universität wien

DISSERTATION / DOCTORAL THESIS

Titel der Dissertation /Title of the Doctoral Thesis

„Biological activities of novel transition metal complexes with heterocyclic ligands“

verfasst von / submitted by

Maria Legina, MSc

angestrebter akademischer Grad / in partial fulfilment of the requirements for the degree of

Doktorin der Naturwissenschaften (Dr. rer. nat.)

Wien, 2018 / Vienna 2018

Studienkennzahl lt. Studienblatt / degree programme code as it appears on the student record sheet:	A 796 605 419
Dissertationsgebiet lt. Studienblatt / field of study as it appears on the student record sheet:	Chemie / Chemistry
Betreut von / Supervisor:	O. Univ.-Prof. Dr. Dr. Bernhard K. Keppler

Acknowledgements

The author is sincerely grateful to all those people who directly or indirectly made this work possible. I would like to express my very great appreciation to O. Univ.-Prof. Dr. Dr. Bernhard K. Keppler for giving me the unique opportunity to conduct my doctoral studies in his multidisciplinary group, as well as for financial support of this work.

I am deeply grateful for the help of Dr. Michael Jakupec with careful and critical supervision of the work at all stages, for valuable and constructive discussions during the planning and development of this dissertation; for his extraordinary overall support.

The author is warmly grateful to the members of the cell culture facility (Anton, Gerhard, Simone, Robert, Klaudia, Erik, Conny, Michaela, Lea and Katharina) for their constant support and participation in the discussion of issues, as well as for the friendly working atmosphere.

I would like to acknowledge all members of the Bioinorganic Chemistry research group, especially Dipl.-Ing. Dr. Wolfgang Kandioller and Dipl.-Ing. Alexander Roller for their active and productive collaboration.

I would like to acknowledge our collaboration partners – Univ.-Prof. Dr. Leticia González and Juan Jose Nogueira Perez, PhD – who contributed significantly to the conduction of this dissertation. I wish to express my special thankfulness to ao. Univ.-Prof. Dr. Vladimir Arion for given opportunities.

I would like to express my deepest gratitude to the people who helped me to overcome administrative difficulties at all stages, especially Elfriede Limberger, who was always ready to help.

The author is infinitely grateful to Dr. Anton Legin for unfailing support, continuous encouragement and endless patience throughout my years of study and through the process of researching and writing this thesis. This work would not have been possible without his daily support and love over the past years of my life.

Heartfelt thanks to my grandmother for all that she did for me.

Finally, I wish to thank my parents, relatives and friends for their support and encouragement.

Table of Contents

Index of figures

Abstract

Many studies suggest possible advantages of using other transition metal ions than platinum for development of anticancer metal complexes. For example, ruthenium-based compounds have attracted the interest of researchers because of the possibility of using this metal to create new drugs that allow treating cancer with more selective cytotoxicity against tumor cells. In this dissertation a library of compounds was investigated, comprising ruthenium- and osmium-based nitrosyl complexes that showed a striking difference in activity, which was attributed to the lability of the Ru–NO bond. Ruthenium(II)–cymene complexes with various substituted 3-hydroxyflavones were found to exhibit not only high antiproliferative activity but also potent inhibitory properties with regard to human topoisomerase IIα activity. Further studies of a series of novel 1,3-dioxoindan-2-carboxamide-based complexes, combining the attributes of half-sandwich complexes and the topoisomerase IIα inhibiting properties of the ligand scaffold, showed only a minor impact on the cytotoxicity but a distinct impact on topoisomerase IIα inhibition properties of these complexes.

Recent analysis of novel ruthenium, osmium, rhodium and iridium complexes featuring thiomaltol ligands suggests that the metal coordination has a distinct impact on their biological activity. The acquired data implied that the introduction of 1-methylimidazole as a leaving group substantially increases the stability in aqueous solution and shields the complex from coordination of biomolecules that would lead to ligand release. This modification allows an accumulation of the intact complexes and controlled activation at the lower pH values within tumor tissues. Whereas the complexes proved to be good topoisomerase IIα inhibitors, the thiomaltol ligand alone proved to be inactive and the tested substances were evidently no topoisomerase IIα poisons. Furthermore, we looked the structure-activity relationships of these complexes in mammary carcinoma cell lines with different level of topoisomerase IIα expression as well as in a newly generated cell line variant with down-regulated enzyme expression in order to understand their biological behavior. In addition, we performed a theoretical analysis of the intermolecular contacts between the metal complexes and the protein as well as an analysis of the solvation spheres around the two complexes that indicated the pocket which is the most likely binding site of the protein domain. Thus, the current study contributes substantially to the knowledge about the biological properties of novel transition metal complexes influencing their anticancer profiles.

Zusammenfassung

Viele Studien legen mögliche Vorteile der Verwendung anderer Übergangsmetallionen als Platin für die Entwicklung antitumoraler Metallkomplexe nahe. Zum Beispiel haben Rutheniumverbindungen das Interesse von Forschern geweckt, weil dieses Metall Möglichkeiten eröffnet, neue Arzneimittel zu kreieren, die eine Krebsbehandlung mit selektiverer Zytotoxizität gegen Tumorzellen erlauben. In dieser Dissertation wurde eine ruthenium- und osmium-basierte Nitrosylkomplexe umfassende Bibliothek von Metallkomplexen untersucht, die einen auffälligen Aktivitätsunterschied aufwiesen, der auf die Labilität der Ru-NO-Bindung zurückzuführen war. An Ruthenium(II)-Cymolkomplexen mit verschiedenen substituierten 3-Hydroxyflavonen wurden nicht nur hohe antiproliferative Aktivitäten, sondern auch starke inhibitorische Eigenschaften im Hinblick auf die Aktivität der menschlichen Topoisomerase IIα festgestellt. Weitere Untersuchungen an einer Reihe von neuartigen 1,3-dioxoindan-2-carboxamid-basierten Komplexen, welche die Eigenschaften von Halbsandwich-Komplexen und die topoisomerase-IIα-hemmenden Eigenschaften des Ligandengerüsts vereinen, zeigten nur eine geringe Auswirkung auf die Zytotoxizität, aber einen deutlichen Einfluss auf die topoisomerase-IIα-inhibitorischen Eigenschaften dieser Komplexe.

Neuere Untersuchungen an Ruthenium-, Osmium-, Rhodium- und Iridiumkomplexen mit Thiomaltolliganden deuten darauf hin, dass die Metallkoordination einen deutlichen Einfluss auf ihre biologische Aktivität hat. Die gewonnenen Daten implizieren, dass die Einführung von 1-Methylimidazol als Abgangsgruppe die Stabilität in wässriger Lösung wesentlich erhöht und den Komplex gegen die Koordination von Biomolekülen abschirmt, die zur Ligandenfreisetzung führen würde. Diese Modifikation ermöglicht eine Akkumulation der intakten Komplexe und eine kontrollierte Aktivierung bei den niedrigeren pH-Werten innerhalb des Tumorgewebes. Während sich die Komplexe als gute Topoisomerase IIα-Inhibitoren erwiesen, zeigte der Thiomaltol-Ligand allein keine Aktivität, und die getesteten Substanzen waren nachweislich keine Topoisomerase IIα-Gifte. Darüber hinaus wurden die Struktur-Aktivitäts-Beziehungen dieser Komplexe in Mammakarzinom-Zelllinien mit unterschiedlicher Topoisomerase-IIα-Expression sowie in einer neu generierten Zelllinienvariante mit herunterregulierter Enzym-Expression untersucht, um deren biologisches Verhalten zu verstehen. Zudem führten wir eine theoretische Analyse der intermolekularen Kontakte zwischen den Metallkomplexen und dem Protein sowie eine Analyse der Solvationssphären um die beiden Komplexe durch, die auf jene Tasche hinwiesen, welche die wahrscheinlichste Bindungsstelle an der Proteindomäne ist. Somit trägt die aktuelle Studie wesentlich zum Wissen über die biologischen Eigenschaften neuer Übergangsmetallkomplexe bei, die ihre antitumoralen Profile beeinflussen.

1. Introduction

1.1 Definition of Cancer

Cancer is a group of diseases involving abnormal cell grow with the acquisition of metastatic properties. Normal cells grow and divide, but every step of every cycle is controlled by many regulatory mechanisms and factors – they only grow when stimulated by growth factors. Cancer cells divide in on unregulated manner and at a rapid pace. Obviously, cancer cells require specific dynamic changes in the genome to become malignant. Carcinogenesis involves uncontrolled cell growth, the activation of oncogenes and inactivation of tumor suppressor genes, while metastasis requires down-regulation of cell adhesion receptors (required for tissue-specific cell-cell attachment) as well as the up-regulation of receptors that increase the mobility of cells [1, 2]. In total, there are more than 100 types of cancer. Usually, they are named after the tissues or organs from which they originate, but some after the cell type that formed them [3], they can be grouped in the following categories:

- carcinoma, formed by epithelial cells;
- sarcoma, formed in bone and mesenchymal soft tissues;
- leukemia, formed in the blood-building tissue of the bone marrow;
- lymphoma, formed from lymphocytes (T cells or B cells);
- multiple myeloma, formed from plasma cells;
- melanoma, formed from melanocytes;
- other types of tumors (neuroendocrine, germ cell tumors and etc.).

According to the original hallmarks of cancer as defined by Douglas Hanahan and Robert A. Weinberg, six different capabilities lead to the development and progression of cancers (**Fig. 1**). Generally, every normal cell requires special signals to grow and divide, but cancer cells are self-sufficient in this, they can produce those signals by themselves. At the same time, many control proteins of cell division or of tumor-suppressor genes may be upregulated in cancer cells, leading to increased growth rate and insensitivity to anti-growth signals. Moreover, these cells become “immortal” due to their ability for a limitless number of divisions. Cancer cells also show a lower propensity for programmed cell death (apoptosis) in case of damage. Finally, these cells are able to stimulate the development of blood vessels to get suffi-

cient amount of oxygen and other important components for them to survive and, finally, they are known to invade neighboring tissues as well as to spread to distant parts of the body (metastasize) [4].

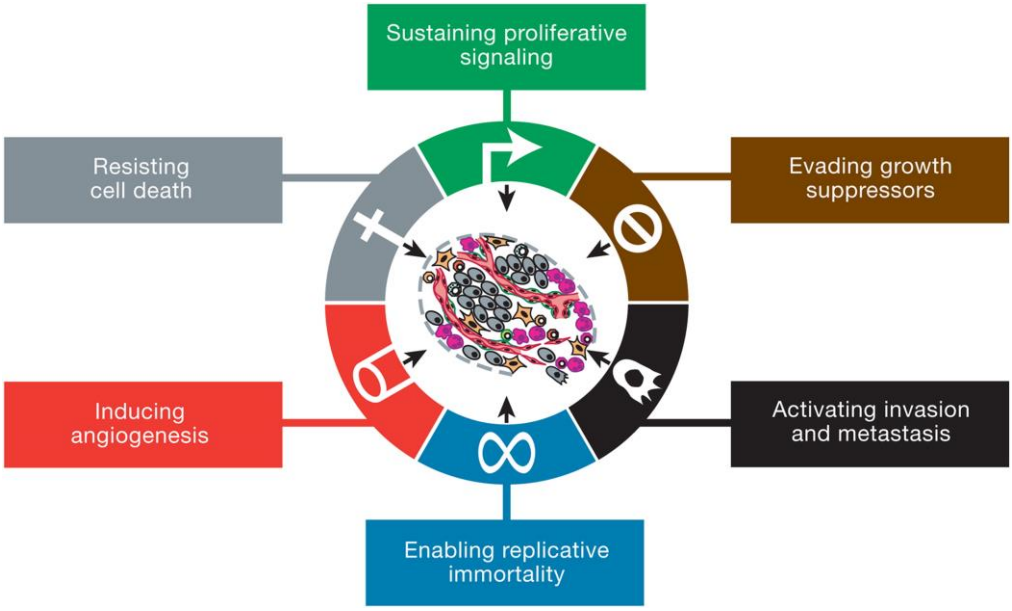

Figure 1. The hallmarks of cancer according to Weinberg and Hanahan 2000 [5].

In 2011 Weinberg and Hanahan published another article where they proposed new hallmarks: abnormal metabolic pathways and evasion of immune control. There authors also mentioned the importance of genomic instability, which generates the genetic diversity that expedites their acquisition, and inflammation, which fosters multiple hallmark functions [5].

Usually, cancer progression is driven by the accumulation of a number of genetic alterations. Those genetic changes or "drivers" of cancer are known to promote cancerogenesis and have effects on three main types of genes namely proto-oncogenes, tumor suppressor genes and DNA repair genes. Notably, the relation of chromosomal abnormalities to tumorigenesis was suggested in 1914 and confirmed half a century later with new cytogenetic techniques. This approach identified the first specific translocation driving the development of human leukemia (Philadelphia chromosome). Since these discoveries, somatic alterations of about 500 genes were linked to cancer development and progression. For example, the analysis of glioblastoma and ovarian cancer samples by the Cancer Genome Atlas project at the genome level revealed a marked contrast regarding somatic copy number alterations, while at the gene level both cancers showed mutations of tumor protein 53, retinoblastoma protein and RTK/RAS/BRAF/PI3K signaling pathway alterations [6, 7].

Understanding how the cancer appears, develops, responds to treatment and promotes metastasis poses a further challenge, but will shed a light on new strategies in cancer therapies (**Fig. 2**).

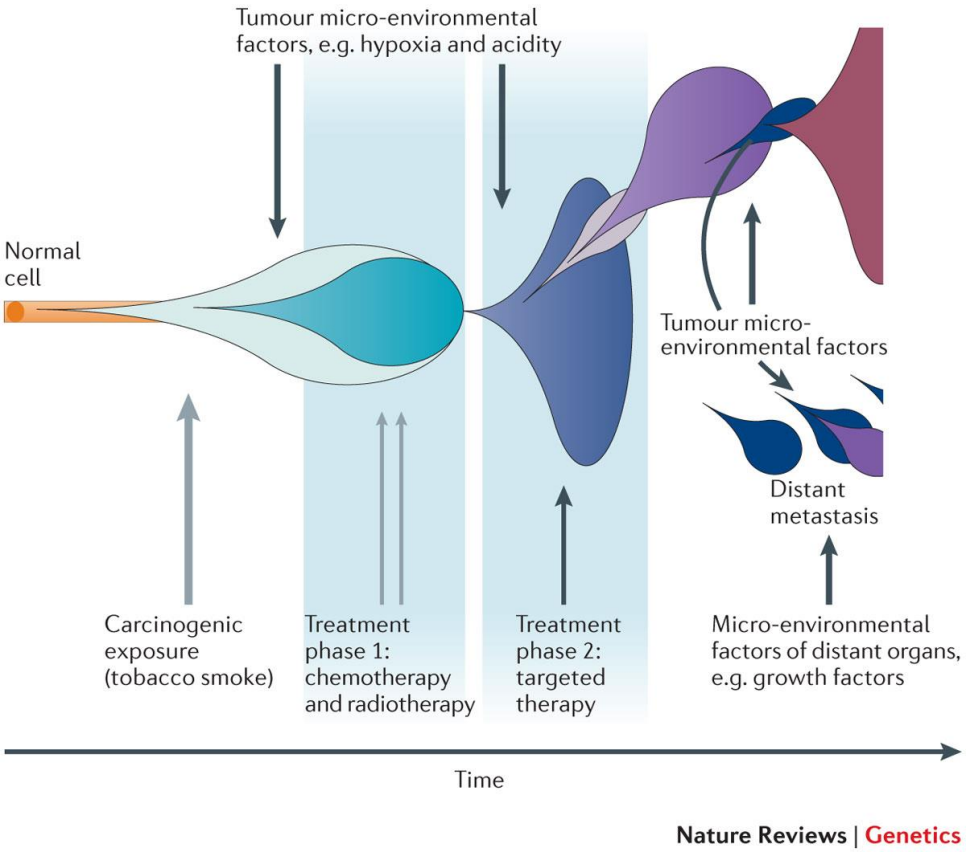

Figure 2. A multitude of environmental factors may shape the evolutionary processes within a single cancer. Blue and purple bubbles represent successive cancer clones, the expansion of which is altered by mutagenic factors (grey arrows) and non-mutagenic factors (black arrows) [10].

Uri David Akavia with co-authors developed a computing structure (CONEXIC), which unites chromosomal copy number and gene expression data for detecting aberrations that promote tumorigenesis. They demonstrated the use of this framework on 62 cultured melanomas and identified 30 scoring modulators as likely "drivers". Recently, BRCA1 and BRCA2 mutations that affect DNA repair have been shown to create a tumor-specific vulnerability to PARP (poly(ADP-ribose) polymerase) inhibitors and have triggered enthusiasm for cancer therapeutic target discovery. These new approaches are very important for identification of candidate drivers with biological importance for cancer treatment [8-10]. Refined definition of cancer with the new approaches will help further research in the fight against cancer. Recognition of the broad application of the hallmarks concepts will influence the development of new means for anti-cancer therapy.

1.2 Epidemiology of Cancer

Cancer is a leading cause of death in both economically developed and developing countries. The significance of the disease is increasing, not only because of the growth and aging of the population but also due to cancer-associated lifestyle habits such as smoking, poor-quality diet or lack of physical activity. Cancer risk and protective factors are identified in epidemiologic studies. The cancerogenic effect of tobacco was the most important discovery in the history of cancer epidemiology. Lung cancer cases increase sharply among constant smokers, but the risk is the highest in those who start smoking young and continue during all life. Cancerogenic effects of tobacco were then thought to be associated with only a limited number of cancer types – lung, pancreatic, bladder, head/neck and esophageal. Later data showed that other types of cancer, which are highly prevalent around the world, also increase by smoking (e.g., gastric, liver and cervical) [11-13].

Dietary epidemiology studies factors such as the variety of food and food components as well as correlations and temporary changes in their use. The question whether the concrete food components or nutrients are connected with increased or reduced risk of a cancer was addressed. However, studies of human populations still did not convincingly show that any dietary component causes or protects from a cancer. Scientists studied many additives, nutrients and other biologically active components for possible associations with cancer. At most, it was shown that some components are associated with cancer risks including alcohol, artificial sweeteners and fried meat [12, 14-16], while other components are known to be associated with cancer prevention – antioxidants, tea, cruciferous vegetables, garlic and vitamin D [17-20].

Other factors, such as reproductive and hormonal, are also known to play a role in the development of breast and ovarian cancers. However, the most important discoveries concern the cancerogenic effects of infectious pathogens, such as *Helicobacter pylori*, human papilloma virus or hepatitis-B virus. About one fifth of all human cancerous tumors around the world appear in stomach, liver or cervix, and the majority of them would be prevented if these infections could be eradicated. Epidemiological data on human cancer rates also provide some information about occupational and environmental carcinogens. The only widespread cancer undoubtedly caused by environmental factors is skin cancer, while there is a little information about other correlations. Presence of asbestos, mineral oils, silica, diesel engine exhaust, coal tars and pitches, dioxins, environmental tobacco smoke, radon, tetrachloroethylene, arsenic and strong inorganic mists are among the most common carcinogens [12, 21].

The American Cancer Society, the International Agency for Research on Cancer, and the Union for International Cancer Control developed the Cancer Atlas to provide a global basis for the fight against cancer. This worldwide report provides information about estimated 14.1 million new cases and 8.2 million

deaths from cancer in 2012 (**Fig. 3**). Around 57% (8 million) of new cancer cases and 65% (5.3 million) of fatal cases occurred in less developed regions of the world. Nearly a half of all new cases and a little more than a half of all deaths comes from Asia, and one quarter of the global burden occurs in China [21]. Based on obtained data it is expected that by the year 2025 there will be an estimated 19.3 million new cancer cases and 11.4 million cancer deaths yearly, and the proportions occurring in less developed regions will increase to 59% and 68%, respectively.

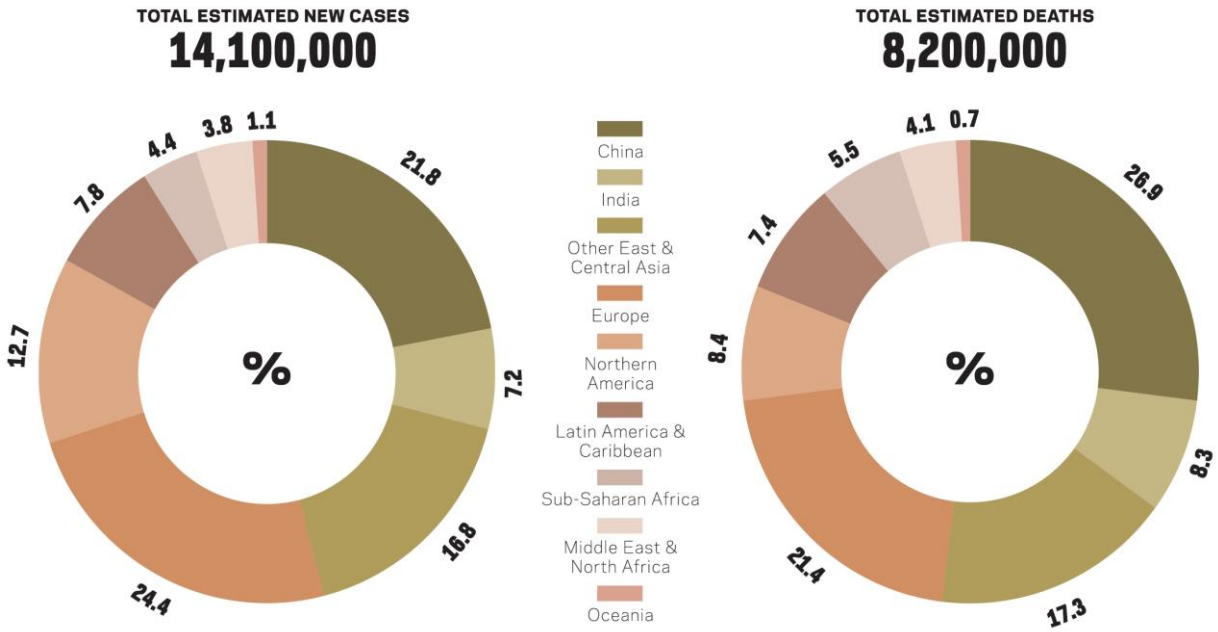

Figure 3. Estimated global numbers of new cases and deaths with proportions by major world regions, for all malignant cancers (excluding non-melanoma skin cancer) in both sexes combined, 2012 [21].

J. Ferlay and co-authors described the key results available in the GLOBOCAN series of the International Agency for Research on Cancer in a more detailed manner. They analyzed the data and assumed that lung cancer remains the most common cancer in the world with 1.8 million cases and 1.6 million deaths (12.9% and 19.4% of total, respectively) because of the higher fatality. Breast cancer is the second most common cancer overall with 1.7 million cases (11.9%) but ranks lower as a cause of death (522,000, 6.4%) because of the more favorable prognosis. These are followed by colorectal cancer (1.4 million cases, 693,000 deaths), prostate cancer (1.1 million cases, 307,000 deaths), stomach cancer (951,000 cases, 723,000 deaths) and liver cancer (782,000 cases and 745,000 deaths). These six cancers represent 55% of the global incidence burden in 2012; in more developed regions, just four cancers – female breast, prostate, lung and colorectal – amount to half of the total incidence, whereas lung, female breast, stomach and colorectal cancers combined with liver and cervical cancers make up more than half of the incidence burden (54%) in less developed regions [22]. These data are presented in the Atlas of Cancer by sex – here we

see the pattern described above – lung and prostate cancer is the most common type of cancer in men, whereas breast cancer is the most common in women (**Fig. 4**).

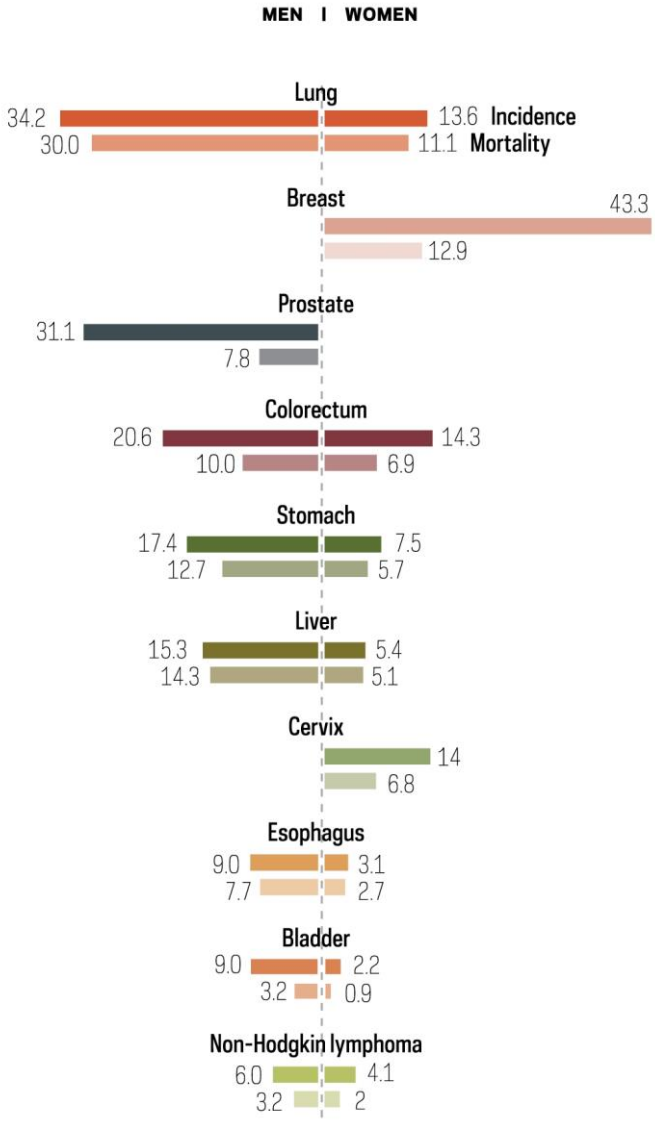

Figure 4. Global estimated age-standardized cancer incidence and mortality rates per 100,000 by major sites in men and women, 2012 [21].

Striking geographical differences in cancer incidents are typical for Europe, where 3.5 million new cases and 1.9 million deaths from cancer were estimated in 2012. More than half of overall new cancer cases are from breast, colorectal, prostate and lung cancers, while the most common causes of cancer death are lung and colorectal cancer. In the male population the most frequent form of cancer incidence is prostate cancer in Northern, Western and Southern European countries, while lung cancer is more common in Central and Eastern Europe. Lung cancer is the leading cause of cancer death among men in almost all

European countries, while breast cancer dominates as the most frequent in women. Generally, in most European countries breast cancer incidence rates continue to increase, while mortality rates decreased, as a result of earlier diagnosis, improved therapies and population-based screening programs [21]. If we look at the most recent available cancer statistics 2018, we will see that not much has changed – breast cancer continues to hold the leading position with new estimated 266,120 cases and an estimated 40,920 deaths, while lung/bronchus cancer follows on the second position with 234,030 and 154,050 estimated cases and deaths, respectively. Prostate cancer closes the top three with 164,690 estimated cases and 29,430 deaths. In 2018, it is estimated that there will be 1,735,350 new cases of cancer of any site and an estimated 609,640 people will die of this disease. Overall cancer incidence rates are higher among men than women. Among racial/ethnic groups, there are more new cases among African American men and white women and fewer new cases among Asian/Pacific Islanders of both sexes. The number of new cases of cancer of any site was 439.2 per 100,000 men and women per year based on 2011–2015 cases. Cancer of any site is most frequently diagnosed among people aged 65–74 with median age of 66. Using statistical models for analysis, rates for new cases of cancer of any site have been falling on average 1.1% each year over the last 10 years. Death rates have been falling on average 1.5% each year over 2006–2015 [23].

1.3 Principles and strategies of anticancer therapy

There are many types of cancer treatment – surgery, radiation therapy, chemotherapy, immunotherapy, targeted and hormone therapy. The type of treatment that a patient receives depends on the type of cancer and how advanced it is. Strategies of anticancer therapy have changed over the last four decades and the time when operation and radiotherapy were the only effective ways of treatment is long past. It is well known that surgery is the most effective type of treatment for localized primary tumors and overall as a single treatment strategy – it cures more patients than any other individual type of treatment. Chemotherapy and radiation therapy in comparison with operations are only able to kill a fraction of tumor cells by each treatment. However, within the last two decades, the use of surgery and radiation in combined therapy considerably reduced the mortality connected with surgery of solid tumors. The most common use of radiotherapy is in combination with surgery and/or chemotherapy. Radiotherapy can be used pre-, post- or intraoperative and chemotherapy approaches can be used with different strategies depending on type of tumor [24].

However, in the treatment of advanced or metastatic stage and in hematological tumors, surgery and radiotherapy are either not an option or insufficient. Chemotherapy is the most effective therapeutic approach – it relieves painful symptoms, prolongs life and/or even heals the disease:

- chance of normal life for some patients with different types of metastatic tumors;

- increased survival, when used in combination with surgical therapy or radiation therapy;
- total remission in more than 25% of the treated patients [25];
- increased response rate with a significant prolongation of life expectancy;
- objective regression in 30-50% of patients who first received a chemical product.

However, it is always important to remember that the use of cytotoxic chemotherapy does not lead to regression of the tumor in all patients, and that has often undesirable side effects. Nevertheless, chemotherapy expands as new effective antitumor drugs are discovered. Anticancer drugs have their own profile of sensitive and resistant primary tumors, and the use of combined drugs leads to a high complexity of possible therapeutic regimens. The objective of chemotherapy in cancer is the selection of drugs and dose levels, which have a chance of eradicating disseminated cancer cells, without causing severe host toxicity [25].

1.3.1 Alkylating agents, antimetabolites and antimitotic drugs

The beginning of the modern era of chemotherapy started with the discovery of nitrogen mustard as an effective cancer therapy by Goodman and Gilman with surgeon Lindskog in 1942. They continued experiments with a desire to understand the mode of action of mustard compounds and found the ability which was later clarified as forming covalent bonds with DNA. Later studies demonstrated specific sites of alkylation on purine bases, leading to crosslinking of strands and induction of apoptosis. Around 1950, it was shown that a four-amino analogue of folic acid (aminopterin) could inhibit proliferation of cells and induces remissions in acute leukemic patients. While, nitrogen mustard and its derivatives are long known to covalently bond alkyl groups of molecules, folic acid analogs are known to interfere with the synthesis of DNA precursors. Up to now, alkylating agents and anti-folates remain major classes of cytotoxic chemotherapy drugs in routine clinical use to treat tumors [26, 27]. Differences in the activity of alkylating agents are explained by differences in absorption, metabolic rate and tissue affinity, and not by differences in the mode of action. With rare exceptions, the resistance of tumor cells to a particular alkylating agent indicates resistance to other alkylating agents. Alkylating agents cause various pharmacological effects, including interference with mitosis, mutagenesis, immunosuppression and carcinogenesis. There are five chemical classes of clinically useful alkylating agents [25]:

- nitrogen mustard derivatives (mechlorethamine, cyclophosphamide, chlorambucil, melphalan);
- ethylene derivatives;
- alkyl sulfonates (busulfan);
- triazine derivatives (dacarbazine);
- nitrosoureas (carmustine, lomustine, semustine).

Antimetabolites directly interact with special metabolic enzymes, which leads to inhibition of this enzyme or the subsequent synthesis of an aberrant molecule that cannot function normally. These antimetabolites are structural analogues of normal metabolites necessary for the biosynthesis of purine and pyrimidine – when introduced into a cell instead of a physiological substance, they lead to inhibition of the cellular function. Antimetabolites are specific for the phases of the cell cycle and act during DNA synthesis (cell phase S). Main antimetabolites are [25]:

- pyrimidine analogues (5-fluorouracil, cytosine-arabinoside, gemcitabine);
- purine analogues (6-mercaptopurine, 6-thioguanine);
- folic acid antagonists (methotrexate).

The class of antimitotic drugs is widely represented by plant alkaloids of which the most famous cancer fighter are Vinca alkaloids – a subset of drugs obtained from the Madagascar periwinkle plant. They are naturally extracted from the pink periwinkle plant, *Catharanthus roseus* and have hypoglycemic as well as cytotoxic effects. They have been used to treat diabetes, high blood pressure, used as disinfectants and anticancer drugs. There are four major Vinca alkaloids in clinical use: vinblastine, vinorelbine, vincristine and vindesine. The main mechanism of Vinca alkaloid cytotoxicity is their interaction with tubulin and disruption of microtubule function, particularly of microtubules comprising the mitotic spindle apparatus, directly causing metaphase arrest [28].

1.3.2 Platinum compounds

In 1965 Rosenberg opened a door to metal-based chemotherapeutic agents by discovering the antitumor properties of cisplatin. Today cisplatin, carboplatin and oxaliplatin are the only FDA-approved platinum drugs and are used worldwide for the treatment of various cancer types. Another three Pt-drugs have gained approval in single markets – nedaplatin in Japan, lobaplatin in China and heptaplatin in Korea (**Fig. 5**). The major cellular processes by which cisplatin attacks cancer cells include formation of DNA adducts, their recognition by damage-response proteins, and signal transduction leading to cell-cycle arrest, DNA repair and/or cell death. Platinum drugs contain two types of ligands attached to a central platinum cation – amine/ammine "carrier" and labile chlorido/carboxylato ligands. Platinum drugs can be viewed as prodrugs as they require aquation of their labile ligands to form bonds with the N7 atom on guanine and adenosine bases of DNA. This type of binding stops DNA replication and transcription and leads to apoptosis [29-32].

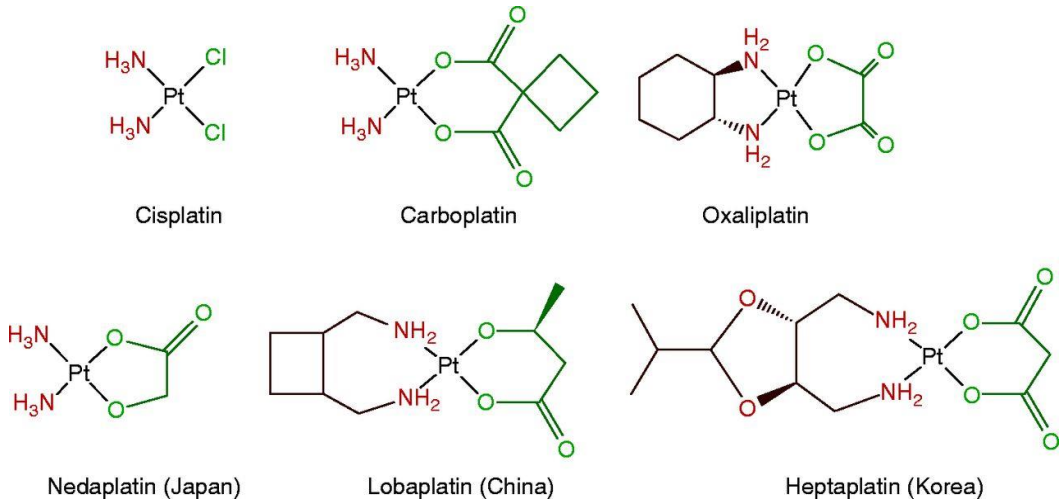

Figure 5. The structures of the approved platinum drugs, showing the "carrier" amine/ammine ligands in red and the labile chlorido- or carboxylate-based ligands in green [32].

Despite their success, platinum drugs have two main limitations: severe side effects (such as neuro- or nephrotoxicity) and drug resistance of several cancer types. The side effects from unspecific damage to rapidly dividing cells (e.g., hair follicles, bone marrow, mucosa of the gut) are much less pronounced for platinum drugs than for many other chemotherapeutics, while drug resistance arises from several mechanisms: down-regulation of cellular uptake and up-regulation of drug efflux, glutathione-associated effects (degradation and detoxification of the drugs in the cell), as well as a decrease in formation of drug-DNA adducts and an increased repair of or tolerance to the DNA damage. Platinum drugs remain one of the most used families of chemotherapeutic drugs and are unlikely to be clinically replaced in the near future. They are not without their shortcomings, with serious side effects limiting the dose that can be prescribed to patients, and the development of drug resistance even by those types of cancer that initially respond to platinum. While the direction is developing and new platinum preparations are appearing, they are likely to suffer from the same problems, and therefore, currently the focus is on developing new substances that are more stable and more selective for cancers [32].

1.3.3 DNA topoisomerase-targeting drugs

DNA topoisomerase-targeting drugs are the next well-known and promising class of anticancer chemotherapeutics. Topoisomerases are essential nuclear enzymes involved in every aspect of DNA function – replication, transcription, recombination and chromosome condensation. In particular, DNA strand separation for transcription and replication, the flawless segregation of two identical copies of entire genomes in two daughter cells following replication, and the formidable genomic compaction in cells exemplify the critical actions of DNA topoisomerases. Topoisomerases are classified as type I and type II according

to the number of DNA strands cut in one round of their catalytic cycle. Thus, topoisomerase I (topo1) cleaves one DNA strand at a time and topoisomerase II (topo2) both strands of the double helix as part of their catalytic functions. The enzyme type II has two isoforms – α and β, encoded by different genes that are expressed in actively dividing cells. Topoisomerase IIα (topo2α) plays a dominant role in mitosis, while topoisomerase IIβ (topo2β) is not absolutely required for cell division, hereby, topo2α became a primary target for a number of anticancer drugs and considered to be more effective in killing cancer cells [33, 34].

The most popular anticancer drugs targeting topoisomerase I are camptothecin (CPT) derivatives. Camptothecin was first identified from the tree *Camptotheca acuminata* ("happy tree") that is growing in southern China and Tibet. The bark and stems of the tree contain the alkaloid CPT that is poisoning the enzyme by reversibly inhibiting religation of DNA strands. However, CPT had some limitations: low solubility and inactivation within minutes at physiological pH by lactone E ring opening. In later studies, structures were improved and two water-soluble CPT derivatives were approved for worldwide clinical use – topotecan and irinotecan (belotecan only in South Korea) (**Fig. 6**). Topotecan is a DNA intercalator and its action disrupts the DNA duplication mechanism, which leads to cell death. Irinotecan works via its active metabolite – SN-38 that is formed via hydrolysis of irinotecan by carboxylesterases and is 1000 times more active than irinotecan itself. The inhibition of topo1 by the active metabolite SN-38 eventually leads to inhibition of both DNA replication and transcription that, obviously, helps to overcome the limitations of topotecan [35].

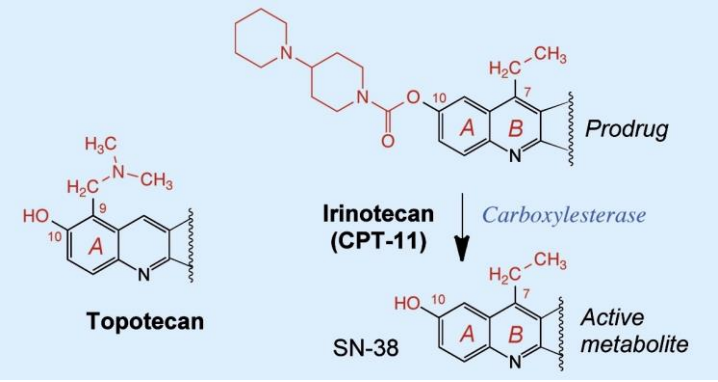

Figure 6. Topotecan and irinotecan are the two FDA-approved camptothecins for anticancer therapy [35].

Agents able to stabilize the covalent DNA topo2 complex (also known as the cleavable complex) are traditionally called topo2 poisons, while agents acting on any of the other steps in the catalytic cycle are called catalytic inhibitors. (**Fig. 7**). The story of topo2 poisons begins with the anthracycline daunorubicin, which was discovered in the 1950s, derived from soil bacteria of the genus *Streptomyces* as an extremely potent anticancer drug. It remains in use today primarily for the treatment of acute leukemia.

Doxorubicin (adriamycin), another bacterial toxin, was discovered soon after daunorubicin and is widely used for treating breast cancer, bone and soft tissue sarcomas, bladder cancer, anaplastic thyroid cancer, Hodgkin's and non-Hodgkin's lymphomas and multiple myeloma. Epirubicin, an active isomer of doxorubicin, was developed later (approved by the FDA in 1999) to avoid the side effects of doxorubicin, possibly due to its faster elimination. The anthracyclines are effective against more types of cancer than any other class of chemotherapeutic agents and have several mechanisms of action: they intercalate into DNA and RNA strands and inhibit their synthesis, they inhibit topo2 by stabilization of the enzyme-DNA cleavage complex and generate free oxygen radicals. Although anthracyclines are used to treat a wide range of cancers, their limitation is long-term cardiotoxicity. Another well-known topoisomerase poison, etoposide (Vepesid), is a glycoside derivative of podophyllotoxin found in the American mayapple (*Podophyllum peltatum*). It was first synthesized in 1966, approved by the FDA in 1983 and is still widely used in oncology for a broad range of solid tumors. Etoposide prevents topo2 from religating cleaved DNA and increases enzyme-mediated double-strand breaks of DNA. Teniposide has a similar mechanism of action, but it is about 10-fold more potent than etoposide in killing malignant cells likely due to higher cellular uptake. The anthracenedione mitoxantrone (Novantrone) was developed as a synthetic analog of anthracyclines at the American Cyanamid Laboratories in the late 1970s and approved by the FDA in 1996 for prostate cancer treatment, it is a potent DNA intercalator and topo2 poison [35-38].

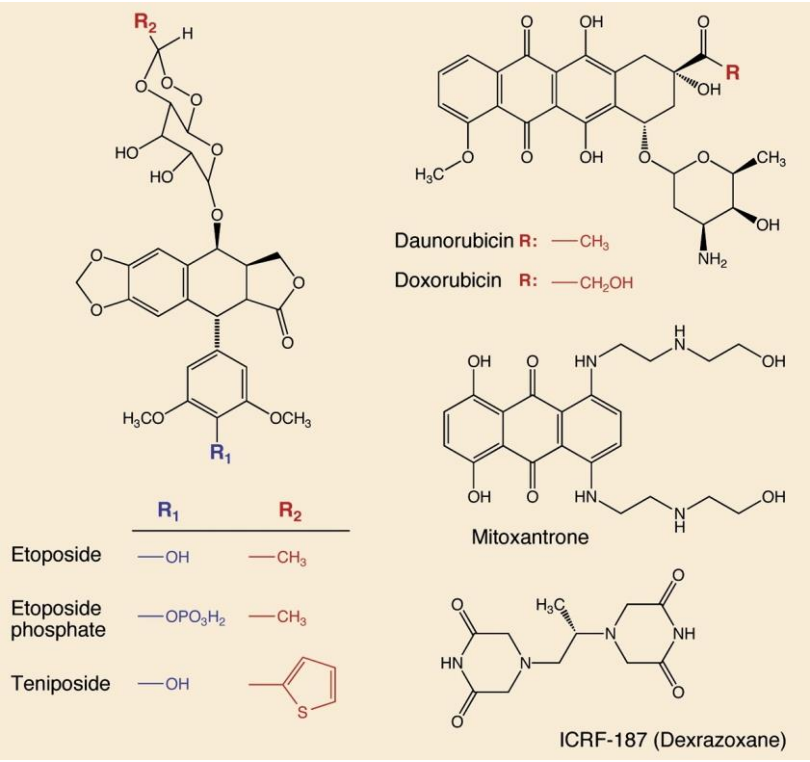

Figure 7. The overview of topo2-targeting drugs including poisons and catalytic inhibitors [35].

Catalytic topo2 inhibitors are a heterogeneous group of compounds that might interfere with the binding between DNA and topo2 (aclarubicin and suramin), stabilize noncovalent DNA topo2 complexes (merbarone, ICRF-187, and structurally related bisdioxopiperazine derivatives), or inhibit ATP binding (novobiocin). The most frequently studied group of topo2 inhibitors are ICRF-187 and related bisdioxopiperazine derivatives. ICRF-187 was in clinical usage primarily for reducing the cardiotoxicity of anthracyclines but since was found to inhibit topoisomerase and in fact now it is under investigation as a catalytic inhibitor. Merbarone is another catalytic inhibitor of topo2 useful for experimental studies – it exhibits curative activity against L1210 leukemia and activity against some other murine tumors. The drug inhibits the catalytic activity of topo2 with some selectivity toward the topo2α isoform; while this drug is not approved for clinical use, it remains a useful tool for studying the enzyme [38]. The main difference between catalytic inhibitors and poisons is the accumulation of double-strand breaks in the latter case. Catalytic inhibitors are mainly disrupting the function of the enzyme by binding to its ATP pocket, by binding to the same sites on DNA that are used by the enzyme or by the simultaneous binding to DNA and the enzyme, leading to the freezing of the whole catalytic cycle, but without increasing levels of DNA cleavage (**Fig. 8**) [35-40].

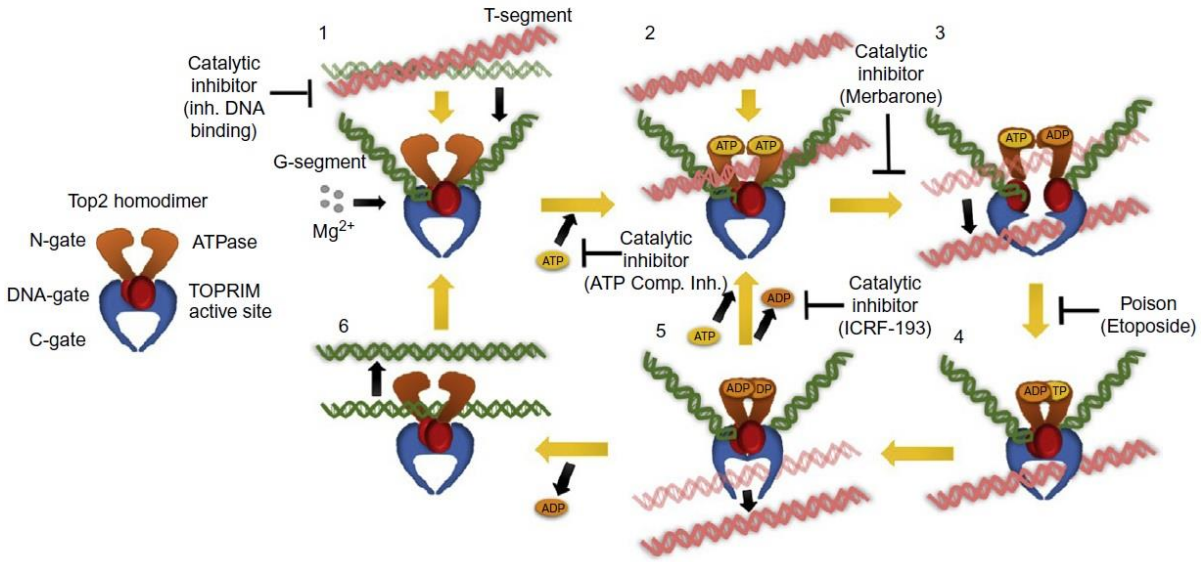

Figure 8. The overview on topo2 catalytic cycle (based on Murphy et al.) [40]

In addition to the above-mentioned inhibitors, the activity against the enzyme was shown by compounds such as curcumin, cannabidiol and resveratrol. The first two agents demonstrated inhibition of topo2α ATP hydrolysis and a decrease in enzyme–DNA binding, while the last agent showed the ability to inhibit relaxation; nevertheless, further work is required to clarify the possible modes of action [40]. In this regard, many scientific groups turned to the methods of theoretical chemistry and went into the field of molecular

simulations. They investigate existing structural data with molecular dynamic simulations and propose models for not yet well characterized DNA–topo2–drug systems. Thus, there are plenty of methods to investigate the possible options for modifying chemical structures to improve existing catalytic inhibitors in order to overcome the main disadvantage of topo2 poisons – the tendency to form secondary malignant tumors [41-42].

It should be noted here that tumor cells show different expression of topo2α compared to normal cells. Among all forms of topoisomerases, this α isoform of the enzyme is closely associated with cell proliferation and is therefore an important therapeutic target in diseases that involve cellular proliferation such as cancers. Different researchers pointed out the prognostic value of topo2α in various types of cancer. Overexpression is related with changes in tumor behavior and responses to medication. The up- or down-regulation of this enzyme alone and sometimes in association with other genes may predict the character of malignancy, therapeutic response, and overall survival of patients [43].

1.3.4 Targeted therapy

For decades systemic anticancer therapy has been based on application of cytotoxic chemotherapeutics. The majority of these drugs are DNA-damaging agents that are intended to destruct or suppress quickly dividing cells. While many researchers were searching for the most effective cytotoxic compounds, others were studying tumor cell characteristics including self-dependence on positive regulatory signals, insensitivity to growth inhibitory signals, limitless proliferation, resistance to apoptosis, angiogenesis and the ability to establish distant metastasis. They found out that networks, which are responsible for these activities or inactivities, are radically altered in cancer cells and set out to target these molecular defects – it was the beginning of a new era of "targeted therapy". Today, there are two main approaches available for use in clinical practice of specific molecular targeting – therapeutic monoclonal antibodies and small-molecule agents. The first can deplete or block tumor growth factors, while the second target different steps in transduction and execution of growth signals. The most famous strategies are anti-HER2 and anti-EGFR targeted therapies (trastuzumab, lapatinib, gefitinib and erlotinib). Many drugs influencing each of the acquired properties necessary for growth and progression of a tumor were developed, are in clinical tests or even approved for clinical application in cancer treatment. Below, the **Figure 9** depicts different classes of those drugs and the wide range of promising targets and modes of action in development for most of these hallmarks of cancer [5, 24, 44].

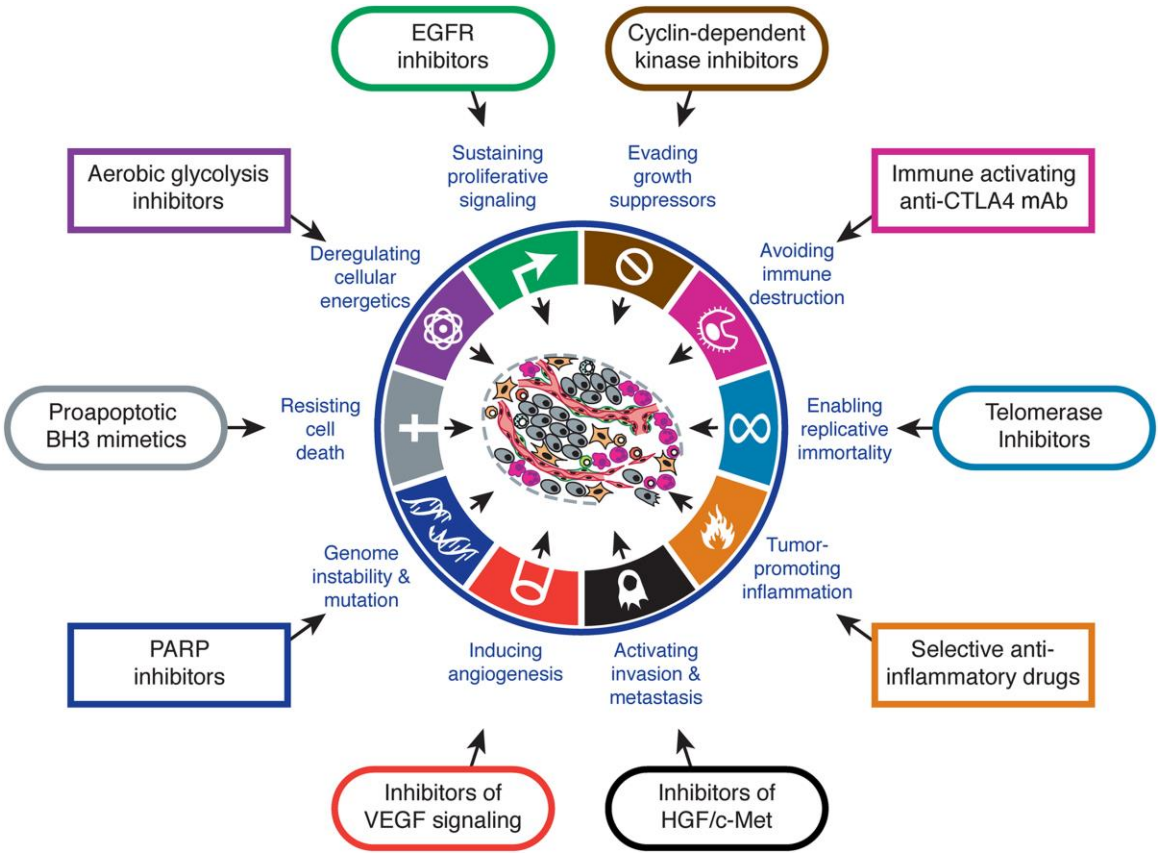

Figure 9. Different classes of drugs that interfere with each of the acquired capabilities necessary for tumor growth and progression [5].

Cancer immunotherapy makes use of a stimulation of the immune system to treat cancer. Active immunotherapy is used to trigger the immune system to attack cancer cells by targeting tumor antigens. The blocking of immune checkpoints is one of the most promising approaches for activation of therapeutic antitumor immunity. Immune checkpoints are excessive inhibitory pathways built into the immune system that are critical for modulating the duration and strength of immune responses. Due to fact that many of the immune checkpoints are initiated by ligand–receptor interactions, they can be blocked by antibodies or modulated by recombinant forms of ligands and receptors. For example, the first of this class of immune-therapeutics were cytotoxic T-lymphocyte-associated antigen 4 (CTLA4) antibodies which were approved by the US Food and Drug Administration (FDA). Preliminary clinical findings with blocking of additional checkpoint proteins such as programmed cell death protein 1 (PD1) indicated broad and diverse opportunities to enhance antitumor immunity with the potential to produce long-lasting clinical responses. Viral vectors or virotherapy is another concept in cancer treatment – the strategy involves oncolytic viruses that grow selectively in tumor cells. An additional mechanism of antitumor activity associ-

ated with the replication of the virus in the tumor is the activation of an immune response against the tumor [24, 45].

1.4 Novel metal-based anticancer drugs

The successful application of cisplatin in oncology has raised the interest in metal-based drugs as potential chemotherapeutics. Transition metals offer a wide range of possibilities in the design of anticancer agents, including the variation of coordination numbers, redox states and ligand substitution. Current studies are focused on metal-based drugs that interact differently with DNA in comparison to classic platinum complexes or with other targets such as proteins, implying alternative ways to kill cancer cells. Many different transition metal complexes have been synthesized and investigated in order to overcome resistance of some tumors to platinum drugs. In this respect, ruthenium and osmium compounds with their lower toxicity and different mechanisms of action, as compared to classic platinum-based complexes, are promising candidates in the field of anticancer drug development [29, 30, 47].

1.4.1 Ruthenium and osmium compounds

Generally, ruthenium has two oxidation states that are relevant for drug design – Ru(II) and Ru(III) which are able to form six-coordinated octahedral species and the rate of ligand exchange is comparable to that of platinum. In 1980, chlorido-ammine-Ru(III) compounds were found to have anticancer activity in rats, which was the starting point in the story of ruthenium-based compounds as experimental cancer therapeutics. Although the activity of these complexes was limited by poor solubility, four years later the new analog *cis*-[$RuCl_2(dmso)_4$] was shown to be active against primary and metastatic cancers with less activity compared to platinum drugs but with milder side effects. The general overview of ruthenium-based compounds shows that three classes of active compounds were most successful for – NAMI-A, KP1019/1339 and organometallic Ru(II)-arene complexes (such as RAPTA-C) (**Fig. 10**). KP1019 is a potent ruthenium anticancer drug but with one significant drawback – poor water solubility. A sodium salt analog, KP1339, was synthesized to overcome this issue and showed a 35-fold higher solubility. In preclinical trials NAMI-A and KP1019/1339 have shown antimetastatic potential and ability to induce apoptosis in primary tumors, respectively. These ruthenium compounds are characterized by a high affinity to proteins of the blood, which has been suggested to be crucial for drug accumulation in the tumor tissue and to be responsible for the minor adverse effects observed in clinical trials. The clinical study showed that NKP-1339 is well tolerated with manageable side effects and single-agent activity was noted in multiple tumors including NET [30, 46-50].

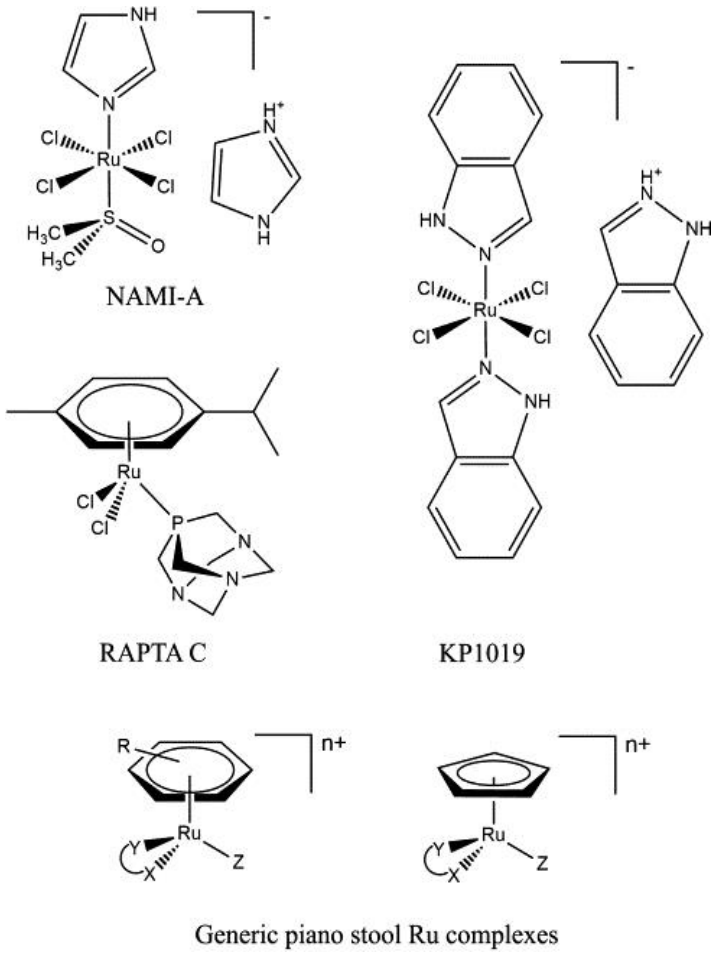

Figure 10. Anticancer ruthenium complexes [46].

The long success of Ru-arene compounds is connected to the amphiphilic properties of the Ru-arene system where a hydrophobic ligand is adjoined by the hydrophilic metal center. The best-known representatives are drugs designed by the group of Dyson (RAPTA-C) and some analog produced by Sadler. Although RAPTA-C only exhibits a low activity *in vitro*, it is active against metastatic tumors *in vivo* [46].

Studies of ruthenium-based compounds could identify a unique combination of properties of certain complexes with respect to their anticancer potency – possible transport into tumor cells by transferrin, given the presumed higher demand for iron of these rapidly dividing cells; their octahedral geometry offering unique possibilities to bind to target molecules; accessibility of different oxidation states under biological conditions. Some ruthenium-based compounds are suitable as NO-delivering agents, while other may reveal topoisomerase-targeting properties. Thus, ruthenium-based anticancer compounds may more selectively attack tumor cells, rather sparing healthy tissues [51].

Osmium is a metal that deserves attention of researchers in search of new effective anticancer therapeutics. Osmium complexes gained increasing interest in this context since several studies revealed them as an interesting alternative to their ruthenium analogs. For instance, NAMI-A-analogous Os(II) and Os(III) complexes are highly resistant to hydrolysis even in chloride-free solution in comparison to their Ru(III) congeners. Of course, these chemical differences reflect in different biological properties – some Os(II) analogues of NAMI-A are inactive, while Os(III) complexes display a significant antiproliferative activity compared to the parent and related compounds. Moreover, there were new osmium-based complexes synthesized as analogs of the clinically active compound KP1019 and RAPTA-like that exert different biological effects. It has been shown that osmium complexes are capable of inducing apoptosis by interaction with various cellular pathways; however, further investigations are necessary to gain deeper knowledge of biological effects of osmium complexes in a cell [46, 52].

Anticancer ruthenium (and osmium) complexes were initially designed to mimic the mode of action of platinum-based agents. However, this point of view changed significantly over the last decade due to the fact that these complexes demonstrated novel mechanisms of action and a strong potential as anticancer therapeutics. Many experimental findings suggest that these metallodrugs do not target DNA exclusively but also some important cellular proteins. Truly, the target identification as well as the evaluation of novel mechanisms of action require a broad experimental base and a special approach that includes an integrated target-profiling, for example. This will ensure a better understanding by linking the potential targets to drug effects by a network analysis as it was described by Meier-Menches and co-authors. The compounds of ruthenium and osmium offer a rich chemical variety that provides many opportunities for fine-tuning the perspective configurations into a metal complex with the desired properties [53-54].

1.4.2 Rhodium and iridium compounds

In contrast to the ruthenium and osmium complexes that have attracted attention as potential chemotherapeutic agents over the past two decades, much fewer investigations on the biological effects of rhodium and iridium compounds have appeared. Surprisingly, the first mention of antitumor properties for a rhodium(III) complex was in 1953 [55]. However, later there were only occasional reports of significant antineoplastic activity for individual complexes and only in the past five years the structure–activity relationships and cellular effects of cytotoxic Rh(III) compounds and their Ir(III) counterparts have been systematically studied. Iridium and rhodium complexes have become popular due to their easily tunable reactivity, higher water solubility and relative availability. This type of compounds exhibits a wide range of properties that might make them promising anticancer drugs. Their activities, binding preferences and cellular uptake are strongly dependent on their ligand combination and coordination geometry, which open up a plentitude of opportunities in the design and development of metal-based chemotherapeutics. Further-

more, the diverse stereochemistry and unique geometries offered by transition metal complexes in general may allow them to cover a wider range of biological targets and to access targets that are not amenable for purely organic compounds [56, 57].

1.4.3 Other metals

Because of increased emphasis on the clinical relevance of metal-based complexes, many potential candidates for anticancer therapeutics are awaiting their chance to be recognized as being useful. Copper is a very promising candidate since it is an essential cellular metal necessary for many biological pathways and it is a cofactor in enzymatic processes, therefore, copper complexes exhibit cytotoxic properties with a wide spectrum of activities that mainly depends on the ligand attached. The cytotoxic potencies of gold complexes have drawn attention recently – gold(III) complexes are an appearing class of metal-based complexes with potential antitumor properties, mainly because of their outstanding cytotoxic properties shown through non-cisplatin-like mechanisms and, therefore, showing a strong effect on cisplatin-resistant cell lines. Metal complexes with silver were known for their antibacterial actions for a long time and are widely used in treatment of the infected wounds and cases of a burn. In the past, silver-based complexes did not receive a lot of attention in comparison with other metals, but recently, cytotoxic properties of silver(I) complexes have attracted an interest as most of them has shown a greater cytotoxic activity than cisplatin with rather low toxicity and greater selectivity toward cancer cell lines [58-60].

2. Results

This cumulative PhD thesis is based on the following research articles and manuscripts.

2.1 Biological evaluation of novel thiomaltol-based organometallic complexes as topoisomerase IIα inhibitors

Legina MS, Nogueira Perez JJ, Kandioller W, Jakupec MA, Gonzales Herrero L, Keppler BK.

Nature Chemical Biology, submitted manuscript

As the first author, I contributed substantially to every step in the making of this article, including the entire experimental work, its description and interpretation. In this manuscript the antiproliferative activity as well as the induction of cell death of thiomaltol-based organometallic complexes was analyzed in mammary carcinoma cell lines with different levels of topo2α expression (SK-BR-3, T47D and MDA-MB468). Their impact on DNA secondary structure and possible DNA double-strand breaks were investigated. Additionally, downregulation of topo2α expression level by RNAi was performed in order to investigate how this affects cancer cell response to treatment with these compounds. Theoretical analysis of the intermolecular contacts between the metal complexes and the protein as well as the analysis of the solvation spheres of the two complexes indicated the pocket that is the most likely binding site of the protein domain. I contributed to all sections of the publication and coordinated the collaboration with the co-authors.

2.2 Thiomaltol-based organometallic complexes with 1-methylimidazole as leaving group: synthesis, stability, and biological behavior

Hackl CM, Legina MS, Pichler V, Schmidlehner M, Roller A, Dömötör O, Enyedy EA, Jakupec MA, Kandioller W, Keppler BK.

Chemistry – a European Journal **2016**, 22(48): 17269–17281. doi: 10.1002/chem.201603206.

Thiomaltol, a potential *S,O*-coordinating molecule, has been utilized for the complexation of four different organometallic fragments, yielding the desired Ru^{II} , Os^{II} , Rh^{III} , and Ir^{III} complexes having a "piano-stool" configuration and which were characterized with standard analytical methods. As the second author of this manuscript, I investigated their cytotoxicity in three different cancer cell lines; furthermore, I elucidated their capacity as topoisomerase IIα inhibitors as well as their effect on the cell cycle distribution and reactive oxygen species (ROS) generation. I contributed with the description and interpretation of the biological data to the preparation of the manuscript.

2.3 1,3-Dioxoindan-2-carboxamides as bioactive ligand scaffolds for the development of novel organometallic anticancer drugs

Mokesch S[*], Novak MS[*], Roller A, Jakupec MA, Kandioller W, Keppler BK.

[*]these authors contributed equally to the manuscript

Organometallics **2015**, 34 (5): 848–85. doi: 10.1021/om501032s.

A series of novel 1,3-dioxoindan-2-carboxamide-based complexes were synthesized and characterized with standard analytical methods. Contributing equally as the first author, I investigated the structure–activity relationships of these substances in three human cancer cell lines by means of the colorimetric MTT assay. In addition, I determined the induced changes in cell cycle distribution and the apoptosis/necrosis induction potential. I also contributed respective parts to the discussion and preparation of the manuscript.

2.4 Topoisomerase IIα inhibition and anticancer activity of 3',4'-dihydroxyflavonol-derived organometallics

Kurzwernhart A, Rossi-Gendron C, Novak MS, Roller A, Jakupec MA, Kandioller W, Keppler BK.

(manuscript prior to submission)

3',4'-Dihydroxyflavonol-derived organometallics were synthesized and characterized with standard analytical methods. As a third author, I determined the antiproliferative activity of these complexes in there human cancer cell lines and investigated their potential to inhibit topoisomerase IIα by means of the DNA plasmid relaxation assay. I also contributed to the discussion and preparation of the manuscript.

2.5 Biological properties of novel ruthenium and osmium nitrosyl complexes with azole heterocycles

Novak MS, Büchel GE, Keppler BK, Jakupec MA.

J Biol Inorg Chem. **2016**, 21(3): 347–56. doi: 10.1007/s00775-016-1345-z.

As the first author, I contributed to every part of the project, in particular the entire experimental work, and coordinated the collaboration with the co-authors. Novel ruthenium- and osmium-nitrosyl complexes with azole heterocycles were studied to elucidate their cytotoxicity and possible interactions with DNA. Apoptosis/necrosis induction, changes of mitochondrial transmembrane potential and possible formation of reactive oxygen species were investigated as indicators of NO-mediated damage by flow cytometry.

Furthermore, I investigated the accumulation of intracellular cyclic guanosine monophosphate. I made a major contribution to the preparation of all chapters of the manuscript.

Unless noted otherwise, the listed articles are published in peer-reviewed international scientific journals and can be openly accessed online with the respective DOIs.

Biological evaluation of novel thiomaltol-based organometallic complexes as topoisomerase IIα inhibitors

Maria S. Legina[a], Juan J. Nogueira[b, c], Wolfgang Kandioller[a, d], Michael A. Jakupec[a, d], Leticia González[b, c] and Bernhard K. Keppler[a, d]

[a] University of Vienna, Institute of Inorganic Chemistry, A-1090 Vienna, Austria

[b] University of Vienna, Institute of Theoretical Chemistry, A-1090 Vienna, Austria

[c] Current address: Australian National University, Research School of Biology, Canberra, ACT 2601, Australia

[d] University of Vienna, Research Cluster "Translational Cancer Therapy Research", A-1090 Vienna, Austria

Corresponding author:

Michael A. Jakupec,

Email: michael.jakupec@univie.ac.at

Tel.: +43 4277 52610

University of Vienna, Institute of Inorganic Chemistry, Währinger Strasse 42, A-1090 Vienna, Austria

Abstract

Topoisomerase IIα (topo2α) is an essential nuclear enzyme involved in DNA replication, transcription, recombination and chromosome condensation. Thus, topo2α targeting has become a very efficient and well-established anticancer strategy. Herein, we investigate the antiproliferative activity of ruthenium-, osmium-, rhodium- and iridium-based thiomaltol organometallics in mammary carcinoma cell lines by means of several biological assays, including downregulation of topo2α expression level. We show that inhibition of topo2α is the key process in the cytotoxic mechanism of some of the drugs, while DNA damage is a minor pathway. In addition, molecular modelling evinces that the metal complexes are able to access the DNA-binding pocket of the enzyme, where the hydrophilic environment favors the interaction with highly polar complexes. These

findings will improve our knowledge of the suitability of these novel complexes to be applied as metallopharmaceuticals, given the growing interest in the design of metal-based anticancer agents capable of overcoming the drawbacks of clinically applied chemotherapeutics.

Keywords: topoisomerase IIα, topoII inhibitors, metal complexes, anticancer drugs, molecular dynamics, Monte Carlo simulations, RNA interference

Introduction

Since the discovery of the cytotoxic properties of cisplatin by Rosenberg in 1965 [1], the field of metal-based chemotherapeutic agents has been rapidly growing and developing every year [2]. Cisplatin, carboplatin and oxaliplatin are the only FDA approved platinum drugs used worldwide for the treatment of various cancer types; however, there are many cases of resistance of tumors to platinum drugs. Drug resistance is a well-known phenomenon that results when diseases become tolerant to pharmaceutical treatments [3]. Some mechanisms of drug resistance are disease-specific, while others, such as the drug efflux observed in microbes and in human drug-resistant cancers, are evolutionarily conserved. Although many types of cancer are initially susceptible to chemotherapy, over time they can develop resistance through different mechanisms, such as DNA mutations and metabolic changes that promote drug inhibition and degradation [3]. The processes by which cells develop resistance to antitumor platinum drugs have been the subject of intense research [4] as it is a major obstacle for their clinical use. A large body of experimental evidence suggests that the antitumor activity of platinum complexes stems from their ability to form with DNA various types of covalent adducts [5,6]; as a result, research on DNA modifications by these drugs and their cellular processing has predominated. The resistance of tumor cells to platinum drugs has been attributed to various processes, such as reduced platinum accumulation, intracellular inactivation, block an induction of apoptosis, an increased repair of platinum-DNA adducts or a combination thereof [4-5]. In order to overcome these obstacles, many different transition metal complexes have been synthesized and investigated [7]. In recent years, ruthenium-based molecules have emerged as promising antitumor agents. Certain ruthenium complexes possess unique biochemical features allowing them to accumulate preferentially in neoplastic tissues and/or to convert to their active state under specific pathophysiological conditions. In this respect, ruthenium (and osmium) compounds with their different mechanisms of action are promising candidates as anticancer drugs [8-10]. In the recent past, the drug development has mainly relied on organic chemistry. This can be attributed to the lack of knowledge on the mechanisms and binding modes of metal-based drugs with biomolecular targets other than DNA. Traditionally, it was believed that the majority of metal-based drugs targeted DNA, but considerable evidence has accumulated that metal-based drugs are also able to bind to protein targets. Recent trends involve metal complexes that inhibit protein and lipid kinases, matrix

metalloproteases, telomerases, topoisomerases, glutathione-S-transferases, and histone deacetylases [11-13]. In the present study, we investigate topoisomerases as targets for metal-based drugs. Topoisomerases are key nuclear enzymes that control the topological states of DNA by generating transient strand breakage. They are, therefore, involved in key processes such as DNA replication and transcription, as well as chromosome formation, enrichment, and separation (**Fig. 1**).

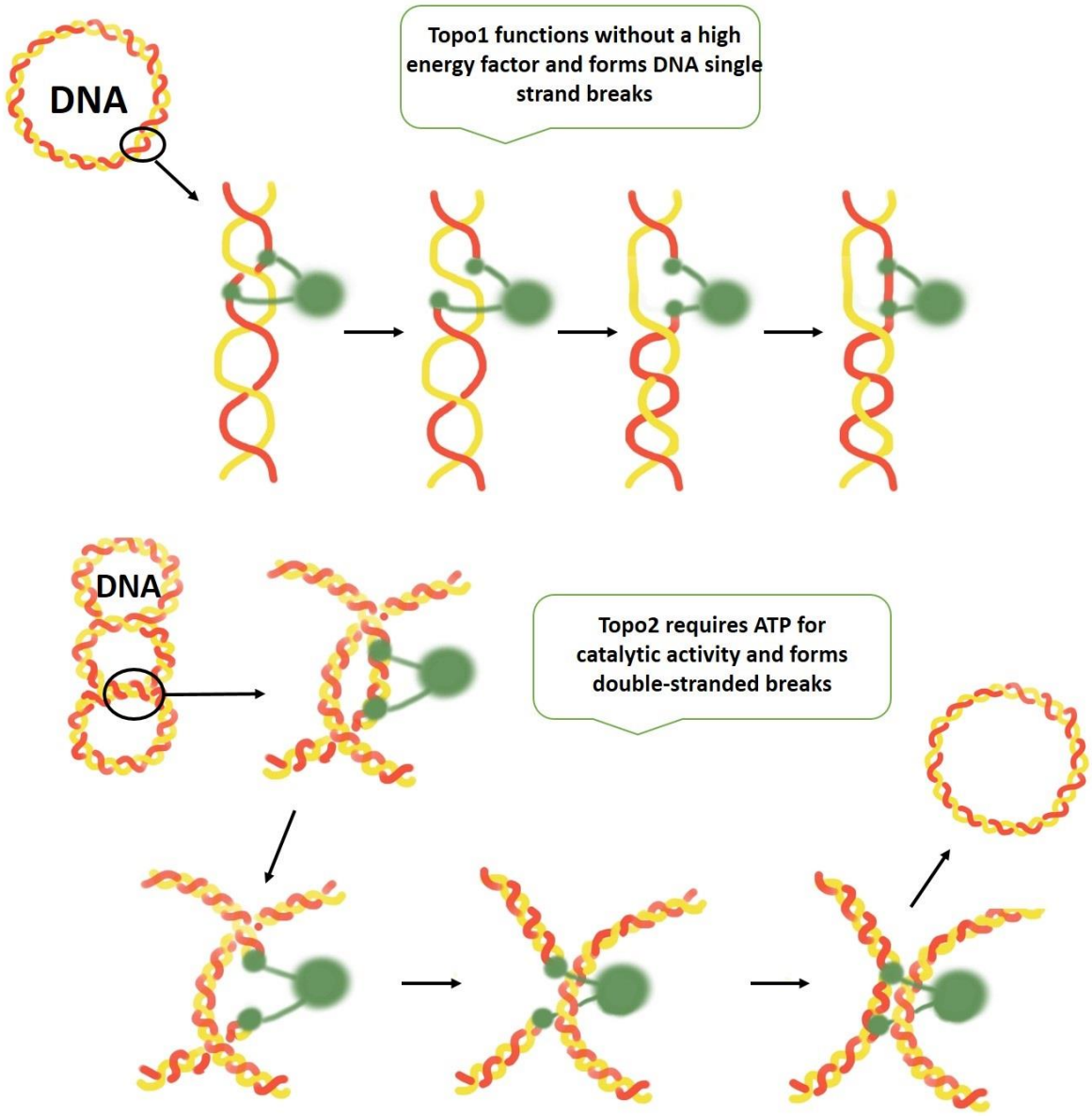

Fig. 1. Catalytic activity of topo1 and topo2 enzymes – topo1 cuts one strand of the DNA double helix, while topo2 cuts both strands requiring ATP (adenosine triphosphate) and is able to religate strands of the end of each cycle (designed based on the publication from John Nitiss [19]).

Mammalian cells encode two type II isozymes – topoisomerase IIα (topo2α) and β (topo2β), which have highly identical N-terminal ATPase and central core domains.

However, they differ in their C-termini as well as in their expression patterns and cannot compensate for each other *in vivo*, i.e., if one of the forms is downregulated the other one cannot replace its functions equivalently. Moreover, the α isoform is produced primarily in the late S-phase, it remains associated with chromosomes at mitosis and plays a dominant role in this context, which makes it apparently more sensitive to pharmaceutical agents [14]. Well-known topo1-targeting drugs include camptothecin and its derivatives, while topo2-targeting drugs include doxorubicin, etoposide, and mitoxantrone. There are different types of topo2-targeting drugs, namely inhibitors and poisons. Topo2 poisons inhibit the enzyme's activity by stabilization of the enzyme–DNA covalent complex, which leads to the accumulation of DNA double-strand breaks. In contrast, topo2 catalytic inhibitors may stop the cycle by preventing binding of the enzyme to DNA, by blocking the ATP-binding site of the enzyme or by inhibiting the cleavage reaction. This kind of topo2-targeting drugs have become established in clinical practice – many studies have shown the efficacy of irinotecan (CPT-11, a derivative of camptothecin), which is approved by the FDA for use in colorectal cancer [15-19].

The topo2α enzyme has been shown to be a proliferation marker associated with tumor grade and cell proliferation index [20]. The prognostic effect of topo2α seems different among different subtypes of breast cancer but, in general, patients with high topo2α expression showed a significantly higher rate of distant metastasis and shorter distant metastasis free survival compared with patients with low topo2α expression [20]. Cancer cell lines expressing different levels of the enzyme would be a powerful tool in the investigation of topo2 behavior and responsiveness to treatment. Our understanding of the molecular biology of cancer cell progression, invasion, metastasis and failure to undergo cell death have led to a new generation of systemic anticancer therapies, which target specific cellular defects in malignant cells. Unlike classic cytotoxic chemotherapy, this new generation of drugs tends to work in tumors with specific genetic defects, allowing personalized treatment. Therefore, topo2 targeting is an effective anticancer strategy [21].

Here we investigate the cytotoxicity of several thiomaltol-based metal complexes. By means of biological assays complemented with computational modeling we show that topo2 is involved in the anticancer mode of action of some of these complexes and we unveil the interaction mechanism between the drugs and the enzyme. Given that

topoisomerases are among the most well-established targets for anticancer therapy, this opens up new avenues for the development of this compound class.

Materials and methods

Compounds

Thiomaltol complexes with ruthenium (Ru^{II}), osmium (Os^{II}), rhodium (Rh^{III}), and iridium (Ir^{III}), bearing either 1-methylimidazole or chloride as leaving group (see **Fig. 2**), were synthesized and characterized according to procedures published elsewhere [22].

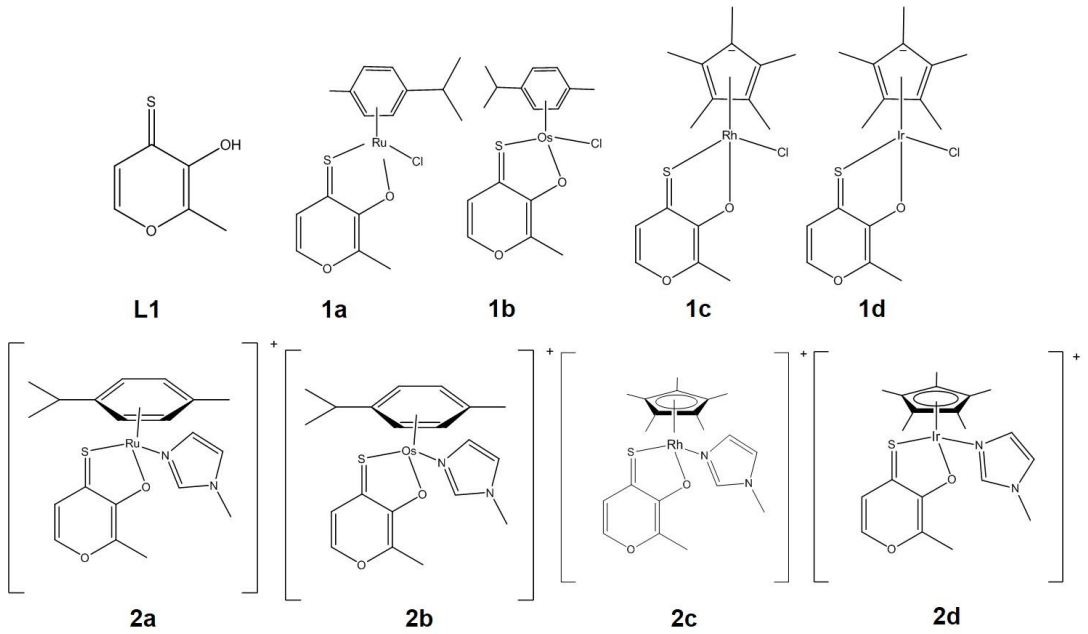

Fig. 2. Structural formulas of tested compounds and ligand.

Cell lines and culture conditions

SK-BR-3, T47D and MDA-MB468 (mammary carcinoma human cells) were kindly provided by Evelyn Dittrich (Department of Medicine I, Medical University of Vienna, Austria). All cell culture media and supplements were purchased from Sigma-Aldrich and plastic ware from Starlab. SK-BR-3 and SW480 cells were grown in 75 cm^2 culture flasks in complete medium (i.e., Minimum Essential Medium supplemented with 10% heat-inactivated fetal bovine serum, 1 mM sodium pyruvate, 4 mM L-glutamine and 1% non-essential amino acids from 100× ready-to-use stock), while T47D and MDA-MB468 cells in RPMI 1640 medium (supplemented with 10% heat-inactivated fetal bovine serum and 4 mM L-glutamine) as adherent monolayer cultures. After successful transfection the cell line T47D-kn was maintained in RPMI 1640 medium with 1.5% of antibiotic (blastidin) according to the manufacturer protocol (Invitrogen by life technologies). Cultures were grown at 37 °C under a humidified atmosphere containing 5% CO_2 and 95% air.

Antiproliferative activity assay (MTT)

Antiproliferative activity *in vitro* was determined by the colorimetric MTT assay (MTT = 3-(4,5-dimethyl-2-thiazolyl)-2,5-diphenyl-2H-tetrazolium bromide). For this purpose, cells were harvested from culture flasks by use of trypsin and seeded in appropriative medium (100 µL/well) into 96-well plates in densities of 5×10^3 (SkBr3), 8×10^3 (T47D) and 2×10^3 (MDA-MB468) as well as 24×10^3 (T47D-kn) cells per well (growth kinetic tests were performed to estimate and confirm the required number of cells for further experiments). Cells were allowed for 24 h to settle and resume proliferation. Test compounds were dissolved in DMSO first, diluted in appropriate medium and instantly added to the plates (100 µL/well), where the DMSO content did not exceed 0.5 %. After exposure for 96 h, the medium was removed and replaced with 100 µL/well of a 1:7 MTT/RPMI 1640 solution (MTT solution, 5 mg/mL of MTT reagent in phosphate-buffered saline; RPMI 1640 medium) and incubated for 4 h at 37 °C. Subsequently, the MTT/RPMI 1640 solution was removed, and the formazan product formed by viable cells was dissolved in DMSO (150 µL/well). Optical densities were measured with a microplate reader (BioTek ELx808) at 550 nm (and a reference wavelength of 690 nm) to yield relative quantities of viable cells as percentages of untreated controls, and 50% inhibitory concentrations (IC50) were calculated by interpolation. Evaluation is based on at least three independent experiments with triplicates for each concentration level.

Flow cytometric detection of apoptotic/necrotic cells

Induction of cell death was analyzed by flow cytometry using FITC-conjugated annexin V (BioVision, USA) and propidium iodide (PI, Fluka) double staining. SkBr3, T47D, MDA-MB468 and SW480 cells were seeded into 12-well plates in a density of $5–13 \times 10^4$ cells per well in complete medium in 12-well plates and allowed to settle for 24 h. The cells were exposed to test compounds in different concentrations for 48 h at 37 °C. Merbarone (Sigma-Aldrich Austria) was used as a positive control at a concentration of 160 µM. After incubation, cells were gently trypsinized, washed with PBS, and suspended with FITC-conjugated annexin V (0.25 µg/mL) and PI (1 µg/mL) in binding buffer (10 mM HEPES/NaOH pH 7.4, 140 mM NaCl, 2.5 mM $CaCl_2$) at 37 °C for 15 min. Stained cells were analysed with a Guava

8HT EasyCyte flow cytometer (Millipore) using InCyte software and analyzed by FlowJo software. Results are based on three independent experiments.

Plasmid DNA interaction studies

pUC19 DNA (2686 bp) plasmid was purchased from Fermentas Life Sciences. 400 ng of pUC19 plasmid were incubated with 10 μM of the test compounds in 0.1× Tris-EDTA (TE) buffer for different time intervals (30 min up to 8 h) at 37 °C. Electrophoresis was performed in agarose (from Sigma-Aldrich) gel 1 % w/v in 1× Tris-borate-EDTA (TBE) buffer for 90 min at 80 V. Gels were stained with ethidium bromide (EtBr) in 1× TBE (0.75 μg/ml) for 20 min. Images were taken with the multi-imaging detection system Fusion SL (Vilber Lourmat). Results are based on two independent experiments.

DNA damage detection assay (γH2AX)

Evaluation of a formation of γ-H2AX in response to DNA double stranded breaks was performed with the Flow Cellect™ Histone H2A.X Phosphorylation Assay Kit (Millipore). SkBr3, T47D, MDA-MB468 and SW480 cells were seeded into 6-well plates in a density of 15–25 × 10^4 cells per well in complete medium in 12-well plates and allowed to settle for 24 h. The cells were exposed to test compounds at different concentrations for 48 h at 37 °C. Etoposide (Sigma-Aldrich) was used as a positive control at a concentration of 100 μM. All following steps for DNA damage evaluation were performed according to the manufacturer's protocol. Numbers of cells and their viability state were determined with a Guava 8HT EasyCyte flow cytometer (Millipore) using ViaCount software. Results are based on three independent experiments.

Regulation of topo2α expression level by RNAi

Single-stranded oligonucleotides specific for the topo2α gene were purchased from Invitrogen by life technologies and the regulation of topo2α expression level by RNAi was performed according to manufacturer's protocol. Details of the single-stranded oligos specific for the topo2α gene: [Homo sapiens] topoisomerase (DNA) II alpha 170 kDa, TOP2A – TOP2A BLOCK-IT™ miR RNAi Select Hmi417628; Hmi417629; Hmi417630; Hmi417631. Double-stranded oligonucleotides were generated and checked for their integrity, then ligation reaction and transformation of

One Shot TOP10 *E. coli* was performed and transformants analysed. Target plasmids were extracted and the rapid BP/LR recombination reaction performed, the expression clones linearized, One Shot Stbl3 *E. coli* transformed and transformants analysed. Plasmid DNA was isolated, the sequence confirmed and transfection reaction in target cells SK-BR-3, T47D and MDA-MB468 performed. The gene knockdown was performed as described in the manufacturer's protocols and illustrated in **Fig. 3**.

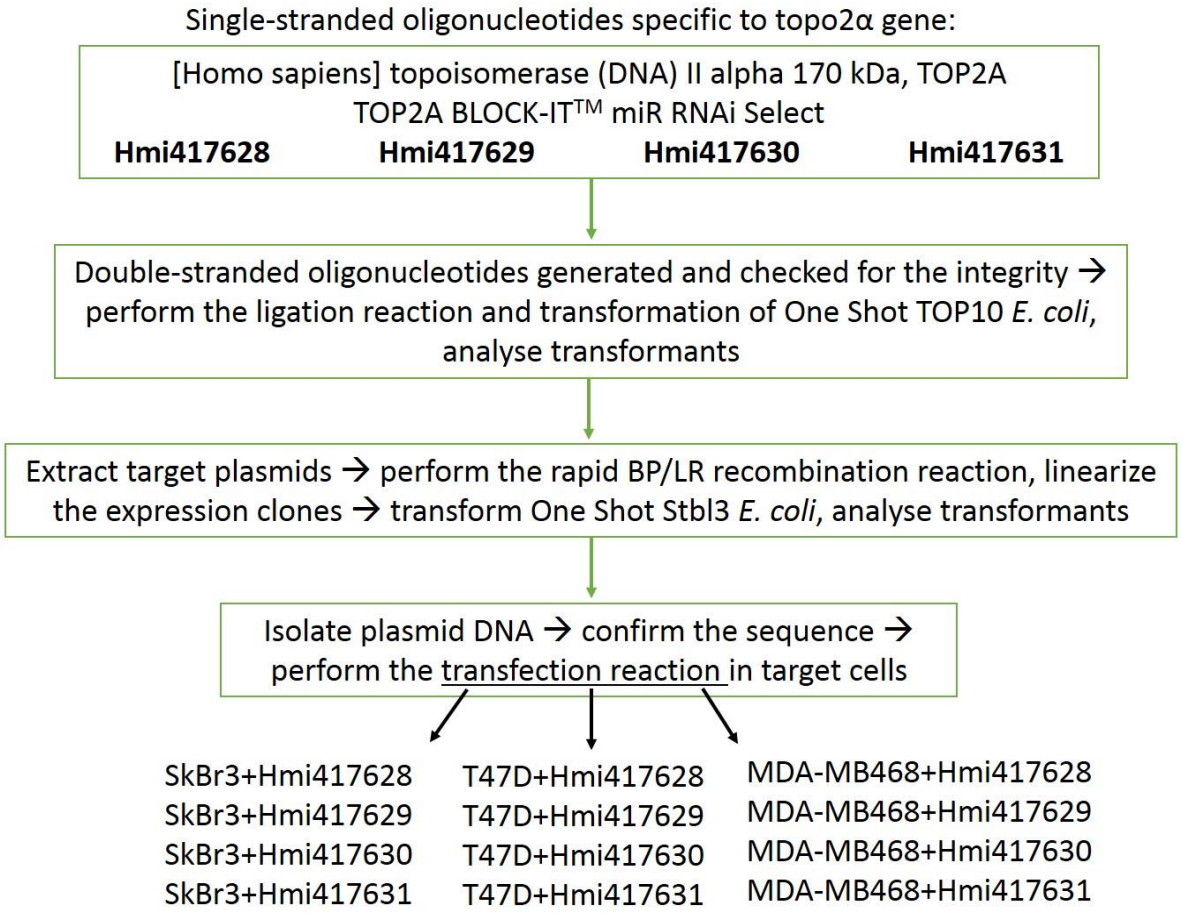

Fig. 3. Scheme of generation of a cell line with downregulated topo2α expression.

In the next few days topo2α knock-down versions of SK-BR-3 and MDA-MB468 cells stopped division or died. T47D cells with sequences Hmi417628 (T47D-kn628) and Hmi417630 (T47D-kn630) were checked for the verification of topo2α knock-down via Western blotting.

Western blotting

The visualization of topo2α protein level in SW480, SK-BR-3, T47D and MDA-MB468 cells as well as the verification of topo2α knock-down in T47D-kn628/630 cells was performed by Western blotting. Cells were seeded in densities of 1.5–2 × 10^5 cells per well into 6-well plates (Starlab) and allowed to resume proliferation for 24 h. After the cells were washed with PBS and lysed by adding 100 µL per well of RIPA lysis buffer (150 mM sodium chloride, 1.0% Triton X-100, 0.5% sodium deoxycholate, 0.1% SDS (sodium dodecyl sulphate), 50 mM Tris, pH 8.0). Cells were carefully scratched and sonicated for 10 sec to shear DNA and reduce sample viscosity. The protein content of lysates was measured with the Pierce Micro BCA Protein Assay (Thermo Scientific). The appropriate volume of cell lysates (20 µg protein content per gel pocket) was mixed with 6´ loading buffer (12% w/v SDS, 30% 2-mercaptoethanol, 60% glycerol, 0.012% bromophenol blue, 0.375 M Tris HCL, pH 6.8) and heated to 95° C for 5 min. The proteins were separated by 8% SDS-polyacrylamide gel electrophoresis and subsequently transferred onto nitrocellulose membranes (Millipore) by using a semi-dry blotting apparatus (Biorad). The membranes were blocked with blocking buffer (1´ TBS, 0.1% Tween-20 with 5% BSA) and immunoblotted with the relevant primary topo2α rabbit antibody diluted in TBS/T buffer in a ratio of 1:1000 (Cell Signaling Technology). Primary antibodies were detected by using anti-rabbit IgG HRP-linked antibody diluted in TBS/T buffer in a ratio of 1:3000 (Cell Signaling Technology) and visualized with the chemiluminescence detection system Fusion SL (Vilber Lourmat) using SuperSignal West Pico Chemiluminescent Substrate (Thermo Scientific). Afterwards the membranes were cleaned by stripping buffer (15 g glycine, 1 g SDS, 10 mL Tween 20, pH 2.2) and immunoblotted with the β-actin rabbit antibody diluted in TBS/T buffer in a ratio of 1:3000 (Cell Signaling Technology) to check the quality of gel loading. Results are based on two independent experiments.

Computational details of binding of thiomaltol complexes to topo2α

Since all metal complexes investigated here are positively charged (the chloride ones after hydrolysis), they may potentially bind to topo2α into a pocket with large polarity, as it is the case of the DNA-binding domain of the protein. In order to explore this possibility, the binding affinity between the complexes **1a** and **2a** (see **Fig. 2**) and the DNA-binding domain of topo2α (PDB code 3L4K) [22] has been

theoretically investigated by means of Monte Carlo (MC) and Molecular Dynamics (MD) simulations following the protocol explained below.

First, the DNA helix that is present in the crystal structure was manually removed. Then, the protein was protonated and solvated by a periodic truncated octahedral box of water molecules extended to a distance of 12 Å from any solute atom by the leap module of AmberTools15 [24]. This results in a solvated protein with one positive charge that was neutralised with one chloride ion. The solvated protein was minimized for 20000 steps, where the first 10000 steps were driven by a steepest-descent algorithm, and the last 10000 steps by a conjugated-gradient algorithm. The system was then heated in the canonical ensemble (NVT ensemble) from 0 to 300 K by a classical MD simulation for 1 ns using a time step of 2 fs. During the heating process the motion of the protein was restrained with a harmonic force constant of 10.0 kcal/(mol$Å^2$). Then, a classical MD simulation was run in the NVT ensemble at 300 K for 1 ns without applying any restrains to the motion of the protein. After heating, the density of the solvent and the structure of the protein was equilibrated in the isothermal–isobaric ensemble (NPT) during a 50 ns simulation with a time step of 2 fs. The Berendsen barostat with a pressure relaxation time of 2 ps was used to maintain a pressure of 1 bar. The Langevin thermostat with a collision frequency gamma of 1.0 ps^{-1} was used in both heating and equilibration steps to control the temperature. Moreover, the bond distances involving H atoms were restrained by the SHAKE algorithm [25]. Along the whole protocol the Coulomb and van der Waals interactions were truncated at 10 Å. The Coulomb interactions were evaluated by the particle mesh Ewald method [26] using a grid spacing of 1 Å in each direction for the charge grid, in which the reciprocal sums are computed by a fourth-order interpolation, and a direct sum tolerance of 10^{-5}. The whole system, i.e., the protein, water molecules, and chloride ion were described by a force field [27-29]. All these steps were run by the Amber14 package [24].

The last snapshot from the previous classical MD simulations, for which the solvated protein is well equilibrated, was selected and the water molecules and the chloride ion were removed. Then, the different binding pockets of the equilibrated protein have been explored by a classical Monte Carlo (MC) simulation of 4000 steps using the Protein Energy Landscape Exploration (PELE) algorithm [30]. Since accurate force fields for Ru-based complexes are not available in the literature, the binding pockets of the protein have been explored by the thiomaltol ligand, which is present in all the

metal complexes investigated here. Therefore, it was assumed that the binding mode of the metal complexes is the same as that of thiomaltol. Due to its small size and rigidity, the thiomaltol ligand was treated as a rigid body. The OPLS-AA force field [31] was used to describe topoisomerase and thiomaltol, while the aqueous solvent was modeled by the implicit surface-general Born continuum model [32]. The default values for the MC parameters implemented in the PELE algorithm [30] were used. The calculation of the binding free energy between thiomaltol and the protein for each of the 4000 MC steps allowed the identification of two favorable binding pockets (see below). These pockets will be named here pocket 1 and pocket 2, with the first one being the DNA-binding pocket.

In the next step, the thiomaltol ligand bound to the two favorable binding pockets has been replaced by the Ru complexes **1a** and **2a** such that the thiomaltol ligands of the complexes are aligned with the isolated thiomaltol ligand inside the pockets to keep the same binding pose. This results in the generation of four different systems: complex-**1a**/pocket-1, complex-**1a**/pocket-2, complex-**2a**/pocket-1, and complex-**2a**/pocket-2. The metal-complex/topoisomerase systems were neutralised by adding two chloride ions and solvated by a periodic truncated octahedral box of water molecules extended to a distance of 12 Å from any solute atom by the leap module of AmberTools15 [24]. Then, the system was classically minimised for 5000 steepest-descent and 5000 subsequent conjugated-gradient steps. After minimisation, a classical MD simulation in the NVT ensemble was run for 20 ps with a time step of 1 fs to heat the system up to 300 K. Afterwards, a simulation in the NPT ensemble was run for 1 ns to equilibrate the density of the solvent and to accommodate the metal complexes inside the binding pockets of the protein. As mentioned above, accurate force fields are not available in the literature for Ru complexes, especially when metal/π interactions are important, as it is the case here (see **Fig. 2**). Therefore, the internal coordinates of the complex were frozen during the classical simulations. This means that intramolecular parameters describing the internal motion of the Ru species are not necessary. However, point charges and Lennard-Jones parameters are still needed to describe the non-bonded interactions between the Ru complexes and the solvated protein environment. The Lennard-Jones parameters for the Ru atom were taken from an MM3 force field developed for Ru(II)-polypyridyl complexes [33], while the Lennard-Jones parameters for the remaining metal-complex atoms were taken from the General Amber Force Field [34]. The charges were derived by, first, optimising

the geometries of the complexes **1a** and **2a** quantum mechanically by density-functional theory (DFT) using the Gaussian09 program [35]. Specifically, the B3LYP functional [36-39] with the D3BJ dispersion correction [40] and the LanL2DZ effective-core potential [41] for Ru and the 6-31G* basis set [42] for the remaining atoms were employed. Then, the Mulliken charges were computed for the optimised geometries at the same level of theory.

In the last step of our protocol, the last snapshot of each of the four previous classical MD simulations (one for each complex/pocket combination) were taken as initial conditions for quantum mechanics/molecular mechanics (QM/MM) MD simulations in the NPT ensemble for 10 ps with a time step of 2 fs. The same thermostat and barostat used in the classical simulations were used here. The metal complexes **1a** and **2a** were described quantum mechanically by the same density functional, basis set, and effective-core potential specified above using TeraChem1.9 [43-44] through the interface to external QM programs implemented in Amber14 [24] and run at GPUs Dispersion corrections were considered by the D3 parameterizations of Grimme and coworkers [45]. The protein, water molecules, and chloride ions were treated by the force field mentioned above. The interaction between the QM and MM region layers was computed by an electrostatic embedding [46]. The Coulomb and van der Waals interactions were truncated at 8 Å and a real-space cutoff was used to compute the long-range QM-QM and QM-MM electrostatic interactions. These simulations allow the relaxation of the structure of the Ru complexes at QM level and, thus, provide a better description of the vibrational motion of the complexes and their interaction with the binding pockets of topoisomerase and with the solvent. From the QM/MM MD simulations 2000 snapshots were printed for analysis. The number of contacts between the Ru complexes and the protein and the number of water molecules in the solvation shells of the Ru complexes (see below) were obtained by the CPPTRAJ module [47] implemented in AmberTools15 [24]. The visualization of the MC and MD simulations and the graphical representations of the systems were carried out by the Visual Molecular Dynamics (VMD) program [48].

Results and discussion

Recently published findings [22] on the anticancer properties of novel Ru^{II}, Os^{II}, Rh^{III}, and Ir^{III} thiomaltol complexes showed that they act as topo2α catalytic inhibitors and have a significantly higher enzyme inhibitory capacity compared to the free ligand. In cell cycle studies the Ru^{II} and Ir^{II} methylimidazole-substituted complexes caused the highest S-phase accumulation (up to 43% and 45%, respectively), which was consistent with enzyme inhibition. Previously acquired data implied that the introduction of 1-methylimidazole as a leaving group substantially increased the stability in aqueous solution. It was suggested that this modification may allow accumulation of the intact complexes and controlled activation at the lower pH values within tumor tissues. The cytotoxicity of thiomaltol ligand **L1** and respective complexes **1a–d** and **2a-d** in A549, CH1/PA-1 and SW480 cells has already been reported [22]; however, new data for SK-BR-3, T47D and MDA-MB468 (mammary carcinoma cells) were acquired within this work. In general, all complexes showed IC_{50} values in the low micromolar to high nanomolar range (**Tab. 1**). Remarkably, Os^{II} complexes are less active than the other complexes. The difference in the monodentate leaving group has only a marginal impact on the activity of the Os^{II} complexes, as the chlorido complex **1b** is only about 1.5 times more active than the 1-methylimidazole analogue **2b** in all tested cell lines. In contrast, a significant impact of the ligand on the cytotoxicity was observed for complexes **1c-d** as well as for **2c-d**; specifically the Rh^{III} and Ir^{III} complexes **2c-d** were more active than their chlorido counterparts by factors of 2–6, depending on the cell line. The P-gp expressing cell line SW480 is mostly as sensitive to all the complexes as the broadly chemosensitive CH1/PA-1 cell line, whereas IC_{50} values in breast carcinoma cell lines (SK-BR-3, T47D and MDA-MB468) expressing different levels of topo2 enzyme are in a similar range with a few exceptions – Os^{II} complexes turned out to be 10-fold less active and Ir^{III} complex **1d** is about 2-fold less active than in untransfected cell lines. In this respect, Ru^{II} analogs are in an intermediate position – they are more active than Os^{II} complexes but almost as active as the Ir^{III}- or Rh^{III}-based complexes with some deviations. In addition, the two Ru^{II} complexes differ from each other, with up to 4 times more activity for complex **2a** with respect to **1a**.

Tab. 1. Inhibition of cancer cell growth by tested substances in six human cancer cell lines; 50% inhibitory concentrations (means ± standard deviations), obtained by the MTT assay (exposure time: 96 h).

IC50 value ± SD							
M	Complex	A549	CH1/PA-1	SW480	SK-BR-3	T47D	MDA-MB468
Ru^{II}	**1a**	12 ± 4	3.3 ± 0.5	11 ± 1	16 ± 4	6.3 ± 1.7	7.2 ± 0.9
Os^{II}	**1b**	4.1 ± 0.3	2.0 ± 0.2	2.0 ± 0.2	12 ± 3	13 ± 2	10 ± 1
Rh^{III}	**1c**	5.9 ± 0.8	1.0 ± 0.1	1.0 ± 0.1	2.9 ± 0.8	1.8 ± 0.3	1.4 ± 0.2
Ir^{III}	**1d**	5.8 ± 1.7	0.57 ± 0.03	0.73 ± 0.10	1.8 ± 0.6	1.3 ± 0.1	1.4 ± 0.1
Ru^{II}	**2a**	7.1 ± 1.6	2.6 ± 0.5	3.0 ± 0.2	11 ± 4	4.4 ± 0.6	5.4 ± 0.7
Os^{II}	**2b**	6.6 ± 0.4	3.0 ± 0.4	3.4 ± 0.7	30 ± 7	21 ± 4	37 ± 5
Rh^{III}	**2c**	2.6 ± 0.6	0.86 ± 0.17	0.48 ± 0.03	1.1 ± 0.3	1.3 ± 0.1	0.53 ± 0.02
Ir^{III}	**2d**	3.4 ± 0.8	0.63 ± 0.07	0.67 ± 0.04	1.6 ± 0.4	1.3 ± 0.6	0.70 ± 0.06
Lig	**L1**	1.3 ± 0.8	0.52 ± 0.04	0.55 ± 0.31	0.86 ± 0.05	0.46 ± 0.12	0.31 ± 0.04
–	Merbarone	n.d.	9.2 ± 1.3	29 ± 3	22 ± 5	18 ± 2	17 ± 1
–	Etoposide	n.d.	0.043 ± 0.010	0.20 ± 0.02	0.51 ± 0.06	0.59 ± 0.20	0.40 ± 0.08

Taking into account that we consider the topo2 to be a target of these drugs, we had to make sure that there is no direct interaction with DNA. The ability to alter the secondary structure of DNA in cell-free experiments was studied by the use of an electrophoretic double-stranded DNA plasmid assay (**Fig. S1**).

In general, these metal-based complexes and the corresponding ligand **L1** did not show any impact on DNA mobility and its secondary structure; however, we saw an unusual behavior of plasmid DNA in the presence of some complexes – either the intensity of open circular (OC) band increased over the time, or additional bands between OC and supercoiled (SC) bands appeared. In order to make sure that this

unusual pattern is not a result of the DNA breakage, we performed an H2AX assay that allows monitoring and accurately measuring phospho-specific histone H2AX activation in a population of cells. Histone H2AX locates downstream of the DNA damage kinase signaling cascade, and phosphorylation of this histone at serine 139 is an important indicator of DNA damage. As the level of DNA damage increases, the level of phospho-histone H2AX (also known as γH2AX) increases, accumulating at the sites of DNA damage. This accumulation is often used to indicate the level of DNA damage present within the cell [49-50]. The evaluation of a formation of γ-H2AX in response to DNA double-strand breaks in SW480, SK-BR-3, T47D and MDA-MB468 cell lines after 48 h of exposure to the studied compounds, showed no significant increase in DNA damage (**Fig. S2**). In general, Rh^{III} complexes **1c** and **2c** were most harmful for DNA and generated double-strand breaks in up to 33% of MDA-MB468 and up to 52% of SW480 cells (the latter cell line was the second most chemosensitive towards the tested substances over all cancer cell lines used). Ru^{II} complexes **1a** and **2a** similarly generated the maximum of DNA damage in up to 13% of T47D cells. Probably due to the expression level of topo2α, T47D cells were relatively sensitive to all tested substances (9–30%) except ligand **L1** (DNA damage in 4% of cell populations). For comparison, DNA double-strand breaks were present in the negative control with 1–2% and in positive control (100 μM of etoposide) with 41–86%. It should be mentioned that in a previous publication the potential of these complexes to raise cellular ROS levels had been investigated. One of the well-known damaging effects of ROS is DNA damage, including double-stand breaks [51]. The obtained data indicated a slight increase in ROS levels for Rh^{III} complex **2c** by a factor 2.7, which may be a reason for the higher percentage of double-strand breaks in cells treated with this complex. In order to substantiate this funding, we investigated the ability of the Ru and Rh compounds to activate programmed cell death. Apoptosis/necrosis induction in SW480, SK-BR-3, T47D and MDA-MB468 cells after 48 h of exposure to the studied compounds and ligand, measured by flow cytometry using annexin V-FITC/propidium iodide double staining, demonstrated the ability of the complexes to induce cell death (**Fig. S3**). Ru^{II} complexes **1a** and **2a** effectively induced apoptosis in SW480 and SK-BR-3 cells with 40–50 and 70–80%, respectively. Rh^{III} complexes **1c** and **2c** induced programmed cell death predominantly in SK-BR-3 cells with 70 and 88%, respectively. Surprisingly, ligand **L1** was able to induce apoptosis in SK-BR-3 and MDA-MB468 cells with 51 and

66%, respectively. For comparison, the positive control (160 μM of merbarone, as well-known topo2α catalytic inhibitor) induced apoptosis only with up to 33%. The percentage of necrosis measured by this assay on average was no more than 12%. The fact that the introduction of an imidazole moiety instead of the chlorido-ligand in complex **2a** increases the stability of complex in the presence of biomolecules and the solubility corresponds to the observation that this complex is more active than its analog **1a**. These two complexes also displayed different capacities of topo2α inhibition (as published previously) – **2a** complex was able to inhibit the enzyme activity at a concentration 4 times lower than the one required for its analog **1a** (2.5 μM vs 10 μM). Moreover, S-phase accumulation in the cell cycle studies (up to 45%) was consistent with enzyme inhibition experiments, and the capacity to induce apoptosis was 1.7-fold higher for **2a** complex than for **1a** [22]. Thus, we can conclude that rhodium complexes induce ROS activation that leads to DNA damage and apoptosis, while ruthenium complexes induce cell death via the enzyme inhibition.

We looked further and established methods to characterize anticancer properties of metal-based compounds with respect to the role of topo2α inhibition. One of the ideas that attracted our attention was that topo2α expression levels affect the cell response to drug treatment. Previous studies suggested that we may expect a different cell response to treatment in case of up/downregulation of topo2α expression levels. Some experiments that have studied the effect of reducing the level of expression have shown that this can lead to either drug resistance or a higher susceptibility to drugs [51-54]. In order to investigate how different levels of topo2α expression may affect the cellular response to the treatment with the compounds studied here, we not just compared the cell lines with intrinsically different levels of topo2α expression but induced a downregulation of the enzyme expression by RNA interference (RNAi). RNAi is a biological process in which RNA molecules inhibit gene expression, typically by causing the destruction of specific mRNA molecules. This system is used to investigate the functions of different genes [55]. We used BLOCK-iT Expression Vector Kits that combine the advantages of traditional RNAi vectors – a stable expression and the ability to use viral delivery with capabilities for tissue-specific expression and multiple target knockdown from the same transcript. The pcDNA vectors of this kit are designed to express artificial miRNAs which are engineered to have 100% homology to the target sequence and will result in target cleavage.

Since the complete inhibition of topo2α production in the cell leads to division failure and cell death [56-57], we established several combinations of cell lines and miRNA sequences in order to reduce the production of the protein but not to inhibit it completely – the topo2α gene sequence was divided into 4 short sequences to produce RNA sequences complementary to different parts of the gene (see **Fig. 3**). Thus, we avoided complete topo2α inhibition of the protein expression and cell death. Still, topo2α downregulated variants of SK-BR-3 and MDA-MB468 cells stopped dividing or died on the following days. Therefore, only T47D-kn628 and T47D-kn630 cells with topo2α downregulation confirmed via Western blotting (**Fig. 4**) were used for further experiments.

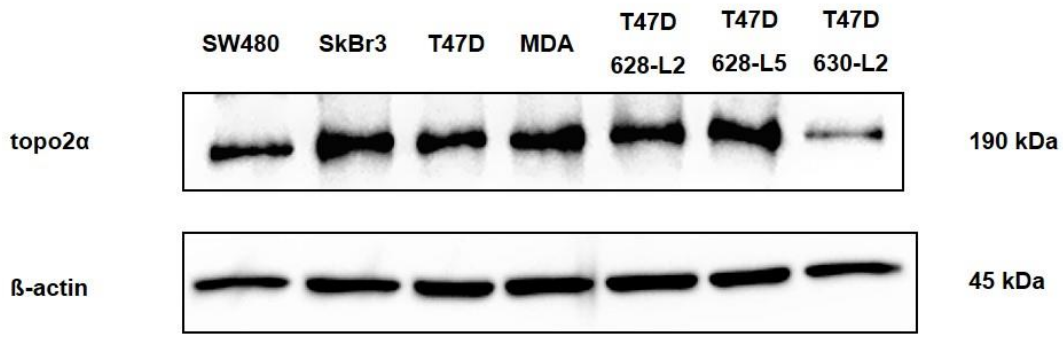

Fig. 4. Western blotting visualization of topo2α protein level in SW480, SK-BR-3, T47D and MDA-MB468 standard cell lines as well as in the topo2α downregulated T47D cell lines (primers Hmi417628 and Hmi417630 – T47D-kn628 and T47D-kn630); β-actin was used as a loading control.

The effect of RNAi was verified at the protein level by Western blotting and these experiments clearly showed the successful downregulation of topo2α expression in one of the three variants – T47D-kn630 cells. Then, the antiproliferative activity of the metal compounds was evaluated in the cell line T47D and its topo2α downregulated variant in order to investigate the possible role of the enzyme in the drug treatment (**Tab. 2**).

Tab. 2. Inhibition of cancer cell growth by tested substances in the human cancer cell line T47D and the down-knocked variant of this cell line T47D-kn630; 50% inhibitory concentrations (means ± standard deviations), obtained by the MTT assay (exposure time: 96 h).

IC50 value ± SD			
M	Complex	T47D	T47D-kn630
Ru^{II}	**1a**	6.3 ± 1.7	3.8 ± 0.8
Ru^{II}	**2a**	4.4 ± 0.6	10 ± 3
Rh^{III}	**1c**	1.8 ± 0.3	1.9 ± 0.3
Rh^{III}	**2c**	1.3 ± 0.1	0.80 ± 0.60
Lig	**L1**	0.46 ± 0.12	1.2 ± 0.5
–	Merbarone	18 ± 2	22 ± 3
–	Etoposide	0.59 ± 0.20	1.2 ± 0.3

The cell line with downregulated topo2α level of expression T47D-kn630 turned out to be 2.3-fold more resistant to complex **2a** and 2.4-fold more resistant to ligand **L1** but 1.6-fold and 1.7-fold more sensitive to complex **2c** and **1a**, respectively. The response to the treatment with complex **1c** remained similar to the behavior of the parental cell line T47D. For comparison, the down-knocked cell line is 2-fold more resistant to the topo2α poison etoposide, but only (a probably irrelevant) 1.2 times more resistant in response to merbarone.

Previously, the sensitivity to different anticancer drugs (amsacrine, doxorubicin, mitoxantrone and etoposide) was studied in a panel of breast cancer cell lines by Houlbrook and co-workers [14]. When the cells were ranked according to their sensitivity to one of the drugs, it was found that the ranking for other compounds did not follow the same pattern (with discrepancies from 2- up 6-times). Later experiments of Burgess and co-workers [58] identified the topo2α expression level as the major determinant of response to the topoisomerase II poison doxorubicin and showed that suppression of the enzyme produces resistance to doxorubicin *in vitro* and *in vivo*. They also mentioned the interesting observation that the effects of topo2α knockdown were specific to topoisomerase II poisons: shTop2A caused resistance to etoposide. A publication by Soubeyrand and co-workers [59] reported that topoII siRNA ablation showed that etoposide cytotoxicity correlates with the inability of cells to

correct topo2α-initiated DNA damage – these results linked the lethality of etoposide to the generation of persistent topo2α-dependent DNA defects within topologically open chromatin domains. Logically, topo2α knockdown would be expected to confer resistance to a poison's cytotoxicity, as decreased topoisomerase expression would produce fewer of the lethal DNA double-strand breaks that result from cleavage complexes. In case of catalytic inhibitors, it is not so easy to make any assumptions due to a limited number of published data. However, based on the IC_{50} values of **Tab. 2**, we can confirm that the sensitivity of the cells to the different drugs depends on the level of enzyme expression. Therefore, it is very likely that the topo2α enzyme is the target biomolecule of many of the inhibitors investigated here. However, the lack of a clear trend suggests that the interaction of metal complexes with topo2α is not the only cytotoxic mechanism and/or that the protein might play different roles in the mode of action of the drugs.

Finally, we investigated the interaction of topo2α and the metal-based complexes by performing theoretical simulations. The first step of our simulations was to investigate the possible binding pockets of the DNA-binding domain of type II topoisomerase, where the thiomaltol ligand can be non-covalently bonded, by means of classical MC simulations. The calculation of the binding free energy along the MC simulation identified favorable binding sites. **Fig. 5a** shows the binding sites of thiomaltol (represented by the red surface) on the surface of the protein for which the (absolute) binding free energy is larger than 15 kcal/mol. As can be seen, two main binding sites are revealed, namely pocket 1 and pocket 2, being the first one the DNA-binding site. A better characterization of both binding pockets can be obtained by computing the binding free energy for both pockets. For that purpose, the snapshots for which thiomaltol is in each of the binding pockets needs to be identified; therefore, the region of the protein where the binding pockets are located must be (arbitrarily) defined. We have selected the residues PHE280 and THR247, which are shown in **Fig. 5b** by blue and magenta van der Waals spheres, respectively, as reference residues along the MC simulation. Then, if for a MC snapshot the centre of mass of thiomaltol is separated from the centre of mass of residue PHE280 (THR247) by less than 15 Å, it is considered that the ligand binds to pocket 1 (pocket 2). By employing this definition of the binding pockets, we have identified 199 and 205 binding events into pockets 1 and 2, respectively, with average binding free energies of -16.9 and -15.0 kcal/mol, as shown in **Fig. 5b**. This result indicates that the binding of thiomaltol

to topoisomerase can occur in both pockets 1 and 2. However, the binding to pocket 1, which is the DNA-binding site, is slightly thermodynamically favored.

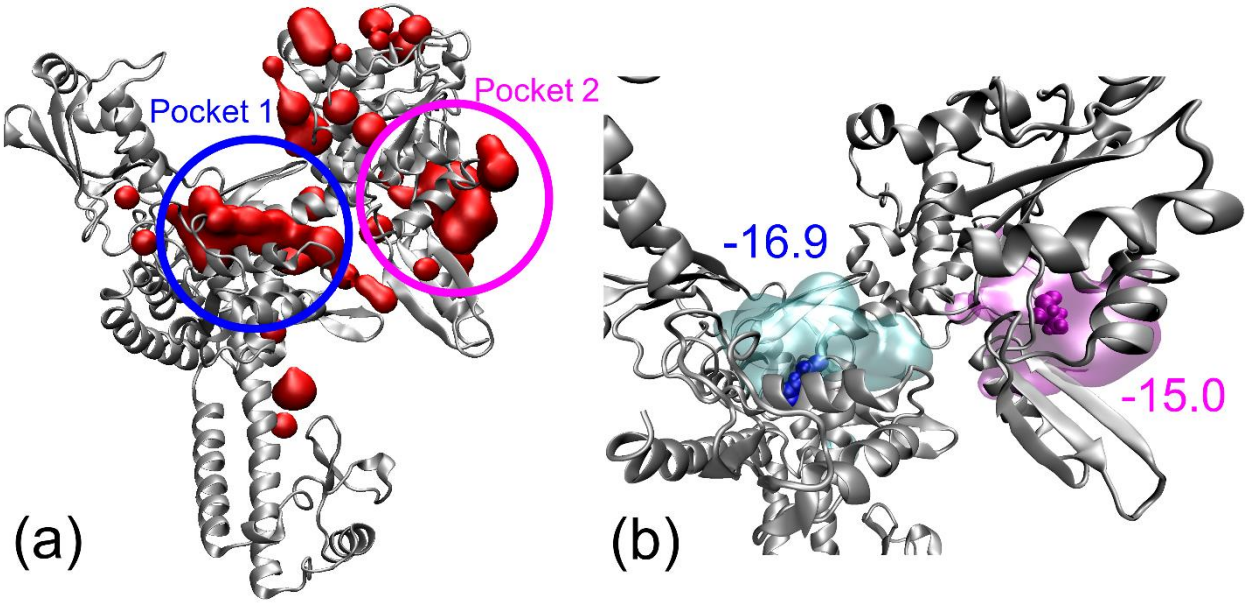

Fig. 5. (a) Binding sites found along the classical MC simulation with binding energies larger (in absolute value) than -15 kcal/mol represented by the red surface. Pockets 1 and 2 are schematically highlighted by blue and pink circles. (b) Binding pockets 1 and 2 represented by the cyan and magenta surfaces defined as the collection of binding sites located at a distance smaller than 15 Å from the residues PHE280 (blue van der Waals representation) and THR247 (magenta van der Waals representation), respectively. Binding free energies for each pocket in kcal/mol are also displayed. The protein is represented in silver color.

In the next step, the two MC snapshots with the largest binding free energy for the pockets 1 and 2 were selected. For these two snapshots, the thiomaltol ligand is replaced by the Ru complexes **1a** and **2a** in both binding pockets. Then, classical MD simulations followed by QM/MM MD simulation are evolved for each of the four complex/pocket combinations. The binding affinity between the complexes and the protein could be analyzed by computing the intermolecular potential energy provided by the force field along the classical MD simulation. However, as discussed above, the force field employed here is not accurate enough for that purpose. Alternatively, the interaction energy between the complex and the protein could be calculated from the energy calculations along the QM/MM MD simulation. However, the present QM/MM computations do not allow the decomposition of the total interaction energy into Ru-complex/solvent and Ru-complex/protein contributions. Therefore, we analyze the binding affinity in terms of intermolecular contacts between the Ru

species and the protein along the QM/MM MD simulation. The number of contacts, defined here as the number of interatomic distances smaller than 3 Å between the complexes and the protein, are listed in **Table 3** for each binding pocket. As can be seen, in both binding pockets the total number of contacts for complex **2a** (61 for pocket 1 and 59 for pocket 2) is larger than that for complex **1a** (56 for pocket 1 and 51 for pocket 2). This suggests that intermolecular interactions between the Ru complexes and the protein are stronger for complex **2a** than for complex **1a**. In addition, the number of contacts per metal-complex atom, defined as the total number of contacts divided by the number of atoms of the metal complex, provides an estimation of the intermolecular interaction undergone by each atom of the complex. As **Table 3** shows, the number of contacts per atom is ca. 1.2 for both complexes and for both binding pockets, indicating that the strength of each Ru-complex/protein interatomic interaction is very similar in both complexes and pockets. By comparing the number of contacts for a particular complex in the different pockets, it is apparent that the intermolecular interactions are stronger for pocket 1 (56 contacts for complex **1a** and 62 for complex **2a**) than for pocket 2 (51 contacts for complex **1a** and 59 for complex **2a**). Therefore, based solely on the analysis of intermolecular contacts, the binding of complex **2a** into pocket 1 is the most favorable binding event.

Tab. 3. Average total number of contacts and average number of contacts per metal-complex atom between the Ru complexes and topoisomerase within a cutoff distance of 3 Å computed along the QM/MM MD simulation. Average number of total water molecules and average number of water molecules per metal-complex atom in the solvation shell of 3 Å of the Ru complexes computed along the QM/MM MD simulations.

	Pocket 1		Pocket 2
	Complex **1a**	Complex **2a**	Complex **1a**
Total contacts	56.3	61.5	51.2
Contacts per atom	1.3	1.2	1.2
Total waters	23.4	33.1	16.6
Waters per atom	0.55	0.65	0.40

The visualization of the QM/MM MD simulations reveals that the complexes embedded into the binding pockets are accompanied by a large solvation sphere, as can be seen in the representative snapshots displayed in **Fig. 6** for the complex **2a** inside the pockets 1 and 2. The solvation sphere stabilizes the positive charge of the complexes and interacts with the polar amino acids of the protein, favoring the binding process. For both Ru compounds, the solvation sphere presents a larger

number of water molecules in pocket 1 than in pocket 2. Specifically, considering a solvation shell of 3 Å from any solute atom, complex **1a** (**2a**) is solvated by 23 (33) and 17 (18) water molecules in pockets 1 and 2, respectively. This can be understood by attending to the protein residues that surrounds the solvated complexes into the two binding sites. As **fig. 6a** shows, pocket 1 presents a large number of polar amino acids (represented by the orange surfaces) at the binding site that create a polar environment that favorably interacts with the solvated complexes. Contrary, pocket 2 presents a more hydrophobic character at the binding site allowing the penetration of less water molecules inside the pocket (**Fig. 6b**). Therefore, pocket 1 is the preferred binding site for the two Ru complexes. This means that complexes **1a** and **2a** can efficiently prevent the binding of DNA to the DNA-binding site (pocket 1) of topo2α and inhibit the enzymatic activity of the protein.

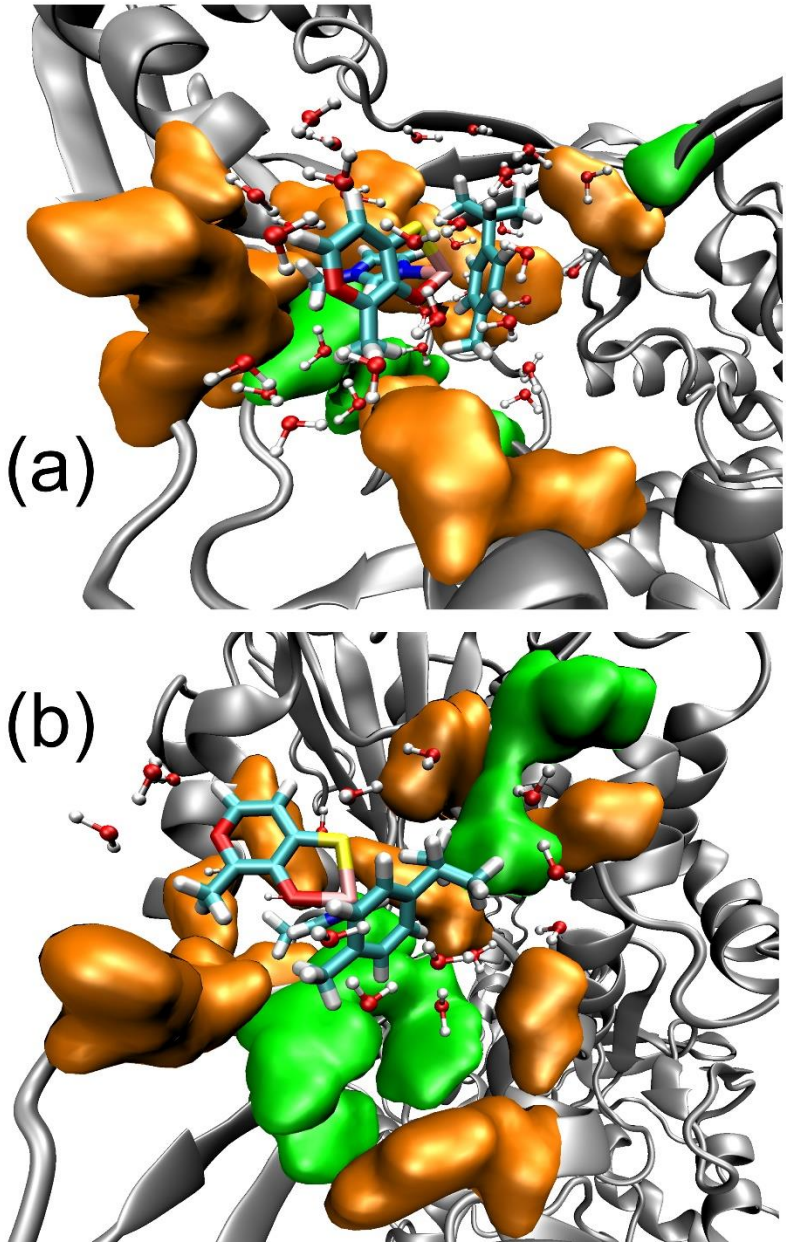

Fig. 6. Polar and nonpolar amino acids represented in orange and green, respectively, that are located at a distance smaller than 6 Å from the metal complex **2a** in (a) pocket 1 and (b) pocket 2. The drug is displayed in tube representation with C in cyan, S in yellow, O in red, Ru in pink, and H in white. The water molecules solvating the complex located at a distance smaller than 3 Å from the complex are represented by balls and tubes, where oxygen is red and hydrogen is white. The protein is represented in silver color.

Next, the different binding affinities between complexes **1a** and **2a** and the protein domain are examined by comparing the solvation spheres of both Ru compounds. In the preferred pocket 1, complex **2a** is solvated by a larger solvation sphere (33 water molecules) than complex **1a** (23 water molecules). This could seem an obvious conclusion since complex **2a** has a larger size than complex **1a** and, thus, a larger

number of water molecules can interact with it. However, if the solvation spheres are compared in terms of number of water molecules per solute atom in order to eliminate the system-size dependency, the same conclusion is drawn. The solvation sphere of complex **2a** has 0.65 water molecules per solute atom, while that of complex **1a** has only 0.54 water molecules per solute atom when the compounds are embedded in pocket 1 (**Tab. 3**). The only structural difference between the two complexes is the substitution of water (complex **1a**) by 3-methylimidazole (complex **2a**), as shown in **Fig. 2** (one should notice that the chlorido group of compounds **1a-d** is replaced by water after hydrolysis). The dipole moment of both ligands was computed by B3LYP/6-31G* using the optimized geometries at the same level of theory. 3-Methylimidazole presents a larger dipole moment (3.9 D) than water (1.9 D). Therefore, complex **2a** should be better solvated, in agreement with what is observed in the MD simulations. Moreover, the better solvated complex **2a** interacts stronger than complex **1a** with the DNA-binding site of topoisomerase, which presents a larger hydrophilicity than pocket 2. The hydrophobic environment found in pocket 2 induces a desolvation effect in both Ru species, which present solvation spheres of only 17 water molecules. Thus, the intermolecular contacts between the metal complexes and the protein and, most importantly, the analysis of the solvation spheres of the two complexes indicate that pocket 1 is the most likely binding site of the protein domain. In addition, complex **2a** interacts stronger with topoisomerase than complex **1a** and, thus, should be able to inhibit the DNA binding in a more effective way. This behavior is in consonance with the generally higher cytotoxicity experimentally observed for the complexes that possess the 3-methylimidazole ligand.

Conclusions

The cytotoxic mechanism of several thiomaltol-based Ru, Os, Rh and Ir complexes has been investigated by means of biological assays and theoretical simulations. Electrophoretic DNA plasmid and H2AX assays have demonstrated that some of the drugs do not induce a relevant degree of damage to the DNA structure and, thus, DNA is most likely not the main target of these drugs. Instead, the modification of the IC_{50} values of the drugs when the cell expression of topo2α is regulated by RNAi is consistent with the assumption that this enzyme is the main target at least for part of the compounds investigated here. Monte Carlo and molecular dynamics simulations have revealed that the metal compounds are able to bind into the DNA-binding pocket of the enzyme. In addition, the drugs enter the binding pocket with their solvation shell to maximize the interactions with the hydrophilic environment of the pocket. This suggests that functionalization of the compounds with highly polar ligands favors their binding to the protein. This behavior agrees with the fact that an enhancement of the inhibition of cancer cell growth was observed upon modification of the structures by substitution of the labile chlorido ligand (which is readily exchanged for an aqua ligand in solution) by 3-methylimidazole. Our experiments also showed that inhibition of topo2α may not be the only way to inhibit cancer for this type of complexes. Thus, more research is required to validate the role of topo2α expression levels and investigate additional cytotoxic mechanisms. Nevertheless, these compounds may serve as potential pharmacophores for further rational design of topo2 catalytic inhibitors. This adds a new aspect to the modes of action of experimental organometallics, which may allow overcoming some of the drawbacks of clinically applied metal-based anticancer agents.

Acknowledgements

The authors would like to thank the Johanna Mahlke née Obermann Foundation for financial support within the project “Exploring Novel Protein Targets of Anticancer Metal Compounds”. The Vienna Scientific Cluster is acknowledged for generous computational support.

Author contributions

Study conception and design: Legina M. S., Nogueira J. J., Jakupec M. A.

Data acquisition: Legina M. S., Nogueira J. J.

Analysis and interpretation of data: Legina M. S., Nogueira J. J., Jakupec M. A.

Drafting of the manuscript: Legina M. S., Nogueira J. J., Jakupec M. A.

Critical revision: Jakupec M. A., Kandioller W., González L., Keppler B.K.

Conflict of interest

The authors declare that they have no conflicts of interest with the contents of this article.

References

1. Rosenberg B., van Camp L., Krigas T. Inhibition of cell division in *Escherichia coli* by electrolysis products from a platinum electrode. *Nature* 205, 698–699 (1965).
2. Medici M. S., Zoroddua A. Noble metals in medicine: Latest advances. *Coord. Chem. Rev.* 284, 329–350 (2015).
3. Housman G., Byler S., Heerboth S., Lapinska K., Longacre M., Snyder N., Sarkar S. Drug resistance in cancer: an overview. *Cancers* (Basel) 6(3), 1769–92 (2014).
4. Brabec V., Kasparkova J. Molecular aspects of resistance to antitumor platinum drugs. *Drug Resist Updat.* 5(3–4), 147–61 (2002).
5. Ohmichi M., Hayakawa J., Tasaka K., Kurachi H., Murata Y. Mechanisms of platinum drug resistance. *Trends Pharmacol Sci.* 26(3), 113–6 (2005).
6. Czapla-Masztafiak J., Nogueira J.J., Lipiec E., Kwiatek W.M., Wood B.R., Deacon G.B., Kayser Y., Fernandes D.L., Pavliuk M.V., Szlachetko J., González L., Sá J. Direct determination of metal complexes' interaction with DNA by atomic telemetry and multiscale molecular dynamics. *J Phys Chem Lett.* 8 (4): 805–811 (2017).
7. Kenneth L. Organometallic transition metal complexes with biological molecules and living cells. 1st edition, *Academic Press* (2017)
8. Antonarakis E. S., Emadi A. Ruthenium-based chemotherapeutics: are they ready for prime time? *Cancer Chemother Pharmacol.* 66(1), 1–9 (2010).
9. Clarke M. J. Ruthenium metallopharmaceuticals. *Coordination Chemistry Reviews* 236, 209–233 (2003).
10. Muhammad N., Guo Z. Metal-based anticancer chemotherapeutic agents. *Current Opinion in Chemical Biology* 19, 144–153 (2014).
11. Che C. M., Siu F. M. Metal complexes in medicine with a focus on enzyme inhibition. *Curr Opin Chem Biol.* 14(2), 255–61 (2010).
12. Abid M., Shamsi F., Azam A. Ruthenium Complexes: An Emerging Ground to the Development of Metallopharmaceuticals for Cancer Therapy. *Mini Rev Med Chem.* 16(10), 772–86 (2016).

13. Griffith D., Parker J. P., Marmion C. J. Enzyme inhibition as a key target for the development of novel metal-based anti-cancer therapeutics. *Anticancer Agents Med Chem.*, 10(5):354–70 (2010).
14. Houlbrook S., Addison C. M., Davies S. L., Carmichael J., Stratford I. J., Harris A. L., Hickson I. D. Relationship between expression of topoisomerase II isoforms and intrinsic sensitivity to topoisomerase II inhibitors in breast cancer cell lines. *Br J Cancer.*, 72(6):1454– 61 (1995)
15. Burris H. A., Hanauske A. R., Johnson R. K., Marshall M. H., Kuhn J. G., Hilsenbeck S. G., Von Hoff D. D. Activity of topotecan, a new topoisomerase inhibitor, against human tumor colony forming units in vitro. *J Natl Cancer Inst.*, 84:1816–1820 (1992).
16. Chen A. Y., Liu L. F. DNA topoisomerases: essential enzymes and lethal targets. *Annu Rev Pharmacol Toxicol.*, 34:191–218 (1994).
17. Fayad W., Fryknäs M., Brnjic S., Olofsson M. H., Larsson R., Linder S. Identification of a novel topoisomerase inhibitor effective in cells overexpressing drug efflux transporters. *PLoS ONE.*, 4(10):e7238 (2009).
18. Pommier Y., Kohn K. W. Cell cycle and checkpoints in oncology: new therapeutic targets. *Med Sci*, 19:173–86 (2003).
19. Nitiss J. L. Targeting DNA topoisomerase II in cancer chemotherapy. *Nat Rev Cancer.*, 9(5):338–50 (2009).
20. An X., Xu F., Luo R., Zheng Q., Lu J., Yang Y., Qin T., Yuan Z., Shi Y., Jiang W., Wang S. The prognostic significance of topoisomerase II alpha protein in early stage luminal breast cancer. *BMC Cancer*, 18(1):331 (2018).
21. Lind M. J. Principles of systemic anticancer therapy. *Medicine* 44, 1, 20–24 (2015).
22. Hackl C. M., Legina M. S., Pichler V., Schmidlehner M., Roller A., Dömötör O., Enyedi E. A., Jakupec M. A., Kandioller W., Keppler B. K. Thiomaltol-based organometallic complexes with 1-methylimidazole as leaving group: synthesis, stability, and biological behavior. *Chemistry – A European Journal* 22, 17269–17281 (2016).
23. Schmidt B. H., Burgin A. B., Deweese J. E., Osheroff N., Berger J. M. A novel and unified two-metal mechanism for DNA cleavage by type II and IA topoisomerases. *Nature*, 465(7298):641–4 (2010).

24. Case D. A.; Berryman J. T.; Betz R. M.; Cerutti D. S.; Cheatham T. E. III; Darden T. A.; Duke R. E.; Giese T. J.; Gohlke H.; Götz A. W.; Homeyer N.; Izadi S.; Janowski P. A.; Kaus J. W.; Kovalenko A.; Lee T.; Le Grand S.; Li P.; Luchko T.; Luo R.; Madej B. D.; Merz K. M.; Monard G.; Needham H.; Nguyen H.; Nguyen H. T.; Omelyan I.; Onufriev A.; Roe D. R.; Roitberg A. E.; Salomon-Ferrer R.; Simmerling C.; Smith W.; Swails J.; Walker R. C.; Wang J.; Wolf R. M.; Wu X.; York D. M.; Kollman P., AMBER 2015, University of California, San Francisco, 2015.
25. Miyamoto S., Kollman P. A. Settle: An analytical version of the SHAKE and RATTLE algorithm for rigid water models. *Computational Chemistry*, 3(8): 952–962 (1992).
26. Crowley M., Darden T., Cheatham T., Deerfield D. Adventures in Improving the Scaling and Accuracy of a Parallel Molecular Dynamics Program. The Journal of Supercomputing, 11(3): 255–278 (1997).
27. Maier J. A., Martinez C., Kasavajhala K., Wickstrom L., Hauser K. E., Simmerling C. ff14SB: Improving the Accuracy of Protein Side Chain and Backbone Parameters from ff99SB. *J. Chem. Theory Comput.*, 11 (8), 3696–3713 (2015).
28. Jorgensen W. L., Chandrasekhar J., Madura J. D., Impey R. W., Klein M. L. Comparison of simple potential functions for simulating liquid water. *Journal of Chemical Physics*, 79(2):926 (1983).
29. Fox T., Kollman P. A. Application of the RESP Methodology in the Parametrization of Organic Solvents. *J. Phys. Chem. B*, 102 (41), 8070–8079 (1998).
30. Borrelli K. W., Vitalis A., Alcantara R., Guallar V. PELE: Protein Energy Landscape Exploration. A Novel Monte Carlo Based Technique. *J. Chem. Theory Comput*, 1 (6), 1304–1311 (2005).
31. Jacobson M. P., Kaminski G. A., Friesner R. A., Rapp C. S. Force Field Validation Using Protein Side Chain Prediction. *J. Phys. Chem. B*, 106 (44), 11673–11680 (2002).
32. Ghosh A., Rapp C. S., Friesner R. A. Generalized Born Model Based on a Surface Integral Formulation. *J. Phys. Chem. B*, 102 (52), pp 10983–10990 (1998).

33. Brandt P., Norrby T., Åkermark B., Norrby P. O. Molecular Mechanics (MM3*) Parameters for Ruthenium(II)−Polypyridyl Complexes. *Inorg. Chem.*, 37 (16), 4120–4127 (1998).
34. Wang J., Wolf R. M., Caldwell J. W., Kollman P. A., Case D. A. Development and testing of a general amber force field. *Computational Chemistry*, 25(9): 1157–1174 (2004).
35. Frisch M. J., Trucks G. W., Schlegel H. B., Scuseria G. E. Robb M. A., Cheeseman J. R., Scalmani G., Barone V., Mennucci B., Petersson G. A., Nakatsuji H., Caricato M., Li X., Hratchian H. P., Izmaylov A. F., Bloino J., Zheng G., Sonnenberg J. L., Hada M., Ehara M., Toyota K., Fukuda R., Hasegawa J., Ishida M., Nakajima T., Honda Y., Kitao O., Nakai H., Vreven T., Montgomery J. A., Jr.; , Peralta J. E., Ogliaro F., Bearpark M., Heyd J. J., Brothers E., Kudin K. N., Staroverov V. N., Kobayashi R., Normand J., Raghavachari K., Rendell A., Burant J. C., Iyengar S. S., Tomasi J., Cossi M., Rega N., Millam N. J., Klene M., Knox J. E., Cross J. B., Bakken V., Adamo C., Jaramillo J., Gomperts R., Stratmann R. E., Yazyev O., Austin A. J., Cammi R., Pomelli C., Ochterski J. W., Martin R. L., Morokuma K., Zakrzewski V. G., Voth G. A., Salvador P., Dannenberg J. J., Dapprich S., Daniels A. D., Farkas Ö., Foresman J. B., Ortiz J. V., Cioslowski J., Fox D. J., Gaussian, Inc., Wallingford CT, 2013.
36. Becke A. D. Density-functional thermochemistry. III. The role of exact exchange *J. Chem. Phys*. 98, 5648 (1993)
37. Lee C., Yang W., Parr R. G. Development of the Colle-Salvetti correlation-energy formula into a functional of the electron density. *Physical review. B, Condensed matter* 37(2):785–789 (1988)
38. Vosko S. H., Wilk L., Nusair M. Accurate spin-dependent electron liquid correlation energies for local spin density calculations: a critical analysis. *Canadian Journal of Physics*, 58(8): 1200–1211 (1980)
39. Stephens P. J., Devlin F. J., Chabalowski C. F., Frisch M.J. Ab Initio Calculation of Vibrational Absorption and Circular Dichroism Spectra Using Density Functional Force Fields. *J. Phys. Chem.*, 98 (45), 11623–11627 (1994)

40. Grimme S., Ehrlich S., Goerigk L. Effect of the damping function in dispersion corrected density functional theory. *Computational Chemistry*, 32 (7): 1456– 1465 (2011)
41. Chiodo S., Russo N., Sicilia E. LANL2DZ basis sets recontracted in the framework of density functional theory. *Journal of Chemical Physics* 125, 104107 (2006)
42. Wood G. P. F., Radom L., Petersson G. A., Barnes E. C. A restricted-open-shell complete-basis-set model chemistry. *Journal of Chemical Physics* 125, 094106 (2006)
43. TeraChem v 1.9, PetaChem, LLC (2009, 2015).
44. Ufimtsev I. S., Martinez T. J. Quantum Chemistry on Graphical Processing Units. 3. Analytical Energy Gradients, Geometry Optimization, and First Principles Molecular Dynamics. *J. Chem. Theory Comput.*, 5 (10), 2619–2628 (2009)
45. Grimme S., Antony J., Ehrlich S., Krieg H. A consistent and accurate ab initio parametrization of density functional dispersion correction (DFT-D) for the 94 elements H-Pu. *Journal of Chemical Physics* 132, 154104 (2010)
46. Walker R. C., Crowley M.F., Case D. A. The implementation of a fast and accurate QM/MM potential method in Amber. *Computational Chemistry*, 29 (7): 1019– 1031 (2008)
47. Roe D. R., Cheatham III T. E. PTRAJ and CPPTRAJ: Software for Processing and Analysis of Molecular Dynamics Trajectory Data. *J. Chem. Theory Comput.*, 9 (7), 3084–3095 (2013)
48. Humphrey W., Dalke A., Schulten K. VMD: visual molecular dynamics. *Journal of Molecular Graphics*, 14(1): 33–8, 27–8 (1996)
49. Tanaka T., Huang X., Halicka H. D., Zhao H., Traganos F., Albino A. P., Dai W., Darzynkiewicz Z. Cytometry of ATM Activation and Histone H2AX Phosphorylation to Estimate Extent of DNA Damage Induced by Exogenous Agents. Cytometry; 71A(9): 648–661 (2007)
50. Ewald B., Sampath D., Plunkett W. H2AX phosphorylation marks gemcitabine-induced stalled replication forks and their collapse upon S-phase checkpoint. Mol Cancer Ther.; 6(4): 1239–48 (2007)

51. Sallmyr A., Fan J., Rassool F. V. Genomic instability in myeloid malignancies: increased reactive oxygen species (ROS), DNA double strand breaks (DSBs) and error-prone repair. *Cancer Lett.* 270(1):1–9 (2008)
52. Fry A. M., Chresta C. M., Davies S. M., Walker M. C., Harris A. L., Hartley J. A., Masters J. R., Hickson I. D. Relationship between topoisomerase II level and chemosensitivity in human tumor cell lines. *Cancer Res.* 51(24): 6592–5 (1991)
53. Chen C. F., He X., Beck W. T. Inducible knockdown of DNA topoisomerase IIα affects drug sensitivity and cell growth. *Cancer Res* 71 (8): 4683–4683 (2011)
54. Koshiyama M., Fujii H., Kinezaki M., Yoshida M. Correlation between Topo II alpha expression and chemosensitivity testing for Topo II-targeting drugs in gynaecological carcinomas. *Anticancer Res.* 21(2A): 905–10 (2001)
55. Satyajit S., Vidyarthi A. S., Prasad D. RNA interference: concept to reality in crop improvement. *Planta*., 239 (3): 543–564 (2014)
56. Gonzalez R. E., Lim C. U., Cole K., Bianchini C. H., Schools G. P., Davis B. E., Wada I., Roninson I. B., Broude E. V. Effects of conditional depletion of topoisomerase II on cell cycle progression in mammalian cells. *Cell Cycle.* 10(20): 3505–14 (2011)
57. Akimitsu N., Adachi N., Hirai H., Hossain M. S., Hamamoto H., Kobayashi M., Aratani Y., Koyama H., Sekimizu K. Enforced cytokinesis without complete nuclear division in embryonic cells depleting the activity of DNA topoisomerase IIalpha. *Genes Cells.* 8(4): 393–402 (2003)
58. Burgess D. J., Doles J., Zender L., Xue W., Ma B., McCombie W. R., Hannon G. J., Lowe S. W., Hemann M. T. Topoisomerase levels determine chemotherapy response *in vitro* and *in vivo*. *Proc Natl Acad Sci U S A.* 105(26): 9053–8
59. Soubeyrand S., Pope L., Haché R. J. Topoisomerase IIalpha-dependent induction of a persistent DNA damage response in response to transient etoposide exposure. *Mol Oncol.* 4(1):38-51 (2010)

Abbreviations

DCFH DA – dichloro-dihydro-fluorescein diacetate

DMSO – dimethyl sulfoxide

FITC – fluorescein isothiocyanate

HEPES – 4-(2-hydroxyethyl)-1-piperazineethanesulfonic acid

MTT – 3-(4,5-dimethylthiazol-2-yl)-2,5-diphenyltetrazolium bromide

NF-kB - nuclear factor kappa-light-chain-enhancer of activated B cells

PBS – phosphate-buffered saline

PI – propidium iodide

ROS – reactive oxygen species

MC – Monte Carlo

MD – Molecular Dynamics

QM/MM – Quantum Mechanics/Molecular Mechanics

SUPPORTING MATERIALS

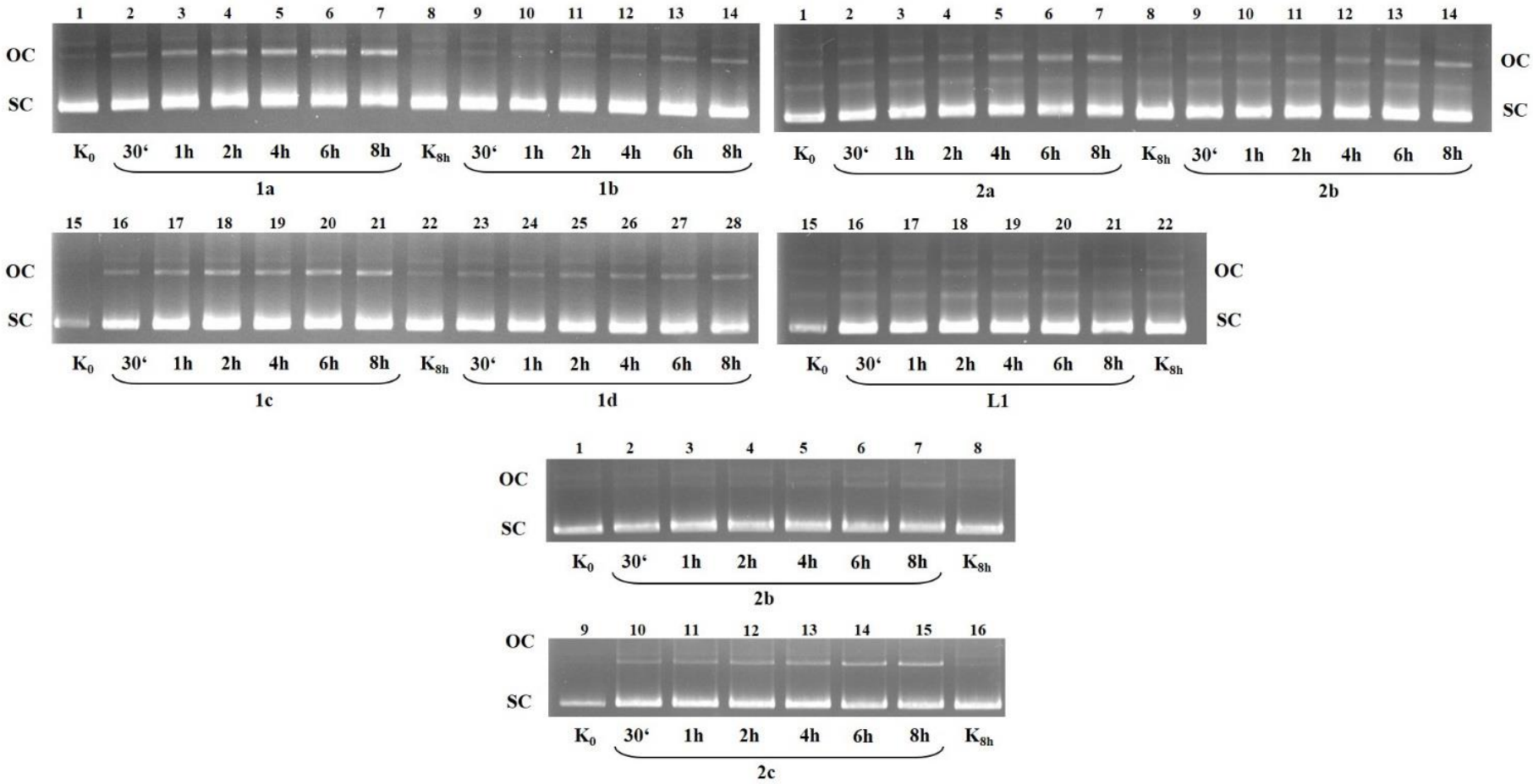

Fig. S1. Electropherograms of dsDNA plasmid pUC19 after exposure to 10 μM solutions of **1a**, **1b**, **1c**, **1d**, **2a**, **2b**, **2c**, **2d** and **L1** for different exposure times (30 min to 8 h) compared to untreated controls K_0 and K_{8h}.

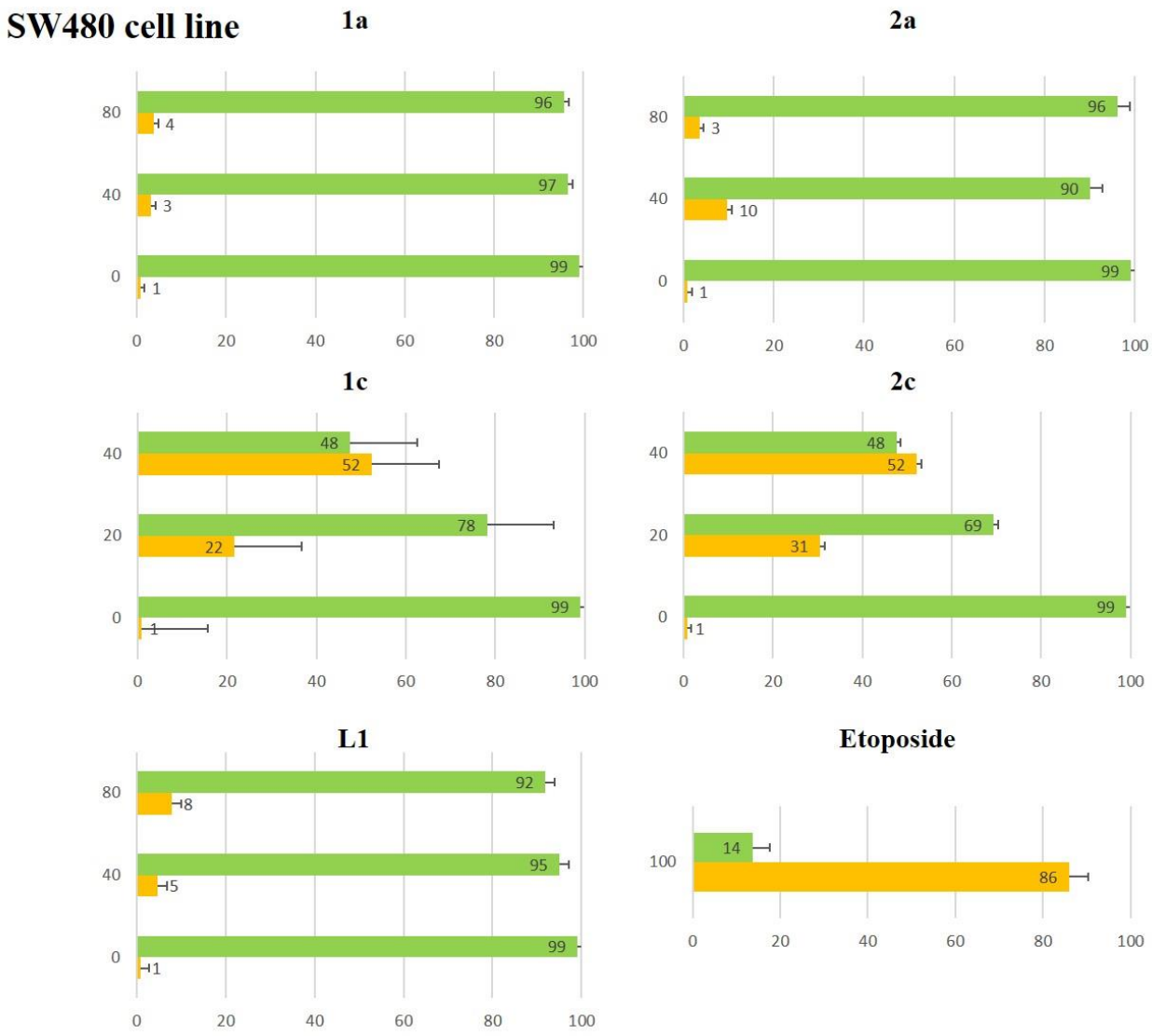

Fig. S2. Evaluation of a formation of γ-H2AX in response to DNA double-strand breaks (DSBs) in SW480, SK-BR-3, T47D and MDA-MB468 cells after 48 h of exposure to the studied compounds and ligand; measured by flow cytometry using the γ-H2AX assay (undamaged cells shown in green, damaged – in yellow).

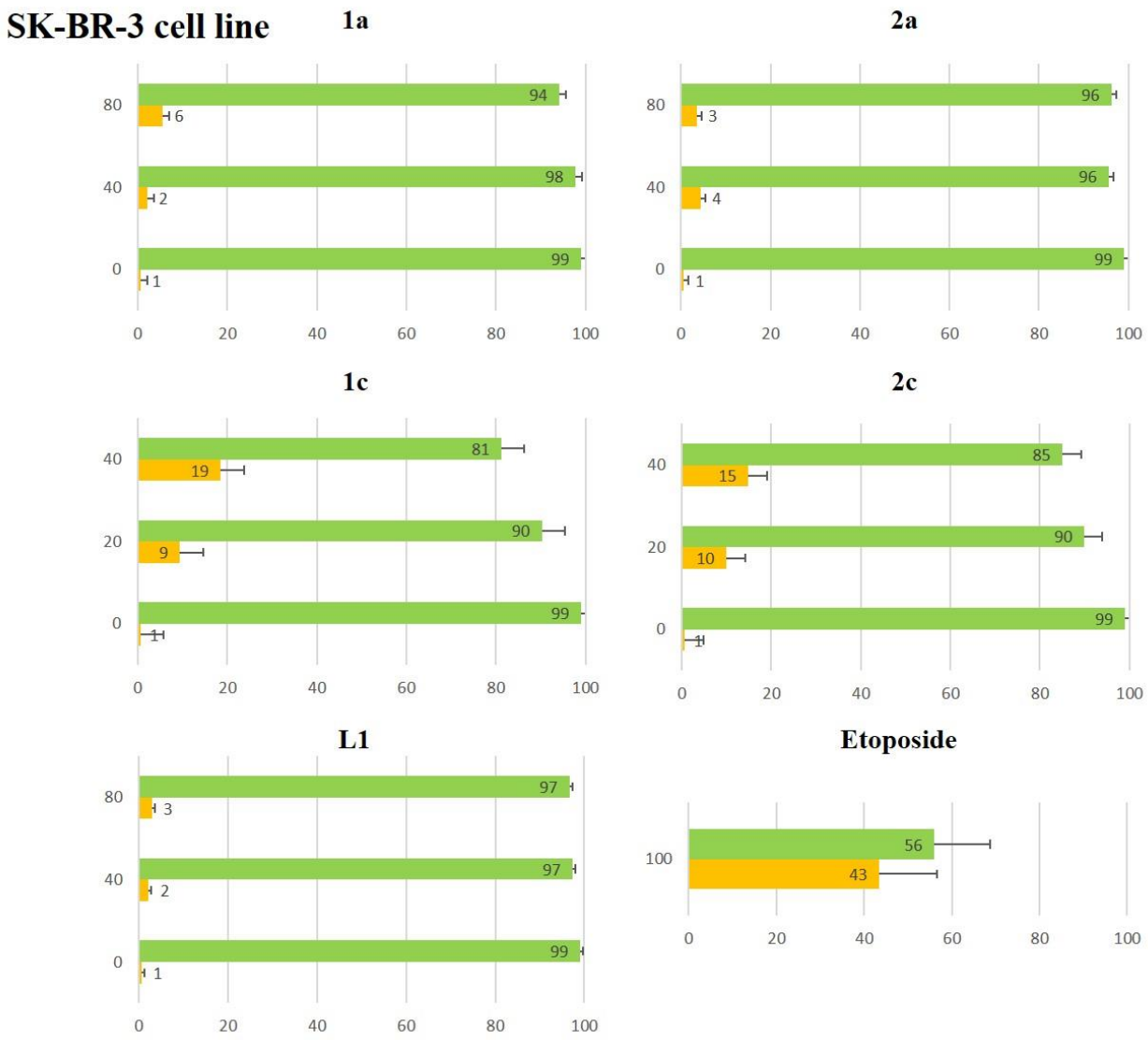

Fig. S2. (continued)

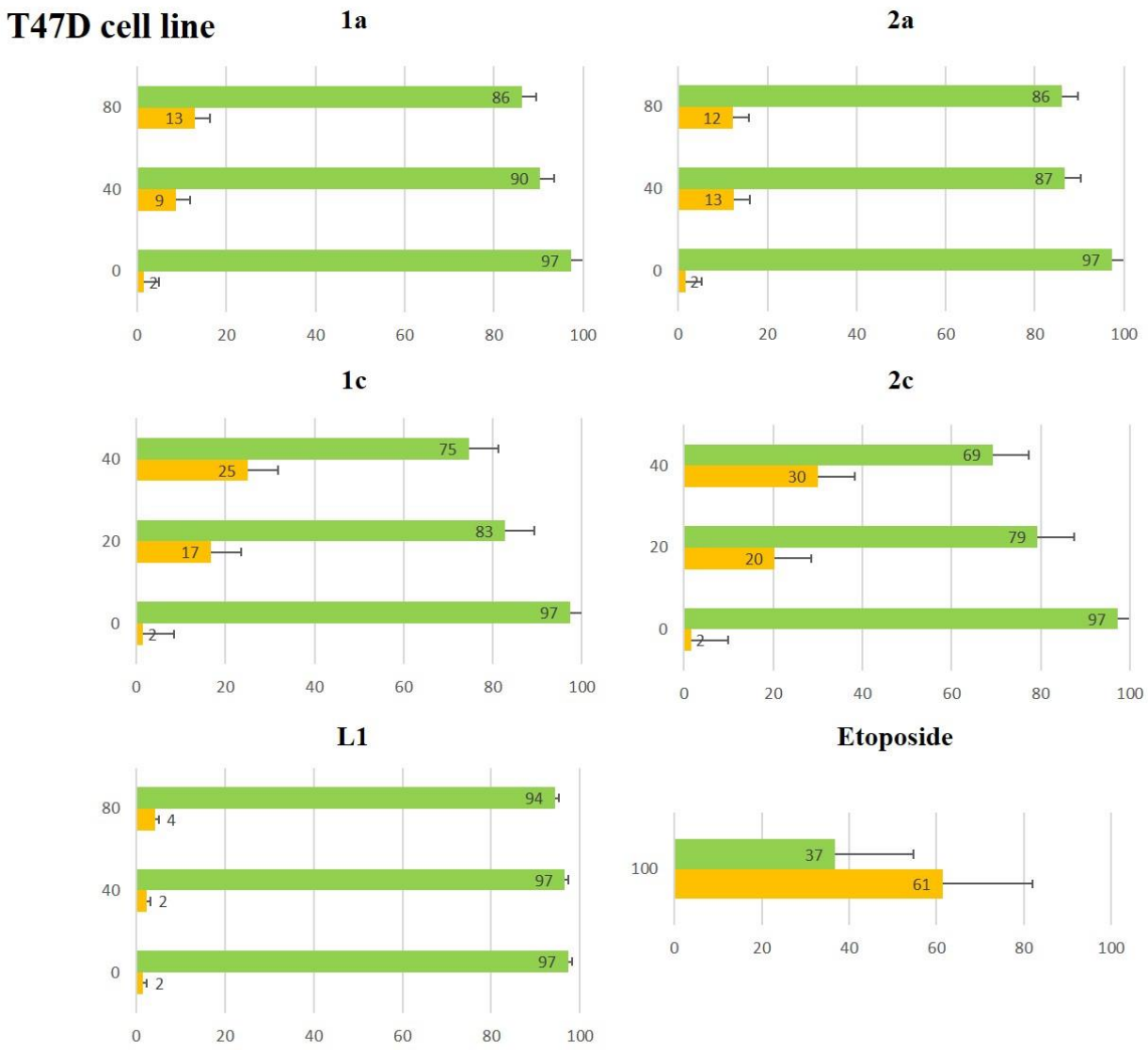

Fig. S2. (continued)

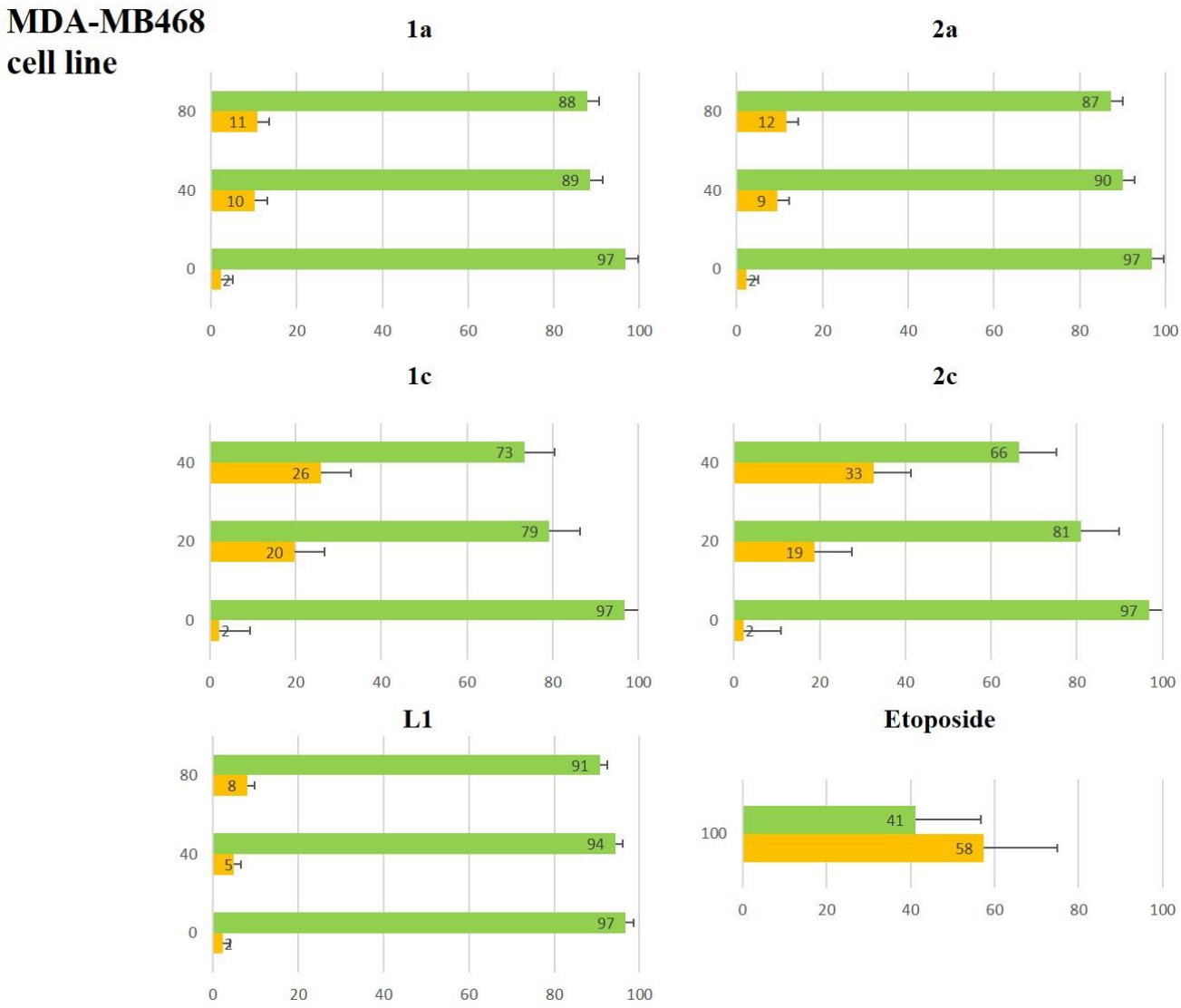

Fig. S2. (continued)

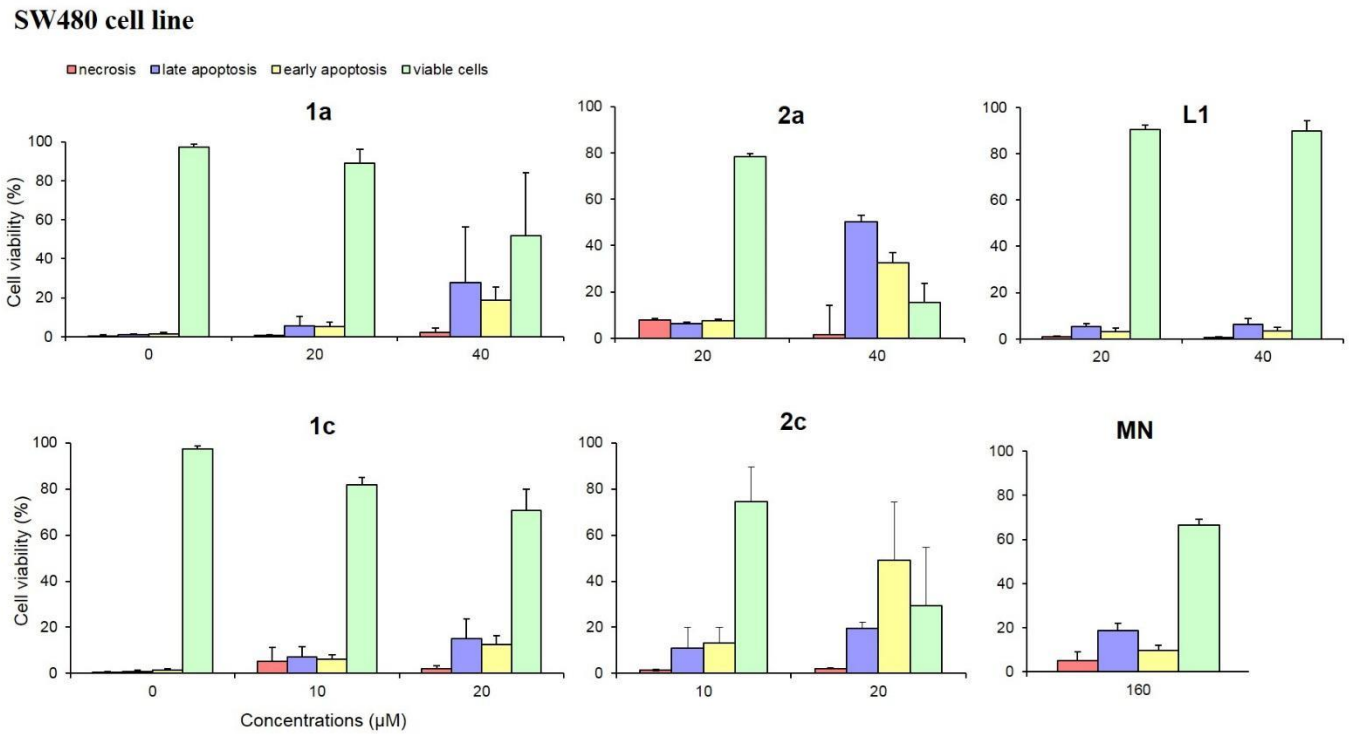

Fig. S3. Apoptosis/necrosis induction in SW480, SK-BR-3, T47D and MDA cells after 48 h of exposure to the studied compounds, ligand and merbarone (MN); measured by flow cytometry using the annexin V-FITC/propidium iodide double staining (viable cells shown in green, early apoptosis – in yellow, late apoptosis – in violet and necrosis – in pink).

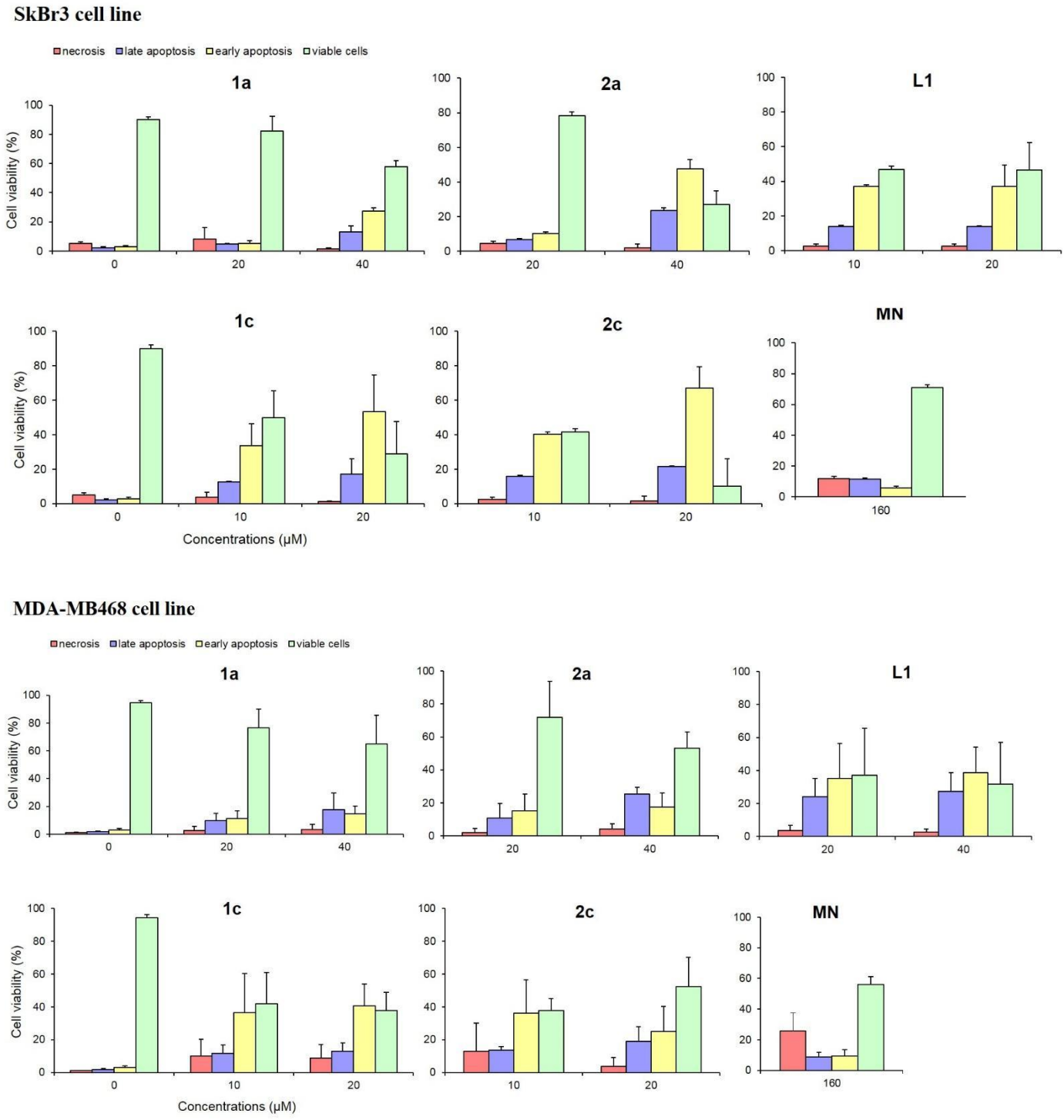

Fig. S3. (continued)

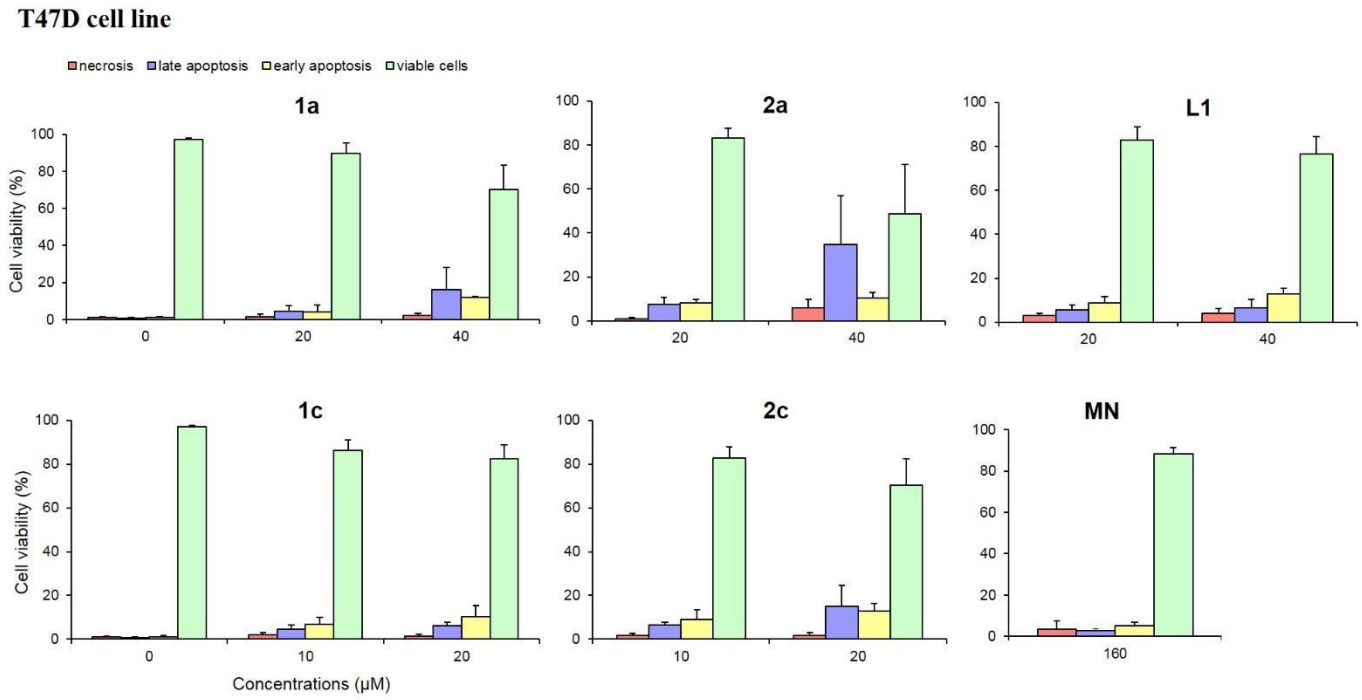

Fig. S3. (continued)

DOI: 10.1002/chem.201603206

Antitumor Agents

Thiomaltol-Based Organometallic Complexes with 1-Methylimidazole as Leaving Group: Synthesis, Stability, and Biological Behavior

Carmen M. Hackl,[a] Maria S. Legina,[a] Verena Pichler,[a] Melanie Schmidlehner,[a] Alexander Roller,[a] Orsolya Dömötör,[b, c] Eva A. Enyedy,[b] Michael A. Jakupec,[a, d] Wolfgang Kandioller,*[a, d] and Bernhard K. Keppler[a, d]

Abstract: Thiomaltol, a potential *S*,*O*-coordinating molecule, has been utilized for the complexation of four different organometallic fragments, yielding the desired Ru^{II}, Os^{II}, Rh^{III}, and Ir^{III} complexes having a "piano-stool" configuration. In addition to the synthesis of these compounds with a chlorido leaving group, the analogous 1-methylimidazole derivatives have been prepared, giving rise to thiomaltol-based organometallics with enhanced stability under physiological conditions. The organometallic compounds have been characterized by NMR spectroscopy, elemental analysis, and X-ray diffraction analysis. Their behavior in aqueous solution and their interactions with certain amino acids have been studied by ESI mass spectrometry. Their pH-dependent stability has been investigated by ^{1}H NMR in aqueous solution, and their cytotoxicity against three different cancer cell lines has been investigated. Furthermore, their capacity as topoisomerase IIα inhibitors as well as their effect on the cell cycle distribution and reactive oxygen species (ROS) generation have been elucidated.

Introduction

In recent years, the development of ruthenium-containing compounds has expanded the spectrum of potential anticancer drugs. Considerable impetus has arisen due to the occurrence of a variety of resistances to treatment of different cancer types with commonly applied platinum-based single-agent or combination chemotherapy strategies.[1] One promising drug candidate featuring a ruthenium core is IT-139 (Figure 1); it was thoroughly studied in a phase I clinical trial, in which it demonstrated activity against different tumor types. It was shown that this Ru^{III}-based drug could be applied in the treatment of non-pancreatic gastrointestinal neuroendocrine tumors, where it influences the GRP78 pathway. GRP78, a regulator of endoplasmic reticulum stress response, has been found to be significantly upregulated in cancer cells and is accredited with a high impact on tumor cell survival and resistance.[2] Furthermore, evidence for synergy of IT-139 was obtained when it was tested in combination with approved anticancer drugs, such as sorafenib.[3] NAMI-A, as another representative of ruthenium(III) anticancer compounds, showed a divergent activity profile compared to IT-139, despite its structural similarities. Even though this drug demonstrated selective activity in metastatic cells and antiangiogenic activity,[4,5] clinical trials were discontinued due to poor clinical responses and the absence of a distinctly assignable target.[6] Besides ruthenium(III) compounds, the development of organometallic complexes that contain the metal in its reduced, active form, stabilized by the coordination of an arene ligand to the metal center, has emerged in the field of anticancer drug research.[7] Two representatives of this group of ruthenium(II) organometallic compounds are RAPTA-C and RM175, which have been extensively studied in the course of various preclinical investigations.[7–9]

Ruthenium(II) half-sandwich complexes provide a promising approach for the development of anticancer metallodrugs with different modes of action. The impact of ligand variation on the most important characteristics of these compounds has been an active field of research and, through a series of studies, it was demonstrated that the nature of the donor atoms has a considerable impact on the in vitro activity.[10] Low anticancer activities could be explained by insufficient complex stability due to replacement of the active ligand by biomole-

[a] C. M. Hackl, M. S. Legina, Dr. V. Pichler, Dr. M. Schmidlehner, A. Roller, Dr. M. A. Jakupec, Dr. W. Kandioller, Prof. Dr. Dr. B. K. Keppler
Institute of Inorganic Chemistry, University of Vienna
Waehringer Str. 42, 1090 Vienna (Austria)
E-mail: wolfgang.kandioller@univie.ac.at

[b] Dr. O. Dömötör, Dr. E. A. Enyedy
Department of Inorganic and Analytical Chemistry
University of Szeged, Dóm tér 7, 6720 Szeged (Hungary)

[c] Dr. O. Dömötör
MTA-SZTE Bioinorganic Chemistry Research Group
University of Szeged, Dóm tér 7, 6720 Szeged (Hungary)

[d] Dr. M. A. Jakupec, Dr. W. Kandioller, Prof. Dr. Dr. B. K. Keppler
Research Platform "Translational Cancer Therapy Research"
University of Vienna, Waehringer Str. 42, 1090 Vienna (Austria)

Supporting information and the ORCID number(s) for the author(s) of this article are available under http://dx.doi.org/10.1002/chem.201603206.

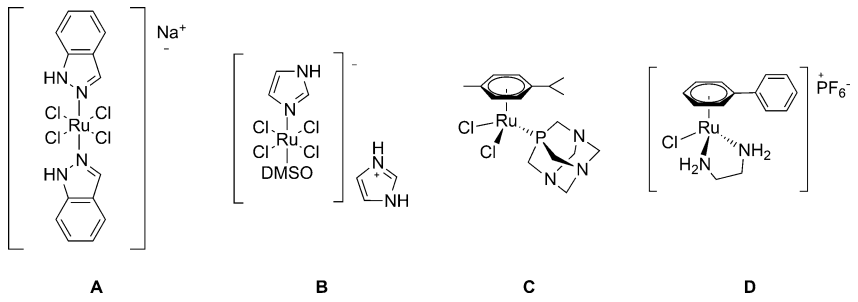

Figure 1. Important representatives of ruthenium-containing compounds as anticancer agents. From left to right: A) IT-139 (NKP-1339), B) NAMI-A, C) RAPTA-C, and D) RM175.

cules, which are omnipresent once the drug has been administered. A thorough investigation and comparison of maltol-derived ruthenium(II) complexes by NMR and ESI-MS supported the assumption that the replacement of an *O*,*O*-donor set by an *S*,*O*-donating moiety could increase both aqueous stability and cytotoxic activity, resulting in IC_{50} values in the low μM range.[11,12] The stronger bond between the metal center and the ligand can be attributed to the softer character of the sulfur atom in comparison to oxygen, which should result in an increased complex stability since ligand-exchange reactions and subsequent inactivation are impeded.[13] As illustrated previously, co-incubation of imidazole with the organoruthenium(II) maltolato complex greatly increased the stability of the complex due to a decelerated aquation process.[12] Since this ligand exchange by a water molecule is thought to be directly related to the activity of a compound, a delayed activation is desired in order to allow for accumulation of the intact drug and subsequent interaction with the cellular target. In this work, we demonstrate that coordination of 1-methylimidazole (MeIm) stabilizes the complexes under alkaline conditions, while at the same time offering an interesting approach towards complex activation at the slightly acidic pH values present in tumor tissues.[14,15] In addition, we have investigated the impacts of metal center and leaving group variation on the physicochemical and biological properties. Preliminary studies have been conducted concerning possible cellular targets, and possible modes of action have been elucidated by investigation of topoisomerase IIα inhibition, reactive oxygen species (ROS) production, and cell cycle analysis.

Results and Discussion

The introduction of an imidazole moiety in place of a chlorido ligand should increase the stability of complexes in the presence of biomolecules, as well as their solubility, depending on the counter ion of the resulting charged organometallic. Commercially available maltol was used as starting point for this synthetic pathway and was converted to its thionated analogue by reaction with Lawesson's reagent under inert conditions. Complexation was performed under the established reaction conditions.[16,17] The first approach was the direct conversion of **1a**–**d** (Scheme 1) by the addition of silver trifluoromethanesulfonate and 1-methylimidazole. However, this attempt resulted in the formation of compound mixtures that could not be separated. Therefore, a different strategy was applied, involving [bis(1-methylimidazole)M(*p*-cym/Cp*)Cl]Cl (*p*-cym = *p*-cymene) precursor complexes. In contrast to the situation with the mono-imidazole analogue, only one product was obtained after treatment with thiomaltol. The four required bis(1-methylimidazole) precursors were synthesized by treatment of the respective dimeric metal compounds $[M(p\text{-cym/Cp*})Cl_2]_2$ ($M = Ru^{II}$, Os^{II}, Rh^{III}, Ir^{III}) with a slight excess of 1-methylimidazole under optimized microwave reaction conditions (Scheme 1).[18] In general, coordination of thiomaltol to organometallic moieties requires strictly inert conditions to avoid the formation of undesired by-products. Therefore, the complexation reactions were performed in distilled methanol by means of Schlenk-line techniques. Thiomaltol was deprotonated by using sodium methoxide in dry methanol. After addition of the respective dimeric metal precursor, the reaction mixture was stirred at room temperature for 1.5–24 h, depending on the metal center present. Extraction with dichloromethane and subsequent filtration allowed the isolation of pure complexes. The desired products were obtained by crystallization from dichloromethane/diethyl ether in low to moderate yields (32–52%). The isolated complexes were characterized by standard analytical methods, such as ^1H and ^{13}C NMR, elemental analysis, ESI-MS measurements, and, where possible, by X-ray diffraction analysis. ^1H NMR spectra of both the chlorido series as well as of the complexes with 1-methylimidazole were recorded from solutions in deuterated methanol and showed characteristic signals (see Figures S1–S4). The chlorido compounds showed only two doublets attributable to the aromatic protons of the η^6-*p*-cymene ligand, although four distinct signals could be expected due to the magnetically inequivalent protons. This effect has also been observed for similar maltolato-based organoruthenium(II) and osmium(II) complexes.[19] Substitution by the more sterically demanding 1-methylimidazole moiety leads to a more complex NMR spectrum, which could be rationalized in terms of hindered inversion at the metal center. ESI-MS studies showed complexes **2a**–**d** to be more stable than their chlorido analogues **1a**–**d** under the applied conditions. **1a**–**d** and **2c**,**d** formed only $[M-Cl]^+$ or $[M-MeIm]^+$ fragments, whereas complexes **2a**,**b** showed signals attributable to the molecular peak $[M]^+$ and $[M-MeIm]^+$.

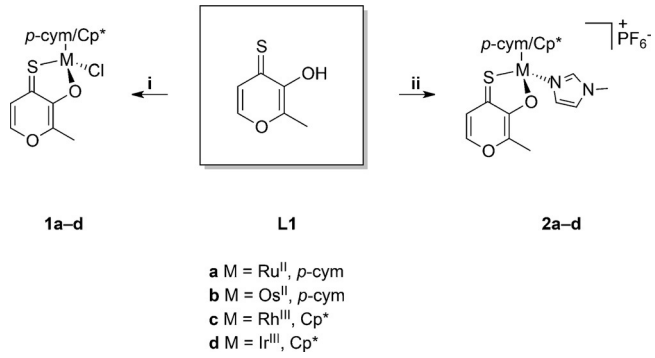

Scheme 1. Overview of synthesized compounds **1a–d** and **2a–d**. i) [(*p*-cym)/(Cp*)$MCl_2]_2$, NaOMe, methanol abs. ii) [(*p*-cym)/(Cp*)M$(MeIm)_2$Cl]Cl, NaOMe, methanol abs., $NaPF_6$.

X-ray diffraction analysis

Single crystals of **1b** and **1c** (Figure 2) as well as of **2a–d** (Figures 3, and Figures S6 and S8 in the Supporting Information) suitable for X-ray diffraction analysis were obtained by precipitation from dichloromethane/*n*-hexane or dichloromethane/diethyl ether. The crystal structure of **1a** has been published previously.[12] All of the complexes adopt the so-called "piano-stool" configuration, whereby the stabilizing aromatic ligand forms the seat and the chelating thiomaltolato ligand as well as the respective leaving group (either chlorido or 1-methylimidazole) constitute the chair legs. Upon coordination of thiomaltol to organometallic fragments, a distorted nonplanar five-membered ring was formed with an O-M-S-C torsion angle ranging from 2.53 to 10.69°. The distortion can be explained by the pronounced difference in bond lengths of the metal ion to the oxygen and sulfur donor atoms [**1a**: 2.080 and 2.373 Å; Ru^{II} maltolato complex: 2.082(3) and 2.108(3) Å,[4] respectively].

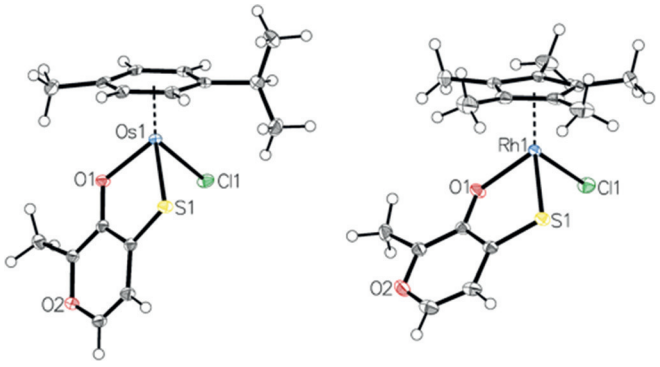

Figure 2. Crystal structures of **1b** and **1c** with ellipsoids drawn at the 50% probability level.

The most salient bond lengths and angles in **1b** and **1c** are summarized in Table 1. Both complexes are representatives of the monoclinic crystal system, with **1b** belonging to the space group $P2_1/c$, whereas **1c** crystallizes in the space group $C2/c$. The M–Cl distances were found to lie in the same range for both the Os^{II} (**1b**) and Rh^{III} (**1c**) complexes [**1b**: 2.4357 Å; **1c**: 2.4222 Å], in good agreement with reported data for **1a** [2.433 Å].[11,12] The C–S bond lengths in **1b** and **1c** were found to be slightly longer than in the free ligand [**1b**: 1.7035 Å, **1c**: 1.7032 Å, **L1**: 1.6770 Å][2] due to the electron-withdrawing effect of the coordinated metal.

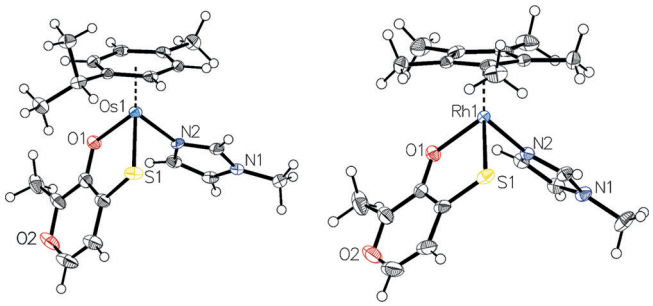

Figure 3. Crystal structures of **2b** and **2c** with ellipsoids drawn at the 50% probability level (PF_6^- counter ion omitted for clarity).

Table 1. Selected bond lengths and angles of Os^{II} and Rh^{III} compounds **1b**, **2b**, **1c**, and **2c**.

Compound	1b	2b	1c	2c
M–S [Å]	2.3775	2.3652	2.3637	2.3399
M–O [Å]	2.0864	2.0754	2.0924	2.0731
M–Cl/–N [Å]	2.4357	2.1011	2.4222	2.0984
C=S [Å]	1.7035	1.7082	1.7032	1.7102
C–O [Å]	1.3172	1.3185	1.3091	1.3130
π-plane centroid distance [Å]	1.6619	1.6684	1.7738	1.7692
ring slippage [Å]	0.039	0.035	0.031	0.033
O-M-S-C [°]	10.69	4.92	9.95	2.53

By comparison of **2a–d**, structural similarity between the Os^{II} and Ru^{II} compounds as well as between the Ir^{III} and Rh^{III} complexes can be observed. Complexes **2a** and **2b** are representatives of the triclinic $P\bar{1}$ space group, whereas compounds **2c** and **2d** belong to the monoclinic space group $P2_1/c$. The metal-azole distance ranges from 2.0981 Å in **2a** to 2.1024 Å in **2d**. The measured metal-azole bond lengths are in good agreement with reported data for the corresponding precursor complex [(*p*-cym)Ru$(MeIm)_2$Cl]Cl [2.121(3) and 2.131(3) Å].[20] Selected bond lengths and angles in the chlorido complexes **1b** and **1c** are also listed in Table 1, along with those in their analogues **2b** and **2c** bearing 1-methylimidazole as the leaving group. Overall, substitution of the chlorido ligands by 1-methylimidazole resulted in slightly shorter distances between the metal center and the *S*,*O*-donor atoms, indicating a higher stability of the attached ligand scaffold. Both pairs of complexes show differences in the M–leaving group bond lengths [**1b**: 2.4357 Å, **2b**: 2.1011 Å; **1c**: 2.4222 Å, **2c**: 2.0984 Å] due to the different donor atoms. Nevertheless, the M–Cl and M–N bond lengths in the investigated complexes are in the same range as those in the Ru^{II} complex RM175 published by Sadler and co-workers.[21] An envelope conformation of the five-membered coordination cycle is apparent in both forms of the Os^{II} and Rh^{III} complexes, but the torsion angle (O-M-S-C) is less pro-

nounced in complexes **2b** and **2c** (4.92° and 2.53°, respectively) compared to their chlorido counterparts **1b** and **1c** (10.69° and 9.95°, respectively), which might be attributed to both the increased steric demand of the 1-methylimidazole ligand and the different donor properties. As expected, slightly shorter π-plane–centroid distances were found for η^6-coordinating moieties compared to the η^5-coordinative bond between the Cp* ligand and the Rh^{III} or Ir^{III} metal centers.

Stability investigations by ESI-MS

The behavior of metal complexes in aqueous media is an important characteristic, since the M–Cl bond is prone to hydrolysis. Aquation is believed to be an important step in the mode of action of this compound class, because the comparatively more reactive aqua complex is assumed to interact with biological targets. Therefore, the stability in aqueous solution was investigated for all of the synthesized organometallics bearing either chlorido (**1a–d**) or 1-methylimidazole (**2a–d**) leaving groups. Samples were prepared according to the procedure described in the Experimental Section and examined after 1, 3, 6, 24, and 48 h of incubation at 37 °C. A general tendency towards increased stability of complexes bearing the 1-methylimidazole leaving group could be discerned among the investigated metal complexes. Overall, immediate cleavage of the chlorido group was observed for **1a–d**, yielding the respective $[M-Cl]^+$ species. Osmium complexes **1b** and **2b** proved to be the most stable in the tested series. Besides the characteristic peak of $[\mathbf{1b}-Cl]^+$ (*m/z* 467.04 ± 0.02, m_{ex} 467.07), the spectrum of compound **2b** showed an additional species with the leaving group 1-methylimidazole still coordinated to the metal center, that is, $[\mathbf{2b}]^+$ (*m/z* 549.09 ± 0.02, m_{ex} 549.12). Ru^{II} complexes **1a** and **2a** behaved similarly to the respective osmium compounds **1b** and **2b**. In accordance with its osmium equivalent **2b**, ruthenium complex **2a** showed a corresponding peak representing the species with the leaving group bound to the metal center during the first 6 h of incubation, that is, $[\mathbf{2a}]^+$ (*m/z* 459.04 ± 0.02, m_{ex} 459.07), besides the peak pertaining to the complex without its leaving group $[\mathbf{2a}-Melm]^+$ (*m/z* 377.01 ± 0.02, m_{ex} 377.02). In contrast to the abovementioned occurrence of an additional peak with the azole leaving group attached to the metal center, no such peak was detected in the mass spectra of the corresponding Ir^{III} and Rh^{III} compounds besides the characteristic $[M-\text{leaving group}]^+$ peaks (**1c**, **2c**: *m/z* 379.01 ± 0.01, m_{ex} 379.02; **1d**, **2d**: *m/z* 469.05 ± 0.02, m_{ex} 469.08). Overall, replacement of the labile chlorido ligand by methylimidazole as an *N*-donor improved the stability of the organometallic complex in aqueous solution, and especially the Ru^{II} and Os^{II} compounds seemed to be more stable under the applied conditions.

Stability of complex 1c and formation equilibrium processes

Due to the different behavior observed in the ESI-MS stability experiments, complex formation equilibrium processes of **1c** were studied in aqueous solution by the combined use of pH-potentiometric, ^{1}H NMR, and UV/Vis titrations in the absence and presence of chloride ions and compared to the reported data for the ruthenium analogue **1a**.[23] The stoichiometry and stability constants of the formed complexes giving the best fits to the experimental data are listed in Table 2.

As chloride ions may possibly coordinate by partly replacing the aqua ligands, the stability constants determined in a chloride-containing medium are regarded as conditional stability constants and are valid only under the given conditions. Thiomaltol can undergo oxidation in the alkaline pH range, and thus anaerobic conditions were applied. According to pH-potentiometric titration curves recorded at a 1:1 metal-to-ligand ratio, proton displacement by the metal ion was complete at a starting pH of around 2 in both experimental setups (I = 0.2 M KCl or KNO_3). Additional signals belonging neither to the methyl protons of the unbound Rh^{III}-Cp* fragment nor to the ligand were detected at this pH by ^{1}H NMR spectroscopy (Figure S9). These findings hampered determination of the stability constant of the mono-ligand complex $[RhCp^*(L)(H_2O)]^+$ denoted as [ML]. Therefore, UV/Vis spectrophotometry was applied

Table 2. Proton dissociation constant (pK_a) of thiomaltol and overall, stepwise, and derived stability constants of its RhCp* complexes in chloride-free and chloride-containing aqueous solutions determined by various methods, and H_2O/Cl^- exchange constant ($\log K$) for the $[ML(H_2O)]^+$ complex {T = 25 °C; I = 0.20 M}.[a]

Constant	Equilibrium	0.2 M KNO_3	0.2 M KCl	Method	Notes
pK_a (HL)	HL⇄H + L	8.16(1)	8.06(1)	pH-metry	–
$\log K$ [ML]	M + L⇄[ML]	> 15.0	> 15.0	UV/Vis (pH 0.7–2)	estimated; = $\log ß$ [ML]
$\log K$ [ML_2H]	[ML] + HL⇄[ML_2H]	4.9(1)	4.9(1)	^{1}H NMR	at pH 2.70 (KNO_3); pH 3.85 (KCl)
$\log ß$ [ML_2H]	M + 2 L + H⇄[ML_2H]	> 28.1	> 28.0	various methods, calculated	= $\log K$ [ML_2H] + $\log K$ [ML] + pK_a (HL)
pK_a [ML_2H]	[ML_2H]⇄[ML_2] + H	6.37(1)	6.33(4)	^{1}H NMR	–
		6.4	6.2	pH-metry, calculated	= $\log ß$ [ML_2H] − $\log ß$ [ML_2]
$\log ß$ [ML_2]	M + 2 L⇄[ML_2]	> 21.7	> 21.7	^{1}H NMR, calculated	= $\log ß$ [ML_2H] − pK_a [ML_2H]
		> 21.6(1)	> 21.8(1)	pH-metry	$\log ß$ [ML] and $\log ß$ [ML_2H] kept constant during the data evaluation
$\log K$ (H_2O/Cl^-)	$[ML(H_2O)]^+ + Cl^- ⇄ [ML(Cl)] + H_2O$	0.95(1)	0.95(1)	UV/Vis	determined at pH 3.1

[a] Charges of the complexes are omitted for simplicity. Standard deviations (SD) are given in parentheses. Hydrolysis products of the organometallic cation: $\log ß$ [M_2H_{-2}] = −11.12, $\log ß$ [M_2H_{-3}] = −19.01 at I = 0.20 M (KCl) and $\log ß$ [M_2H_{-2}] = −8.53, $\log ß$ [M_2H_{-3}] = −14.26 at I = 0.20 M (KNO_3) taken from the literature.[22]

under more dilute conditions in the pH range 0.7–2.0 to force dissociation of the complex. These spectra were found to be identical (Figure S10), suggesting that the complex is still intact in this pH range due to its outstandingly high stability, similar to that of **1a**.[23] Therefore, only a threshold limit could be estimated for $\log\beta$ [ML] (Table 2). It is noteworthy that thiomaltol forms significantly more stable complexes than analogous (*O*,*O*)-hydroxypyrones, with $\log\beta$ values at least six orders of magnitude higher.[21] Deprotonation of $[RhCp^*(L)(H_2O)]^+$ was observed at pH > 6, leading to precipitation of the product (Figure 4).

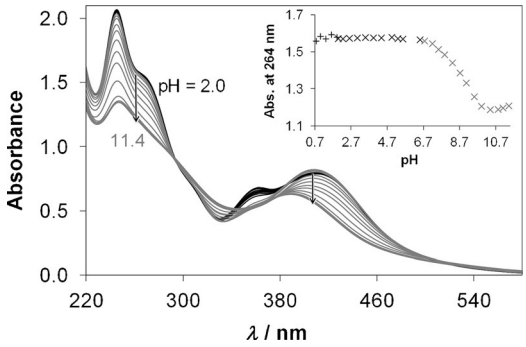

Figure 4. UV/Vis spectra recorded for the $[RhCp^*(H_2O)_3]^{2+}$–thiomaltol (1:1) system in the pH range 2.0–11.4. The inset shows the pH-dependence of absorbance values at 264 nm at pH > 2 (×) and in the pH range 0.7–2.0 using individual samples (+) {c_L = 48 μM; c_M = 48 μM; T = 25 °C; I = 0.20 M (KCl/HCl); l = 2 cm}.

The speciation in the RhCp*-thiomaltol system was found to be different and more complicated in the presence of excess ligand compared to the complexes of other types of bidentate *O*,*O*-, *O*,*N*-, or *N*,*N*-ligands,[21–23] since the latter form exclusively mono-ligand [ML] and [ML(OH)] complexes in aqueous solution. Careful analysis of the ^{1}H NMR spectra recorded at various metal-to-ligand ratios revealed the formation of bis-ligand complexes of thiomaltol, besides the respective species [ML], in which an additional thiomaltol ligand coordinates in a monodentate fashion through its thio group (Scheme S1 and Figures S11 and S12). Similar mixed coordination modes have been reported for the Ru^{II}(*p*-cym) complexes of hydroxypyr(idin)ones.[23,24] The Cl^-/H_2O exchange process was found to be fast (Figure S13) and the obtained $\log K$ (H_2O/Cl^-) of 0.95 is similar to those obtained for the RhCp* complexes of hydroxypyr(idin)ones with an *O*,*O*-donor set (maltol: 1.17, allomaltol: 1.38,[22] deferiprone: 0.78,[25] and the Ru^{II}(*p*-cym) complex of thioallomaltol: 0.71[23]), although it is considerably lower than the values obtained for the biologically inactive complexes with *N*,*N*-donor ligands 2,2′-bipyridine or ethylenediamine.[26]

Investigation of amino acid interaction by ESI-MS

In order to acquire more detailed information about the behavior of the synthesized complexes in biological media and with regard to possible binding partners on entering the body by intravenous administration, their reactivity towards the amino acids glycine, L-histidine, and L-cysteine was tested. As previously demonstrated in the literature,[13] in the presence of amino acids or proteins such as ubiquitin, ruthenium(II) (thio)pyr(id)one compounds react with these molecules by cleavage of the ligand scaffold, forming adducts of the form [(*p*-cym)Ru+Ub/amino acid]$^+$. Whereas this effect is observed to a great extent within the first few hours in the case of *O*,*O*-coordinating ligands, the thiomaltolato complex was found to persist for longer in the presence of the tested biomolecules. Only after 24 h of incubation were the first biomolecule adducts and ligand release detected. To investigate the change in stability imparted by the introduction of the 1-methylimidazole leaving group, the two ruthenium compounds **1a** and **2a** as well as the two rhodium complexes **1c** and **2c** were chosen. Samples were prepared as described in the Experimental Section. Investigation of compound **1a** revealed the formation of L-histidine (His) adducts after 6 h [**1a**−Cl+His]$^+$ (m/z 532.10 ± 0.02, m_{ex} 532.08). After 24 h of incubation, the thiomaltol ligand was cleaved, giving rise to His- as well as L-cysteine (Cys)-containing adducts [(*p*-cym)Ru+His]$^+$ (m/z 390.05 ± 0.02, m_{ex} 390.08) and [(*p*-cym)Ru+Cys]$^+$ (m/z 356.01 ± 0.02, m_{ex} 356.03). In general, the formation of L-histidine adducts seems to be favored in the recorded spectra of **1a** compared to L-cysteine coordination. In the spectrum recorded after 48 h, a small amount of a ligand-bearing dimeric species [(*p*-cym)$_2$Ru$_2$**L1**(OH)$_2$(CH$_3$OH)]$^+$ (m/z 678.10, m_{ex} 678.06) was detected. In the case of **2a**, increased stability compared to its chlorido analogue can be inferred since the intact compound [**2a**−MeIm]$^+$ was detected throughout the whole incubation period. During the first 6 h of incubation, only two species could be observed, namely [**2a**−MeIm]$^+$ (m/z 377.01, m_{ex} 377.02) and [**2a**]$^+$ (m/z 459.04 ± 0.02, m_{ex} 459.07). After 6 h, the adduct [**2a**−MeIm+His]$^+$ (m/z 532.10 ± 0.02, m_{ex} 532.08) was found besides the two intact compound species described above. Cleavage of the ligand had only occurred to a very small extent after 24 h, leading to the species [(*p*-cym)Ru+His]$^+$ and [(*p*-cym)Ru+Cys]$^+$. Equal amounts of three species were found after 48 h of incubation: [**2a**−MeIm]$^+$ (m/z 377.10, m_{ex} 377.02), [(*p*-cym)Ru+His]$^+$ (m/z 390.05 ± 0.02, m_{ex} 390.08), and the ligand-bearing dimeric species [(*p*-cym)$_2$Ru$_2$**L1**(OH)$_2$(CH$_3$OH)]$^+$ (m/z 678.10, m_{ex} 678.06). Enhanced stability was also observed for the 1-methylimidazole-bearing organorhodium complex **2c** compared to the chlorido analogue **1c**. After just 3 h, **1c** had started to form the [(Cp*)Rh+Cys] adduct (m/z 358.01 ± 0.02, m_{ex} 358.03), which became the predominant species at the end of the incubation period along with [(Cp*)Rh+His]$^+$ (m/z 392.05 ± 0.02, m_{ex} 392.08). In contrast, **2c** resisted ligand cleavage induced by amino acid binding for more than 24 h, and this was found only to a very small degree thereafter. Therefore, substitution of the labile chlorido group by 1-methylimidazole is a successful strategy to increase the stability of the organometallic thiomaltol complexes, enabling them to reach tumor tissue intact, in contrast to the respective chlorido analogues or complexes with comparable *O*,*O*-coordinating ligands.

pH-Dependent cleavage of the 1-methylimidazole leaving group

Given the indication of a characteristically lowered pH level by 0.5 to 1 units in tumor tissues, depending on the size and tumor type,[14,27] the behavior of the synthesized compounds under pH variation was of great interest. Thus, pH-dependent stability studies of complexes **2a–d** were conducted by ^{1}H NMR measurements in order to gain knowledge about the formation of the respective aqua species upon pH-induced cleavage of the coordinated azole ligand. In general, all four complexes behaved very similarly on varying the pH. Compounds **2a–d** were dissolved in D_2O, and pD values were adjusted by the addition of DCl and NaOD over a wide pH range (2.5–12). The obtained pD values were converted to the corresponding pH values according to Equation (2), as described in the Experimental Section. The shifts of the 1-methylimidazole and arene signals were monitored, and in the case of compounds **2a** and **2b** the formation of the aqua species led to an additional set of signals corresponding to the aromatic cymene protons. The intact complexes exhibited four signals corresponding to the four aromatic protons, whereas the replacement of the leaving group by a water molecule led to the appearance of two broad peaks in the aromatic region. Another indication of the formation of the aqua species was provided by the emergence of peaks attributable to the free 1-methylimidazole ligand. These signals were also used to assess the behavior of compounds **2c** and **2d** under pH variation. Formation of the respective aqua species could be observed starting at pH 6, until it became the predominant species at values around pH 3.5 (Figure 5). Complexes **2a–d** showed very high stabilities under alkaline conditions and no degradation products could be detected at up to pH 11 (Table S15 in the Supporting Information). Based on these findings, it can be assumed that under the hypoxic conditions of the tumor microenvironment, the leaving group may be partly cleaved to form the corresponding more reactive aqua complex.

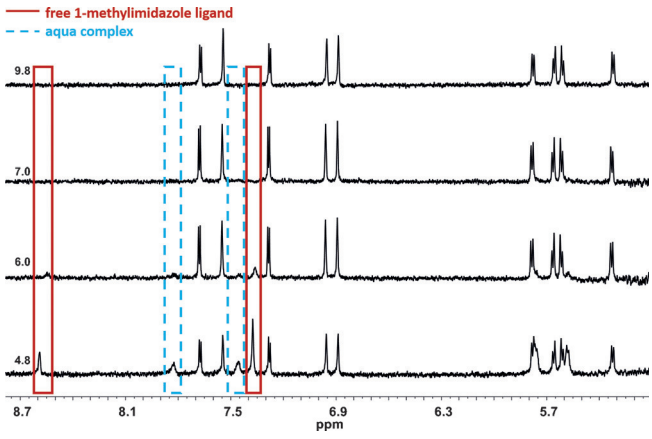

Figure 5. ^{1}H NMR spectra of compound **2a** in D_2O at different pH values (4.8–9.8).

Cytotoxicity

Analogous maltol and allomaltol Rh^{III} Cp* complexes were recently reported to show moderate anticancer activity against the human cancer cell lines CH1/PA-1 (ovarian teratocarcinoma), SW480 (colon carcinoma), and A549 (non-small cell lung carcinoma).[22] The cytotoxicity of complex **1a** in CH1/PA-1 and SW480 cells has been reported previously, whereas data pertaining to A549 cells have been determined for the first time here. The thiomaltolato complexes **1a–2d** and the respective free thiomaltol ligand **L1** were tested against the same human cancer cell lines. In general, all complexes showed IC_{50} values in the low micromolar to submicromolar range (Table 3), and are therefore far more potent than their pyrone analogues.[19] Surprisingly, even the free ligand **L1** proved to be highly cytotoxic against the tested cell lines and overall it seems that thiomaltol is the activity-determining factor for this class of complexes. In general, the chlorido complexes **1b–d** showed similar activities, but were found to be more active than **1a**. The two different monodentate leaving groups have only a marginal impact on the activity because the supposed activation of the organometallics requires release of the leaving group. In contrast to the chlorido complexes **1a–d**, a small effect of the metal center on the cytotoxicity was observed for complexes **2a–d**. In particular, the Ru^{II} and Rh^{III} representatives **2a** and **2c** were found to be more active than their chlorido counterparts by factors of up to 3.7, depending on the cell line. The P-glycoprotein (P-gp) expressing cell line SW480 proved to be as sensitive to most of the complexes as the broadly chemosensitive CH1/PA-1 cell line, whereas IC_{50} values against the more chemoresistant cell line A549 were up to ten-fold higher. This feature of the investigated set of compounds is in sharp contrast to the well-established Pt^{II} complexes, such as cisplatin, which is about 20 times less potent against SW480 than against CH1 cells (data taken from the literature).[28] As SW480 cells express low levels of ABCB1 (P-gp)[29] and A549 cells overexpress multiple transporters of the ABC family (e.g., ABCC2 (MRP2), ABCC4 (MRP4), ABCC5 (MRP5)),[30–32] investigations concerning the influence of such transporters on the activity of organometallic complexes will be a subject of future research.

Topoisomerase IIα inhibition

Topoisomerase IIα is an essential nuclear enzyme involved in almost every aspect of DNA functionality: replication, transcription, recombination, and chromosome condensation. Topoisomerase IIα is a primary target for active anticancer drugs. Several studies have revealed that clinically active drugs that target topoisomerase IIα generate enzyme-mediated DNA damage.[35–37] The compounds reported here were studied by a DNA relaxation assay for their topoisomerase IIα inhibitory properties. Complexes **1a–d** and **2b–d** displayed inhibitory capacity at a concentration of 10 μM. In addition, the Ru^{II} complex **2a** proved to be a potent enzyme inhibitor at just 2.5 μM, which is in contrast to the comparatively high IC_{50} values of **2a** within the series of 1-methylimidazole-substituted compounds. In comparison, the corresponding ligand **L1** did not inhibit the

Table 3. Inhibition of cancer cell growth by the tested substances in three human cancer cell lines; 50% inhibitory concentrations (means ± standard deviations), obtained by MTT assay (exposure time: 96 h).

Compound	M	IC_{50} value ± SD A549	CH1/PA-1	SW480
1a	Ru^{II}	12±4	3±1	11±1
1b	Os^{II}	4.1±0.3	2.0±0.2	2.0±0.2
1c	Rh^{III}	5.9±0.8	1.0±0.1	1.0±0.1
1d	Ir^{III}	5.8±1.7	0.57±0.03	0.7±0.1
2a	Ru^{II}	7.1±1.6	2.6±0.5	3.0±0.2
2b	Os^{II}	6.6±0.4	3.0±0.4	3.4±0.7
2c	Rh^{III}	2.6±0.6	0.9±0.2	0.48±0.03
2d	Ir^{III}	3.4±0.8	0.6±0.1	0.67±0.04
L1	–	1.3±0.8	0.52±0.04	0.55±0.31
cisplatin[a]	Pt^{II}	1.3±0.4	0.16±0.03	3.5±0.3
NKP-1339[b]	Ru^{III}	156±11	50±6	62±9

[a] See ref. [33]. [b] See ref. [34].

enzyme appreciably at the applied concentrations. Figures 6 and 7 show that the tested compounds did not act as topoisomerase poisons, since the linear DNA band was only present in the positive control, whereby the action of the poison generates a high level of TopoII–DNA covalent complexes, resulting in the accumulation of DNA double-strand breaks. It is more likely that the tested complexes act as catalytic inhibitors, blocking the ATP-binding site of the enzyme, preventing binding of the enzyme to DNA or the release of DNA.[36] Similar behavior in the presence of topoisomerase IIα was observed for Ru^{II} and Rh^{III} complexes of comparable architecture, with inhibitory effects on topoisomerase IIα starting at concentrations between 5 and 20 μM.[38,39]

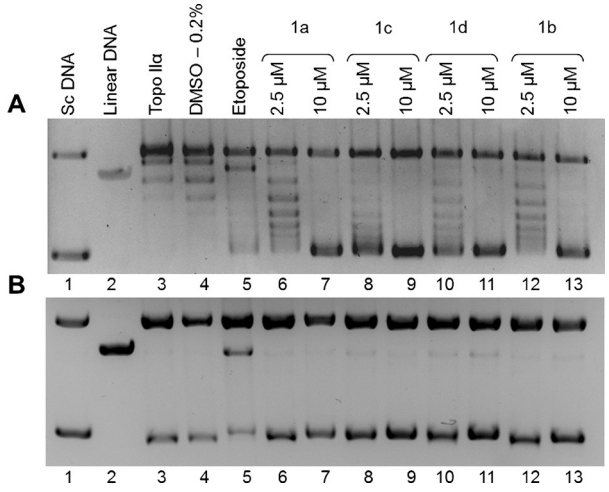

Figure 6. Topoisomerase IIα-inhibitory capacities of complexes **1a–d** determined by the plasmid DNA relaxation assay. Supercoiled and linear DNA used as references (lanes 1 and 2, respectively); relaxed DNA bands (lane 3) indicating intact enzyme activity; DMSO control corresponding to maximum content in test compound solutions (lane 4); linear DNA band induced by 0.8 mM etoposide (positive control, lane 5). Lanes 6–13 display the reaction of topoisomerase IIα with supercoiled DNA in the presence of the test compounds. The top gel (A) was post-stained and the bottom gel (B) was pre-stained with 0.7 μg mL^{-1} ethidium bromide.

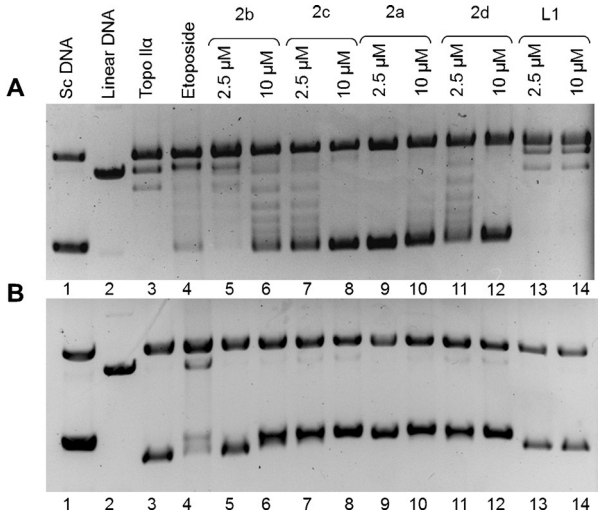

Figure 7. Topoisomerase IIα-inhibitory capacities of complexes **2a–d** and ligand **L1** determined by the plasmid DNA relaxation assay. Supercoiled and linear DNA used as references (lanes 1 and 2, respectively); relaxed DNA bands (lane 3) indicating intact enzyme activity; linear DNA band induced by 0.8 mM etoposide (positive control, lane 4). Lanes 5–14 display the reaction of topoisomerase IIα with supercoiled DNA in the presence of the test compounds. The top gel (A) was post-stained and the bottom gel (B) was pre-stained with 0.7 μg mL^{-1} ethidium bromide.

Cell cycle and ROS studies

Since the tested compounds exhibited properties of topoisomerase IIα catalytic inhibitors and may disrupt some essential processes, such as transcription and replication, we examined the changes in cell cycle distribution by flow cytometry using propidium iodide staining. As illustrated in Figure 8, the effects on SW480 cells after 12 h of treatment were pronounced: the highest S-phase accumulations were seen for ruthenium(II) and iridium(III) complexes (**2a** and **2d**), with an increase to around 45% at a concentration of 20 μM. Detailed cell cycle distribution data are summarized in Table S16.

Furthermore, we investigated whether the thiomaltol-based organometallic complexes could alter the levels of reactive oxygen species (ROS) in cancer cells (Figure 9) by means of a 2′,7′-dichlorofluorescein diacetate (DCF-DA) assay. It has been reported by Sadler and co-workers that certain organoruthenium complexes are able to catalytically reduce GSH levels, leading to an increase of ROS formation.[40,41] Our complexes were studied with regard to their potential to raise cellular ROS levels, and the obtained data indicated slight increases in ROS levels for the rhodium(III) 1-methylimidazole-substituted complex **2c** by a factor of 2.7 and for the iridium(III) 1-methylimidazole-substituted complex **2d** by a factor of 1.5, but no discernible effect for the other tested substances. Table S17 shows the detailed ROS generation data. Based on these findings, the formation of ROS does not convincingly contribute to the cytotoxicity of thiopyrone-based organometallics.

In summary, these results suggest that topoisomerase IIα may be a target for organometallic thiomaltol-based complexes, whereas the free ligand is devoid of enzyme inhibitory properties at the same concentration. None of these com-

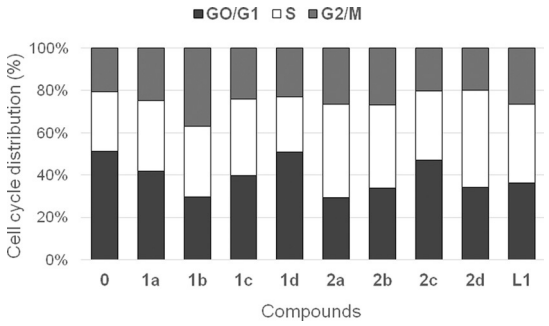

Figure 8. Concentration-dependent impact of thiomaltol-based organometallic complexes **1a–d** and **2a–d** and the corresponding ligand **L1** at a concentration of 20 μM on the cell-cycle distribution of SW480 cells after 12 h of continuous exposure.

pounds act as topoisomerase IIα poisons. Cell cycle distribution analyses revealed a moderate increase of the S-phase fraction upon exposure to the organometallics, consistent with inhibition of this key enzyme. In addition, ROS production appears unlikely to play a central role in the cellular response to treatment with these metal complexes. A general overview of cytotoxicity, enzyme inhibition, cell cycle perturbations, and ROS activation of thiomaltol-based complexes suggests that metal coordination has a distinct impact on the biological activity.

Conclusions

Thiomaltol-based organometallics are characterized by increased stability compared to their pyrone analogues, making them more suitable for metallodrug development. In this work, thiomaltol-bearing complexes with Ru^{II}, Os^{II}, Rh^{III}, and Ir^{III}, bearing either 1-methylimidazole or chloride as leaving group, have been synthesized, and the effects of different metal centers and leaving groups on the physicochemical and biological properties have been investigated. The acquired data implied that the introduction of 1-methylimidazole as a leaving group substantially increases the stability in aqueous solution and shields the complex from coordination of biomolecules that would lead to ligand release. This modification may allow accumulation of the intact complexes and controlled activation at the lower pH values within tumor tissues. The synthesized substances were tested against three different human cancer cell lines with regard to their anticancer potential, and promising IC_{50} values in the low μM to sub-μM range were observed. Whereas the complexes proved to be good topoisomerase IIα inhibitors, the thiomaltol ligand alone proved to be inactive and the tested substances were evidently not poisons to the enzyme. The complexes induce changes in the cell cycle, such that an accumulation of cells in the S-phase was observed. According to these findings, topoisomerase IIα might be a possible target of organometallic thiopyrones. Based on the data presented herein, thiomaltol-based organometallic complexes can be regarded as promising candidates for the further development of anticancer agents with topoisomerase IIα inhibitory properties.

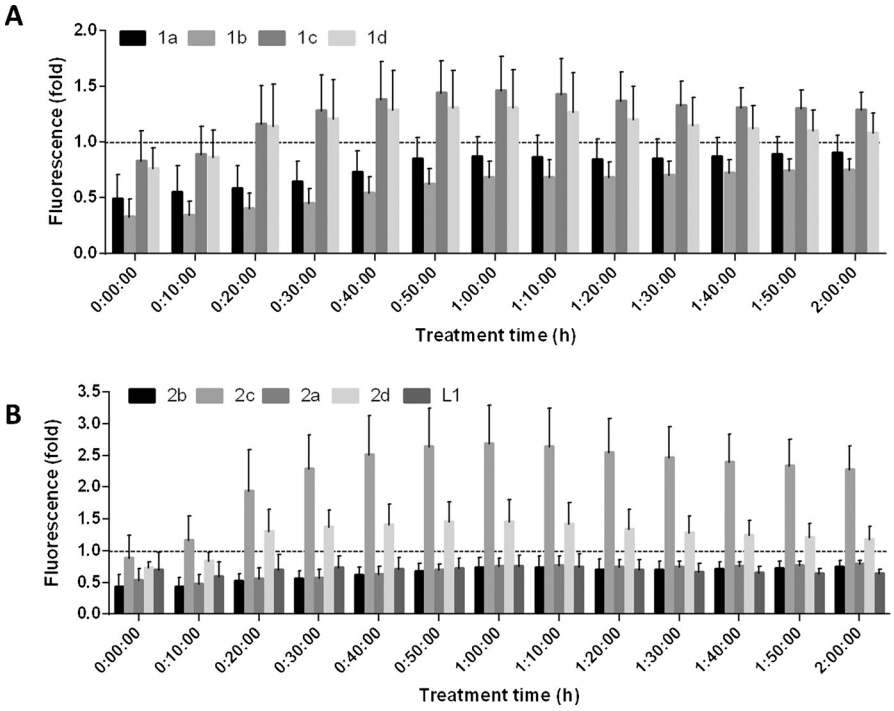

Figure 9. Generation of ROS as indicated by DCF-DA microplate assay using complexes: A) **1a–d**, B) **2a–d** and **L1**. Mean ± standard deviation is plotted for three replicates at each concentration. The relative fluorescence unit (RFU) for all samples was normalized to the RFU of stained untreated control (indicated by a dashed line).

Experimental Section

Materials

The dimeric metal precursors $[Ru(p\text{-cym})Cl_2]_2$, $[Os(p\text{-cym})Cl_2]_2$, $[Rh(Cp^*)Cl_2]_2$, and $[Ir(Cp^*)Cl_2]_2$ were prepared according to literature procedures.[16,42,43] The solvents used were purchased from commercial sources and distilled prior to use. Methanol (HPLC grade, Fisher) and Millipore water (MilliQ H_2O; 18.2 MΩ; Synergy 185 UV Ultrapure Water System, Millipore) were used for mass spectrometric investigations and titrations. 3-Hydroxy-2-methyl-4*H*-pyran-4-one (≥99.0%, Aldrich), Lawesson's reagent (99%, Acros), osmium(VIII) tetroxide (Johnson Matthey), hydrazine dihydrochloride (>98%, Aldrich), hydrochloric acid (37%, Acros), α-terpinene (90%, Acros), iridium(III) chloride (Johnson Matthey), 1,2,3,4,5-pentamethylcyclopentadiene (95%, Aldrich), ruthenium(III) chloride hydrate (Johnson Matthey), rhodium(III) chloride hydrate (Johnson Matthey), 1-methylimidazole (99%, Aldrich), sodium methoxide (ca. 95%, Fluka), sodium hexafluorophosphate (98%, Aldrich), glycine (Merck), L-cysteine (Fluka), and L-histidine (Merck) were purchased and used as received. KCl, KNO_3, $AgNO_3$, HCl, HNO_3, KOH, and 4,4-dimethyl-4-silapentane-1-sulfonic acid (DSS) were purchased from Sigma–Aldrich in puriss quality. NMR spectra were recorded at 25 °C on a Bruker Avance III™ 500 MHz FT-NMR spectrometer. ^{1}H NMR spectra were measured at 500.10 MHz and ^{13}C NMR spectra at 125.75 MHz from solutions in deuterated dimethyl sulfoxide, methanol, or chloroform. DCl (35%) and NaOD (4%) were used for the stability investigation of complexes at varying pH values. CHNS elemental analyses were carried out on a Eurovector EA3000 elemental analyzer in the microanalytical laboratory of the University of Vienna.

General procedures

General procedure for the synthesis of Os^{II}/Ru^{II} cymene and Ir^{III}/Rh^{III} Cp* chlorido complexes: Ligand **L1** (1 equiv) and sodium methoxide (1.1 equiv) were dissolved in absolute methanol and the solution was stirred for 15 min under inert conditions. The yellow solution was then transferred to a Schlenk flask containing the respective dimer (0.45 equiv), whereupon it underwent an immediate color change. The mixture was stirred under argon atmosphere at 40 °C for 1.5 h. Thereafter, the solvent was evaporated under reduced pressure and the residue was redissolved in dichloromethane. Filtration allowed the removal of reaction by-products, and the filtrate was concentrated in vacuo. Precipitation from *n*-hexane afforded the pure product in good to excellent yields (63–92%).

General procedure for the synthesis of Os^{II}/Ru^{II} cymene and Ir^{III}/Rh^{III} Cp* 1-methylimidazole complexes: The ligand **L1** (1 equiv) and sodium methoxide (1.1 equiv) were dissolved in absolute methanol and the solution was stirred for 15 min under inert conditions. The yellow solution was then transferred to a Schlenk flask containing the respective precursor complex (0.9 equiv), whereupon it underwent an immediate color change. The mixture was stirred under argon atmosphere at 40 °C for 4–48 h, depending on the relevant precursor metal complex. In order to separate the desired product from uncharged side products, sodium hexafluorophosphate was added and the resulting mixture was stirred for a further 1 h at room temperature. Thereafter, the solvent was evaporated under reduced pressure and the residue was taken up in dichloromethane. Filtration allowed the removal of reaction by-products and the filtrate was concentrated in vacuo. Precipitation from dichloromethane/diethyl ether afforded the pure product in low to moderate yields (32–52%).

[Chlorido(2-methyl-3-(oxo-κ*O*)-pyran-4(1*H*)-thionato-κ*S*)(η^6-*p*-cymene)osmium(II)] (1b): The reaction was performed according to the general procedure for chlorido complexes using **L1** (60 mg, 0.42 mmol, 1 equiv), sodium methoxide (25 mg, 0.46 mmol, 1.1 equiv), and $[(\eta^6\text{-}p\text{-cym})Os^{II}Cl_2]_2$ (150 mg, 0.19 mmol, 0.45 equiv). The product was isolated as a red solid. Yield: 135 mg (71%). ^{1}H NMR (500.10 MHz, $CDCl_3$, 25 °C): $\delta = 1.28$ (d, $^3J(H,H) = 7$ Hz, 6H; $CH_{3,cym}$), 2.33 (s, 3H; $CH_{3,cym}$), 2.51 (s, 3H; CH_3), 2.67–2.75 (m, 1H; CH_{cym}), 5.62 (br s, 2H; CH_{Ar}), 5.82 (br s, 2H; CH_{Ar}), 7.26 (d, $^3J(H,H) = 5$ Hz, 1H; CH-5), 7.43 ppm (d, $^3J(H,H) = 5$ Hz, 1H; CH-6); ^{13}C NMR (125.75 MHz, $CDCl_3$, 25 °C): $\delta = 15.4$ (CH_3), 18.5 ($CH_{3,cym}$), 22.4 & 22.9 (2$CH_{3,cym}$), 31.4 (CH_{cym}), 73.2 (CH_{Ar}), 75.0 (CH_{Ar}), 90.3 ($C_{q,Ar}$), 90.8 ($C_{q,Ar}$), 120.7 (CH-5), 144.6 (CH-6), 153.5 (C_q-2), 168.5 (C_q-3), 181.9 ppm (C_q-4); elemental analysis calcd (%) for $C_{16}H_{19}ClO_2OsS$: C 38.35, H 3.82, S 6.40; found: C 38.48, H 3.98, S 6.30.

[Chlorido(2-methyl-3-(oxo-κ*O*)-pyran-4(1*H*)-thionato-κ*S*)(η^5-1,2,3,4,5-pentamethylcyclopentadienyl)rhodium(III)] (1c): The reaction was performed according to the general procedure for chlorido complexes using **L1** (78 mg, 0.55 mmol, 1 equiv), sodium methoxide (32 mg, 0.60 mmol, 1.1 equiv), and $[(\eta^5\text{-}Cp^*)Rh^{III}Cl_2]_2$ (150 mg, 0.24 mmol, 0.45 equiv). The product was isolated as a red solid. Yield: 189 mg (95%). ^{1}H NMR (500.10 MHz, $CDCl_3$, 25 °C): $\delta =$ 1.75 (s, 15H; CH_{3,Cp^*}), 2.45 (s, 3H; CH_3), 7.17 (d, $^3J(H,H) = 5$ Hz, 1H; CH-5), 7.45 ppm (d, $^3J(H,H) = 5$ Hz, 1H; CH-6); ^{13}C NMR (125.75 MHz, $CDCl_3$, 25 °C): $\delta = 9.0$ (CH_{3,Cp^*}), 15.5 (CH_3), 94.0 (d, $^1J(Rh,C) = 10$ Hz; C_{Cp^*}), 120.9 (CH-5), 143.7 (CH-6), 153.7 (C_q-2), 165.5 (C_q-3), 180.0 ppm (C_q-4); elemental analysis calcd (%) for $C_{16}H_{19}ClO_2RhS{\cdot}0.5\,H_2O$: C 45.46, H 4.77, S 7.59; found: C 45.35, H 4.92, S 7.70.

[Chlorido(2-methyl-3-(oxo-κ*O*)-pyran-4(1*H*)-thionato-κ*S*)(η^5-1,2,3,4,5-pentamethylcyclopentadienyl)iridium(III)] (1d): The reaction was performed according to the general protocol for chlorido complexes using **L1** (60 mg, 0.42 mmol, 1 equiv), sodium methoxide (25 mg, 0.46 mmol, 1.1 equiv), and $[(\eta^5\text{-}Cp^*)Ir^{III}Cl_2]_2$ (150 mg, 0.19 mmol, 0.45 equiv). The product was isolated as a red solid. Yield: 165 mg (86%). ^{1}H NMR (500.10 MHz, $CDCl_3$, 25 °C): $\delta = 1.78$ (s, 15H; CH_{3,Cp^*}), 2.52 (s, 3H; CH_3), 7.18 (d, $^3J(H,H) = 5$ Hz, 1H; CH-5), 7.45 ppm (d, $^3J(H,H) = 5$ Hz, 1H; CH-6); ^{13}C NMR (125.75 MHz, $CDCl_3$, 25 °C): $\delta = 8.9$ (CH_{3,Cp^*}), 15.5 (CH_3), 86.2 (d, $^1J(Ir,C) = 10$ Hz; C_{Cp^*}), 121.8 (CH-5), 143.7 (CH-6), 154.2 (C_q-2), 167.7 (C_q-3), 179.4 ppm (C_q-4); elemental analysis calcd (%) for $C_{16}H_{20}ClIrO_2S{\cdot}H_2O$: C 36.81, H 4.25, S 6.14; found: C 36.72, H 3.98, S 6.43.

[(1-Methylimidazole-κ*N*^{3})(2-methyl-3-(oxo-κ*O*)-pyran-4(1*H*)-thionato-κ*S*)(η^6-*p*-cymene)ruthenium(II)] hexafluorophosphate (2a): The reaction was performed according to the general procedure for the synthesis of metal complexes with 1-methylimidazole as leaving group, using ligand **L1** (51 mg, 0.354 mmol, 1 equiv), sodium methoxide (21 mg, 0.390 mmol, 1.1 equiv), and $[(\eta^6\text{-}p\text{-cym})Ru^{II}(MeIm)_2Cl]Cl$ (150 mg, 0.319 mmol, 0.9 equiv). The mixture was stirred at 40 °C for 40 h, affording the desired product after work-up as orange crystals. Yield: 79 mg (41%). ^{1}H NMR (500.10 MHz, [D$_4$]methanol, 25 °C): $\delta =$ 1.25–1.28 (m, 6H; $CH_{3,cym}$), 2.07 (s, 3H; $CH_{3',cym}$), 2.50 (s, 3H; CH_3), 2.67–2.76 (m, 1H; CH_{cym}), 3.72 (s, 3H; $CH_{3,MeIm}$), 5.46–5.55 (m, 2H; CH_{Ar}), 5.69–5.75 (m, 2H; CH_{Ar}), 6.95 (s, 1H; CH_{MeIm}), 7.07 (s, 1H; CH_{MeIm}), 7.28 (d, $^3J(H,H) = 5$ Hz, 1H; CH-5), 7.70 (s, 1H; CH_{MeIm}), 7.75 ppm (d, $^3J(H,H) = 5$ Hz, 1H; CH-6); ^{13}C NMR (125.75 MHz, [D$_4$]methanol, 25 °C): $\delta = 13.7$ (CH_3), 16.8 ($CH_{3,cym}$), 21.0 & 21.7 (2$CH_{3,cym}$), 30.9 (CH_{cym}), 33.2 ($CH_{3,MeIm}$), 81.1 & 82.6 (2CH_{Ar}), 83.5 & 84.6 (2CH_{Ar}), 100.2 ($C_{q,Ar}$), 103.0 ($C_{q,Ar}$), 119.8 (CH-5), 121.6 (CH_{MeIm}), 129.5 (CH_{MeIm}), 139.8 (CH_{MeIm}), 145.9 (C-6), 154.1 (C_q-2), 164.9 (C_q-3), 180.1 ppm (C_q-4); elemental analysis calcd

(%) for $C_{20}H_{25}F_6N_2O_2PRuS$: C 39.80, H 4.18, N 4.64, S 5.31; found: C 39.81, H 4.14, N 4.67, S 5.23.

[(1-Methylimidazole-κ*N*^{3})(2-methyl-3-(oxo-κ*O*)-pyran-4(1*H*)-thionato-κ*S*)(η^6-*p*-cymene)osmium(II)] hexafluorophosphate (2b): The reaction was performed according to the general procedure for the synthesis of metal complexes with 1-methylimidazole as leaving group, using ligand **L1** (43 mg, 0.298 mmol, 1 equiv), sodium methoxide (18 mg, 0.328 mmol, 1.1 equiv), and [(η^6-*p*-cym)Os^{II}(MeIm)$_2$Cl]Cl (150 mg, 0.268 mmol, 0.9 equiv). The mixture was stirred at 40 °C for 48 h affording the desired product after work-up as red-brown crystals. Yield: 75 mg (40 %). ^{1}H NMR (500.10 MHz, [D$_4$]methanol, 25 °C): δ = 1.22–1.28 (m, 6H; $CH_{3,cym}$), 2.13 (s, 3H; $CH_{3,cym}$), 2.53 (s, 3H; CH_3), 2.57–2.66 (m, 1H; CH_{cym}), 3.74 (s, 3H; $CH_{3,MeIm}$), 5.68–5.77 (m, 2H; CH_{Ar}), 5.85–5.94 (m, 2H; CH_{Ar}), 6.94 (s, 1H; CH_{MeIm}), 7.04 (s, 1H; CH_{MeIm}), 7.36 (d, ^3J(H,H) = 5 Hz, 1H; CH-5), 7.72 (s, 1H; CH_{MeIm}), 7.75 ppm (d, ^3J(H,H) = 5 Hz, 1H; CH-6); ^{13}C NMR (125.75 MHz, [D$_4$]methanol, 25 °C): δ = 13.8 (CH_3), 16.7 ($CH_{3,cym}$), 21.3 & 22.1 (2$CH_{3,cym}$), 31.1 (CH_{cym}), 33.2 ($CH_{3,MeIm}$), 71.7 & 73.3 (2CH_{Ar}), 74.9 & 76.2 (2CH_{Ar}), 92.0 ($C_{q,Ar}$), 93.3 ($C_{q,Ar}$), 120.2 (CH-5), 121.4 (CH_{MeIm}), 128.9 (CH_{MeIm}), 139.5 (CH_{MeIm}), 146.7 (CH-6), 154.6 (C_q-2), 167.5 (C_q-3), 180.7 ppm (C_q-4); elemental analysis calcd (%) for $C_{20}H_{25}F_6N_2O_2OsPS$: C 34.68, H 3.64, N 4.04, S 4.63; found: C 34.69, H 3.56, N 4.02, S 4.54.

[(1-Methylimidazole-κ*N*^{3})(2-methyl-3-(oxo-κ*O*)-pyran-4(1*H*)-thionato-κ*S*)(η^5-1,2,3,4,5-pentamethylcyclopentadienyl)rhodium(III)] hexafluorophosphate (2c): The reaction was performed according to the general procedure for the synthesis of metal complexes with 1-methylimidazole as leaving group, using ligand **L1** (50 mg, 0.352 mmol, 1 equiv), sodium methoxide (21 mg, 0.387 mmol, 1.1 equiv), and [(η^5-Cp*)Rh^{III}(MeIm)$_2$Cl]Cl (150 mg, 0.317 mmol, 0.9 equiv). The mixture was stirred at 40 °C for 4 h, affording the desired product after work-up as orange crystals. Yield: 100 mg (52 %). ^{1}H NMR (500.10 MHz, [D$_4$]methanol, 25 °C): δ = 1.70 (s, 15H; $CH_{3,Cp*}$), 2.53 (s, 3H; CH_3), 3.77 (s, 3H; $CH_{3,MeIm}$), 7.02 (br s, 1H; CH_{MeIm}), 7.17 (br s, 1H; CH_{MeIm}), 7.27 (d, ^3J(H,H) = 5 Hz, 1H; CH-5), 7.79 ppm (br s, 2H; CH_{MeIm} & CH-6); ^{13}C NMR (125.75 MHz, [D$_4$]methanol, 25 °C): δ = 7.5 ($CH_{3,Cp*}$), 13.7 (CH_3), 33.5 ($CH_{3,MeIm}$), 95.3 (d, ^1J(Rh,C) = 10 Hz; C_{Cp*}), 120.5 (CH-5), 122.1 (CH_{MeIm}), 123.1 (CH_{MeIm}), 129.1 (CH_{MeIm}), 146.7 (CH-6), 154.8 (C_q-2), 164.8 (C_q-3), 179.3 ppm (C_q-4); elemental analysis calcd (%) for $C_{20}H_{26}F_6N_2O_2PRhS$: C 39.62, H 4.32, N 4.62, S 5.29; found: C 39.66, H 4.33, N 4.56, S 5.30.

[(1-Methylimidazole-κ*N*^{3})(2-methyl-3-(oxo-κ*O*)-pyran-4(1*H*)-thionato-κ*S*)(η^5-1,2,3,4,5-pentamethylcyclopentadienyl)iridium(III)] hexafluorophosphate (2d): The reaction was performed according to the general procedure for the synthesis of metal complexes with 1-methylimidazole as leaving group, using ligand **L1** (42 mg, 0.296 mmol, 1 equiv), sodium methoxide (18 mg, 0.326 mmol, 1.1 equiv), and [(η^6-Cp*)Ir^{III}(MeIm)$_2$Cl]Cl (150 mg, 0.267 mmol, 0.9 equiv). The mixture was stirred at 40 °C for 4 h, affording the desired product after work-up as orange-brown crystals. Yield: 61 mg (32 %). ^{1}H NMR (500.10 MHz, [D$_4$]methanol, 25 °C): δ = 1.72 (s, 15H; $CH_{3,Cp*}$), 2.55 (s, 3H; CH_3), 3.79 (s, 3H; $CH_{3,MeIm}$), 7.00 (br s, 1H; CH_{MeIm}), 7.15 (br s, 1H; CH_{MeIm}), 7.31 (br s, 1H; CH-5), 7.78 ppm (br s, 2H; CH_{MeIm} & CH-6); ^{13}C NMR (125.75 MHz, [D$_4$]methanol, 25 °C): δ = 7.4 ($CH_{3,Cp*}$), 13.7 (CH_3), 33.4 ($CH_{3,MeIm}$), 87.7 (d, ^1J(Ir,C) = 10 Hz; C_{Cp*}), 121.3 (CH-5), 122.0 (CH_{MeIm}), 123.3 (CH_{MeIm}), 129.4 (CH_{MeIm}), 146.1 (CH-6), 154.9 (C_q-2), 165.8 (C_q-3), 179.1 ppm (C_q-4); elemental analysis calcd (%) for $C_{20}H_{26}F_6IrN_2O_2PS$: C 34.53, H 3.77, N 4.03, S 4.61; found: C 34.19, H 3.65, N 3.98, S 4.67.

Single-crystal X-ray diffraction analysis

X-ray intensity data were measured on a Bruker D8 Venture diffractor equipped with a multilayer monochromator, an $Mo_{K\alpha}$ INCOATEC microfocus sealed tube, and a Kryoflex II cooling device. Structures were solved by direct methods and refined by full-matrix least-squares techniques. Non-hydrogen atoms were refined with anisotropic displacement parameters. Hydrogen atoms were inserted at calculated positions and refined with riding coordinates. The following software was used: frame integration, Bruker SAINT software package[44] using a narrow-frame algorithm; absorption correction, SADABS;[45] structure solution, SHELXS-2013;[46] refinement, SHELXL-2013,[46] OLEX2,[47] and SHELXLE;[48] molecular diagrams, OLEX2.[47] CCDC1486550 (**1b**), 1486549 (**1c**), 1486552 (**2a**), 1486554 (**2b**), 1486551 (**2c**), and 1486553 (**2d**) contain the supplementary crystallographic data for this paper. These data are provided free of charge by The Cambridge Crystallographic Data Centre. Experimental data, crystal data, data collection parameters, and structure refinement details are listed in the Supporting Information (Tables S1–S14). Molecular structures and packings are displayed in Figures S5–S8.

ESI-MS measurements

Electrospray ionization mass spectra were recorded on a Bruker AmaZon SL ion-trap mass spectrometer (Bruker Daltonics GmbH). Data were acquired and processed using Compass 1.3 and Data Analysis 4.0 (Bruker Daltonics GmbH). Mass spectra were recorded following direct infusion with a sample concentration of 5 μM and a flow rate of 240 μL h^{-1}. Small molecules were measured with the following settings: dry temperature: 180 °C, nebulizer: 8.00 psi, dry gas: 6.00 L min^{-1}, and the high-voltage capillary was set to −4500 V or +4500 V for positive and negative mode, respectively. The target mass was set to 600 *m/z*. Samples for stability measurements and small molecule samples were diluted with water/methanol (50:50). Stock solutions of complexes **1a–d** and **2a–d** were prepared in DMSO and diluted to a final concentration of 1 % in DMSO/H_2O. The molar ratios used for interaction studies were complex:L-histidine:L-cysteine:glycine (1:1:1:1). Mass spectra were recorded after 0, 1, 3, 6, 24, and 48 h of incubation at 37 °C.

pH-Potentiometric titrations

An Orion 710A pH-meter equipped with a Metrohm combined electrode (type 6.0234.100) or Metrohm combined double-junction electrode (type 6.0255.100) and a Metrohm 665 Dosimat burette were used for the pH-potentiometric measurements. The exact concentrations of the ligand stock solutions together with the proton dissociation constants were determined by pH-potentiometric titrations with the help of the computer program HYPERQUAD.[49] RhCp* stock solutions were obtained by dissolving a known amount of [RhCp*(μ-Cl)Cl]$_2$ in water. A stock solution of [RhCp*$(H_2O)_3$]$(NO_3)_2$ was obtained from an aqueous solution of [RhCp*(μ-Cl)Cl]$_2$ after removal of chloride ions using an equivalent amount of $AgNO_3$. Concentrations of RhCp* stock solutions were checked by pH-potentiometric titrations employing stability constants for [(RhCp*)$_2$(hydroxido)$_i$] (i = 2 or 3) complexes.[22] The pH-potentiometric measurements were carried out at 25.0 ± 0.1 °C in water, and at an ionic strength of 0.20 M KCl or KNO_3. Titrations were performed with carbonate-free KOH solution (0.20 M). The exact concentrations of HCl, HNO_3, and KOH solutions were determined by pH-potentiometric titrations. The electrode system was calibrated to the pH = −log [H$^+$] scale by means of blank titrations (strong acid vs. strong base: HCl/HNO_3 vs. KOH), as suggested by

Irving et al.[50] The average water ionization constant, pK_w, was determined as 13.76±0.01 at 25.0 °C, I=0.20 M (KCl, KNO_3), which corresponds well to literature values.[51] The reproducibility of the titration points included in the calculations was within 0.005 pH units. The pH-potentiometric titrations were performed in the pH range between 2.0 and 11.5. The initial volume of the samples was 10.0 mL. The ligand concentration was 1.0 mM and was investigated at metal ion-to-ligand ratios of 1:1, 1:1.5, and 1:2. The accepted fitting between the measured and calculated titration data points regarding the volume of the titrant was < 10 μL. The software PSEQUAD[52] was utilized to calculate the stoichiometry of the complexes as well as their overall stability constants. $\beta(M_pL_qH_r)$ is defined in Equation (1) for the general equilibrium:

$$pM + qL + rH \rightleftharpoons M_pL_qH_r \text{ as } \beta(M_pL_qH_r) = [M_pL_qH_r]/[M]^p[L]^q[H]^r \quad (1)$$

where M denotes the metal moiety RhCp* and L is the completely deprotonated ligand. Values of log ß of various $[(RhCp^*)_2(hydroxido)_i]$ ($i=2$ or 3) complexes were calculated on the basis of pH-potentiometric titration data in the absence and presence of chloride ions, and were in good agreement with our previously published data.[22]

UV/Vis spectrophotometric and ^{1}H NMR titrations

A Hewlett Packard 8452 A diode-array spectrophotometer was used to record UV/Vis spectra in the interval 200–800 nm. The pathlength (l) was either 1 or 2 cm. Titrations were performed with samples containing only thiomaltol (48 μM), RhCp* (48 μM), or a 1:1 molar ratio of RhCp* and the ligand over the pH range 2.0–11.5 at an ionic strength of 0.20 M (KCl or KNO_3) and at 25.0±0.1 °C under anaerobic conditions. Measurements were carried out in the absence and presence of chloride ions, whereas the 0.20 M KCl or KNO_3 was partially or completely replaced by HCl or HNO_3, and pH values in the range 0.7–2.0 were calculated from the content of strong acid in the solutions. UV/Vis spectra were recorded to investigate the dependence of the H_2O/Cl^- exchange processes in the $[RhCp^*(L)(H_2O)]^+$ complex at pH 3.1 on the Cl^- concentration (0–0.64 M). Stability constants for the co-ligand exchange were calculated with the software PSEQUAD.[52] ^{1}H NMR studies were carried out on a Bruker Ultrashield 500 Plus instrument or on a 600 MHz Bruker Avance III spectrometer equipped with a 5 mm cryo-TXI (^{1}H, ^{13}C, ^{15}N) probe. All ^{1}H NMR spectra were recorded with the WATERGATE water suppression pulse scheme using DSS as an internal standard. Thiomaltol was dissolved in a 10% (v/v) D_2O/H_2O mixture to yield a concentration of 1 or 0.1 mM, and each solution was titrated at 25 °C, at I=0.20 M (KCl or KNO_3), in the absence or presence of RhCp* at a 1:1 metal-to-ligand ratio. Samples containing RhCp* and thiomaltol at various ratios (1:1–1:5) at constant concentration of the ligand (1 mM) at pH 3.85 (I=0.2 M KCl) and 2.70 (I=0.2 M KNO_3) were measured. Stability (log K) and proton dissociation (pK_a) constants for the complex $[ML_2H]$ were calculated using the software PSEQUAD.[52]

Stability measurements under pH variation

An Eco Scan pH6 pH meter equipped with a glass-micro combination pH electrode (Orion 9826 BN) was used. It was calibrated with standard buffer solutions of pH 4.00, 7.00, and 10.00. Complexes **2a–d** were dissolved in D_2O (0.5 mL) and pD values were determined instantly in the NMR tubes. The pH titrations were performed by addition of NaOD (0.4–0.0004% in D_2O) and DCl (0.4–0.0004% in D_2O). After each addition of either DCl or NaOD, the samples were directly measured at 25 °C using a Bruker Avance III™ 500 MHz FT-NMR spectrometer. The experimentally obtained pD values were corrected according to Equation (2)[53] in order to convert the measured values to the corresponding pH values in aqueous solution.

$$pH = 0.936\,pH^* - 0.412 \quad (2)$$

Cell lines and culture conditions

CH1/PA-1 cells (identified by STR profiling as PA-1 ovarian teratocarcinoma cells by Multiplexion, Heidelberg, Germany) were obtained from Lloyd R. Kelland, CRC Centre for Cancer Therapeutics, Institute of Cancer Research, Sutton, UK. SW480 (human adenocarcinoma of the colon) and A549 (human non-small cell lung cancer) cells were kindly provided by Brigitte Marian (Institute of Cancer Research, Department of Medicine I, Medical University of Vienna, Austria). All cell culture media and reagents were purchased from Sigma–Aldrich Austria and plastic ware from Starlab Germany. Cells were grown in 75 cm^2 culture flasks as adherent monolayer cultures in Minimum Essential Medium (MEM) supplemented with 10% heat-inactivated fetal calf serum, 1 mM sodium pyruvate, 4 mM L-glutamine, and 1% non-essential amino acids (from 100× ready-to-use stock). Cultures were maintained at 37 °C in humidified atmosphere composed of 95% air and 5% CO_2.

Cytotoxicity assay

Cytotoxic effects of the tested compounds were determined by means of a colorimetric microculture assay [MTT assay; MTT=3-(4,5-dimethyl-2-thiazolyl)-2,5-diphenyl-2*H*-tetrazolium bromide]. Cells were harvested from culture flasks by trypsinization and seeded at densities of 1×10^3 (CH1/PA-1), 2×10^3 (SW480), and 3×10^3 (A549) in 100 μL per well aliquots in 96-well microculture plates. Before drug exposure, cells were allowed to settle and resume proliferation for 24 h. Test compounds were first dissolved in DMSO, diluted with complete culture medium, and added to the plates, whereby the final DMSO content did not exceed 0.5%. After 96 h of exposure, the medium was removed and replaced with 100 μL/well of a 1:7 MTT/RPMI 1640 solution (MTT solution, 5 mg mL^{-1} of MTT reagent in phosphate-buffered saline; RPMI 1640 medium, supplemented with 10% heat-inactivated fetal calf serum (FCS), and 4 mM L-glutamine) and incubated for 4 h at 37 °C. Subsequently, the MTT/RPMI 1640 solution was removed from all wells, and the formazan crystals formed by viable cells were dissolved in 150 μL of DMSO per well. Optical densities at 550 nm were measured with a microplate reader (Biotek EL×808), using a reference wavelength of 690 nm to correct for nonspecific absorption. The quantity of viable cells was expressed in terms of T/C values (relative to untreated controls), and 50% inhibitory concentrations (IC_{50}) were calculated from concentration–effect curves by interpolation. Evaluation was based on mean values from three independent experiments.

Topoisomerase IIα inhibition

The topoisomerase IIα inhibitory capacities of the tested compounds were determined by means of a DNA plasmid relaxation assay. For this purpose, we used a topoisomerase drug screening kit and human recombinant topoisomerase IIα enzyme from TopoGen Inc. The supercoiled pHOT1 plasmid DNA was incubated for 30 min at 37 °C with topo IIα in the presence of various concentrations of the test compounds. Etoposide (VP-16) was used as a posi-

tive control at a concentration of 0.8 mM. The reaction was stopped by the rapid addition of 10% SDS followed by digestion with proteinase K for 15 min at 37 °C. The samples were divided and loaded onto two different 1% agarose gels with equal amounts of reaction products. One gel (Figures 6A and 7A) was post-stained (after electrophoresis incubated in a 1× TAE buffer containing 0.7 μg mL^{-1} ethidium bromide) and the other gel (Figures 6B and 7B) was pre-stained (0.7 μg mL^{-1} ethidium bromide added to the gel before electrophoresis). Both were analyzed by visualization with the detection system Fusion SL (Vilber Lourmat). Evaluation was based on two independent experiments.

Cell cycle studies

For this assay, SW480 cells were harvested by trypsinization and 1.2×10^5 cells were seeded into 12-well plates. In the first 24 h, the cells were allowed to settle and resume proliferation. Thereafter, DMSO stock solutions of the tested compounds were diluted with MEM, and the medium in the plates was replaced with medium containing the test compounds so that the final DMSO content did not exceed 0.5%. After continuous exposure for 12 h at 37 °C and under 5% CO_2, the cells were trypsinized and centrifuged at 300 *g* for 3 min. They were then washed with PBS (1 mL) and resuspended in PI/HSF buffer (600 μL; 0.1% Triton X-100, 0.1% sodium citrate, in PBS) containing 50 μg mL^{-1} propidium iodide. After incubation overnight at 4 °C in the dark, 5×10^3 cells were measured by flow cytometry with a Millipore guava easyCyte 8HT instrument. Data were evaluated by means of FlowJo software (Tree Star) using Dean–Jett–Fox algorithms.

Detection of intracellular reactive oxygen species

DCF-DA (2′,7′-dichlorofluorescein diacetate) was used to detect the production of ROS. SW480 cells were seeded at densities of 2.5×10^4 cells in 100 μL/well aliquots in 96-well microculture plates and were allowed to proliferate for 24 h. The cells were washed with Hanks' balanced salt solution (HBSS) supplemented with 1% FCS, and were stained with 25 μM DCF-DA for 40 min at 37 °C under 5% CO_2. The cells were again washed with HBSS supplemented with 1% FCS, and complexes were added in phenol-red-free MEM supplemented with 1% FCS at the indicated concentrations. Fluorescence measurements were carried out with a Synergy HT microplate reader (BioTek Instruments) set to 37 °C. Measurements were performed with a 480 nm excitation and a 516 nm emission filter pair and a PMT sensitivity setting of 50. Readings were conducted at intervals of 10 min for 120 min. A 200 μM solution of *tert*-butyl hydroperoxide (*t*bHP) was used as a positive control. Background (non-stained cells) was subtracted from all measurements, and fold change relative to the untreated control was determined.

Acknowledgements

The authors would like to thank the University of Vienna, the FWF Austrian Science Fund (project number P24659-N28), TÉT 15-1-2016-0024 bilateral research project, and the Hungarian Research Foundation OTKA project PD103905 for financial support.

Keywords: antitumor agents · leaving group variation · medicinal chemistry · organometallics · thiomaltol

[1] P. Heffeter, U. Jungwirth, M. Jakupec, C. Hartinger, M. Galanski, L. Elbling, M. Micksche, B. Keppler, W. Berger, *Drug Resist. Updates* **2008**, *11*, 1–16.
[2] L. S. Flocke, R. Trondl, M. A. Jakupec, B. K. Keppler, *Invest. New Drugs* **2016**, *34*, 261–268.
[3] P. Heffeter, B. Atil, K. Kryeziu, D. Groza, G. Koellensperger, W. Körner, U. Jungwirth, T. Mohr, B. K. Keppler, W. Berger, *Eur. J. Cancer* **2013**, *49*, 3366–3375.
[4] F. Frausin, V. Scarcia, M. Cocchietto, A. Furlani, B. Serli, E. Alessio, G. Sava, *J. Pharmacol. Exp. Ther.* **2004**, *313*, 227–233.
[5] A. Vacca, M. Bruno, A. Boccarelli, M. Coluccia, D. Ribatti, A. Bergamo, S. Garbisa, L. Sartor, G. Sava, *Br. J. Cancer* **2002**, *86*, 993–998.
[6] S. Leijen, S. A. Burgers, P. Baas, D. Pluim, M. Tibben, E. van Werkhoven, E. Alessio, G. Sava, J. H. Beijnen, J. H. M. Schellens, *Invest. New Drugs* **2015**, *33*, 201–214.
[7] Y. K. Yan, M. Melchart, A. Habtemariam, P. J. Sadler, *Chem. Commun.* **2005**, 4764–4776.
[8] W. H. Ang, A. Casini, G. Sava, P. J. Dyson, *J. Organomet. Chem.* **2011**, *696*, 989–998.
[9] B. S. Murray, M. V. Babak, C. G. Hartinger, P. J. Dyson, *Coord. Chem. Rev.* **2016**, *306*, 86–114.
[10] R. Fernández, M. Melchart, A. Habtemariam, S. Parsons, P. J. Sadler, *Chem. Eur. J.* **2004**, *10*, 5173–5179.
[11] W. Kandioller, C. G. Hartinger, A. A. Nazarov, C. Bartel, M. Skocic, M. A. Jakupec, V. B. Arion, B. K. Keppler, *Chem. Eur. J.* **2009**, *15*, 12283–12291.
[12] W. Kandioller, C. G. Hartinger, A. A. Nazarov, M. L. Kuznetsov, R. O. John, C. Bartel, M. A. Jakupec, V. B. Arion, B. K. Keppler, *Organometallics* **2009**, *28*, 4249–4251.
[13] S. M. Meier, M. Hanif, W. Kandioller, B. K. Keppler, C. G. Hartinger, *J. Inorg. Biochem.* **2012**, *108*, 91–95.
[14] I. F. Tannock, D. Rotin, *Cancer Res.* **1989**, *49*, 4373–4384.
[15] L. E. Gerweck, K. Seetharaman, *Cancer Res.* **1996**, *56*, 1194–1198.
[16] M. A. Bennett, A. K. Smith, *J. Chem. Soc. Dalton Trans.* **1974**, 233–241.
[17] M. Hanif, H. Henke, S. M. Meier, S. Martic, M. Labib, W. Kandioller, M. A. Jakupec, V. B. Arion, H.-B. Kraatz, B. K. Keppler, *Inorg. Chem.* **2010**, *49*, 7953–7963.
[18] M. Schmidlehner, P.-S. Kuhn, C. M. Hackl, A. Roller, W. Kandioller, B. K. Keppler, *J. Organomet. Chem.* **2014**, *772–773*, 93–99.
[19] A. F. A. Peacock, M. Melchart, R. J. Deeth, A. Habtemariam, S. Parsons, P. J. Sadler, *Chem. Eur. J.* **2007**, *13*, 2601–2613.
[20] C. A. Vock, C. Scolaro, A. D. Phillips, R. Scopelliti, G. Sava, P. J. Dyson, *J. Med. Chem.* **2006**, *49*, 5552–5561.
[21] R. E. Morris, R. E. Aird, P. del Socorro Murdoch, H. Chen, J. Cummings, N. D. Hughes, S. Parsons, A. Parkin, G. Boyd, D. I. Jodrell, *J. Med. Chem.* **2001**, *44*, 3616–3621.
[22] O. Dömötör, S. Aicher, M. Schmidlehner, M. S. Novak, A. Roller, M. A. Jakupec, W. Kandioller, C. G. Hartinger, B. K. Keppler, É. A. Enyedy, *J. Inorg. Biochem.* **2014**, *134*, 57–65.
[23] É. A. Enyedy, É. Sija, T. Jakusch, C. G. Hartinger, W. Kandioller, B. K. Keppler, T. Kiss, *J. Inorg. Biochem.* **2013**, *127*, 161–168.
[24] M. Gras, B. Therrien, G. Süss-Fink, P. Štěpnička, A. K. Renfrew, P. J. Dyson, *J. Organomet. Chem.* **2008**, *693*, 3419–3424.
[25] É. A. Enyedy, O. Dömötör, C. M. Hackl, A. Roller, M. S. Novak, M. A. Jakupec, B. K. Keppler, W. Kandioller, *J. Coord. Chem.* **2015**, *68*, 1583–1601.
[26] É. A. Enyedy, J. P. Mészáros, O. Dömötör, C. M. Hackl, A. Roller, B. K. Keppler, W. Kandioller, *J. Inorg. Biochem.* **2015**, *152*, 93–103.
[27] J. L. Wike-Hooley, J. Haveman, H. S. Reinhold, *Radiother. Oncol.* **1984**, *2*, 343–366.
[28] V. Pichler, S. Göschl, S. M. Meier, A. Roller, M. A. Jakupec, M. Galanski, B. K. Keppler, *Inorg. Chem.* **2013**, *52*, 8151–8162.
[29] A. Kanzaki, Y. Takebayashi, X.-Q. Ren, H. Miyashita, S. Mori, S. Akiyama, Y. Pommier, *Mol. Cancer Ther.* **2002**, *1*, 1327–1334.
[30] H. M. Leitner, R. Kachadourian, B. J. Day, *Biochem. Pharmacol.* **2007**, *74*, 1677–1685.
[31] W. Berger, L. Elbling, E. Hauptmann, M. Micksche, *Int. J. Cancer* **1997**, *73*, 84–93.
[32] W. Berger, L. Elbling, M. Micksche, *Int. J. Cancer* **2000**, *88*, 293–300.
[33] V. Pichler, S. M. Valiahdi, M. A. Jakupec, V. B. Arion, M. Galanski, B. K. Keppler, *Dalton Trans.* **2011**, *40*, 8187–8192.
[34] P.-S. Kuhn, V. Pichler, A. Roller, M. Hejl, M. A. Jakupec, W. Kandioller, B. K. Keppler, *Dalton Trans.* **2015**, *44*, 659–668.

[35] J. M. Fortune, N. Osheroff, *J. Biol. Chem.* **1998**, *273*, 17643 – 17650.
[36] J. L. Nitiss, *Nat. Rev. Cancer* **2009**, *9*, 338 – 350.
[37] N. Osheroff, *Biochim. Biophys. Acta* **1998**, *1400*, 1 – 2.
[38] M. Schmidlehner, L. S. Flocke, A. Roller, M. Hejl, M. A. Jakupec, W. Kandioller, B. K. Keppler, *Dalton Trans.* **2015**, *44*, 724 – 733.
[39] S. Mokesch, M. S. Novak, A. Roller, M. A. Jakupec, W. Kandioller, B. K. Keppler, *Organometallics* **2015**, *34*, 848 – 857.
[40] J. J. Soldevila-Barreda, P. J. Sadler, *Curr. Opin. Chem. Biol.* **2015**, *25*, 172 – 183.
[41] S. J. Dougan, A. Habtemariam, S. E. McHale, S. Parsons, P. J. Sadler, *Proc. Natl. Acad. Sci. USA* **2008**, *105*, 11628 – 11633.
[42] B. L. Booth, R. N. Haszeldine, M. Hill, *J. Chem. Soc. Inorg. Phys. Theor.* **1969**, 1299 – 1303.
[43] J. W. Kang, K. Moseley, P. M. Maitlis, *J. Am. Chem. Soc.* **1969**, *91*, 5970 – 5977.
[44] Bruker SAINT V8.32B Copyright © 2005 – 2015 Bruker AXS.
[45] Bruker (**2001**). SADABS Vers. 2012/1. Bruker AXS Inc., Madison, Wisconsin, USA.
[46] G. Sheldrick, *Acta Crystallogr. Sect. A* **2008**, *64*, 112 – 122.
[47] O. V. Dolomanov, L. J. Bourhis, R. J. Gildea, J. A. K. Howard, H. Puschmann, *J. Appl. Crystallogr.* **2009**, *42*, 339 – 341.
[48] SHELXLE, G. Hübschle, *J. Appl. Cryst.* **2011**, *44*, 1281.
[49] P. Gans, A. Sabatini, A. Vacca, *Talanta* **1996**, *43*, 1739 – 1753.
[50] H. M. Irving, M. G. Miles, L. D. Pettit, *Anal. Chim. Acta* **1967**, *38*, 475 – 488.
[51] SCQuery, The IUPAC Stability Constants Database, Academic Software (Version 5.5), RSC, **1993 – 2005**.
[52] L. Zekany, I. Nagypal, in *Comput. Methods Determ. Form. Constants* (Ed.: D. J. Leggett), Springer, Boston, **1985**, pp. 291 – 353.
[53] A. Kréżel, W. Bal, *J. Inorg. Biochem.* **2004**, *98*, 161 – 166.

Received: July 5, 2016
Published online on October 19, 2016

Supporting Information

[EXTRACT]

Contents

5) Cell cycle distribution data

Table S16. Impact of tested substances on the cell cycle distribution of SW480 cells after 12 h continuous exposure. Merbarone was used as a positive control with a concentration of 640 µM (REF Mokesch S., Novak M.S., Roller A., Jakupec M.A., Kandioller W., Keppler B.K. Organometallics, 2015, 34 (5), pp 848–857.).

Cell cycle distribution (%)				
Compound	Concentration	SW480		
		G0/G1	S	G2
Control	0	51 ± 2	28 ± 2	20 ± 3
1a	2.5	43 ± 9	33 ± 6	21 ± 3
	10	41 ± 8	37 ± 6	21 ± 4
	20	41 ± 5	33 ± 3	24 ± 3
1b	2.5	49 ± 6	32 ± 4	18 ± 1
	10	41 ± 12	35 ± 9	24 ± 2
	20	29 ± 0.1	33 ± 7	37 ± 7
1c	2.5	36 ± 3	32 ± 7	31 ± 4
	10	35 ± 3	30 ± 3	33 ± 6
	20	39 ± 2	36 ± 4	24 ± 6
1d	2.5	52 ± 2	21 ± 0.3	26 ± 1
	10	45 ± 2	24 ± 2	30 ± 0.2
	20	49 ± 0.2	25 ± 2	22 ± 3
2a	2.5	41 ± 4	38 ± 1	20 ± 6
	10	34 ± 2	38 ± 2	27 ± 6
	20	29 ± 5	43 ± 0.0	26 ± 5

2b	2.5	44 ± 2	31 ± 2	24 ± 4
	10	42 ±2	32 ± 4	26 ± 6
	20	34 ± 0.0	39 ± 0.5	27 ± 1
2c	2.5	40 ± 8	28 ± 4	31 ± 4
	10	46 ± 4	30 ± 3	20 ± 1
	20	46 ± 4	32 ± 6	20 ± 2
2d	2.5	30 ± 5	38 ± 2	29 ± 2
	10	33 ± 3	41 ± 3	25 ± 2
	20	34 ± 2	45 ± 2	20 ± 4
L1	2.5	29 ± 12	36 ± 6	34 ± 18
	10	29 ± 2	34 ± 4	35 ± 7
	20	36 ± 10	37 ± 5	26 ± 5
Merbarone	640	33 ± 5	38 ± 3	27 ± 3

6) ROS generation data

Table S17. Impact of thiomaltol-based organometallic complexes on levels of ROS in SW480 cells after 2 h continuous exposure. tbHP was used as a positive control with a concentration of 200 µM.

Treatment time (h)	Fluorescence (fold)										
	Compound										
	tbHP	µM	1a	1b	1c	1d	2a	2b	2c	2d	L1
00:00:00	1.5 ± 0.5	10	0.57 ± 0.15	0.51 ± 0.24	0.79 ± 0.21	0.82 ± 0.26	0.74 ± 0.31	0.69 ± 0.27	0.91 ± 0.28	0.86 ± 0.20	0.71 ± 0.25
		20	0.49 ± 0.22	0.33 ± 0.16	0.83 ± 0.27	0.76 ± 0.19	0.53 ± 0.19	0.43 ± 0.19	0.88 ± 0.36	0.73 ± 0.09	0.70 ± 0.27
00:10:00	2.8 ± 0.9	10	0.55 ± 0.11	0.52 ± 0.19	0.80 ± 0.20	0.84 ± 0.24	0.64 ± 0.25	0.61 ± 0.22	0.99 ± 0.28	0.80 ± 0.14	0.59 ± 0.24
		20	0.55 ± 0.24	0.34 ± 0.13	0.89 ± 0.25	0.86 ± 0.25	0.47 ± 0.15	0.43 ± 0.15	1.16 ± 0.39	0.84 ± 0.13	0.59 ± 0.23
00:20:00	7.7 ± 3.1	10	0.61 ± 0.11	0.56 ± 0.18	0.97 ± 0.26	1.07 ± 0.33	0.68 ± 0.22	0.67 ± 0.18	1.39 ± 0.38	1.11 ± 0.28	0.70 ± 0.24
		20	0.58 ± 0.21	0.40 ± 0.14	1.16 ± 0.35	1.14 ± 0.38	0.55 ± 0.18	0.52 ± 0.12	1.93 ± 0.66	1.30 ± 0.35	0.70 ± 0.24
00:30:00	11 ± 3	10	0.62 ± 0.07	0.58 ± 0.17	1.04 ± 0.22	1.14 ± 0.31	0.70 ± 0.19	0.67 ± 0.16	1.59 ± 0.35	1.16 ± 0.23	0.71 ± 0.19
		20	0.64 ± 0.19	0.45 ± 0.13	1.28 ± 0.32	1.21 ± 0.35	0.57 ± 0.14	0.55 ± 0.13	2.28 ± 0.54	1.37 ± 0.27	0.73 ± 0.19
00:40:00	14 ± 3	10	0.68 ± 0.08	0.62 ± 0.14	1.09 ± 0.21	1.18 ± 0.28	0.71 ± 0.15	0.69 ± 0.17	1.74 ± 0.37	1.17 ± 0.29	0.69 ± 0.18
		20	0.73 ± 0.19	0.54 ± 0.15	1.38 ± 0.34	1.29 ± 0.35	0.62 ± 0.13	0.61 ± 0.13	2.51 ± 0.62	1.41 ± 0.33	0.71 ± 0.18
00:50:00	17 ± 3	10	0.73 ± 0.09	0.67 ± 0.13	1.14 ± 0.21	1.21 ± 0.27	0.74 ± 0.13	0.74 ± 0.16	1.81 ± 0.37	1.17 ± 0.29	0.68 ± 0.17

		20	0.85 ± 0.19	0.62 ± 0.14	1.44 ± 0.29	1.31 ± 0.33	0.69 ± 0.10	0.67 ± 0.13	2.64 ± 0.60	1.45 ± 0.32	0.72 ± 0.16
01:00:00	18 ± 2	10	0.79 ± 0.11	0.72 ± 0.15	1.17 ± 0.23	1.22 ± 0.28	0.79 ± 0.16	0.77 ± 0.18	1.84 ± 0.37	1.18 ± 0.30	0.69 ± 0.16
		20	0.87 ± 0.18	0.68 ± 0.15	1.46 ± 0.31	1.31 ± 0.34	0.75 ± 0.13	0.73 ± 0.16	2.68 ± 0.61	1.46 ± 0.34	0.75 ± 0.18
01:10:00	19 ± 2	10	0.79 ± 0.13	0.72 ± 0.16	1.16 ± 0.23	1.20 ± 0.28	0.81 ± 0.18	0.77 ± 0.19	1.82 ± 0.37	1.16 ± 0.31	0.69 ± 0.17
		20	0.86 ± 0.20	0.68 ± 0.16	1.43 ± 0.32	1.27 ± 0.35	0.77 ± 0.15	0.73 ± 0.19	2.64 ± 0.60	1.42 ± 0.34	0.74 ± 0.21
01:20:00	19 ± 2	10	0.76 ± 0.11	0.68 ± 0.13	1.11 ± 0.19	1.13 ± 0.23	0.77 ± 0.14	0.73 ± 0.17	1.75 ± 0.33	1.09 ± 0.26	0.66 ± 0.16
		20	0.84 ± 0.19	0.68 ± 0.14	1.37 ± 0.26	1.20 ± 0.30	0.74 ± 0.12	0.70 ± 0.17	2.54 ± 0.54	1.34 ± 0.31	0.69 ± 0.17
01:30:00	19 ± 1	10	0.74 ± 0.09	0.67 ± 0.11	1.08 ± 0.16	1.08 ± 0.20	0.74 ± 0.11	0.70 ± 0.14	1.69 ± 0.30	1.05 ± 0.23	0.65 ± 0.13
		20	0.85 ± 0.18	0.70 ± 0.13	1.33 ± 0.22	1.15 ± 0.25	0.74 ± 0.09	0.70 ± 0.14	2.46 ± 0.49	1.28 ± 0.27	0.66 ± 0.14
01:40:00	18 ± 1	10	0.75 ± 0.07	0.67 ± 0.10	1.06 ± 0.14	1.06 ± 0.17	0.74 ± 0.09	0.70 ± 0.11	1.64 ± 0.27	1.03 ± 0.21	0.63 ± 0.11
		20	0.87 ± 0.17	0.72 ± 0.12	1.31 ± 0.18	1.12 ± 0.21	0.75 ± 0.07	0.71 ± 0.11	2.39 ± 0.44	1.24 ± 0.24	0.65 ± 0.10
01:50:00	18 ± 1	10	0.75 ± 0.08	0.67 ± 0.09	1.05 ± 0.14	1.05 ± 0.16	0.75 ± 0.08	0.70 ± 0.10	1.61 ± 0.25	1.02 ± 0.20	0.63 ± 0.09
		20	0.89 ± 0.16	0.74 ± 0.11	1.30 ± 0.17	1.10 ± 0.19	0.77 ± 0.06	0.72 ± 0.11	2.33 ± 0.42	1.21 ± 0.22	0.64 ± 0.08
02:00:00	17 ± 1	10	0.76 ± 0.07	0.68 ± 0.09	1.05 ± 0.13	1.03 ± 0.15	0.76 ± 0.07	0.71 ± 0.09	1.57 ± 0.23	1.01 ± 0.18	0.63 ± 0.08
		20	0.90 ± 0.16	0.75 ± 0.10	1.29 ± 0.16	1.08 ± 0.18	0.79 ± 0.05	0.74 ± 0.10	2.27 ± 0.38	1.18 ± 0.21	0.64 ± 0.07

ORGANOMETALLICS

Article

pubs.acs.org/Organometallics

1,3-Dioxoindan-2-carboxamides as Bioactive Ligand Scaffolds for the Development of Novel Organometallic Anticancer Drugs

Stephan Mokesch,[†] Maria S. Novak,[†] Alexander Roller,[†] Michael A. Jakupec,[†,‡] Wolfgang Kandioller,*[,†,‡] and Bernhard K. Keppler[†,‡]

[†]Institute of Inorganic Chemistry, Faculty of Chemistry, and [‡]Research Platform "Translational Cancer Therapy Research", University of Vienna, Waehringer Straße 42, A-1090 Vienna, Austria

Supporting Information

ABSTRACT: A series of novel 1,3-dioxoindan-2-carboxamide-based complexes were synthesized, designed to employ both the attributes of half-sandwich complexes and the topoisomerase inhibiting properties of the ligand scaffold. The compounds were characterized with standard analytical methods. Their stability in aqueous systems and the impact of either the metal center or the ligand scaffold on the affinity toward small biomolecules such as amino acids, DNA model compounds, and small proteins were determined by IT-ESI mass spectrometry. The cytotoxicity was investigated in three human cancer cell lines by means of a colorimetric MTT assay, and preliminary structure−activity relationships were derived. The benzyl derivatives showed the highest in vitro activity and promising topoisomerase IIα inhibition in the range of the IC_{50} values. In addition, the induced changes in the cell cycle distribution were determined and the apoptosis induction potential elucidated.

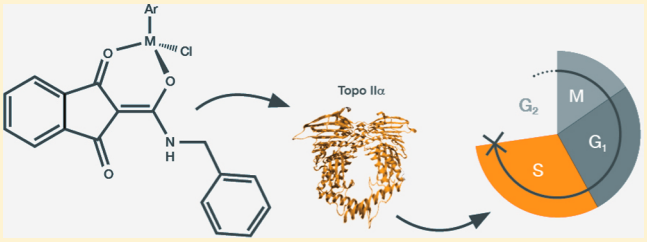

INTRODUCTION

"Piano-stool" configured metal complexes (especially with Ru) bearing facial arene ligands have become increasingly popular among the scientific community, due to their extreme synthetic versatility and broad range of potential applications.[1] The arene represents the seat of the piano stool and the mono- or bidentate ligands the legs. Hydrolysis of the labile chlorido ligand yields positively charged aqua-complexes, which are then able to attack biological targets in the cell.[2] The coordinated aromatic system (e.g., η^6-*p*-cymene (cym) and η^5-1,2,3,4,5-pentamethylcyclopentadienyl (Cp*)) stabilizes low oxidation states of transition metals (e.g., Ru^{II}) and acts as a hydrophobic face, thereby enhancing cell membrane permeation. Variation of the leaving group has effects on the ligand exchange rate.[3] Complexes bearing N,N-chelates or PTA have been the most intensely studied in this compound class and are currently in an advanced preclinical stage.[4−6] Recently, bidentate ligand systems with biological activity on their own, such as flavones[7] and paullones,[8] have been employed to exploit possible synergistic effects.[9]

Topoisomerases I and II (topo I and topo II) are key enzymes in DNA transcription and replication. DNA occurs in an extremely condensed form in the nucleus and needs to be uncoiled to allow the polymerase enzyme complex to read the encoded information. Uncontrolled uncoiling would involve rotations and torsions and could potentially lead to uncontrolled DNA strand breaks. Topoisomerases perform controlled single-strand breaks (isoforms of class I) or double-strand breaks (isoforms of class II) and the respective religations. Of the two isoforms of topo II (α and β), only topo IIα plays a central role in mitosis, while topo IIβ is not imperative for cell division.[10,11] As this class of enzymes is essential for cell replication, they present an attractive point of attack for novel chemotherapeutic agents. The mechanisms of topoisomerase inhibition can be divided into two categories. The first is topoisomerase toxicity, where the topoisomerase poison stabilizes the enzyme−DNA complex and consequently prevents strand religation (e.g., podophyllotoxins such as etoposide[12] and anthracyclines such as doxorubicin;[13] see Chart 1). The second is actual topoisomerase inhibition, where

Chart 1. Chemical Structures of Doxorubicin, TAS-103, and 1,3-Dioxoindan-2-carboxamides

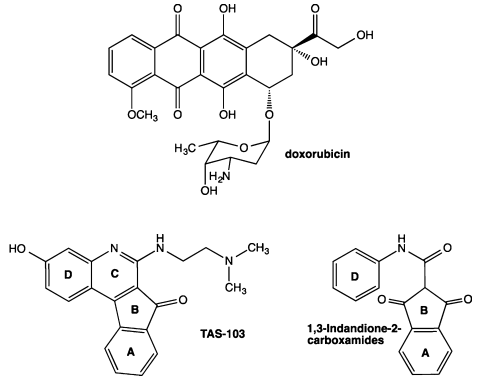

Received: October 17, 2014
Published: February 19, 2015

DOI: 10.1021/om501032s
Organometallics 2015, 34, 848−857

the inhibitor forms a stable complex with the enzyme and keeps it from DNA cleavage (e.g., delphinidin, cyanidin).[14,15] Intrinsic reparative processes usually maintain cell viability. However, with increasing concentration of inhibited topoisomerases, genotoxic events accumulate. Proliferating cells were found to express a higher concentration of topoisomerase II, rendering them more vulnerable to the inhibitors' toxicity.[16] Topo IIα, especially, has become a popular target for a number of anticancer drugs.

In the late 1990s a new promising dual topoisomerase I and II inhibitor was developed, namely 6-[[2-(dimethylamino)-ethyl]amino]-3-hydroxy-7*H*-indeno[2,1-*c*]-quinolin-7-one dihydrochloride (TAS-103; Chart 1). Since topo I inhibition can be partially circumvented by topo II, the dual targeting of this compound is thought to be a promising strategy[17] and synergistic effects with cisplatin[18] as well as efficacy against (multi)drug resistant cancer cell lines[17] have been observed. Jung et al. developed 1,3-dioxoindane-2-carboxamide derivatives structurally related to TAS-103 (Chart 1) and tested them on four different cancer cell lines. They exhibited potent in vitro cytotoxicity; however, their IC_{50} values were about 100-fold higher than that of doxorubicin.[19]

The aim of this study was to design novel organometallic compounds by coordination of the organometallic half-sandwich ruthenium/rhodium scaffold to 1,3-dioxoindan-2-carboxamides with potential topoisomerase inhibiting properties.

RESULTS AND DISCUSSION

Synthesis. 1,3-Indanedione-2-carboxamides actually first aroused attention as one of the few classes of amides which can be stabilized in their enolic form.[20] The enolization was found to occur on the amide side rather than on the C1/C3-carbonyl groups. In solvents with low polarity they exist solely as enols of the amide.[21] This compound class can be obtained starting from the zwitterionic precursor 2-oxido-3-phenyl-iodonio-1,4-naphthoquinone (**P1**), which was synthesized by the reaction of lawsone with (diacetoxyiodo)benzene[22] in excellent yields (91%). The 1,3-dioxoindan-2-carboxamide ligands were then obtained by reaction of the precursor with the respective primary amine (methylamine, ethylamine, propylamine, and benzylamine), where the reaction time varied depending on the applied amine. Aqueous workup afforded the desired compounds in excellent purity and in good yields (74–96%). The attack of the amine followed a preceding Wolff-type rearrangement, where the elimination of iodobenzene led to the highly reactive ketocarbene intermediate, which subsequently rearranged to the respective ketene via ring contraction (Scheme 1). This highly reactive intermediate then reacted with the amine, leading to the ligands **L1**–**L4**.

Of the four, only ligand **L4** has previously been synthesized by Malamidou–Xenikaki et al.;[23] however, the optimized aqueous purification process within this work improved the yield by 23%. These ligands were then converted to the respective ruthenium (**1a**–**4a**) and rhodium complexes (**1b**–**4b**) by deprotonation of **L1**–**L4** with sodium methoxide followed by addition of the respective dimeric metal precursor bis[dichlorido(cym)ruthenium(II)] or bis[dichlorido(Cp*)-rhodium(III)] under an argon atmosphere. The yields of the complexations ranged from 57 to 85% (Scheme 2).

The characterization of these novel compounds was carried out via conventional techniques (see the Experimental Section and Figures S1–S12 in the Supporting Information).

Scheme 1. Wolff Rearrangement during Ligand Synthesis

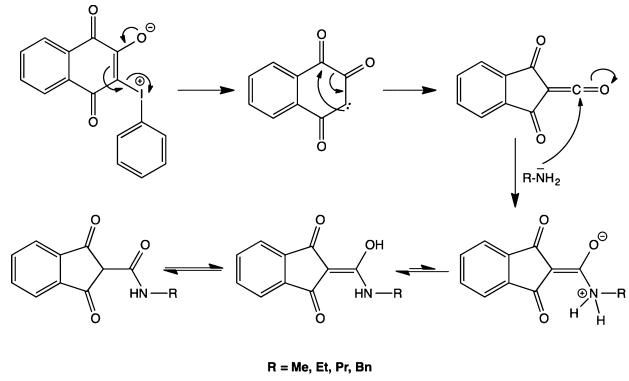

Scheme 2. Synthesis of Compounds 1a,b–4a,b and the supposed Behavior in Biological Media

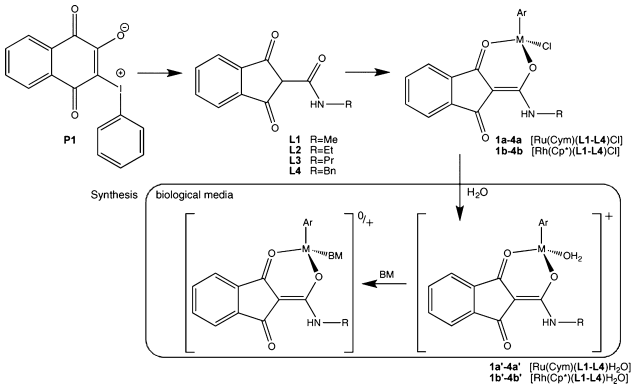

The symmetry of the aromatic signals in the ^{1}H NMR and the $^{13}C\{^1H\}$ spectra of ligands **L1**–**L4** supports the assumed ring contraction of the 1,4-naphthoquinone backbone to the corresponding 1,3-dioxoindane. The ligands seem to enolize at the amide carbon via formation of an exocyclic double bond. All rhodium organometallics exhibited the characteristic ^1J(Rh,C) value of the metal center to the facially coordinated Cp* ligand, where the coupling constant of 10 Hz is in good accordance with the literature.[24] Furthermore, the methylene protons of the benzyl group of **4a,b** show two separate signals, both occurring as a doublet of doublets, where a geminal coupling (^2J(H–H) = 15 Hz) and the coupling to the amine proton (^3J(H–H) = 6 Hz) were detected. Similar behavior of methylene groups was reported for 1-substituted 2-pyridones upon coordination to organometallic fragments.[25]

Single crystals of **3a** and **4a** were obtained by the slow diffusion method from chloroform/pentanes and analyzed by X-ray diffraction (Chart 2). Crystallographic data, collection parameters, and structure refinement details are presented in Table S1 in the Supporting Information. Complex **3a** crystallized in a monoclinic crystal system, in the space group $P2_1/c$; **4a**, on the other hand, crystallized in a triclinic crystal system in the centrosymmetric space group $P\bar{1}$. Both compounds showed the typical piano-stool configuration, with the facial cym ligand being the seat, whereas the chlorido and the chelating ligand represent the legs. In both cases, the two enantiomeric forms of the metal complexes cocrystallized in the unit cell. The anionic O,O-chelating 1,3-dioxoindan-2-carboxamide ligands bind in a bidentate fashion to the ruthenium center, forming a nonplanar six-membered ring. The Ru–O1/O2 bond lengths were slightly different in both

DOI: 10.1021/om501032s
Organometallics 2015, 34, 848–857

Chart 2. Crystal Structures of 3a and 4a drawn at the 50% Probability Level[a]

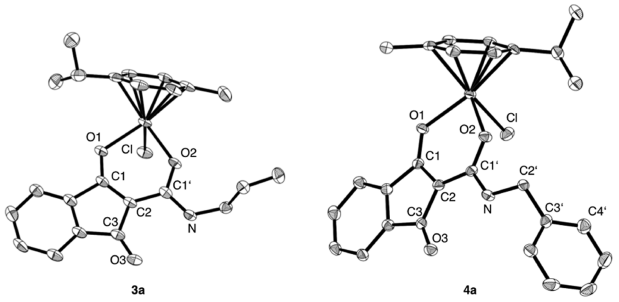

[a]Hydrogen atoms are omitted for clarity.

cases (**3a**, Ru−O1 = 2.0948(29) Å, Ru−O2 = 2.1145(26) Å; **4a**, Ru−O1 = 2.1075(20) Å, Ru−O2 = 2.0798(20) Å). The Ru−Cl bond was found in the same range in both complexes (**3a**, 2.4038(9) Å; **4a**, 2.3703(10) Å). The facially coordinated cym ligand was found to be disordered in the case of **3a**. Overall, the observed bond lengths are in good accordance with those in recently published papers for half-sandwich ruthenium and rhodium complexes.[5] The coordination of the ligand scaffold also has an observable impact on the electron density of the 1,3-indanedione-2-carboxamide backbone. The carbonyl C1−O1 bond (**3a**, 1.2718(46) Å; **4a**, 1.2671(34) Å) is slightly longer than C3−O3 (**3a**, 1.2310(52) Å; **4a**, 1.2217(34) Å), which can be explained by the electron-withdrawing effect of the transition-metal center, and both carbonyl bonds of **3a** are longer than that in the literature for the uncoordinated backbone (1.222 Å).[26] In the case of **4a**, the effect of the benzyl substituent counteracts the ruthenium's electron withdrawal, leading to a carbonyl bond length in the expected vicinity. The measured bond lengths for C1−C2 (**3a**, 1.4647(49) Å; **4a**, 1.4066(39) Å), C2−C1′ (**3a**, 1.4536(53) Å; **4a**, 1.4401(38) Å), and the bond length of the carboxamide carbonyl C1′-O1′ (**3a**, 1.2781(46) Å; **4a**, 1.2663(34) Å) to C1−O1 suggests no distinct double bonds in the chelate ring system but π-electron delocalization. Hydrogen bonding was observed in both cases (N−H···O3: 3.113 Å for **3a** and 2.976 Å for **4a**). The benzyl side chain of **4a** is twisted out of the dioxoindane plane with a torsion angle of 116.05(31)°.

Stability in Aqueous Solution. The stability under physiological conditions is of crucial importance for intravenously administered drugs. It has already been reported that neutral half-sandwich complexes hydrolyze rapidly in aqueous media, yielding the corresponding positively charged aqua species, assumed to interact with the biological targets: i.e. proteins, enzymes, and/or nucleobases[4,27] (Scheme 2). The longevity of the hydrolyzed species **1a**′,**b**′−**4a**′,**b**′ was investigated via IT-ESI-MS measurements. Obviously, the leaving group is lost in the electron beam of the mass spectrometer. Thus, the measurements only give information on the stability of the $[M - Cl]^+$ fragment, not on whether the leaving group was a chloride ion or a water molecule. The complex solutions (1% DMSO/H_2O, 50 μM) were incubated at 37 °C, and samples were taken after 1, 3, 6, 24, and 48 h. All investigated complexes showed remarkable stability under these conditions. Only the characteristic $[M - Cl]^+$ signals were found (**1a**, m/z 438.06 ± 0.01, m_{th} 438.06; **2a**, m/z 452.07 ± 0.01, m_{th} 452.08; **3a**, m/z 466.09 ± 0.01, m_{th} 466.10; **4a**, m/z 514.06 ± 0.01, m_{th} 514.09; **1b**, m/z 440.07 ± 0.01, m_{th} 440.07; **2b**, m/z 454.09 ± 0.01, m_{th} 454.08; **3b**, m/z 468.09 ± 0.01, m_{th} 468.10; **4b**, m/z 516.08 ± 0.01, m_{th} 516.09), and no solvent adducts with either water or DMSO were detected. Due to the very similar behavior of the investigated complexes, only the biomolecular interactions of compounds **1a**,**b** (R = methyl) and **4a**,**b** (R = benzyl) were further investigated, in order to determine whether the lipophilicity has an influence on the reactivity.

Reactivity toward Small Biomolecules. Upon intravenous drug administration, the first possible binding partners are blood proteins. It is therefore of utmost importance to obtain information on the binding preferences of newly designed drugs. The reactivity toward the following model compounds was determined via IT-ESI-MS: selected amino acids (L-histidine (His), L-cysteine (Cys), and glycine (Gly)), proteins (ubiquitin (Ub) and cytochrome C (cyt)), and deoxynucleoside triphosphates (5′-dATP and 5′-dGTP). Due to the poor solubility of the investigated complexes (0.02−0.1 mg/mL in water with 1% DMSO for **1a**,**b** and **4a**,**b**, respectively), mass spectrometric investigations were conducted instead of employing NMR methods.

The complexes' behavior toward amino acids was determined by incubation with an equimolar mixture of Gly, Cys, and His. None of the complexes showed any reactivity toward Gly (see Figures S13−S16 in the Supporting Information). Coordination compounds **1a**′,**b**′ showed a general affinity toward Cys, where only 20% of Rh(Cp*) of **1b**′ forms a His adduct ($[Rh(Cp^*)(His)]^+$; m/z 392.04 ± 0.03, m_{th} 392.08). A total of 60% of Ru(cym) of **1a**′ binds His ($[Ru(cym)(His)]^+$; m/z 390.03 ± 0.03, m_{th} 390.08) until 24 h of incubation; however, after that more than 80% of the Ru was found coordinated to Cys ($[Ru(cym)(Cys)]^+$; m/z 355.97 ± 0.04, m_{th} 356.02). The complexes of ligand **L4**, on the other hand, have an affinity for His. **4a**′ only forms His adducts, and 80% of **4b**′ Rh(Cp*) occurs as $[Rh(Cp^*)(His)]^+$ over the entire incubation period.

The reactivity of the complexes toward the proteins Ub and cyt was investigated (see Figures S17−S20 in the Supporting Information). The model protein Ub was chosen to depict the innate reactivity toward proteins in general and cyt as a redox-active and apoptosis-inducing mitochondrial protein. Ub possesses two potential binding sites (Met1 and His68), whereas cyt offers three (His26, His33, and Met65). Due to the fact that these samples were diluted with formic acid (0.02% (v/v)) in order to denature the present proteins, they occur in various positively charged states (Ub, 7−14; cyt, 11−19). Therefore, deconvolution of the measured spectra was necessary. All investigated organometallics exhibited a clear affinity toward Ub, and the spectra were dominated by the characteristic $[M(Ar)(Ub)]^+$ peak (**1a**′ and **4a**′, M = Ru and Ar = cym, m/z 8798.1 ± 1.2, m_{th} 8798.6; **1b**′ and **4b**′, M = Rh and Ar = Cp*, m/z 8801.1 ± 1.4, m_{th} 8800.6). The ruthenium spectra even showed the initial formation of a $[Ru_2(cym)_2(Ub)]^+$ adduct (m/z 9030.6 ± 2.1, m_{th} 9031.6), which after 24 h only makes up about 8% of the entire ruthenium population. However, the complexes show very low affinity for cyt binding, forming a $[M(Ar)(cyt)]^+$ adduct (**1a**′, M = Ru and Ar = cym, m/z 12592.8 ± 2.0, m_{th} 12593.4; **1b**′ and **4b**′, M = Rh and Ar = Cp*, m/z 12594.4 ± 1.0, m_{th} 12595.4). **4a**′ does not bind cyt at all, and the other complexes never bind more than 12% of all present cytochrome C. These results suggest that reaction with cyt is not a likely pathway for the biological activity.

Once biologically active compounds enter cells, they again encounter proteins and might reach the DNA. In order to

DOI: 10.1021/om501032s
Organometallics 2015, 34, 848−857

identify the mode of action of the synthesized organometallics, they were incubated with a mixture of 5′-dATP and 5′-dGTP. The intensity of the formed adducts was very low (see Figures S21 and S22 in the Supporting Information). However, only complexes of the ligand **L1** formed such adducts at all, showing that there is a very low binding affinity of the Ru(cym) and Rh(Cp*) moieties toward deoxynucleoside triphosphates (dNTPs). Nevertheless, when it was incubated with the dNTP-mixture, **1a**′ revealed a clear selectivity of the Ru(cym) moiety toward guanine. About 75% of ruthenium was found as the $[Ru(cym)(5'\text{-dGTP})]^{2-}$ adduct (m/z 377.47 ± 0.01, m_{th} 377.49). The remaining 25% were bound to adenosine; $[Ru(cym)(5'\text{-dATP})]^{2-}$ (m/z 369.48 ± 0.01, m_{th} 369.49). The rhodium complex **1b**′ revealed selectivity toward 5′-dATP, as 88% of all rhodium was bound to the adenosine moiety. However, 28% of all present rhodium was $[Rh(\eta^5\text{-Cp*})(5'\text{-dADP})]^{-}$ (m/z 662.04 ± 0.01, m_{th} 662.03), and 5% was found as $[Rh(\eta^5\text{-Cp*})(5'\text{-dGDP})]^{-}$ (m/z 678.02 ± 0.02, m_{th} 678.02). The occurrence of deoxynucleoside diphosphates suggests binding of the organorhodium complex to the phosphate chain, leading to elimination of the terminal phosphate. The fact that no diphosphate adducts were found in the analogous spectra of **1a**′ rules out phosphate elimination due to the spraying process and allows the conclusion that the Rh(Cp*) moiety binds not only to the N6 and the O6 of guanosine and adenosine, respectively, but to the triphosphate group as well.

All complexes were incubated with amino acids and dNTPs concurrently, in order to determine which kind of nucleophiles preferably interact with the organometallics. No significant amounts of deoxynucleoside adducts and the same distribution of amino acid adducts as before was observed. This result indicates that the biological activity of this compound class might be attributed to interactions with proteins.

Biological Activity of the Compounds. The antiproliferative activity of ligands **L1**−**L4** and the respective ruthenium (**1a**−**4a**) and rhodium (**1b**−**4b**) complexes was evaluated in human ovarian (CH1/PA-1), colon (SW480), and non-small-cell lung carcinoma (A549) cell lines (Table 1). In general, CH1/PA-1 cells were found to be the most sensitive of these cell lines. The antiproliferative potential of the ligands seems to depend on the lipophilicity and increases in the following order: **L1** (Me) ≤ **L2** (Et) < **L3** (Pr) < **L4** (Bn). Differences in cytotoxicity of the complexes are somewhat less pronounced, but they are usually at least as potent as the corresponding ligand; differences between ruthenium and rhodium analogues are mostly small to negligible. The most potent of all tested compounds are complexes **4a** (Ru) and **4b** (Rh), with IC_{50} values of 13 and 9 μM, respectively, in CH1/PA-1 cells, which was the most sensitive to the investigated compounds.

The most cytotoxic compounds (**4a**,**b**) were further investigated by means of a DNA relaxation assay for their topoisomerase IIα inhibitory properties, due to the structural similarities of this class of compounds to TAS-103.[28] For this purpose, two differently treated gels were prepared for each experiment. One gel (Figure 1A) was stained with ethidium bromide after electrophoresis to assess topo II catalytic activity. Another gel (Figure 1B) contained ethidium bromide already during electrophoresis and served to detect cleavage products caused by double-strand breaks (induced by topo II poisons only). In the latter case, the effects of ethidium bromide on the secondary structure causes the relaxed circular forms to migrate together with the unnicked supercoiled form of the plasmid, allowing identification of linear DNA in the presence of a relaxed circular plasmid.

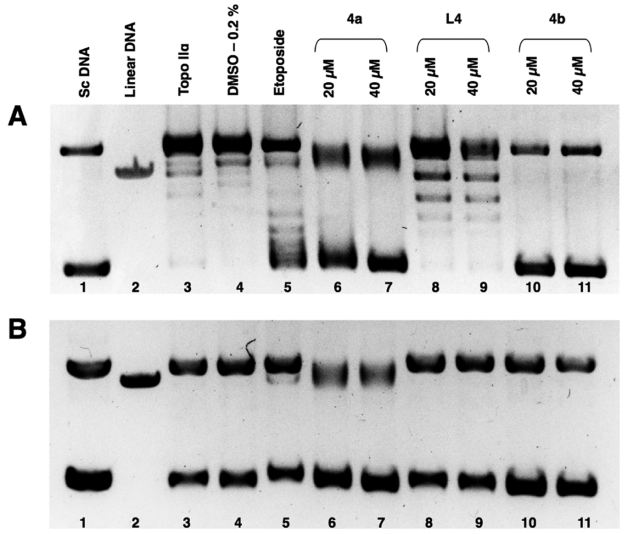

Figure 1. Topoisomerase IIα inhibitory capacity of **L4** and **4a**,**b** determined by the plasmid DNA relaxation assay. The top gel (A) is poststained and the bottom gel (B) is prestained with 0.5 μg/mL ethidium bromide. Gel A: supercoiled and linear DNA used as references (lanes 1 and 2, respectively); relaxed DNA bands (lane 3) indicating intact enzyme activity; DMSO control (lane 4); inhibition of enzyme relaxation activity by positive control (0.8 mM etoposide, lane 5). Lanes 6−11 display the effect of topo IIα on supercoiled plasmid DNA in the presence of the test compounds. Gel B serves for detecting topo II cleavage products such as the linear DNA band induced by 0.8 mM etoposide.

Remarkably, the metal complexes **4a**,**b** displayed a pronounced capacity of inhibiting topo IIα, whereas the uncoordinated ligand **L4** in the applied concentrations did not (Figure 1A). As illustrated by Figure 1B, none of these compounds act as a topo IIα poison since a linear DNA band is present only in the positive control, reflecting double-strand breaks as a result of stabilized topo II-DNA adducts. Thus, the complexes are able to catalytically inhibit topo II in one of the following ways; they either block the ATP-binding site of the enzyme, preventing the binding of the enzyme to DNA or

Table 1. Inhibition of Cancer Cell Growth in Three Human Cancer Cell Lines: 50% Inhibitory Concentrations (Means ± Standard Deviations), obtained by the MTT Assay[a]

	IC_{50} values/μM		
compound	CH1/PA-1	SW480	A549
L1	83 ± 20	>200	>200
1a	17 ± 5	76 ± 15	>200
1b	62 ± 5	76 ± 11	>200
L2	108 ± 7	143 ± 8	179 ± 10
2a	60 ± 2	82 ± 5	118 ± 9
2b	53 ± 23	107 ± 20	242 ± 15
L3	37 ± 1	55 ± 6	72 ± 4
3a	35 ± 1	43 ± 3	64 ± 4
3b	36 ± 2	44 ± 3	72 ± 11
L4	14 ± 2	29 ± 5	34 ± 4
4a	13 ± 3	20 ± 1	37 ± 10
4b	9 ± 2	21 ± 6	28 ± 2

[a]Exposure time: 96 h.

DOI: 10.1021/om501032s
Organometallics 2015, 34, 848−857

impeding the cleavage of DNA.[29] DNA interactions of **4a** might explain the observed smearing of the bands in the electropherograms (Figure 1B, lanes 6 and 7). The inhibitory effects of TAS-103 on topo II catalytic activity was evaluated by Minderman and co-workers.[17] They showed that TAS-103 at concentrations of 24.6 μM and higher inhibits DNA relaxation (as etoposide does) but does not cause the formation of linear DNA species as would be expected for topo II poisons. Compounds **4a**,**b** showed the ability to inhibit enzyme activity at concentrations of 20 μM and higher without formation of linear DNA, suggesting that these compounds might be as potent as TAS-103 for catalytic topo II inhibitors.

The ability to alter the secondary structure of DNA in cell-free experiments was studied by the use of an electrophoretic dsDNA plasmid assay (Figure 2). Retardation of the super-coiled (SC) form by the ruthenium complex **4a** indicates untwisting by DNA binding (Figure 2, lanes 2−6). In contrast, the rhodium complex **4b** and the corresponding ligand **L4** did not show any impact on DNA mobility and secondary structure. Since compounds **4a**,**b** exhibit catalytic topo II inhibitory potential, the changes in cell cycle distribution were examined by flow cytometry using propidium iodide staining. Merbarone, a catalytic inhibitor that is in clinical trials as an anticancer drug, was used as a positive control. Merbarone acts primarily by blocking topo II mediated DNA cleavage, resulting in cell cycle delay.[30,31] As illustrated in Figure 3A, the most pronounced effect was observed in the case of **4a** in CH1/PA-1 cells after 12 h of treatment, showing an increase of the S-phase fraction from 27% to 43%, and a similar trend was found in SW480 cells (29% to 38%); both are comparable to the effects of merbarone (see Table S2 in the Supporting Information). These data are consistent with topoisomerase inhibition tests and support the assumption that the tested compounds act as catalytic topoisomerase inhibitors.

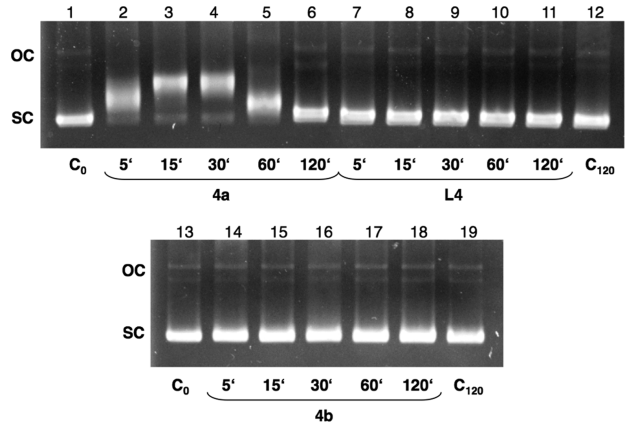

Figure 2. Electropherogram of dsDNA plasmid pUC19 after exposure to a 40 μM solution of ligand **L4** (lanes 7−11), ruthenium complex **4a** (lanes 2−6), and rhodium complex **4b** (lanes 14−18) for different exposure times (5 min to 2 h) in comparison to untreated controls (C_0).

There is evidence that topo II inhibitors effectively block transcription and replication and cells subsequently undergo apoptosis.[29] The potential for the induction of apoptosis of ruthenium(II) complexes **1a**−**4a** and rhodium(III) complexes **1b**−**4b** was elucidated by annexin V-FITC/propidium iodide double staining in SW480 cells and subsequent flow cytometric analysis (Figure 4). Only a total of 11% of the SW480 cells were found in early- or late-stage apoptosis upon treatment with **4a** (up to a concentration of 320 μM), which is 2.8 times more than that in the negative control (4%) but 3.9 times less than that of the positive control merbarone (43%). After treatment with **4b** about 36% of cells were in apoptosis and 32% after exposure to free ligand **L4** (see Table S3 in the Supporting Information). Thus, the ruthenium complex seems to induce stronger cell cycle perturbations, whereas the free ligand and the rhodium complex are stronger inducers of apoptosis.

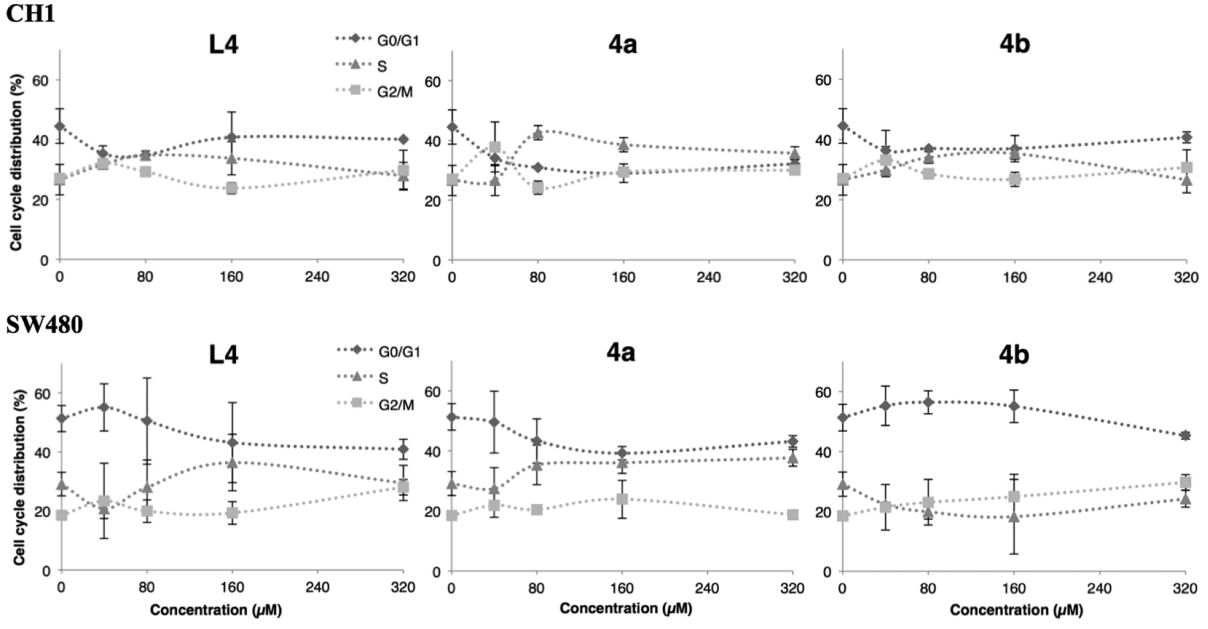

Figure 3. Concentration-dependent impact of compounds **L4** and **4a**,**b** on the cell cycle distribution of CH1/PA-1 and SW480 cells after 12 h of exposure.

DOI: 10.1021/om501032s
Organometallics 2015, 34, 848−857

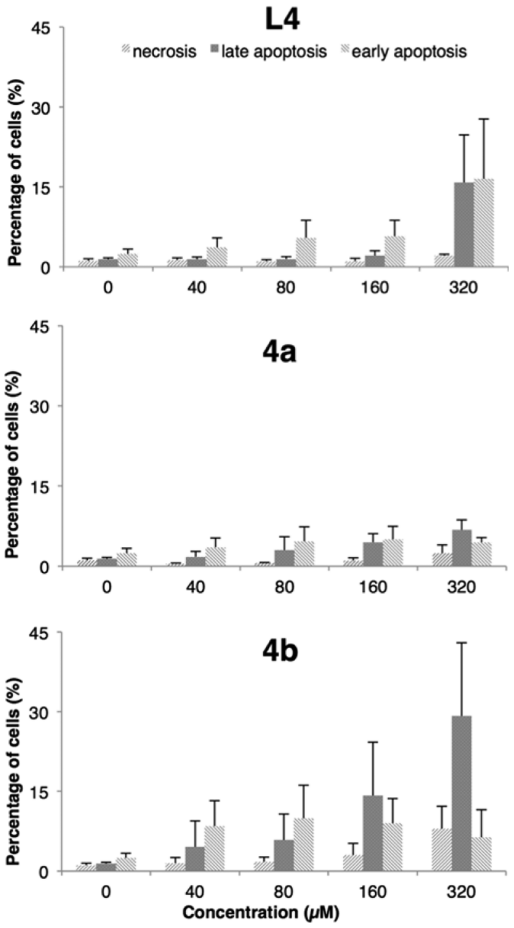

Figure 4. Apoptosis/necrosis induction in SW480 cells after 24 h of exposure to the studied compounds, measured by flow cytometry using annexin V-FITC/propidium iodide double staining.

CONCLUSIONS

Within this work, four N-substituted 1,3-dioxoindan-2-carboxamides and their corresponding organometallic ruthenium and rhodium complexes were synthesized. The obtained compounds were characterized by standard analytical methods, and for two substances the respective solid-state structure was determined. All complexes quickly hydrolyzed under physiological conditions, and the formed aqua complexes were stable for at least 48 h in aqueous systems. The affinity toward small biomolecules such as amino acids and model proteins was elucidated and preferential binding to proteins of the organometallics was observed. The utilized metal centers showed different affinity toward dNTPs. Ru(II) interacted preferably with dGTP, whereas Rh(III) reacts either with the N7 of the purine ring or with the triphosphate residue of dATP. However, the affinity of the investigated compounds toward dNTPs was determined to be very low in competition experiments with amino acids. The biological activity was determined in three different human cancer cell lines, and IC_{50} values were found in the low micromolar range for the benzyl derivatives. It seems that coordination of the bioactive ligand scaffold to the organometallic fragments has only a minor impact on the cytotoxicity; however, there is a distinct impact on topoisomerase IIα inhibition properties of the compounds. The metal complexes were able to catalytically inhibit topo IIα in the concentration range of their IC_{50} values, in contrast to the free ligand. Cell cycle distribution analyses revealed an increase of the S-phase fraction upon exposure to the organometallics, due to the inhibition of this key enzyme, especially the Ru(II) representative. In addition, the metal complexes were investigated for their apoptosis induction properties and the Rh(III) complex showed a significantly higher potential than the analogous Ru(II) compound.

Overall, this novel class of organometallic complexes bearing bioactive 1,3-dioxoindane ligand systems showed very promising in vitro results and will be further investigated for their anticancer potential.

EXPERIMENTAL SECTION

Materials and Methods. All solvents were purchased from commercial sources and distilled prior to use. Chloroform was dried over molecular sieves (3 Å) before use. 2-Hydroxy-1,4-naphthoquinone (99%; Acros Organics), (diacetoxyiodo)benzene (Aldrich), methylamine (40% solution in water; Merck), ethylamine (70% solution in water; Merck), propylamine (≥99.0%; Fluka), benzylamine (≥99.0%; Fluka), sodium hydroxide (≥98%; Sigma-Aldrich), hydrochloric acid (30−33%; Donauchem), sodium sulfate (anhydrous; 99%; Acros Organics), ruthenium(III) chloride trihydrate (Johnson Matthey), α-terpinene (90%; Acros Organics), rhodium(III) chloride hydrate (Johnson Matthey), 1,2,3,4,5-pentamethylcyclopentadiene (95%; Aldrich), sodium methoxide (~95%; Fluka), glycine (Merck), L-cysteine (Fluka), L-histidine (Merck), guanosine 5′-triphosphate sodium salt hydrate (≥95%; Sigma), adenosine 5′-triphosphate disodium salt (Calbiochem), ammonium bicarbonate (≥99.5%; Fluka), ubiquitin (≥98%; bovine erythrocytes; Sigma), cytochrome C (99%; horse heart; Sigma), and formic acid (p.a.; Fluka) were purchased and used without further purification. 2-Oxido-phenyliodonio-1,4-naphthoquinone (**P1**) was synthesized as described elsewhere.[22]

Melting points were determined with a Büchi Melting Point M-560 instrument. The solubility was determined by dissolving the compound in DMSO and subsequent dilution to a final concentration of 1% DMSO/PBS (phosphate buffered saline) and 1% DMSO/MSP (medium with serum proteins). The highest concentrated dilution, where no precipitation of the compound occurred, was the determined solubility. The NMR spectra were recorded at 25 °C using a Bruker FT-NMR spectrometer Avance III 500 MHz. ^{1}H NMR spectra were measured at 500.10 MHz and ^{13}C NMR spectra at 125.75 MHz in deuterated dimethyl sulfoxide (DMSO-d_6) or chloroform ($CDCl_3$). 2D NMR spectra were measured using a gradient-enhanced mode. CHN elemental analyses were performed with a Eurovector EA3000 Elemental Analyzer in the microanalytical laboratory of the University of Vienna. Single crystals of **3a** and **4a** suitable for X-ray diffraction analysis were grown by a slow diffusion method from chloroform and pentanes at 4 °C. The X-ray diffraction data were recorded on a Bruker X8 APEX II CCD diffractometer at 100 K. The single crystals were positioned at 40 and 35 mm from the detector, and 1204 and 1380 frames were measured, each for 30 and 5 s over 1° scan width. The data were processed using the SAINT software package.[32] The structures were solved by direct methods and refined by full-matrix least-squares techniques. Non-hydrogen atoms were refined with anisotropic displacement parameters. H atoms were inserted at calculated positions and refined with a riding model. The following computer programs were used: structure solution, SHELXS-97[33] and Platon;[34] refinement, SHELXL-97[33] and Olex2;[35] molecular diagrams, ORTEP-3.[36] The crystallographic data files for **3a** and **4a** have been deposited with the Cambridge Crystallographic Database as CCDC 1019295 and 1019294, respectively. Electrospray ionization mass spectra were recorded on a Bruker AmaZon SL ion trap mass spectrometer (Bruker Daltonics GmbH). Data were attained and processed with Compass 1.3 and Data Analyis 4.0 (Bruker Daltonics GmbH). Protein spectra were deconvoluted by the use of the maximum entropy algorithm with a m/z 0.2 mass step and m/z 0.5 instrument peak width. Mass spectra were recorded via direct infusion with a sample concentration of 5 μM and a flow rate of 240 μL/h.

DOI: 10.1021/om501032s
Organometallics 2015, 34, 848−857

Small molecules were measured with the following settings: dry temperature, 180 °C; nebulizer, 8.00 psi; dry gas, 6.00 L/min; the high voltage capillary was set to −4500 V or +4500 V for positive and negative mode, respectively. The target mass was set to m/z 600. Proteins were measured with the following settings: dry temperature, 180 °C; nebulizer, 6.00 psi; dry gas, 6.00 L/min; the high voltage capillary set to −3500 V, and target mass set to m/z 1000.

General Procedure for the Synthesis of 1,3-Dioxo-2-indancarboxamides. After 2-oxido-3-phenyliodonio-1,4-naphthoquinone (**P1**; 1 equiv) was suspended in dry chloroform (10 mL for every 100 mg of **P1**), the amine (1 equiv) was added. The mixture was refluxed under argon until TLC analysis (*n*-hexane/ethyl acetate 1/1) showed full conversion of the educt (reaction times varied from 8 h to 3 days). The reaction mixture was extracted with aqueous sodium hydroxide (1 M). The alkaline extracts were then combined and washed with DCM. The aqueous layer was acidified with hydrochloric acid (30%/33%), leading to precipitation of the product. The resulting suspension was extracted with DCM, and the combined organic layers were dried over anhydrous sodium sulfate, filtered, evaporated to dryness, and dried in vacuo.

General Complexation Procedure. The appropriate 1,3-dioxoindan-2-carboxamides ligand **L1**−**L4** (1 equiv) was deprotonated by sodium methoxide (1.1 equiv) in methanol (10 mL) and stirred for 15 min. Afterward, a solution of the respective dimeric precursor bis[dichlorido(cym)ruthenium(II)] or bis[dichlorido(Cp*)rhodium-(III)] (0.9 equiv) in DCM (10 mL) was added and the reaction mixture was stirred for 30−35 h. Half-sandwich ruthenium(II) complexes can generally be synthesized without inert conditions; however, it was decided to prepare all complexes under an argon atmosphere to avoid possible side reactions. The solvent was removed, the residue was dissolved in DCM, and the solution was filtered and concentrated under reduced pressure to a final volume of about 2 mL. The complex was then precipitated by addition of *n*-hexane and the formed solid separated by filtration. The product was washed with cold *n*-hexane and dried in vacuo. Rh(Cp*) complexes needed to be precipitated twice for sufficient purity.

*2-(Hydroxy(methylamino)methylene)-1H-indene-1,3(2H)-dione (**L1**).* The synthesis was performed according to the general procedure of 1,3-dioxo-2-indancarboxamides, using **P1** (405 mg, 1.08 mmol) and methylamine (40%, 93 μL, 1.08 mmol) with a reaction time of 30 h, yielding a green solid (217 mg, 85%); mp 147−148 °C, solubility 0.43 mg/mL ≡ 2.12 mM (PBS, 1% DMSO) and 0.60 mg/mL ≡ 2.88 mM (MSP, 1% DMSO); ^{1}H NMR (500.10 MHz, DMSO-d_6) δ 2.92 (s, 3H, H2′), 7.55−7.66 (m, 4H, H4, H5, H6, H7), 8.69 (br s, 1H, NH) ppm; ^{13}C NMR (125.75 MHz, DMSO-d_6) δ 26.5 (C2′), 93.0 (C2), 120.8 (C4, C7), 133.1 (C5, C6), 137.8 (C3a, C7a), 166.0 (C1′), 190.7 (C1, C3) ppm. Anal. Calcd for $C_{11}H_9NO_3$: C, 65.02; H, 4.46; N, 6.89. Found: C, 65.07; H, 4.44, 6.85.

*2-((Ethylamino)(hydroxy)methylene)-1H-indene-1,3(2H)-dione (**L2**).* The synthesis was performed according to the general procedure of 1,3-dioxo-2-indancarboxamides, using **P1** (200 mg, 0.532 mmol) and ethylamine (70%, 42 μL, 0.532 mmol) with a reaction time of 30 h, yielding an orange solid (95 mg, 83%): mp 103−107 °C; solubility 0.30 mg/mL ≡ 1.38 mM (PBS, 1% DMSO) and 0.15 mg/mL ≡ 0.69 mM (MSP, 1% DMSO); ^{1}H NMR (500.10 MHz, DMSO-d_6) δ 1.17 (t, ^3J(H,H) = 7 Hz, 3H, H3′), 3.36−3.43 (m, 2H, H2′), 7.54−7.66 (m, 4H, H4, H5, H6, H7), 8.75 (br s, 1H, NH) ppm; ^{13}C NMR (125.75 MHz, DMSO-d_6) δ 14.6 (C3′), 34.7 (C2′), 92.8 (C2), 120.8 (C4, C7), 133.1 (C5, C6), 137.8 (C3a, C7a), 165.5 (C1′), 190.8 (C1, C3) ppm. Anal. Calcd for $C_{12}H_{11}NO_3$: C, 66.35; H, 5.10; N, 6.45. Found: C, 66.41; H, 5.01; N, 6.01.

*2-(Hydroxy(propylamino)methylene)-1H-indene-1,3(2H)-dione (**L3**).* The synthesis was performed according to the general procedure of 1,3-dioxo-2-indancarboxamides, using **P1** (751 mg, 1.99 mmol) and *n*-propylamine (137 μL, 1.99 mmol) with a reaction time of 72 h, yielding an orange solid (341 mg, 74%): mp 78−80 °C; solubility 0.50 mg/mL ≡ 2.16 mM (PBS, 1% DMSO) and 0.43 mg/mL ≡ 1.86 mM (MSP, 1% DMSO); ^{1}H NMR (500.10 MHz, DMSO-d_6) δ 0,89 (t, ^3J(H,H) = 7 Hz, 3H, H4′), 1.55−1.62 (m, 2H, H3′), 3.28−3.37 (m, 2H, H2′), 7.55−7.67 (m, 4H, H4, H5, H6, H7), 8.73 (br s, 1H, NH) ppm; ^{13}C NMR (125.75 MHz, DMSO-d_6) δ 11.0 (C4′), 22.2 (C3′), 45.1 (C2′), 92.9 (C2), 120.8 (C4, C7), 133.1 (C5, C6), 137.8 (C3a, C7a), 165.7 (C1′), 190.8 (C1, C3) ppm. Anal. Calcd for $C_{13}H_{13}O_3N$: C, 67.52; H, 5.67; N, 6.06. Found: C, 67.47; H, 5.73; N, 5.86.

*2-((Benzylamino)(hydroxy)methylene)-1H-indene-1,3(2H)-dione (**L4**).* The synthesis was performed according to the general procedure of 1,3-dioxo-2-indancarboxamides, using **P1** (100 mg, 0.266 mmol) and benzylamine (29 μL, 0.266 mmol) with a reaction time of 8 h, yielding a yellow solid (71 mg, 96%): mp 141−143 °C, solubility 0.20 mg/mL ≡ 0.72 mM (PBS, 1% DMSO) and 0.3 mg/mL ≡ 1.07 mM (MSP, 1% DMSO); ^{1}H NMR (500.10 MHz, DMSO-d_6) δ 4.57(s, 2H, H2′), 7.26−7.30 (m, 1H, H6′), 7.32−7,39 (m, 4H, H4′, H5′, H7′, H8′), 7.56−7.66 (m, 4H, H4, H5, H6, H7), 9.18 (br s, 1H, NH) ppm; ^{13}C NMR (125.75 MHz, DMSO-d_6) δ 42.9 (C2′), 93.4 (C2), 120.9 (C4,C7), 127.3 (C6′), 127.4 (C4′), 128.5 (C5′), 133.1 (C5, C6), 137.67 (C3a, C7a), 137.73 (C3′), 165.6 (C1′), 190.6 (C1, C3) ppm. Anal. Calcd for $C_{17}H_{13}NO_3$: C, 73.11; H, 4.69; N, 5.02. Found: C, 72.81; H, 4.43; N, 4.69.

*(Chlorido)((1,3-dioxo-κO1-1H-inden-2(3H)-ylidene)-(methylamino)methanolato-κO2)(p-cymene)ruthenium(II) (**1a**).* The synthesis was performed according to the general complexation procedure, using bis[dichlorido(*p*-cymene)ruthenium(II)] (200 mg, 32 μmol), ligand **L1** (146 mg, 717 μmol), and sodium methoxide (45 mg, 832 μmol) to afford brown crystals (217 mg, 70%): mp >159 °C dec; solubility 0.08 mg/mL ≡ 0.17 mM (PBS, 1% DMSO) and 0.08 mg/mL ≡ 0.17 mM (MSP, 1% DMSO); ^{1}H NMR (500.10 MHz, $CDCl_3$) δ 1.39−1.45 (m, 6H, $2CH_3$-f), 2.30 (s, 3H, CH_3-g), 2.96−3.04 (m, 4H, H2′,He), 5.31−5.37 (m, 2H, Hb), 5.57−5.66 (m, 2H, Hc), 7.37−7.43 (m, 3H, H5, H6, H7), 7.50−7.54 (m, 1H, H4), 8.43 (q, ^3J(H,H) = 4.9 Hz, 1H, NH) ppm; ^{13}C NMR (125.75 MHz, $CDCl_3$) δ 17.9 (CH_3-g), 22.40 and 22.43 ($2CH_3$-f), 26.1 (C2′), 31.1 (Ce), 79.2 and 79.3 (Cb), 82.7 and 82.8 (*Cc*), 96.6 (Ca), 98.4 (C2), 99.4 (Cd), 120.6 (C7), 120.8 (C4), 132.0 (C5), 132.2 (C6), 136.4 (C7a), 137.8 (C3a), 166.6 (C1′), 190.7 (C3), 192.5 (C1) ppm. Anal. Calcd for $C_{21}H_{22}ClNO_3Ru{\cdot}0.25CH_2Cl_2$: C, 51.64; H, 4.59; N, 2.83. Found: C, 51.72; H, 4.25; N, 2.77.

*(Chlorido)((1,3-dioxo-κO1-1H-inden-2(3H)-ylidene)(ethylamino)-methanolato-κO2)(p-cymene)ruthenium(II) (**2a**).* The synthesis was performed according to the general complexation procedure, using bis[dichlorido(*p*-cymene)ruthenium(II)] (250 mg, 0.408 mmol), compound **L2** (194 mg, 0.895 mmol), and sodium methoxide (54 mg, 1.01 mmol) to afford a brown solid (317 mg, 80%): mp >142 °C dec; solubility 0.10 mg/mL ≡ 0.21 mM (PBS, 1% DMSO) and 0.39 mg/mL ≡ 0.8 mM (MSP, 1% DMSO); ^{1}H NMR (500.10 MHz, $CDCl_3$) δ 1.23 (t, ^3J(H,H) = 7 Hz, 3H, H3′), 1.38−1.45 (m, 6H, $2CH_3$-f), 2.30 (s, 3H, CH_3-g), 2.95−3.04 (m, 1H, He), 3.40−3.49 (m, 2H, H2′), 5.31−5.36 (m, 2H, Hb), 5.57−5.65 (m, 2H, Hc), 7.36−7.42 (m, 3H, H5, H6, H7), 7.50−7.54 (m, 1H, H4), 8.48 (t, ^3J(H,H) = 5 Hz, 1H, NH) ppm; ^{13}C NMR (125.75 MHz, $CDCl_3$) δ 15.1 (C3′), 17.9 (CH_3-g), 22.39 and 22.42 ($2CH_3$-f), 31.1 (Ce), 34.4 (C2′), 79.2 and 79.4 (Cb), 82.6 and 82.7 (*Cc*), 96.6 (Ca), 98.3 (C2), 99.4 (Cd), 120.6 (C7), 120.8 (C4), 132.0 (C5), 132.2 (C6), 136.4 (C7a), 137.8 (C3a), 166.0 (C1′), 190.7 (C3), 192.5 (C1) ppm. Anal. Calcd for $C_{22}H_{24}ClNO_3Ru$: C, 54.26; H, 4.97; N, 2.88. Found: C, 53.98; H, 5.05; N, 2.83.

*(Chlorido)((1,3-dioxo-κO1-1H-inden-2(3H)-ylidene)-(propylamino)methanolato-κO2)(p-cymene)ruthenium(II) (**3a**).* The synthesis was performed according to the general complexation procedure, using bis[dichlorido(*p*-cymene)ruthenium(II)] (50 mg, 81 μmol), compound **L3** (39 mg, 168 μmol), and sodium methoxide (11 mg, 206 μmol) to afford red-brown crystals (46 mg, 56%): mp >148 °C dec; solubility 0.15 mg/mL ≡ 0.30 mM (PBS, 1% DMSO) and 0.35 mg/mL ≡ 0.69 mM (MSP, 1% DMSO); ^{1}H NMR (500.10 MHz, $CDCl_3$) δ 0.98 (t, ^3J(H,H) = 7 Hz, 3H, H4′), 1.39−1.44 (m, 6H, $2CH_3$-f), 1.55−1.66 (m, 2H, H3′), 2.30 (s, 3H, CH_3-g), 2.95−3.04 (m, 1H, He), 3.32−3.43 (m, 2H, H2′), 5.31−5.36 (m, 2H, Hb), 5.57−5.64 (m, 2H, Hc), 7.38−7.42 (m, 3H, H5, H6, H7), 7.50−7.55 (m, 1H, H4), 8.56 (t, ^3J(H,H) = 6 Hz, 1H, NH) ppm; ^{13}C NMR (125.75 MHz, $CDCl_3$) δ 11.7 (C4′), 18.0 (CH_3-g), 22.41 and 22.45 ($2CH_3$-f), 23.1 (C3′), 31.1 (Ce), 41.2 (C2′), 79.1 and 79.4 (Cb), 82.6 and 82.8 (*Cc*),

DOI: 10.1021/om501032s
Organometallics 2015, 34, 848−857

96.6 (Ca), 98.3 (C2), 99.4 (Cd), 120.6 (C7), 120.8 (C4), 132.0 (C5), 132.2 (C6), 136.5 (C7a), 137.8 (C3a), 166.1 (C1′), 190.7 (C3), 192.5 (C1) ppm. Anal. Calcd for $C_{23}H_{26}O_3ClNRu·0.25H_2O$: C, 54.65; H, 5.28; N, 2.77. Found: C, 54.46; H, 5.36; N, 2.65.

(Chlorido)(1(,3-dioxo-κO1-1H-inden-2(3H)-ylidene)-(benzylamino)methanolato-κO2)(p-cymene)ruthenium(II) (**4a**). The synthesis was performed according to the general complexation procedure, using bis[dichlorido(*p*-cymene)ruthenium(II)] (200 mg, 327 μmol), compound **L4** (201 mg, 719 μmol), and sodium methoxide (43 mg, 791 μmol) to afford red crystals (302 mg, 84%): mp >155 °C dec; solubility 0.02 mg/mL ≡ 0.04 mM (PBS, 1% DMSO) and 0.14 mg/mL ≡ 0.25 mM (MSP, 1% DMSO); ^{1}H NMR (500.10 MHz, $CDCl_3$) δ 1.28−1.35 (m, 6H, $2CH_3$-f), 2.21 (s, 3H, CH_3-g), 2.77−3.58 (m, 1H, He), 4.53 (dd, ^2J(H,H) = 15 Hz, ^3J(H,H) = 6 Hz, 1H, H2′), 4.72 (dd, ^2J(H,H) = 15 Hz, ^3J(H,H) = 6 Hz, 1H, H2′), 5.23−5.31 (m, 2H, Hb), 5.43−5.55 (m, 2H, Hc), 7.25−7.30 (m, 1H, H6′), 7.31−7.37 (m, 4H, H4′, H5′, H7′, H8″), 7.39−7.45 (m, 3H, H5, H6, H7), 7.52−7.57 (m, 1H, H4), 8.94 (t, ^3J(H,H) = 6 Hz, 1H, NH) ppm; ^{13}C NMR (125.75 MHz, $CDCl_3$) δ 17.9 (CH_3-g), 22.3 and 22.4 ($2CH_3$-f), 30.9 (Ce), 43.4 (C2′), 78.9 and 79.3 (Cb), 82.4 and 82.7 (Cc), 96.7 (Ca), 98.2 (C2), 99.6 (Cd), 120.7 (C7), 120.9 (C4), 127.28 (C4′, C8′), 127.30 (C6′), 128.7 (C5′, C7′), 132.1 (C5), 132.3 (C6), 136.5 (C7a), 137.8 (C3a), 138.8 (C3′), 166.1 (C1″), 190.9 (C3), 192.5 (C1) ppm. Anal. Calcd for $C_{27}H_{26}ClNO_3Ru$: C, 59.07; H, 4.77; N, 2.55%. Found: C, 58.93; H, 4.60; N, 2.42.

(Chlorido)((1,3-dioxo-κO1-1H-inden-2(3H)-ylidene)-(methylamino)methanolato-κO2)(Cp)rhodium(III)* (**1b**). The synthesis was performed according to the general complexation procedure, using bis[dichlorido(Cp*)rhodium(III)] (50 mg, 81 μmol), compound **L1** (37 mg, 181 μmol), and sodium methoxide (11 mg, 209 μmol) to afford an orange solid (58 mg, 76%): mp >246 °C dec; solubility 0.10 mg/mL ≡ 0.21 mM (PBS, 1% DMSO) and 0.06 mg/mL ≡ 0.13 mM (MSP, 1% DMSO); ^{1}H NMR (500.10 MHz, $CDCl_3$) δ 1.69 (s, 15H, Cp*-CH_3), 2.99 (d, ^3J(H,H) = 5 Hz, 3H, H2′), 7.37−7.46 (m, 3H, H5, H6, H7), 7.53−7.59 (m, 1H, H4), 8.58 (br q, ^3J(H,H) = 4 Hz, 1H, NH) ppm; ^{13}C NMR (125.75 MHz, $CDCl_3$) δ 8.8 (Cp*-CH_3), 25.9 (C2′), 92.4 (d, ^1J(Rh,C) = 10 Hz, Cp*), 92.5 (C2), 120.5 (C7), 120.7 (C4), 131.9 (C5), 132.0 (C6), 136.8 (C7a), 138.6 (C3a), 166.7 (C1′), 190.7 (C3), 192.9 (C1) ppm. Anal. Calcd for $C_{21}H_{23}ClNO_3Rh$: C, 53.01; H, 4.87; N, 2.94. Found: C, 53.15; H, 4.68; N, 2.55.

(Chlorido)((1,3-dioxo-κO1-1H-inden-2(3H)-ylidene)(ethylamino)-methanolato-κO2)(Cp)rhodium(III)* (**2b**). The synthesis was performed according to the general complexation procedure, using bis[dichlorido(Cp*)rhodium(III)] (250 mg, 0.405 mmol), compound **L2** (195 mg, 0.895 mmol), and sodium methoxide (54 mg, 1.01 mmol) to afford an orange solid (324 mg, 82%): mp >203 °C dec; solubility 0.09 mg/mL ≡ 0.18 mM (PBS, 1% DMSO) and 0.08 mg/mL ≡ 0.16 mM (MSP, 1% DMSO); ^{1}H NMR (500.10 MHz, $CDCl_3$) δ 1.23 (t, ^3J(H,H) = 7 Hz, 3H, H3′), 1.69 (s, 15H, Cp*-CH_3), 3.41−3.53 (m, 2H, H2′), 7.38−7.44 (m, 3H, H5, H6, H7), 7.54−7.57 (m, 1H, H4), 8.63 (br t, ^3J(H,H) = 5 Hz, 1H, NH) ppm; ^{13}C NMR (125.75 MHz, $CDCl_3$) δ 8.8 (Cp*-CH_3), 15.08 (C3′), 34.1 (C2′), 92.4 (d, ^1J(Rh,C) = 10 Hz, Cp*), 92.5 (C2), 120.4 (C7), 120.7 (C4), 131.9 (C5), 132.0 (C6), 136.8 (C7a), 138.6 (C3a), 166.0 (C1″), 190.8 (C3), 192.9 (C1) ppm. Anal. Calcd for $C_{22}H_{25}ClNO_3Rh·0.1H_2O$: C, 53.75; H, 5.17; N, 2.85. Found: C, 53.46; H, 5.14; N, 2.84.

(Chlorido)((1,3-dioxo-κO1-1H-inden-2(3H)-ylidene)-(propylamino)methanolato-κO2)(Cp)rhodium(III)* (**3b**). The synthesis was performed according to the general complexation procedure, using bis[dichlorido(Cp*)rhodium(III)] (189 mg, 306 μmol), compound **L3** (158 mg, 683 μmol), and sodium methoxide (40 mg, 748 μmol) to afford orange crystals (262 mg, 85%): mp >149 °C dec; solubility 0.20 mg/mL ≡ 0.40 mM (PBS, 1% DMSO) and 0.45 mg/mL ≡ 0.88 mM (MSP, 1% DMSO); ^{1}H NMR (500.10 MHz, $CDCl_3$) δ 0.98 (t, ^3J(H,H) = 7 Hz, 3H, H4′), 1.58−1.64 (m, 2H, H3′), 1.68 (s, 15H, Cp*-CH_3), 3.30−3.49 (m, 2H, H2′), 7.37−7.44 (m, 3H, H5, H6, H7), 7.53−7.56 (m, 1H, H4), 8.71 (br t, ^3J(H,H) = 6 Hz, 1H, NH) ppm; ^{13}C NMR (125.75 MHz, $CDCl_3$) δ 8.8 (Cp*-CH_3), 11.8 (C4′), 23.1 (C3′), 40.9 (C2′), 92.36 (d, ^{1}J(Rh−C) = 9 Hz, Cp*), 92.44 (C2), 120.4 (C7), 120.7 (C4), 131.9 (C5), 132.0 (C6), 136.8 (C7a), 138.6 (C3a), 166.1 (C1′), 190.8 (C3), 192.9 (C1) ppm. Anal. Calcd for $C_{23}H_{27}ClNO_3Rh$: C, 54.82; H, 5.40; N, 2.78. Found: C, 54.58; H, 5.60; N, 2.55.

(Chlorido)((1,3-dioxo-κO1-1H-inden-2(3H)-ylidene)-(benzylamino)methanolato-κO2)(Cp)rhodium(III)* (**4b**). The synthesis was performed according to the general complexation procedure, using bis[dichlorido(Cp*)rhodium(III)] (134 mg, 216 μmol), compound **L4** (135 mg, 483 μmol), and sodium methoxide (43 mg, 791 μmol) to afford an orange solid (203 mg, 85%); mp >132 °C dec; solubility 0.10 mg/mL ≡ 0.18 mM (PBS, 1% DMSO) and 0.25 mg/mL ≡ 0.45 mM (MSP, 1% DMSO); ^{1}H NMR (500.10 MHz, $CDCl_3$) δ 1.58 (s, 15H, Cp*-CH_3), 4.48 (dd, ^2J(H,H) = 16 Hz, ^3J(H,H) = 6 Hz, 1H, H2′), 4.83 (dd, ^2J(H,H) = 16 Hz, ^3J(H,H) = 6 Hz, 1H, H2′), 7.22−7.28 (m, 1H, H6′), 7.31−7.34 (m, 4H, H4′, H5′, H7′, H8′), 7.40−7.47 (m, 3H, H5, H6, H7), 7.56−7.59 (m, 1H, H4), 9.13 (br t, ^3J(H,H) = 6 Hz,1H, NH) ppm; ^{13}C NMR (125.75 MHz, $CDCl_3$) δ 8.7 (Cp*-CH_3), 43.1 (C2′), 92.5 (d, ^1J(Rh,C) = 10 Hz, Cp*), 92.6 (C2), 120.6 (C7), 120.8 (C4), 127.1 (C6′), 127.2 (C4′, C8′), 128.7 (C5′, C7′), 132.0 (C5), 132.2 (C6), 136.9 (C7a), 138.6 (C3a), 139.1 (C3′), 166.3 (C1′), 191.0 (C3), 192.9 (C1) ppm. Anal. Calcd for $C_{27}H_{27}ClNO_3Rh·0.75H_2O$: C, 57.36; H, 5.08; N, 2.48. Found: C, 57.31; H, 5.01; N, 2.54.

Mass Spectroscopic Investigations. Stability measurement and small-molecule samples were diluted with water/methanol (50/50), whereas protein samples were diluted with water/methanol/formic acid (49.9/49.9/0.2), where proteins have their highest possible positive charge. Stock solutions of complexes **1a**,**b** and **4a**,**b** were prepared in DMSO and diluted to a final concentration of 1% DMSO/H_2O. The molar ratios used for interaction studies were complex/L-histidine/L-cysteine/glycine (1/1/1/1), complex/5′-dATP/5′-dGTP (1/1/1), complex/amino acids/nucleoside triphosphates (1/1/1), and complex/ubiquitin/cytochrome C (1/1/1). Mass spectra were recorded after 1, 3, 6, 24, and 48 h of incubation at 37 °C. The relative intensities discussed refer to the percent peak area of all assignable rhodium or ruthenium adduct areas in the respective spectrum.

Cell Lines and Culture Conditions. CH1 cells (identified via STR profiling as PA-1 ovarian teratocarcinoma cells by Multiplexion, Heidelberg, Germany; compare Korch et al.[37]) were obtained from Lloyd R. Kelland, CRC Centre for Cancer Therapeutics, Institute of Cancer Research, Sutton, U.K. SW480 (human adenocarcinoma of the colon) and A549 (human nonsmall cell lung cancer) cells were kindly provided by Brigitte Marian (Institute of Cancer Research, Department of Medicine I, Medical University of Vienna, Vienna, Austria). All cell culture media and reagents were purchased from Sigma-Aldrich Austria, and plasticware was obtained from Starlab Germany. Cells were grown in 75 cm^2 culture flasks as adherent monolayer cultures in minimum essential medium (MEM) supplemented with 10% heat-inactivated fetal calf serum, 1 mM sodium pyruvate, 4 mM L-glutamine, and 1% nonessential amino acids (from 100× ready-to-use stock). Cultures were maintained at 37 °C in a humidified atmosphere containing 95% air and 5% CO_2.

Cytotoxicity Assay. Cytotoxic effects of the test compounds were determined by means of a colorimetric microculture assay (MTT assay, MTT = 3-(4,5-dimethyl-2-thiazolyl)-2,5-diphenyl-2*H*-tetrazolium bromide). Cells were harvested from culture flasks by trypsinization and seeded by using a pipetting system (Biotek Precision XS Microplate Sample Processor) in densities of 1×10^3 (CH1/PA-1), 2×10^3 (SW480), and 3×10^3 (A549) cells in 100 μL/well aliquots in 96-well microculture plates. Before drug exposure, cells were allowed to settle and resume proliferation for 24 h. Test compounds were then dissolved in DMSO first, diluted in complete culture medium, and added to the plates where the final DMSO content did not exceed 0.5%. After 96 h of exposure, the medium was removed and replaced with 100 μL/well of a 1/7 MTT/RPMI 1640 solution (MTT solution, 5 mg/mL of MTT reagent in phosphate-buffered saline; RPMI 1640, supplemented with 10% heat-inactivated fetal bovine serum and 4 mM L-glutamine) and incubated for 4 h at 37 °C. Subsequently, the MTT/RPMI solution was removed from all

DOI: 10.1021/om501032s
Organometallics 2015, 34, 848−857

wells, and the formazan crystals formed by viable cells were dissolved in 150 μL of DMSO per well. Optical densities at 550 nm were measured with a microplate reader (Biotek ELx808), using a reference wavelength of 690 nm to correct for unspecific absorption. The quantity of viable cells was expressed relative to untreated controls, and 50% inhibitory concentrations (IC_{50}) were calculated from concentration−effect curves by interpolation. Evaluation was based on means from three independent experiments.

Topoisomerase IIα Inhibition. The topoisomerase IIα inhibitory capacity of tested compounds was determined by means of the DNA plasmid relaxation assay. For this purpose, we used the topoisomerase drug screening kit and the human recombinant topoisomerase IIα enzyme from TopoGen Inc. The supercoiled pHOT1 plasmid DNA was incubated for 30 min at 37 °C with topo IIα in the presence of various concentrations of the test compounds. Etoposide (VP-16) was used as a positive control in a concentration of 0.8 mM. The reaction was stopped by the rapid addition of 10% SDS followed by digestion with proteinase K for 15 min at 37 °C. The samples were divided and loaded onto two different 1% agarose gels with equal amounts of reaction products. One gel was poststained (after electrophoresis incubated in a 1x TAE buffer containing 0.5 μg/mL ethidium bromide) and the other gel prestained (0.5 μg/mL ethidium bromide added to the gel before electrophoresis). Both were analyzed by visualization with the detection system Fusion SL (Vilber Lourmat). Two independent experiments were performed.

Impact on Secondary Structure of DNA. A 500 ng portion of plasmid DNA pUC19 (2686bp) purchased from Fermentas Life Sciences was incubated with 40 μM of the test compounds in a 0.1× Tris-EDTA (TE) buffer for different time intervals (5−15−30−60−120 min) at 37 °C. Electrophoresis was performed in a 1% agarose gel (Sigma-Aldrich) in 1× Tris-borate-EDTA (TBE) buffer for 90 min at 80 V. Gels were stained with ethidium bromide in 1× TBE (0.75 μg/mL) for 20 min. Images were taken with the detection system Fusion SL (Vilber Lourmat). Three independent experiments were performed.

Cell Cycle Studies. CH1/PA-1 and SW480 cells were harvested by trypsinization, and 1×10^5 and 1.2×10^5 cells, respectively, were seeded into 12-well plates. In the first 24 h the cells were allowed to settle and resume proliferation. Thereafter, the DMSO stocks of the test compounds were diluted in MEM so that the final DMSO content did not exceed 0.5%, and the medium in the plates was replaced with these dilutions. After continuous exposure for 12 h at 37 °C under 5% CO_2, the cells were trypsinized and centrifuged at 300*g* for 3 min. Then the cells were washed with 1 mL of PBS and resuspended in 600 μL of PI/HSF buffer (0.1% Triton X-100, 0.1% sodium citrate, in PBS) containing 50 μg/mL propidium iodide. After incubation overnight at 4 °C in the dark, 5×10^3 cells was measured by flow cytometry with a Millipore guava easyCyte 8HT instrument. The obtained data were evaluated by FlowJo software (Tree Star) using Dean−Jett−Fox algorithms.

Flow Cytometric Detection of Apoptotic Cells. Induction of cell death was analyzed by using FITC-conjugated annexin V (BioVision, USA) and propidium iodide (PI, Fluka) double staining. SW480 cells were seeded into 12-well plates (Starlab) in a density of 1×10^5 cells per well in complete medium and allowed to settle for 24 h. The cells were exposed to the test compound in different concentrations for 24 h at 37 °C. The topo IIα inhibitor merbarone (Sigma-Aldrich Austria) was used as a positive control in concentration of 320 μM on SW480 cells. After the incubation, cells were gently trypsinized, washed with 1 mL of PBS, and suspended with FITC-conjugated annexin V (0.25 μg/mL) and PI (1 μg/mL) in binding buffer (10 mM HEPES/NaOH pH 7.4, 140 mM NaCl, 2.5 mM $CaCl_2$) at 37 °C for 15 min. Stained cells (5×10^3 cells per analysis) were measured with a guava easyCyte 8HT flow cytometer (Merck Millipore, Guava, USA) using InCyte software. The data were evaluated by FlowJo software (Tree Star).

■ ASSOCIATED CONTENT

Supporting Information

Figures, tables, and CIF files giving NMR spectra, IT-ESI-MS adduct distribution over 48 h, and data on the FACS experiments, and crystallographic data. This material is available free of charge via the Internet at http://pubs.acs.org.

■ AUTHOR INFORMATION

Corresponding Author

*W.K.: fax, +43-1-4277-9526; e-mail, wolfgang.kandioller@univie.ac.at.

Author Contributions

The manuscript was written through contributions of all authors. All authors have given approval to the final version of the manuscript. The first two authors contributed equally.

Notes

The authors declare no competing financial interest.

■ ACKNOWLEDGMENTS

We thank the University of Vienna and the Research Platform "Translational Cancer Therapy Research" and the Johanna Mahlke née Obermann Foundation (FA 526005) for financial support. Furthermore, we gratefully acknowledge Filip Groznica for his assistance and Prof. Vladimir Arion for the refinement of the X-ray diffraction data. Dedicated to Prof. Christian Robl, University of Jena, for the occasion of his 60th birthday.

■ ABBREVIATIONS USED

A549, human nonsmall cell lung carcinoma cell line; CH1/PA-1, human ovarial cystadenocarcinoma cell line; Cp*, 1,2,3,4,5-pentamethylcyclopentadienyl ligand; cym, *p*-isopropyltoluene; cyt, cytochrome C; dec, decomposition; IT-ESI-MS, ion trap−electron spray ionization−mass spectrometry; FITC, fluorescein isothiocyanate; MEM, minimum essential medium; MSP, medium with serum proteins; MTT, 3-(4,5-dimethyl-2-thiazolyl)-2,5-diphenyl-2*H*-tetrazolium bromide; PBS, phosphate buffered saline; RPMI-1640, medium developed at Roswell Park Memorial Institute; SW480, human colon adenocarcinoma cell line; TAE, buffer solution containing a mixture of Tris base, acetic acid and EDTA topo I and II, topoisomerase I and II; Ub, ubiquitin

■ REFERENCES

(1) Yan, Y. K.; Melchart, M.; Habtemariam, A.; Sadler, P. J. *Chem. Commun.* **2005**, 4764−4776.
(2) Levina, A.; Mitra, A.; Lay, P. A. *Metallomics* **2009**, *1*, 458−470.
(3) Bugarcic, T.; Habtemariam, A.; Deeth, R. J.; Fabbiani, F. P. A.; Parsons, S.; Sadler, P. J. *Inorg. Chem.* **2009**, *48*, 9444−9453.
(4) Ang, W. H.; Casini, A.; Sava, G.; Dyson, P. J. *J. Organomet. Chem.* **2011**, *696*, 989−998.
(5) Kljun, J.; Bytzek, A. K.; Kandioller, W.; Bartel, C.; Jakupec, M. A.; Hartinger, C. G.; Keppler, B. K.; Turel, I. *Organometallics* **2011**, *30*, 2506−2512.
(6) Liu, H.-K.; Sadler, P. J. *Acc. Chem. Res.* **2011**, *44*, 349−359.
(7) Kurzwernhart, A.; Kandioller, W.; Baechler, S.; Bartel, C.; Martic, S.; Buczkowska, M.; Muehlgassner, G.; Jakupec, M. A.; Kraatz, H.-B.; Bednarski, P. J.; Arion, V. B.; Marko, D.; Keppler, B. K.; Hartinger, C. G. *J. Med. Chem.* **2012**, *55*, 10512−10522.
(8) Schmid, W. F.; John, R. O.; Arion, V. B.; Jakupec, M. A.; Keppler, B. K. *Organometallics* **2007**, *26*, 6643−6652.

DOI: 10.1021/om501032s
Organometallics 2015, 34, 848−857

(9) Kandioller, W.; Kurzwernhart, A.; Hanif, M.; Meier, S. M.; Henke, H.; Keppler, B. K.; Hartinger, C. G. *J. Organomet. Chem.* **2011**, *696*, 999−1010.
(10) Osheroff, N. *Biochim. Biophys. Acta Gene Struct. Expr.* **1998**, *1400*, 1−2.
(11) Null, A. P.; Hudson, J.; Gorbsky, G. J. *Cell Growth Differ.* **2002**, *13*, 325−333.
(12) Rubtsov, M. A.; Glukhov, S. I.; Allinne, J.; Pichugin, A.; Vassetzky, Y. S.; Razin, S. V.; Iarovaia, O. V. *Biopolym Cell* **2011**, *27*, 398−403.
(13) Vanderbeeken, M.-C.; Aftimos, P. G.; Awada, A. *Curr. Breast Cancer Rep.* **2013**, *5*, 31−41.
(14) Habermeyer, M.; Fritz, J.; Barthelmes, H. U.; Christensen, M. O.; Larsen, M. K.; Boege, F.; Marko, D. *Chem. Res. Toxicol.* **2005**, *18*, 1395−1404.
(15) Wink, M. *Alkaloids* **2007**, *64*, 1−47.
(16) Hsiang, Y. H.; Wu, H. Y.; Liu, L. F. *Cancer Res.* **1988**, *48*, 3230−3235.
(17) Minderman, H.; Wrzosek, C.; Cao, S.; Utsugi, T.; Kobunai, T.; Yamada, Y.; Rustum, Y. M. *Cancer Chemother. Pharmacol.* **2000**, *45*, 78−84.
(18) Sunami, T.; Nishio, K.; Kanzawa, F.; Fukuoka, K.; Kudoh, S.; Yoshikawa, J.; Saijo, N. *Cancer Chemother Pharmacol* **1999**, *43*, 394−401.
(19) Jung, J.-K.; Ryu, J.; Yang, S.-I.; Cho, J.; Lee, H. *Arch Pharm. Res.* **2004**, *27*, 997−1000.
(20) Song, J.; Mishima, M.; Rappoport, Z. *Org. Lett.* **2007**, *9*, 4307−4310.
(21) Lei, Y. X.; Rappoport, Z. *J. Org. Chem.* **2002**, *67*, 6971−6978.
(22) Hatzigrigoriou, E.; Spyroudis, S.; Varvoglis, A. *Liebigs Ann. Chem.* **1989**, 167−170.
(23) Malamidou-Xenikaki, E.; Spyroudis, S.; Tsanakopoulou, M. *J. Org. Chem.* **2003**, *68*, 5627−5631.
(24) Pettinari, C.; Pettinari, R.; Fianchini, M.; Marchetti, F.; Skelton, B. W.; White, A. H. *Inorg. Chem.* **2005**, *44*, 7933−7942.
(25) Hanif, M.; Henke, H.; Meier, S. M.; Martic, S.; Labib, M.; Kandioller, W.; Jakupec, M. A.; Arion, V. B.; Kraatz, H.-B.; Keppler, B. K.; Hartinger, C. G. *Inorg. Chem.* **2010**, *49*, 7953−7963.
(26) Carey, F. A.; Sundberg, R. J. *Advanced Organic Chemistry, Part A: Structure and Mechanisms*, 5th ed.; Springer: New York, 2008.
(27) Peacock, A. F. A.; Melchart, M.; Deeth, R. J.; Habtemariam, A.; Parsons, S.; Sadler, P. J. *Chem. Eur. J.* **2007**, *13*, 2601−2613.
(28) Fortune, J. M.; Velea, L.; Graves, D. E.; Utsugi, T.; Yamada, Y.; Osheroff, N. *Biochemistry (Mosc.)* **1999**, *38*, 15580−15586.
(29) Nitiss, J. L. *Nat. Rev. Cancer* **2009**, *9*, 338−350.
(30) Fortune, J. M.; Osheroff, N. *J. Biol. Chem.* **1998**, *273*, 17643−17650.
(31) Wang, L.; Roy, S. K.; Eastmond, D. A. *Mutat. Res.* **2007**, *616*, 70−82.
(32) Pressprich, M. R.; Chambers, J. *SAINT + Integration Engine, Program for Crystal Structure Integration*; Bruker Analytical X-ray systems: Madison, WI, 2004.
(33) Sheldrick, G. M. *Acta Crystallogr., Sect. A* **2008**, *64*, 112−122.
(34) Spek, A. L. *Acta Crystallogr.. Sect. D* **2009**, *65*, 148−155.
(35) Dolomanov, O. V.; Bourhis, L. J.; Gildea, R. J.; Howard, J. A. K.; Puschmann, H. *J. Appl. Crystallogr.* **2009**, *42*, 339−341.
(36) Farrugia, L. J. *J. Appl. Crystallogr.* **1997**, *30*, 565−565.
(37) Korch, C.; Spillman, M. A.; Jackson, T. A.; Jacobsen, B. M.; Murphy, S. K.; Lessey, B. A.; Jordan, V. C.; Bradford, A. P. *Gynecol. Oncol.* **2012**, *127*, 241−248.

DOI: 10.1021/om501032s
Organometallics 2015, 34, 848−857

SUPPORTING INFORMATION

[EXTRACT]

1,3-Dioxoindan-2-carboxamides as bioactive ligand scaffold for the development of novel organometallic anticancer drugs

Stephan Mokesch,[‡,a] Maria S. Novak,[‡,a] Alexander Roller,[a] Michael A. Jakupec,[a,b] Wolfgang Kandioller,[*,a,b] Bernhard K. Keppler [a,b]

[a] Institute of Inorganic Chemistry, University of Vienna, Waehringer Straße 42, 1090 Vienna, Austria

[b] Research Platform "Translational Cancer Therapy Research", University of Vienna, Waehringer Straße 42, 1090 Vienna, Austria

Table of Contents

4 Biological experiments

Table S2 Impact of compounds **L4**, **4a** and **4b** on the cell cycle distribution of CH1/PA-1 and SW480 cells after 12 h exposure.

		CH1/PA-1			SW480		
Compound	Concentration [μM]	G0/G1	S	G2/M	G0/G1	S	G2/M
		Percentage of cells [%]			Percentage of cells [%]		
Control	0	44 ± 6	27 ± 5	27 ± 1	51 ± 4	29 ± 4	18 ± 1
L4	40	35 ± 3	32 ± 1	32 ± 1	55 ± 8	21 ± 3	23 ± 13
	80	35 ± 0.3	35 ± 2	29 ± 1	50 ± 15	28 ± 9	20 ± 4
	160	41 ± 9	34 ± 6	24 ± 2	43 ± 14	36 ± 10	19 ± 4
	320	40 ± 0.2	28 ± 4	30 ± 7	41 ± 3	29 ± 6	28 ± 3
4a	40	34 ± 3	27 ± 5	38 ± 8	50 ± 10	27 ± 7	22 ± 4
	80	31 ± 0.4	43 ± 2	24 ± 2	43 ± 7	35 ± 7	20 ± 0.3
	160	29 ± 3	39 ± 2	29 ± 0.2	39 ± 2	36 ± 4	24 ± 6
	320	32 ± 1	36 ± 2	30 ± 1	43 ± 2	38 ± 3	19 ± 0.1
4b	40	36 ± 7	30 ± 2	33 ± 5	55 ± 7	22 ± 1	21 ± 8
	80	37 ± 0.2	34 ± 2	29 ± 2	56 ± 4	20 ± 2	23 ± 8
	160	37 ± 4	35 ± 2	27 ± 2	55 ± 5	18 ± 13	25 ± 8
	320	41 ± 2	27 ± 4	31 ± 6	45 ± 1	24 ± 3	30 ± 3
Merbarone	320	21 ± 28	34 ± 11	43 ± 15	-	-	-
	640	-	-	-	33 ± 5	38 ± 3	27 ± 3

Table S3 Impact of compounds **L4**, **4a** and **4b** on the cell viability of SW480 cells after 24 h exposure.

Compound	Concentration [μM]	Necrosis	Late apoptosis	Early apoptosis	Viable cells
		Percentage of cells [%]			
Control	0	1 ± 0.4	1 ± 0.3	2 ± 0.9	95 ± 1
L4	40	1 ± 0.4	1 ± 0.4	4 ± 1.8	94 ± 3
	80	1 ± 0.3	1 ± 0.4	5 ± 3.3	92 ± 4
	160	1 ± 0.6	2 ± 0.9	6 ± 3.0	91 ± 5
	320	2 ± 0.2	16 ± 9	17 ± 11	65 ± 20
4a	40	0 ± 0.2	2 ± 1.0	4 ± 1.7	94 ± 3
	80	1 ± 0.1	3 ± 2.5	5 ± 2.7	92 ± 5
	160	1 ± 0.6	4 ± 1.6	5 ± 2.4	89 ± 4
	320	2 ± 1.5	7 ± 1.8	4 ± 0.9	86 ± 4
4b	40	2 ± 1.0	5 ± 4.9	8 ± 4.8	85 ± 9
	80	2 ± 0.9	6 ± 4.9	10 ± 6.3	82 ± 11
	160	3 ± 2.2	14 ± 10	9 ± 4.6	74 ± 17
	320	8 ± 4.2	29 ± 14	6 ± 5.2	56 ± 20
Merbarone	320	4 ± 1.6	30 ± 9	13 ± 4.2	53 ± 14

Topoisomerase IIα inhibition and anticancer activity of 3',4'-dihydroxyflavonol-derived organometallics

Andrea Kurzwernhart,[a,b] Caroline Rossi-Gendron,[c] Maria S. Novak,[a] Alexander Roller,[a] Michael A. Jakupec,[a,b] Wolfgang Kandioller*[a,b] and Bernhard K. Keppler[a,b]

[a] Institute of Inorganic Chemistry, University of Vienna, Waehringer Strasse 42, 1090 Vienna, Austria

[b] Research Platform "Translational Cancer Therapy Research", University of Vienna, Waehringer Strasse 42, 1090 Vienna, Austria

[c] Department of Chemistry, Ecole Normale Supérieure, 24 rue Lhommond, 75005 Paris, France

Supporting Information Placeholder

ABSTRACT: Three Ru(II)-, Os(II)- and Rh(III)-arene complexes are studied, in which a flavonol-ligand containing a piperonyl group has been designed to imitate the general structure of 3',4'-dihydroxyflavonols (*e.g.* quercetin) and to elucidate the importance of the catechol moiety for topoisomerase inhibition. The antiproliferative activity was determined in human cancer cell lines, and IC_{50} values in the low micromolar range were observed. The change of metal centers showed only minor impact on cytotoxicity, confirming the flavonol ligand as the main active moiety. The compounds inhibit topoisomerase IIα by acting as catalytic inhibitors, but not as topoisomerase poisons at the tested concentrations.

Ruthenium complexes are considered as promising candidates to overcome the disadvantages of the currently clinically-applied platinum drugs.[1] The most prominent representatives of this substance class are indazolium *trans*-[tetrachloridobis(1*H*-indazole)ruthenate(III)] (KP1019) and imidazolium *trans*-[tetrachlorido(dimethylsulfoxide)(1*H*-imidazole)ruthenate(III)] (NAMI-A) (Figure 1), which are currently undergoing clinical trials with very promising results.[2] In recent years, organometallic Ru(II)-arene complexes have clearly shown their potential to complement the clinically applied spectrum of anticancer metallodrugs.[3] These half-sandwich complexes offer multiple possibilities for drug design by modification of the arene ligand and functionalization of the three remaining coordination sites, providing the opportunity to control the reactivity and fine-tune important pharmacological properties such as cellular uptake and interactions with biomolecules.[4] Important examples for this compound class are ethylene-1,2-diamine complexes developed by Sadler and coworkers.[2] It is supposed that the underlying mode of action for these complexes is the interaction with DNA by covalent binding and intercalation of the coordinated arene ligand.[2, 5] Further biological investigations revealed the activity of the Ru(II) complex RM175 (Chart 1) against MCa mammary carcinoma *in vivo*.[2] In contrast, the RAPTA-type compounds of Dyson *et al.* (Chart 1) exhibit only minor cytotoxicity *in vitro*, but possess antimetastatic and antiangiogenic properties[2] and show activity against the Ehrlich ascites carcinoma *in vivo*.[6]

Chart 1. Chemical structures of anticancer-active Ru complexes.

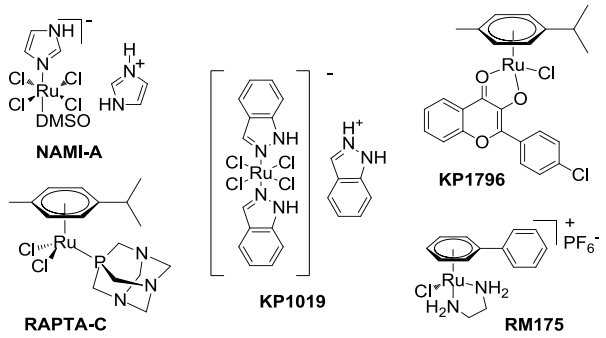

The coordination of biologically active ligand systems to metal centers is a promising strategy for the development of innovative anticancer agents with novel modes of action,[7] especially the inhibition of specific enzymes involved in cancer-related metabolic pathways.[8] Carbonic anhydrase (CA) is known to be overexpressed in many types of cancer. By linking metallocenes to CA inhibitors, Poulsen *et al.* designed compounds with improved activity compared to the metal-free analogues and even higher selectivity for cancer-associated CAs over CAs located in healthy cells.[9] Dyson *et al.* applied the concept to RAPTA-type Ru(II)-arene complexes by tethering ethacrynic acid, a known inhibitor of gluthathione-S-transferase (GST), to the arene moiety, leading to compounds with improved cytotoxicity compared to RAPTA-C and able to inhibit GST, which is often related to drug resistance in some forms of cancer.[10]

Recently, we have reported on a series of novel Ru(II)-arene complexes bearing bioactive flavonols as chelating ligands (*e.g.* KP1796, Chart 1).[11-14] The flavonoid backbone is a naturally occurring secondary metabolite of plants and exhibits favorable biological effects such as antioxidant, anti-inflammatory, antimicrobial and anticancer activity, mainly by scavenging free radicals and reactive oxygen species (ROS) and by the inhibition of several enzymes, *e.g.* human topoisomerases and receptor tyrosine kinases.[15] Some examples of metal-flavonoid complexes are already known to exhibit promising biological properties with often higher activity than the free ligands. These compounds were investigated for the treatment of bacterial and viral infections,

diabetes mellitus and cancer.[16] Coordination of the flavone backbone to organoruthenium fragments afforded compounds with high *in vitro* anticancer activity, which may bind covalently to DNA and on the other hand are potent inhibitors of human topoisomerase IIα, which is often overexpressed in cancer cells.[11-13]

The aim of this work is to extend the structure-activity-relationship (SAR) studies of these novel anticancer active metal-arene complexes featuring bioactive flavonoids with regard to the general structure of naturally occurring flavonoids such as quercetin, where the catechol moiety has a major influence on the bioactivity of these compounds.[15] For this purpose, a piperonyl-substituted flavonol has been linked to a Ru(II)-*p*-cymene moiety. The piperonyl substituent in principle constitutes the protected form of the catechol unit of 3',4'-dihydroxyflavonol and was used in order to avoid undesired side reactions upon coordination of the organometallic fragment. It is likely that, under physiological conditions, the CH_2 group dissociates, leading to the two free hydroxyl groups at position 3' and 4' of the phenyl substituent.[17] In order to study the impact of the metal center, the Os(II)-*p*-cymene and the Rh(III)-pentamethylcyclopentadienyl (Cp*) analogues have been synthesized, and the influence on biological activity has been evaluated with regard to *in vitro* cytotoxicity and the inhibition of topoisomerase IIα.

Scheme 1. Synthesis of ligand 1 and complexes 2-4: a) NaOH, H_2O_2; b) $NaOCH_3$, $[M(arene)Cl_2]_2$ (2: M = Ru(II), 3: M = Os(II), arene = *p*-cymene; 4: M = Rh(III), arene = Cp*).

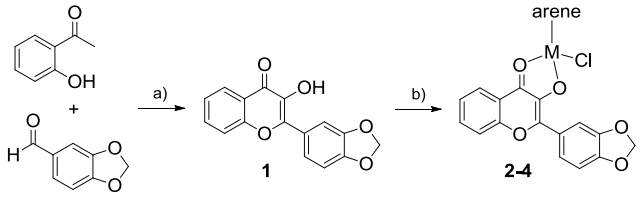

Ligand **1** was synthesized over two steps by a Claisen-Schmidt condensation of 2-hydroxyacetophenone with piperonal followed by an Algar-Flynn-Oyamada cyclization reaction (Scheme 1, Supporting Information).[18-20] The corresponding Ru(II), Os(II)- and Rh(III)-arene complexes **2-4** were isolated in moderate to good yields (44-71%) by deprotonation of the ligand **1** with sodium methoxide and subsequent conversion with the respective dimeric metal precursor bis[dichlorido(η^6-*p*-cymene)ruthenium(II)], bis[dichlorido(η^6-*p*-cymene)osmium(II)] or bis[dichlorido(η^5-pentamethylcyclopentadienyl)rhodium(III)] (Scheme 1, Supporting Information).

The compounds were characterized by standard analytical methods (SI). The ^{1}H NMR spectra of ligand **1** shows a singlet for the CH_2 group of the piperonyl substituent at 6.13 ppm. Upon coordination, the CH_2 signal split into a dd with a coupling constant of $^2J(H,H)$ = 6 Hz and $^2J(H,H)$ = 1 Hz in **2-3** and $^2J(H,H)$ = 7 Hz and $^2J(H,H)$ = 2 Hz in the Rh(III)-Cp* complex **4** (Figure 1). This observation showed to be due to a geminal coupling of the two CH_2 protons, which - in the case of the free [1,3]dioxolane moiety - have a geminal coupling constant of $^2J(H,H) = \pm 0$ Hz and therefore appear as singlet.[21] The coordination to the metal centers leads to a change of electron density in the flavonol ligand of compounds **2-4**, and the signal of the two protons split into a doublet. This observation was verified by 2D NMR spectroscopy (SI).

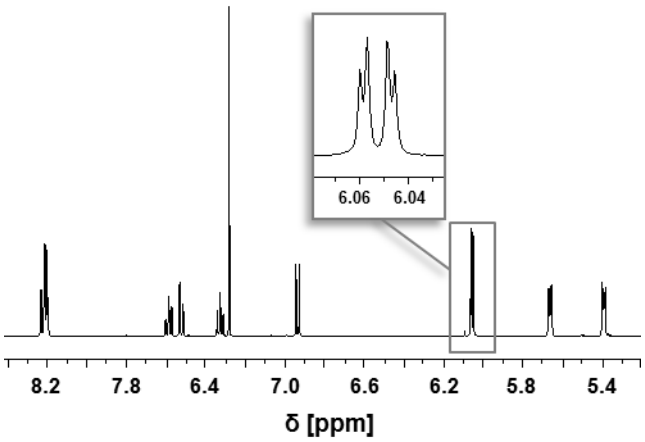

Figure 1. ^{1}H NMR of complex **2** with geminal coupling of the piperonyl-CH_2 protons.

In order to confirm the proposed compound structures, single crystals of **2-4** were analyzed by X-ray diffraction analysis (Figure 2, SI). Compounds **2** and **3** crystallized in the monoclinic space group $P2_1/n$, **4** in the orthorhombic space group *Pbca;* and they adopt the typical pseudo-octahedral "piano-stool" configuration. The flavonol acts as anionic *O,O*-chelate, forming an envelope-like five-membered ring upon coordination to the respective metal center. The phenyl substituent of the ligand is twisted with a torsion angle of ca. 8° in **2** and **3** and 12° in **4**, with the piperonyl group showing an envelope-like conformation. The two metal-O bonds were found slightly different in all complexes (2.1195(12) Å and 2.0794(12) Å in **2**, 2.113(2) and 2.079(2) in **3**, 2.113(3) and 2.141(3) in **4**), in agreement with structurally related compounds[11, 13, 22, 23] and independently of the coordinated metal center. The metal-Cl bonds of **2** and **3** are in the same range (2.4114(5) Å in **2**, 2.4023(9) Å in **3**) and comparable to Ru(II)-Cl bonds of recently published related organometallic complexes,[11, 22] whereas the Rh(III)-Cl bond in compound **4** is slightly shorter (2.376(2) Å).

Table 1. *In vitro* anticancer activity (IC_{50} values in µM, 96 h exposure) of 2-4 and KP1796[a] in human ovarian (CH1), colon (SW480) and non-small cell lung (A549) carcinoma cell lines.

	IC_{50} values/µM		
compound	CH1	SW480	A549
2	1.4 ± 0.3	6.7 ± 0.6	11 ± 1
3	1.8 ± 0.3	13 ± 3	20 ± 4
4	1.68 ± 0.02	9.0 ± 0.8	44 ± 9
KP1796[a]	0.86 ± 0.06	3.8 ± 0.5	9.5 ± 0.5

[a] taken from ref.[11].

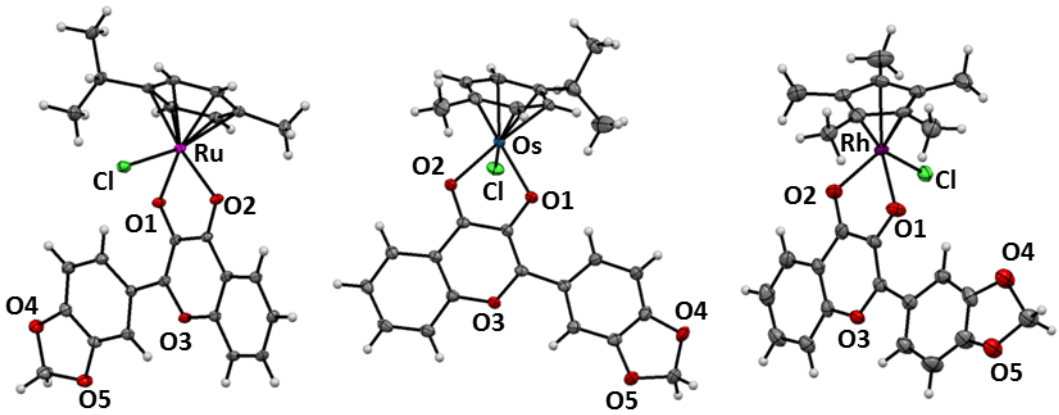

Figure 2. Molecular structures of complexes **2-4** (from left to right) bearing the piperonyl-substituted flavonol ligand **1**.

The *in vitro* anticancer activity of complexes **2-4** was determined in the human cancer cell lines CH1 (ovarian carcinoma), SW480 (colon carcinoma) and A549 (non-small cell lung carcinoma) by means of the colorimetric MTT assay (Table 1). KP1796 (Chart 1) is the *p*-chloro substituted flavonol derivative, which has been the most active of the recently published related flavonol-derived Ru(II)-arene series,[11] and is included for comparison. The new compounds exhibit promising tumor-inhibiting properties with IC_{50} values in the low µM range and show a similar cytotoxicity pattern as KP1796.[11] The highest *in vitro* activity has been found in the generally more chemosensitive cell line CH1 with IC_{50} values of 1.4–1.8 µM, followed by SW480. The lowest cytotoxic potency was found for the more chemoresistant A549 cells. However, the role of the piperonyl substituent seems to be of minor importance, and only a small impact on cytotoxicity is observed concerning the variation of the metal-arene moiety, with the Ru(II)-*p*-cymene compound **2** being the most potent of the new complex series. The minor impact of the metal center on the cytotoxic activity may be explained by the biologically active ligand system, which seems to be mainly responsible for the high *in vitro* potency.[12]

DNA topoisomerases are participating in nearly all biological processes involving DNA, including replication, transcription, recombination, and chromatin remodeling. Their function thereby is to change the topology of DNA by forming a catalytic complex with the DNA strand and creating a transient break, which is reannealed after relaxing or unknotting. These enzymes are well-recognized targets because they are often overexpressed in many cancer types, and established topoisomerase inhibitors, such as doxorubicin, etoposide and mitoxantrone, are routinely used in cancer treatment.[24] Compounds that target topoisomerase II are classified into topoisomerase poisons and catalytic inhibitors. Topoisomerase poisons target the enzyme-DNA complex, stimulate formation of the cleavage complexes and inhibit the ligation of the DNA double-strand break induced. Catalytic inhibitors may affect enzyme activity by blocking access to the DNA substrate or altering ATPase action and enzyme turnover.[25] The enzymes are known targets of flavonoids, but due to their poor solubility in aqueous solutions the natural compounds are hardly suitable for pharmaceutical applications. Flavonol-derived Ru(II)-arene complexes have recently been shown to inhibit topoisomerase IIα in correlation to their cytotoxic activity and furthermore exhibit approximately 10-fold higher solubility in water than the respective flavonoid ligands.[11, 12]

The inhibition of topoisomerase IIα was investigated by means of the DNA plasmid relaxation assay. The complexes **2-4** showed the capacity to inhibit topoisomerase IIα at 40 µM and to some extent at 20 µM (Figure 3, A). The extent of inhibition is comparable for all three complexes, thus the change of the metal center seems to have a minor influence on topoisomerase IIα inhibition, in accordance with cytotoxicity data. KP1796 was included for comparison and showed the same behavior as **2-4**, indicating that introduction of the piperonyl substituent does not dramatically affect topoisomerase IIα inhibition. KP1796 and **2-4** do not act as topoisomerase poisons at the tested concentrations (Figure 3, B). However, the known topoisomerase poison etoposide, which was included as control, was used at a concentration of 0.8 mM. Due to the limited solubility, it was not possible to increase the concentration of the complexes, thus it cannot be excluded that compounds **2-4** are topoisomerase poisons at higher concentrations.

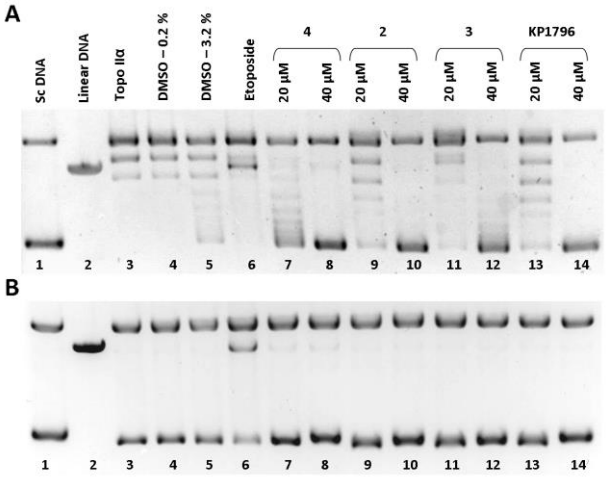

Figure 3. Topoisomerase IIα-inhibitory capacity of **2–4** and KP1796, determined by the plasmid DNA relaxation assay. Supercoiled and linear DNA used as references (lane 1 and 2, respectively); relaxed DNA bands (lane 3) indicating intact enzyme activity; DMSO controls corresponding to test compounds and positive control (lane 4 and 5, respectively); linear DNA band induced by 0.8 mM etoposide (positive control, lane 6). Lanes 7–14 display the reaction of topoisomerase IIα with supercoiled DNA in the presence of test compounds. The top gel (A) is post-stained and the bottom gel (B) is prestained with 0.5 µg/mL ethidium bromide.

Flavonol-derived Ru(II)-arene complexes have already been shown to be promising candidates for the development of novel anticancer drugs.[11,] Herein, the compound library of organometallic complexes featuring flavonoid ligands has been extended by

three metal-arene complexes bearing a piperonyl-substituted flavonol ligand. The compounds probably act as prodrugs, since the piperonyl moiety (the protected form of catechol, which can be found in naturally occurring flavonoids such as quercetin) presumably dissociates to the free OH groups under physiological conditions. The tested complexes are potent inhibitors of cancer cell growth and act as catalytic inhibitors of topoisomerase IIα in the DNA plasmid relaxation assay. The change of metal centers and the piperonyl substitution show a minor impact on antiproliferative activity and capacity for topoisomerase inhibition. It is assumed that rather the flavonoid backbone than different substituents at the phenyl ring are crucial for the high anticancer potency of this substance class.

ASSOCIATED CONTENT

Supporting Information

Information about materials and methods used, detailed experimental part including synthesis and characterization, 1D and 2D NMR spectra, single crystal X-ray diffraction data for compounds **2**-**4** and topoisomerase experiments. This material is available free of charge via the Internet at http://pubs.acs.org.

AUTHOR INFORMATION

Corresponding Author

* Dr. W. Kandioller
Fax: +43-1-4277-52680
E-Mail: wolfgang.kandioller@univie.ac.at

Notes

The authors declare no competing financial interests.

ACKNOWLEDGMENT

We thank the University of Vienna, the Austrian Science Fund (FWF), the Johanna Mahlke née Obermann Foundation, and COST D39 for financial support.

REFERENCES

1. Allardyce, C. S.; Dyson, P. J., Ruthenium in medicine: Current clinical uses and future prospects. *Platinum Met. Rev.* **2001,** 45, (2), 62-69.
2. Bergamo, A.; Gaiddon, C.; Schellens, J. H. M.; Beijnen, J. H.; Sava, G., Approaching tumour therapy beyond platinum drugs Status of the art and perspectives of ruthenium drug candidates. *J Inorg Biochem* **2012,** 106, (1), 90-99.
3. Yan, Y. K.; Melchart, M.; Habtemariam, A.; Sadler, P. J., Organometallic chemistry, biology and medicine: ruthenium arene anticancer complexes. *Chem Commun* **2005**, (38), 4764-4776.
4. Meggers, E., Exploring biologically relevant chemical space with metal complexes. *Current Opinion in Chemical Biology* **2007,** 11, (3), 287-292.
5. Bergamo, A.; Masi, A.; Peacock, A. F. A.; Habtemariam, A.; Sadler, P. J.; Sava, G., In vivo tumour and metastasis reduction and in vitro effects on invasion assays of the ruthenium RM175 and osmium AFAP51 organometallics in the mammary cancer model. *J Inorg Biochem* **2010,** 104, 79-86.
6. Chatterjee, S.; Kundu, S.; Bhattacharyya, A.; Hartinger, C. G.; Dyson, P. J., The ruthenium(II)–arene compound RAPTA-C induces apoptosis in EAC cells through mitochondrial and p53–JNK pathways. *Journal of biological inorganic chemistry* **2008,** 13, 1149-1155.
7. Smith, G. S.; Therrien, B., Targeted and multifunctional arene ruthenium chemotherapeutics. *Dalton Transactions* **2011,** 40, (41), 10793-10800.
8. Kilpin, K. J.; Dyson, P. J., Enzyme inhibition by metal complexes: concepts, strategies and applications. *Chemical science* **2013,** 4, 1410-1419.
9. Salmon, A. J.; Williams, M. L.; Quoc, K. W.; Morizzi, J.; Gregg, D.; Charman, S. A.; Vullo, D.; Supuran, C. T.; Poulsen, S.-A., Metallocene-Based Inhibitors of Cancer-Associated Carbonic Anhydrase Enzymes IX and XII. *Journal of Medicinal Chemistry* **2012,** 55, 5506-5517.
10. Chatterjee, S.; Biondi, I.; Dyson, P. J.; Bhattacharyya, A., A bifunctional organometallic ruthenium drug with multiple modes of inducing apoptosis. *Journal of biological inorganic chemistry* **2011,** 16, 715-724.
11. Kurzwernhart, A.; Kandioller, W.; Bachler, S.; Bartel, C.; Martic, S.; Buczkowska, M.; Muhlgassner, G.; Jakupec, M. A.; Kraatz, H. B.; Bednarski, P. J.; Arion, V. B.; Marko, D.; Keppler, B. K.; Hartinger, C. G., Structure-Activity Relationships of Targeted Ru-II(eta(6)-p-Cymene) Anticancer Complexes with Flavonol-Derived Ligands. *Journal of Medicinal Chemistry* **2012,** 55, (23), 10512-10522.
12. Kurzwernhart, A.; Kandioller, W.; Bartel, C.; Bachler, S.; Trondl, R.; Muhlgassner, G.; Jakupec, M. A.; Arion, V. B.; Marko, D.; Keppler, B. K.; Hartinger, C. G., Targeting the DNA-topoisomerase complex in a double-strike approach with a topoisomerase inhibiting moiety and covalent DNA binder. *Chem Commun* **2012,** 48, (40), 4839-4841.
13. Schwarz, M. B.; Kurzwernhart, A.; Roller, A.; Kandioller, W.; Keppler, B. K.; Hartinger, C. G., Rhodium(Cp*) Compounds with Flavone-derived Ligand Systems: Synthesis and Characterization. *Zeitschrift fuer Anorganische und Allgemeine Chemie* **2013,** 639, (8-9), 1648-1654.
14. Kurzwernhart, A.; Kandioller, W.; Enyedy, E. A.; Novak, M.; Jakupec, M. A.; Keppler, B. K.; Hartinger, C. G., 3-Hydroxyflavones vs. 3-hydroxyquinolinones: structure-activity relationships and stability studies on RuII(arene) anticancer complexes with biologically active ligands. *Dalton Trans.* **2013**, DOI: 10.1039/C2DT32206D.
15. Middleton, E., Jr.; Kandaswami, C.; Theoharides, T. C., The effects of plant flavonoids on mammalian cells: Implications for inflammation, heart disease, and cancer. *Pharmacological Reviews* **2000,** 52, (4), 673-751.
16. Grazul, M.; Budzisz, E., Biological activity of metal ions complexes of chromones, coumarins and flavones. *Coordination Chemistry Reviews* **2009,** 253, (21-22), 2588-2598.
17. Fukuto, J. M.; Kumagai, Y.; Cho, A. K., Determination of the Mechanism of Demethylenation of (Methylenedioxy)phenyl Compounds by Cytochrome P450 Using Deuterium Isotope Effects. *Journal of Medicinal Chemistry* **1991,** 34, 2871-2876.
18. Geissman, T. A.; Fukushima, D. K., Flavanones and related compounds. V. The oxidation of 2'-hydroxychalcones with alkaline hydrogen peroxide. *Journal of the American Chemical Society* **1948,** 70, 1686-9.
19. Bennett, M.; Burke, A. J.; O'Sullivan, W. I., Aspects of the Algar-Flynn-Oyamada (AFO) reaction. *Tetrahedron* **1996,** 52, (20), 7163-7178.
20. Qin, C. X.; Chen, X.; Hughes, R. A.; Williams, S. J.; Woodman, O. L., Understanding the Cardioprotective Effects of Flavonols: Discovery of Relaxant Flavonols without Antioxidant Activity. *Journal of Medicinal Chemistry* **2008,** 51, (6), 1874-1884.
21. Hesse, M.; Meier, H.; Zeeh, B., Spektroskopische Methoden in der organischen Chemie. In Georg Thieme Verlag Stuttgart, New York: 1991; Vol. 4, pp 103-104.
22. Kandioller, W.; Hartinger, C. G.; Nazarov, A. A.; Kasser, J.; John, R.; Jakupec, M. A.; Arion, V. B.; Dyson, P. J.; Keppler, B. K., Tuning the anticancer activity of maltol-derived ruthenium complexes by derivatization of the 3-hydroxy-4-pyrone moiety. *Journal of Organometallic Chemistry* **2009,** 694, (6), 922-929.
23. Kandioller, W.; Balsano, E.; Meier, S. M.; Jungwirth, U.; Göschl, S.; Roller, A.; Jakupec, M. A.; Berger, W.; Keppler, B. K.; Hartinger, C. G., Organometallic anticancer complexes of lapachol: metal center-dependent formation of reactive oxygen species and correlation with cytotoxicity. *Chem Commun* **2013,** 49, 3348-3350.
24. Larsen, A. K.; Escargueil, A. E.; Skladanowski, A., Catalytic topoisomerase II inhibitors in cancer therapy. *Pharmacology and therapeutics* **2003,** 99, 167-181.
25. Bailly, C., Contemporary challenges in the design of topoisomerase II inhibitors for cancer chemotherary. *Chemical reviews* **2012,** 112, 3611-3640.

SUPPORTING INFORMATION

[EXTRACT]

Topoisomerase IIα inhibition and anticancer activity of 3',4'-dihydroxyflavonol-derived organometallics

Andrea Kurzwernhart,[a,b] Caroline Rossi-Gendron,[c] Maria S. Novak,[a] Alexander Roller,[a] Michael A. Jakupec,[a,b] Wolfgang Kandioller*[a,b] and Bernhard K. Keppler[a,b]

Table of Contents

5. Biological experiments

5.1. Cytotoxicity in cancer cell lines

5.1.1. Cell lines and culture conditions

CH1 cells originate from an ascites sample of a patient with a papillary cystadenocarcinoma of the ovary and were a generous gift from Lloyd R. Kelland, CRC Centre for Cancer Therapeutics, Institute of Cancer Research, Sutton, UK. SW480 (human adenocarcinoma of the colon) and A549 (human non-small cell lung cancer) cells were kindly provided by Brigitte Marian (Institute of Cancer Research, Department of Medicine I, Medical University of Vienna, Austria). All cell culture media and reagents were purchased from Sigma-Aldrich Austria and plasticware from Starlab Germany. Cells were grown in 75 cm² culture flasks as adherent monolayer cultures in Minimum Essential Medium (MEM) supplemented with 10% heat-inactivated fetal calf serum, 1 mM sodium pyruvate, 4 mM L-glutamine and 1% non-essential amino acids (from 100x ready-to-use stock). Cultures were maintained at 37 °C in humidified atmosphere containing 95% air and 5% CO_2.

5.1.2. Inhibition of cancer cell growth

Cytotoxic effects of the test compounds were determined by means of a colorimetric microculture assay [MTT assay, MTT = 3-(4,5-dimethyl-2-thiazolyl)-2,5-diphenyl-2H-tetrazolium bromide]. Cells were harvested from culture flasks by trypsinisation and seeded by using a pipetting system (Biotek Precision XS Microplate Sample Processor) in densities of 1×10^3 (CH1), 2×10^3 (SW480) and 3×10^3 (A549) in 100 µL/well aliquots in 96-well microculture plates. Before drug exposure, cells were allowed to settle and resume proliferation for 24 h. Test compounds were then dissolved in DMSO first, diluted in complete culture medium and added to the plates where the final DMSO content did not exceed 0.5%. After 96 h of exposure, the medium was removed and replaced with 100 µL/well of a 1:7 MTT/RPMI 1640 solution (MTT solution, 5 mg/mL of MTT reagent in phosphate-buffered saline; RPMI, supplemented with 10% heat-inactivated fetal bovine serum and 4 mM L-glutamine) and incubated for 4 h at 37 °C. Subsequently, the MTT/RPMI solution was removed from all wells, and the formazan crystals formed by viable cells were dissolved in 150 µL of DMSO per well. Optical densities at 550 nm were measured with a microplate reader (Biotek ELx808), using a reference wavelength of 690 nm to correct for unspecific absorption. The quantity of viable cells was expressed in terms of the T/C values (relative to untreated controls), and 50% inhibitory concentrations (IC_{50}) were calculated from concentration-effect curves by interpolation. Evaluation is based on means from three independent experiments.

5.2. Topoisomerase IIα inhibition

The topoisomerase IIα-inhibitory capacity of **2–4** and KP1796 was determined by means of the DNA plasmid relaxation assay. For this purpose, we used the topoisomerase drug screening kit and the human recombinant topoisomerase IIα enzyme from TopoGen Inc. The supercoiled pHOT1 plasmid DNA was used as a substrate and was incubated for 30 min at 37 °C with topo IIα in the presence of various concentrations of the test compounds. Etoposide (0.8 mM) was used as a positive control. The reaction was stopped by the rapid addition of 10% SDS followed by digestion with proteinase K for 15 min at 37° C. The samples were divided and loaded onto two different 1% agarose gels with equal amount of reaction products. One gel (Fig. 3, A) was poststained (after electrophoresis incubated in a 1x TAE buffer containing 0.5 μg/mL ethidium bromide) and the other gel (Fig. 3, B) prestained (0.5 μg/mL ethidium bromide added to the gel before electrophoresis). Both were analyzed by visualization with the detection system Fusion SL (Vilber Lourmat). Evaluation is based on two independent experiments.

J Biol Inorg Chem (2016) 21:347–356
DOI 10.1007/s00775-016-1345-z

ORIGINAL PAPER

Biological properties of novel ruthenium- and osmium-nitrosyl complexes with azole heterocycles

Maria S. Novak[1] · Gabriel E. Büchel[2] · Bernhard K. Keppler[1] · Michael A. Jakupec[1]

Received: 17 December 2015 / Accepted: 6 February 2016 / Published online: 9 March 2016

Abstract Since the discovery that nitric oxide (NO) is a physiologically relevant molecule, there has been great interest in the use of metal nitrosyl compounds as antitumor pharmaceuticals. Particularly interesting are those complexes which can deliver NO to biological targets. Ruthenium- and osmium-based compounds offer lower toxicity compared to other metals and show different mechanisms of action as well as different spectra of activity compared to platinum-based drugs. Novel ruthenium- and osmium-nitrosyl complexes with azole heterocycles were studied to elucidate their cytotoxicity and possible interactions with DNA. Apoptosis induction, changes of mitochondrial transmembrane potential and possible formation of reactive oxygen species were investigated as indicators of NO-mediated damage by flow cytometry. Results suggest that ruthenium- and osmium-nitrosyl complexes with the general formula (indazolium)[*cis*/*trans*-MCl_4(NO)(1*H*-indazole)] have pronounced cytotoxic potency in cancer cell lines. Especially the more potent ruthenium complexes strongly induce apoptosis associated with depolarization of mitochondrial membranes, and elevated reactive oxygen species levels. Furthermore, a slight yet not unequivocal trend to accumulation of intracellular cyclic guanosine monophosphate attributable to NO-mediated effects was observed.

Keywords Ruthenium · Nitrosyl complexes · Cancer · Apoptosis · cGMP level

Abbreviations

CCCP	Carbonyl cyanide 3-chlorophenylhydrazone
cGMP	Cyclic guanosine monophosphate
DCFH DA	Dichloro-dihydro-fluorescein diacetate
DMSO	Dimethyl sulfoxide
FITC	Fluorescein isothiocyanate
HEPES	4-(2-hydroxyethyl)-1-piperazineethanesulfonic acid
HRP	Horseradish peroxidase
JC-1	5,5′,6,6′-tetrachloro-1,1′,3,3′-tetraethylbenzimidazolylcarbocyanine iodide
MTT	3-(4,5-dimethylthiazol-2-yl)-2,5-diphenyltetrazolium bromide
NF-kB	Nuclear factor kappa-light-chain-enhancer of activated B cells
NO	Nitric oxide
PBS	Phosphate-buffered saline
PI	Propidium iodide
ROS	Reactive oxygen species
sGC	Soluble guanylate cyclase

Introduction

Efforts of many scientists around the world have been focused on the design of metal-based agents that can be successfully used in cancer therapy with a proper balance between activity and toxicity profiles, being active against cancer cells, but not too harmful to normal cells.

Electronic supplementary material The online version of this article (doi:10.1007/s00775-016-1345-z) contains supplementary material, which is available to authorized users.

✉ Michael A. Jakupec
michael.jakupec@univie.ac.at

[1] Institute of Inorganic Chemistry, University of Vienna, 1090 Vienna, Austria

[2] Division of Physical Sciences and Engineering, KAUST Catalysis Center, King Abdullah University of Science and Technology, Thuwal 23955-6900, Saudi Arabia

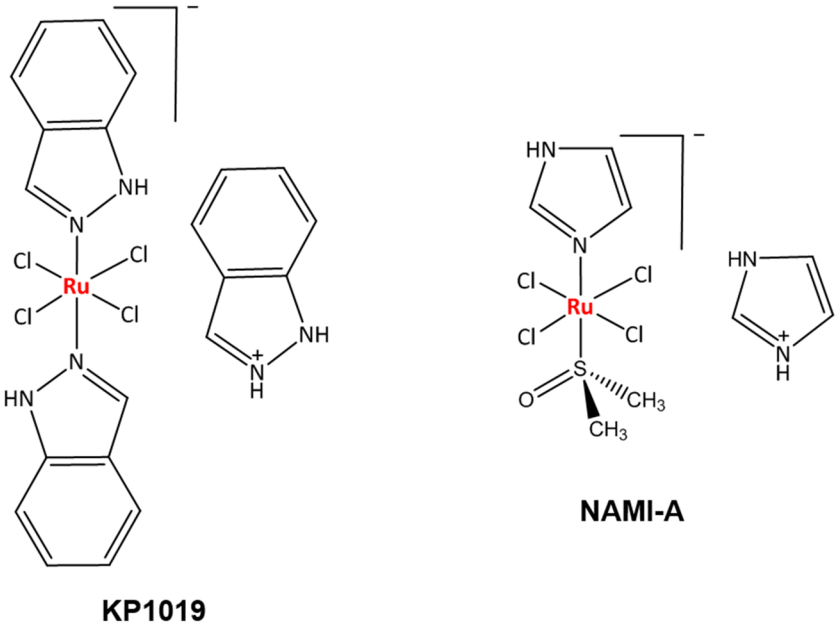

Fig. 1 Structures of indazolium *trans*-tetrachloridobis(1*H*-indazole)ruthenate(III) (KP1019) and imidazolium *trans*-tetrachlorido(dimethylsulfoxide)imidazoleruthenate(III) (NAMI-A)

Ruthenium-based complexes show great promise, not only because of their lower toxicity compared to some other metals, but also because of different mechanisms of action and a different preference for protein rather than DNA binding in comparison to platinum drugs and a different spectrum of activity without pronounced cross-resistance [1, 2]. Over time, several ruthenium complexes were developed and studied for their antiproliferative activities against various cancer models, with the clinical development of NAMI-A, KP1019 (Fig. 1) and NKP-1339 being the major milestones in this field of research. NAMI-A shows little activity against primary tumors, but was found to be highly active against secondary tumors, particularly lung metastases, while the activity of KP1019 affects primary tumors as well, such as colorectal cancers which are resistant to cisplatin therapy [3–8]. Recently, NKP-1339 has been studied against solid tumors and showed promising results in a phase I clinical trial, most remarkably in patients with gastrointestinal neuroendocrine tumors [9]. It was suggested that the tumor targeting properties of KP1019 and NKP-1339 are based on their reversible binding to serum proteins [10–12].

Nitric oxide releasing (pro)drugs of an organic (nitroglycerin) and inorganic (sodium nitroprusside) kind were already in clinical use for decades before the discovery that such a small molecule could act as a signaling molecule in biological systems [13–15]. In recent years, several classes of exogenous NO donors have been synthesized with the aim to investigate physiological processes controlled by different concentrations of nitric oxide in the cell. Some research groups studied the photochemistry of

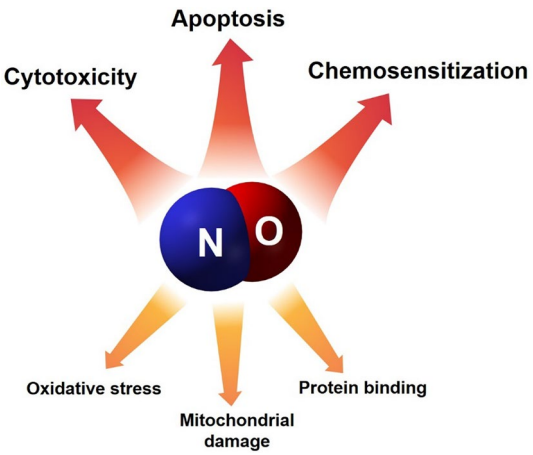

Fig. 2 Nitric oxide is highly reactive molecule that is able to regulate a wide range of cell physiological processes

such compounds, and various strategies were developed to activate these compounds to release NO under the influence of visible or UV/IR light [16]. Generally, ruthenium nitrosyl complexes are attractive because of the thermal stability of the Ru–NO bond, which upon photochemical or electrochemical stimulation may release NO [17–21]. Besides this, it was proposed that the high affinity of NO to ruthenium might play a role in the mechanism of action of KP1019, which may act as an NO scavenger.

Nitric oxide is a highly reactive free radical containing an unpaired electron in its outermost orbital, allowing it to take part in many different reactions as an electron donor or

acceptor and is capable of enhancing various reactions and processes (Fig. 2). Thereby, NO is able to react with other inorganic molecules, DNA, prosthetic groups or with proteins [22]. As a ligand in inorganic chemistry, NO is also known as a "non-innocent ligand", implying that NO can adopt several oxidation states rendering the assignment of oxidation states for the ligand and the metal complicated. Furthermore, the geometry of NO bound to a metal can vary largely from being bound linearly to strongly bent, and being coordinated via N, O or both atoms at the same time. In biological systems, nitric oxide is an endogenous molecule that is produced by nitric oxide synthase (NOS) through the conversion of L-arginine to L-citrulline and NO [23]. Additionally, NOS-independent NO generation pathways starting from nitrate (NO_3^-) and nitrite (NO_2^-), previously thought to be inert, were discovered recently [24]. Activation of soluble guanylate cyclase (sGC), formation of cGMP, and concomitant protein phosphorylation is considered the main physiological signaling pathway of NO. This cGMP-dependent pathway activates various downstream targets including protein kinases, phosphodiesterases and ion channels; whereas cGMP-independent pathways can be related to *S*-nitrosylation, which leads to an inhibition of mitochondrial cytochrome oxidase. The physiological functions of NO include blood pressure control, neurotransmission, immunological responses, and antioxidant defense. All these effects are strongly dependent on the local NO bioavailability and concentration—while low concentrations of nitric oxide contribute to host defense, high concentrations may promote apoptosis [1, 20, 25]. The administration of NO donors reduces NF-kB activation and downstream expression of anti-apoptotic gene products, which is relevant for NO-dependent sensitization of chemotherapy-resistant tumor cells [26–28]. Mitochondrial damage during NO-mediated apoptosis could be linked to the decrease of mitochondrial transmembrane potential due to the opening of mitochondrial permeability transition pores followed by massive ROS production [29].

To characterize in more detail the biological features of ruthenium- and osmium-nitrosyl complexes with the general formula (indazolium)[*cis/trans*-MCl_4(NO)(1*H*-indazole)] (Fig. 3), we report here on cytotoxicity tests, flow cytometric detection of mitochondrial membrane depolarization, ROS generation and apoptotic cells, measurement of intracellular cGMP levels as well as plasmid DNA interaction studies. Synthesis, physicochemical measurements and stability in aqueous solutions as well as reactivity toward ascorbic acid, ubiquitin and myoglobin of these

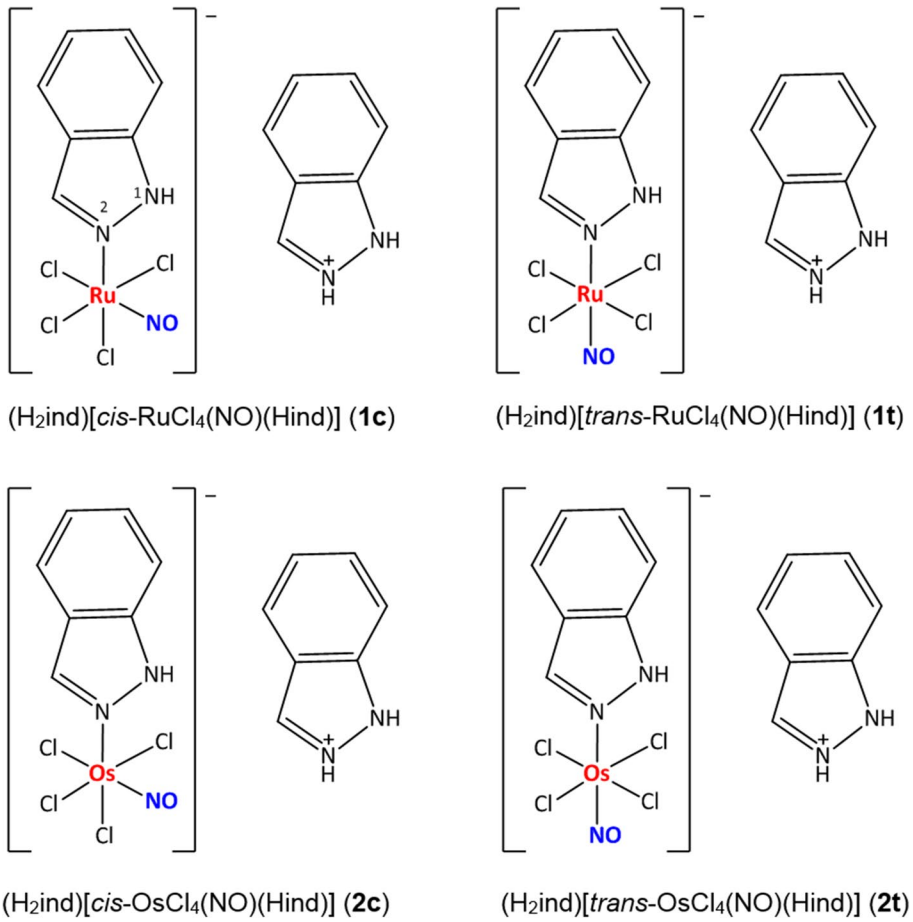

Fig. 3 Structures of ruthenium- and osmium-based nitrosyl complexes. Nitrogen atom labeling was introduced in **1c**

complexes have been published previously [30]. It has also be shown by crystallographic structure determination that indazole binds only via N2 to the metal centers and not via N1 as recently found in particular for osmium compounds, an effect also influencing biological properties [31, 32]. X-ray crystallography also reveals that NO is bound linearly via the nitrogen atom, as already indicated by IR spectroscopic data as well as calculations [33]. Potentially biologically relevant *cis*/*trans* isomerization reactions of these complexes were studied, revealing lower activation barriers for ruthenium than osmium compounds [34].

Materials and methods

Cell lines and culture conditions

CH1/PA-1 cells (identified via STR profiling as PA-1 ovarian teratocarcinoma cells by Multiplexion, Heidelberg, Germany; compare Ref. [35]) were obtained from Lloyd R. Kelland, CRC Centre for Cancer Therapeutics, Institute of Cancer Research, Sutton, UK. SW480 (human adenocarcinoma of the colon), A549 (human non-small cell lung cancer) and HL-60 (human promyelocytic leukemia) cells were kindly provided by the Institute of Cancer Research, Department of Medicine I, Medical University of Vienna, Austria. All cell culture media and supplements were purchased from Sigma-Aldrich, Austria and plastic ware from Starlab, Germany. Cells were grown in 75 cm^2 culture flasks in complete medium (i.e., Minimum Essential Medium supplemented with 10 % heat-inactivated fetal bovine serum, 1 mM sodium pyruvate, 4 mM L-glutamine and 1 % non-essential amino acids from 100× ready-to-use stock) as adherent monolayer cultures. Cultures were grown at 37 °C under a humidified atmosphere containing 5 % CO_2 and 95 % air.

MTT assay

Antiproliferative activity in vitro was determined by the colorimetric MTT assay (MTT = 3-(4,5-dimethyl-2-thiazolyl)-2,5-diphenyl-2*H*-tetrazolium bromide). For this purpose, cells were harvested from culture flasks by use of trypsin and seeded in complete medium (100 µL/well) into 96-well plates in densities of 3×10^3 (A549), 1×10^3 (CH1/PA-1) and 2×10^3 (SW480) cells per well. Cells were allowed for 24 h to settle and resume proliferation. Test compounds were dissolved in DMSO first, appropriately diluted in complete medium and instantly added to the plates (100 µL/well), where the DMSO content did not exceed 0.5 %. After exposure for 96 h, the medium was removed and replaced with 100 µL/well of a 1:7 MTT/RPMI 1640 solution (MTT solution, 5 mg/mL of MTT reagent in phosphate-buffered saline; RPMI 1640 medium, supplemented with 10 % heat-inactivated fetal bovine serum and 4 mM L-glutamine) and incubated for 4 h at 37 °C. Subsequently, the MTT/RPMI 1640 solution was removed, and the formazan product formed by viable cells was dissolved in DMSO (150 µL/well). Optical densities were measured with a microplate reader (BioTek ELx808) at 550 nm (and a reference wavelength of 690 nm) to yield relative quantities of viable cells as percentages of untreated controls, and 50 % inhibitory concentrations (IC_{50}) were calculated by interpolation. Evaluation is based on at least three independent experiments with triplicates for each concentration level.

Neutral red uptake assay

Additionally, cell viability in vitro was investigated by the neutral red uptake assay (neutral red = 3-amino-7-dimethylamino-2-methylphenazine hydrochloride, Sigma). A549, CH1/PA-1 and SW480 cells were seeded in complete medium (100 µL/well) into 96-well plates in the same densities as for MTT tests and were allowed for 24 h to settle and resume proliferation. Test compounds **1c** and **1t** were dissolved in DMSO first, appropriately diluted in complete medium and instantly added to the plates (100 µL/well), where the DMSO content did not exceed 0.5 %. After expose for 96 h, medium was replaced with 100 µL/well of a neutral red-containing medium. A neutral red stock solution (5 mg/mL) was prepared in phosphate-buffered saline, then diluted 1:100 in RPMI 1640 medium (supplemented with 10 % heat-inactivated fetal bovine serum and 4 mM L-glutamine) and pre-incubated overnight at 37 °C. Plates were incubated with this neutral red solution for 2 h at 37 °C to allow for the uptake into the lysosomes of viable cells. After incubation the medium was removed, cells were washed with phosphate-buffered saline two times (150 µL/well) and fixed with 1 % acetic acid in 70 % ethanol (150 µL/well). After incubation for 10 min at RT, the absorption was measured with a microplate reader (BioTek ELx808) at 550 nm (and a reference wavelength of 690 nm) to yield relative quantities of viable cells as percentages of untreated controls, and 50 % inhibitory concentrations (IC_{50}) were calculated by interpolation. Evaluation is based on at least three independent experiments with triplicates for each concentration level.

Impact on mitochondrial membrane potential (JC-1 assay)

Impairment of mitochondrial transmembrane potential was studied by flow cytometry using the lipophilic cationic dye 5,5′,6,6′-tetrachloro-1,1′,3,3′-tetraethylbenzimidazolylcarbocyanine iodide (JC-1). For this purpose, SW480 cells

were exposed to test compounds in different concentrations for 48 h at 37 °C and then collected in a density of 2×10^5 cells/mL by centrifugation at 500*g* for 5 min. Afterwards, cells were washed with PBS and stained with 2 µg/mL JC-1 mix in complete medium for 15 min in the dark at 37 °C. Then cells were washed and suspended in 500 µL of warm PBS and analyzed with a Guava 8HT EasyCyte flow cytometer (Millipore) using InCyte software. Carbonyl cyanide 3-chlorophenylhydrazone (CCCP) was used as a positive control in a concentration of 0.9 mM.

Flow cytometric detection of apoptotic cells

Induction of cell death was analyzed by flow cytometry using FITC-conjugated annexin V (BioVision, USA) and propidium iodide (PI, Fluka) double staining. SW480 cells were seeded into 12-well plates in a density of 5×10^4 cells per well in complete medium and allowed to settle for 24 h. The cells were exposed to test compounds in different concentrations for 48 h at 37 °C. The platinum complex KP1988 (synthesized at the Institute of Inorganic Chemistry, University of Vienna) was used as a positive control in a concentration of 200 µM. After incubation, cells were gently trypsinized, washed with PBS, and suspended with FITC-conjugated annexin V (0.25 µg/mL) and PI (1 µg/mL) in binding buffer (10 mM HEPES/NaOH pH 7.4, 140 mM NaCl, 2.5 mM $CaCl_2$) at 37 °C for 15 min. Stained cells were analyzed with a Guava 8HT EasyCyte flow cytometer (Millipore) using InCyte software.

Detection of intracellular reactive oxygen species (ROS)

For the fluorimetric analysis of ROS, non-adherent HL60 cells (promyelocytic leukemia, human) were stained for 30 min at 37 °C under 5 % CO_2 with 1 µM DCF-DA (2′,7′-dichlorofluorescein diacetate) in Hanks' Balanced Salt Solution supplemented with 1% heat-inactivated fetal bovine serum. Cells were transferred into 96-well plates in a density of 6×10^4 cells/well and treated with the test substances at different concentrations for 30 min at 37 °C under 5 % CO_2. A freshly prepared 500 µM H_2O_2 solution was used as a positive control and added 10 min before measurement. Cellular ROS levels were measured by flow cytometry on a Guava 8HT EasyCyte flow cytometer (Millipore). The resulting histograms of green fluorescence were quantified by FlowJo software (Tree Star). Results are presented as the ratios of green fluorescence intensities of the drug-treated samples and that of the untreated control.

Competition enzyme-linked immunoassay (cGMP assay)

The intracellular cGMP levels after treatment with nitrosyl complexes were assessed by using the Cyclic GMP XP™ Assay Kit (Cell Signaling Technology). The teratocarcinoma cell line CH1/PA-1 was grown in 12-well plates under standard conditions and treated with various concentrations of test compounds for 2 h. Then, cells were solubilized in lysis buffer, and intracellular cGMP levels were assessed according to manufacturer's instructions. The absorbance was measured with a microplate reader (BioTek ELx808) at 450 nm, and the absolute amount of cGMP in samples was calculated by using a standard curve. Evaluation is based on at least three independent experiments with duplicates for each concentration level.

Plasmid DNA interaction studies

pUC19 DNA (2686 bp) plasmid was purchased from Fermentas Life Sciences. 500 ng of pUC19 plasmid was incubated with 50 µM of the test compounds in 0.1× Tris-EDTA (TE) buffer for different time intervals (5 min up to 6 h) at 37 °C. The electrophoresis was performed in agarose (from Sigma-Aldrich) gel 1 % w/v in 1× Tris-borate-EDTA (TBE) buffer for 90 min at 80 V. Gels were stained with ethidium bromide (EtBr) in 1× TBE (0.75 µg/mL) for 20 min. Images were taken with the multi-imaging detection system Fusion SL (Vilber Lourmat).

Results and discussion

As reported previously, ruthenium complexes **1c** and **1t** yielded IC_{50} values in the low micromolar range and turned out to be much more cytotoxic than osmium complexes **2c** and **2t** (Table 1). Since the aqueous solubility of these

Table 1 Inhibition of cancer cell growth by studied compounds in three human cancer cell lines; 50 % inhibitory concentrations (means ± standard deviations), obtained by the MTT assay and neutral red uptake assay (exposure time: 96 h)

Compounds	IC50, µM (MTT)[a]			IC50, µM (neutral red)		
	A549	CH1/PA-1	SW480	A549	CH1/PA-1	SW480
1c	14 ± 3	2.7 ± 0.6	2.6 ± 0.3	20 ± 8	5.7 ± 2.5	4.3 ± 1.7
1t	8.0 ± 1.3	1.3 ± 0.3	1.1 ± 0.3	9.3 ± 2.9	2.3 ± 0.7	1.5 ± 0.4
2c	128 ± 18	48 ± 13	43 ± 6	n.d.	n.d.	n.d.
2t	>640	145 ± 12	450 ± 35	n.d.	n.d.	n.d.

[a] Taken from Ref. [30]

complexes at 294 K is in the very low mM range, compounds had to be dissolved in DMSO, but were diluted to acceptable DMSO contents to enable the application of up to very high submillimolar concentrations in biological test. According to UV-vis spectroscopy (and ESI-MS) studies, complexes remain intact in aqueous solution for at least 24 h (Ru) and 72 h (Os), respectively. ESI-MS studies had also revealed that, in contrast to osmium analogs, the biologically much more active ruthenium compounds are prone to reduction by ubiquitous natural reducing agents such as ascorbic acid, suggesting that they can be activated by biological nucleophiles [30].

The strongest difference in cytotoxicity was observed between *trans*-configured ruthenium indazole complex **1t** and its osmium analog **2t** with a maximum factor of about 400. The difference between the corresponding *cis* isomers **1c** and **2c** was also pronounced with a maximum factor of 18. In addition, the *trans*-configured ruthenium complex **1t** is up to 2.4-fold more potent than its *cis* analog **1c**, while the *cis*-configured osmium indazole complex **2c** is up to tenfold more potent than its *trans* isomer **2t**. For comparison, the antiproliferative activity of KP1019 tested previously yielded IC_{50} values of 44 ± 11 μM in CH1/PA-1 and 79 ± 5 in SW480 cells [31]. Obviously, the exchange of one indazole present in KP1019 by NO increased the cytotoxic potency of ruthenium-based nitrosyl analog **1t** about 72 times in SW480 and about 34 times in CH1/PA-1 cells.

The first cytotoxicity tests had been performed using the MTT assay, which is based on the reduction of a tetrazolium salt to an insoluble formazan, reflecting the number of viable cells present. This reduction is catalyzed by mitochondrial enzymes as well as by cytoplasmic and cell membrane components [36]. Since nitric oxide can disrupt the mitochondrial respiratory system, the NO-mediated damage of mitochondria might distort the results of MTT-based cytotoxic tests. Therefore, the activity of the most active compounds was confirmed by the neutral red uptake assay. This assay is based on the ability of viable cells to incorporate and bind the neutral red dye into lysosomes and likewise provides a quantitative estimation of the number of viable cells [37].

IC_{50} values obtained by the neutral red uptake assay are systematically slightly higher than those obtained by the MTT assay, with a maximum factor of 2.1 (for **1c** in CH1/PA-1 cells). However, these differences are too small to be taken as an indication for distortion of MTT-based cytotoxicity data by NO-mediated mitochondrial damage upon treatment with the tested substances.

The possible influence on mitochondria was additionally investigated in SW480 cells by the lipophilic cationic dye JC-1. The JC-1 assay reveals depolarization of mitochondrial membranes in up to 55 and 68 % of cells after 48 h exposure to ruthenium-based complexes **1c** and **1t**, respectively, and up to 20 and 4 % of cells for osmium-based complexes **2c** and **2t**, respectively (Fig. 4). Thus, these experiments indicate a difference in the capacities of tested analogs to depolarize mitochondria: *trans*-configured ruthenium complex **1t** induces mitochondrial membrane depolarization to an about 17 times higher extent than its osmium analog **2t**, whereas *cis*-configured ruthenium complex **1c** does so only to an about 3 times higher extent than its osmium analog **2c**.

Since the depolarization of mitochondrial membranes plays a role in the intrinsic apoptotic pathway, apoptosis induction was examined by annexin V-FITC/propidium iodide double staining in SW480 cells and subsequent flow cytometric analysis (Fig. 5). This assay is based on detection of phosphatidylserine externalization from the inner to the outer side of the plasma membrane upon apoptosis induction; the protein annexin V is able to bind to this externalized lipid, and the fluorescent tag FITC serves as a label for the flow cytometric detection of apoptotic cells. This is combined with propidium iodide, which indicates the loss of cell membrane integrity, differentiating necrotic and late apoptotic from early apoptotic and viable cells. These experiments indicate induction of apoptosis by ruthenium-based complexes **1c** and **1t** (50 μM) after 48 h in up to 80 and 83 % of cells, respectively, and by osmium-based complexes **2c** and **2t** (250 μM) in up to 3 and 5 % of cells. Thus, the capacity of the *cis*-configured ruthenium indazole complex **1c** to induce apoptosis is about 27 times higher than that of its osmium-based analog **2c**. The *trans*-configured ruthenium indazole complex **1t** is about 17 times more potent in this respect than its osmium analog **2t**. Together with the results of the JC-1 assay, this suggests that only ruthenium, but not osmium-based nitrosyl complexes strongly induce programmed cell death via the intrinsic pathway involving depolarization of mitochondrial membranes.

Since the generation of oxidative stress is one of the known NO-mediated disturbances of the cell [39], we investigated by the DCF-DA assay the impact of nitrosyl complexes on the intracellular level of ROS in promyelocytic leukemia cells HL60 (Fig. 6). The assay employs the cell-permeable fluorogenic probe DCF-DA, which is rapidly oxidized to highly fluorescent DCF by ROS and its fluorescence intensity is proportional to the ROS levels within the cell. As an NO-free reference compound we used KP1019. The studies indicate a pronounced increase in ROS level by the *trans*-configured ruthenium indazole complex **1t** only at the very high concentration of 250 μM (by a factor of 5.7), whereas the reference compound KP1019 consistently induces stronger increases (by up to 13 times) and the other tested complexes only induce up to 2.5-fold increases (at 250 μM). Thus, the *trans*-configured complex KP1019 lacking an NO ligand is about 2.3 times

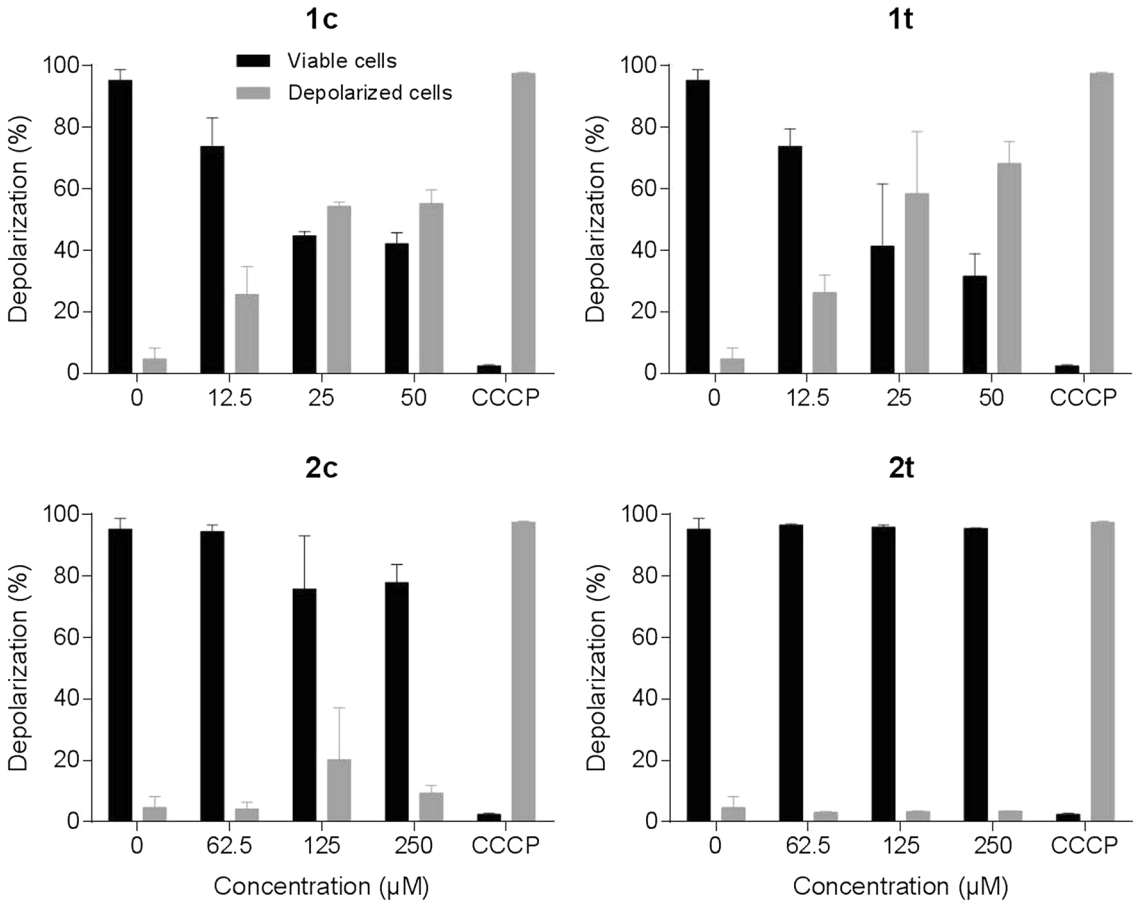

Fig. 4 Depolarization of mitochondrial membranes in SW480 cells after 48 h exposure to the tested compounds, measured by flow cytometry using JC-1 staining. Positive control was treated with 0.9 mM CCCP

more potently inducing ROS than the corresponding ruthenium nitrosyl complex **1t** and about 5 times more potent than the other complexes.

The possible involvement of the cGMP pathway, as a main NO-dependent signaling pathway in the cell, was examined by the competition enzyme-linked immunoassay in CH1/PA-1 cells (Fig. 7). Because of the competitive nature of this assay, the magnitude of the absorbance is inversely proportional to the quantity of cGMP in the sample. Measurement of absorbance using a cGMP standard curve allows calculating the absolute amount of cGMP in a sample of interest. Obtained data suggest an up to 1.5-fold increase in intracellular cGMP level upon treatment with *trans*-configured ruthenium indazole complex **1t** at a concentration of 100 μM and a comparable effect of the *cis*-configured ruthenium indazole complex **1c** at the highest concentration of 500 μM, but all effects are within the ranges of standard deviations and should therefore be taken with caution.

The interactions with plasmid DNA had been studied previously for KP1019, showing its ability to untwist and to bend DNA [10]. As analogs of KP1019, the nitrosyl complexes were now studied for their ability to interact with DNA. Cell-free experiments showed no significant activity versus a dsDNA plasmid (Fig. S1). These experiments suggest that ruthenium- and osmium-based nitrosyl complexes are unable to induce DNA damage under the experimental conditions.

In summary, the metal center variation and *cis*/*trans* isomerism in nitrosyl complexes bearing azole heterocycles have an unexpectedly large impact on their potency in human cancer cell lines. Generally, ruthenium nitrosyl complexes showed a stronger capacity to inhibit cancer cell proliferation, to induce depolarization of mitochondrial membranes and apoptosis, and to increase intracellular ROS and cGMP levels than the osmium analogs. Overall, the *cis*-configured ruthenium nitrosyl complex is nearly as potent as the *trans*-configured complex except for ROS and cGMP assays.

The observed stronger activity of ruthenium complexes is remarkable and can be explained by differences in M–NO bond stabilities. There is evidence that the Os–NO

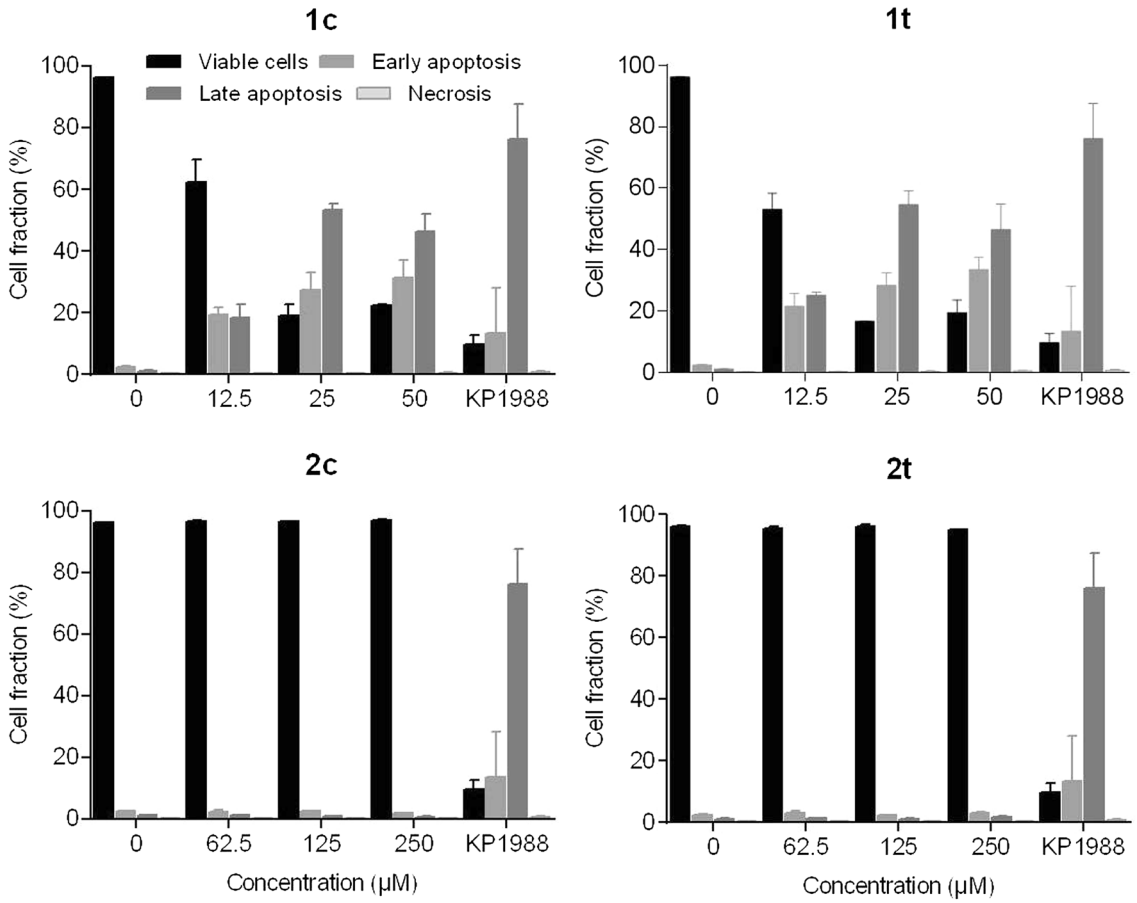

Fig. 5 Apoptosis induction in SW480 cells after 48 h of exposure to the tested compounds, measured by flow cytometry using annexin V-FITC/propidium iodide double staining. Positive control was treated with 200 μM of platinum(II) oxime complex KP1988 [38]

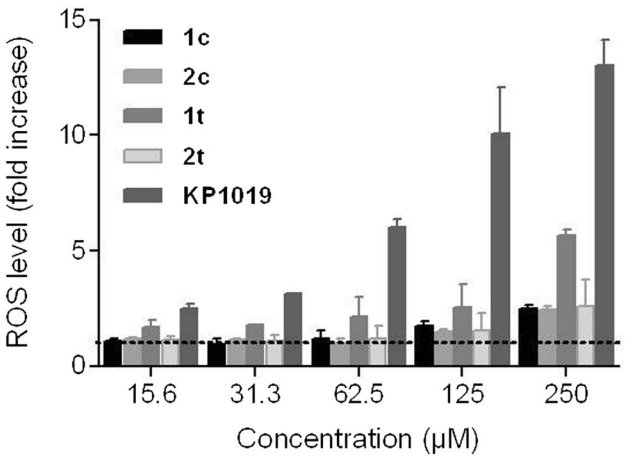

Fig. 6 Intracellular ROS levels in HL60 cells induced by tested compounds, determined by the DCF-DA assay. RFUs of all samples were normalized to the RFU of stained untreated control (indicated by a *dashed line*)

bond is stronger compared to the Ru–NO analog [40]. As a consequence, the ruthenium compounds are prone to reduction in the biological environment due to the decreased stabilization of the NO ligand compared to the Os counterparts. Furthermore the ruthenium analogs can be activated by ascorbic acid, leading to hydrolysis of one chloride ligand in contrast to osmium analogs [30]. Ford has pointed out a "*trans*-effect" for ruthenium nitrosyls, which was more recently reviewed for octahedral transition metal complexes in general by Coe and Glenwright [18, 41]. Ford claims that the identity of the *trans*-ligand affects the M–NO and N–O stretching frequencies; notably, X-ray structures of ruthenium nitrosyls showed that in the *trans* position the M–ligand bond was significantly longer than in the *cis*-position. This is in line with previous research where it was shown that Ru−NO bonds in the *cis* isomer **1c** are significantly shorter than in the *trans* isomer **1t** because of the stronger *trans* effect of indazole compared to the

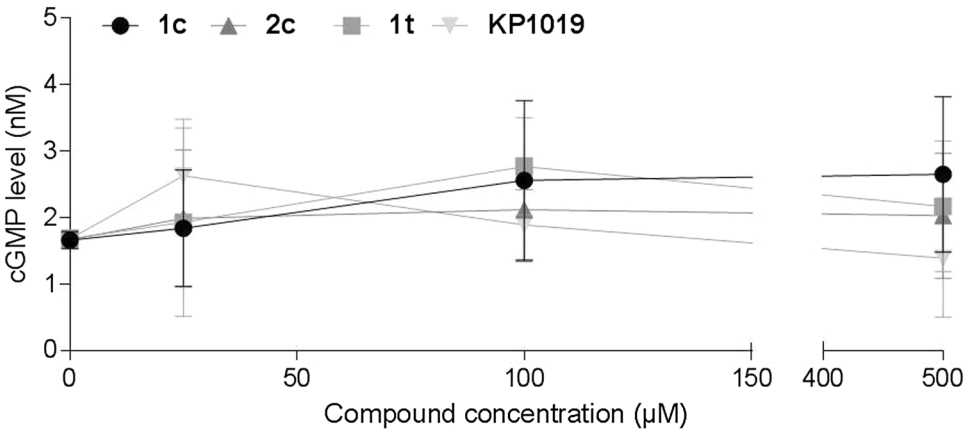

Fig. 7 Intracellular cGMP levels in CH1/PA-1 cells upon treatment with ruthenium- and osmium-based nitrosyl complexes or KP1019, determined by the competition enzyme-linked immunoassay (cGMP assay)

chlorido ligand [30]. This is also confirmed by thermodynamic data showing a preference for the *cis* compound: *cis* to *trans* isomerization [−18.6 J/(mol K)] and [31.0 J/(mol K)] for the *trans* to *cis* conversion. Kinetic data reveal the same picture with rate constants of 5.51×10^{-6} for the *cis*→*trans* process and 12.2×10^{-6} for the *trans*→*cis* process at 100 °C in an aprotic solvent [34].

We come to the point that the understanding of the intracellular Ru–NO bond behavior is crucial for structure–activity relationships of this class of metallodrugs. If we take into account that the Ru–NO bond is more labile than the Os–NO bond, we may expect the release of NO under biological conditions as mentioned above. The role of NO in mitochondria-mediated cell death was reported several times before. Brown and co-workers describe a broad range of NO actions on mitochondria: it inhibits mitochondrial respiration, stimulates the production of superoxide, hydrogen peroxide and peroxynitrite, induces the transition permeability and release of cytochrome C, and NO potentially sensitizes cells to hypoxic damage [39]. Toledo et al. reported the ability of ruthenium(II) ammine nitrosyl complexes to release NO under biological conditions, where the reduction of these complexes is concomitant with mitochondrial NADH oxidation [42]. Curti and co-authors also observed NO release for this compound class which was occurring as a result of NAD(P)H oxidation and led to dissipation of mitochondrial membrane potential, ATP depletion and generation of ROS. As described in the most recent publication, oxidation of mitochondrial NADH promotes NO release from nitrosyl ruthenium complexes, which is accompanied by the release of cytochrome C [43, 44].

Thus far, our results demonstrate that the studied ruthenium nitrosyl complexes induce apoptosis by the mitochondrial pathway, at least partially associated with ROS generation, and may represent promising drug candidates for further preclinical evaluation.

Acknowledgments Austrian Science Fund (FWF). We are deeply grateful to Prof. Dr. Vladimir Arion for overall support and collaborations. Authors wish to thank Anatolie Gavriluta (Université Claude Bernard Lyon 1, France) for cooperation. This work was performed as part of an Austrian-French joint project supported in France by ANR (Agence Nationale de la Recherche) through the project VILYGRu (No. ANR-09-BLAN-0420-01) and in Austria by the Austrian Science Fund (FWF) through the project I374-N19. Partial support by the Austrian Science Fund through the project P-22339-N19 is also acknowledged.

Compliance with ethical standards

Conflict of interest The authors declare that they have no conflicts of interest regarding the contents of this article.

References

1. Tfouni E, Truzzi DR, Tavares A, Gomes AJ, Figueiredo LE, Franco DW (2012) Nitric Oxide 26(1):38–53
2. Wu B, Ong MS, Groessl M, Adhireksan Z, Hartinger CG, Dyson PJ, Davey CA (2011) Chem Eur J 17:3562–3566
3. Bergamo A, Gaiddon C, Schellens JH, Beijnen JH, Sava G (2012) J Inorg Biochem 106(1):90–99
4. Muhammad N, Guo Z (2014) Curr Opin Chem Biol 19:144–153
5. Sava G, Bergamo A (2009) In: Bonetti A, Leone R, Muggia FM, Howell SB (eds) Platinum and other heavy metal compounds in cancer chemotherapy. Humana Press, Totowa, pp 57–66
6. Spreckelmeyer S, Orvig C, Casini A (2014) Molecules 19(10):15584–15610
7. Alessio E, Mestroni G, Bergamo A, Sava G (2004) Curr Top Med Chem 4:1525–1535
8. Bergamo A, Sava G (2007) Dalton Trans 1267–1272
9. Thompson DS, Weiss GJ, Jones SF, Burris HA, Ramanathan RK, Infante JR, Bendell JC, Ogden A, Von Hoff DD (2012) J Clin Oncol 30 **(suppl; abstr 3033)**

10. Hartinger CG, Zorbas-Seifried S, Jakupec MA, Kynast B, Zorbas H, Keppler BK (2006) J Inorg Biochem 100(5–6):891–904
11. Heinrich TA, Von Poelhsitz G, Reis RI, Castellano EE, Neves A, Lanznaster M, Machado SP, Batista AA, Costa-Neto CM (2011) Eur J Med Chem 46(9):3616–3622
12. Jakupec MA, Kandioller W, Alte B, Trondl R, Berger W, Keppler BK **(submitted manuscript)**
13. Butler AR, Megson IL (2002) Chem Rev 102(4):1155–1166
14. Ignarro LJ (1999) Biosci Rep 19(2):51–71
15. Marsh N, Marsh A (2000) Clin Exp Pharmacol Physiol 27(4):313–319
16. Rose MJ, Mascharak PK (2008) Coord Chem Rev 252(18–20):2093–2114
17. Bučinský L, Büchel GE, Ponec R, Rapta P, Breza M, Kožíšek J, Gall M, Biskupič S, Fronc M, Schiessl K, Cuzan O, Prodius D, Turta C, Shova S, Zając DA, Arion VB (2013) Eur J Inorg Chem 14:2505–2519
18. Ford PC (1970) Coord Chem Rev 5:75–99
19. Freitag L, González L (2014) Inorg Chem 53(13):6415–6426
20. Oliveira F, Togniolo V, Pupo T, Tedesco AC, Silva RS (2004) Inorg Chem Commun 7:160–164
21. Trondl R, Heffeter P, Kowol CR, Jakupec MA, Berger W, Keppler BK (2014) Chem Sci 5:2925–2932
22. Mocellin S, Bronte V, Nitti D (2007) Med Res Rev 27(3):317–352
23. Palmer RM, Ashton DS, Moncada S (1988) Nature 333(6174):664–666
24. Lundberg JO, Weitzberg E, Gladwin MT (2008) Nat Rev Drug Discov 7(2):156–167
25. Guo Z, Sadler PJ (1999) Angew Chem Int Ed 38:1512–1531
26. Bonavida B, Khineche S, Huerta-Yepez S, Garbán H (2006) Drug Resist Updat 9(3):157–173
27. Brüne B, von Knethen A, Sandau KB (1998) Eur J Pharmacol 351(3):261–272
28. Muntané J, De la Rosa AJ, Marín LM, Padillo FJ (2013) Mitochondrion 13(3):257–262
29. Ushmorov A, Ratter F, Lehmann V, Dröge W, Schirrmacher V, Umansky V (1999) Blood 93(7):2342–2352
30. Büchel GE, Gavriluta A, Novak M, Meier SM, Jakupec MA, Cuzan O, Turta C, Tommasino JB, Jeanneau E, Novitchi G, Luneau D, Arion VB (2013) Inorg Chem 52(11):6273–6285
31. Büchel GE, Stepanenko IN, Hejl M, Jakupec MA, Keppler BK, Arion VB (2011) Inorg Chem 50:7690–7697
32. Büchel GE, Stepanenko IN, Hejl M, Jakupec MA, Keppler BK, Heffeter P, Berger W, Arion VB (2012) J Inorg Biochem 113:47–54
33. Delcey MG, Freitag L, Pedersen TB, Aquilante F, Lindh R, González L (2014) J Chem Phys 140(17):174103
34. Gavriluta A, Büchel GE, Freitag L, Novitchi G, Tommasino JB, Jeanneau E, Kuhn PS, González L, Arion VB, Luneau D (2013) Inorg Chem 52(11):6260–6272
35. Korch C, Spillman MA, Jackson TA, Jacobsen BM, Murphy SK, Lessey BA, Jordan VC, Bradford AP (2012) Gynecol Oncol 27(1):241–248
36. Berridge MV, Herst PM, Tan AS (2005) Biotechnol Annu Rev 11:127–152
37. Repetto G, del Peso A, Zurita JL (2008) Nat Protoc 3(7):1125–1131
38. Scaffidi-Domianello YY, Legin AA, Jakupec MA, Arion VB, Kukushkin VY, Galanski M, Keppler BK (2011) Inorg Chem 50(21):10673–10681
39. Brown GC, Borutaite V (2001) IUBMB Life 52:189–195
40. Cleare MJ (1968) Platinum Met Rev 12:131–133
41. Coe BJ, Glenwright SJ (2000) Coord Chem Rev 203:5–80
42. Toledo JC Jr, Lopes LG, Alves AA, Pereira da Silva L, Franco DW (2002) J Inorg Biochem 89(3–4):267–271
43. Pestana CR, Phelippin DP, Polizello AC, Dorta DJ, Uyemura SA, Santos AC, Doro FG, Rodrigues FP, Tfouni E, Curti C (2009) Nitric Oxide 20(1):24–30
44. Rodrigues FP, Pestana CR, Polizello AC, Pardo-Andreu GL, Uyemura SA, Santos AC, Alberici LC, da Silva RS, Curti C (2012) Nitric Oxide 26(3):174–181

Supplementary information

Biological properties of novel ruthenium and osmium nitrosyl complexes with azole heterocycles

Maria S. Novak, Gabriel E. Büchel, Bernhard K. Keppler and Michael A. Jakupec

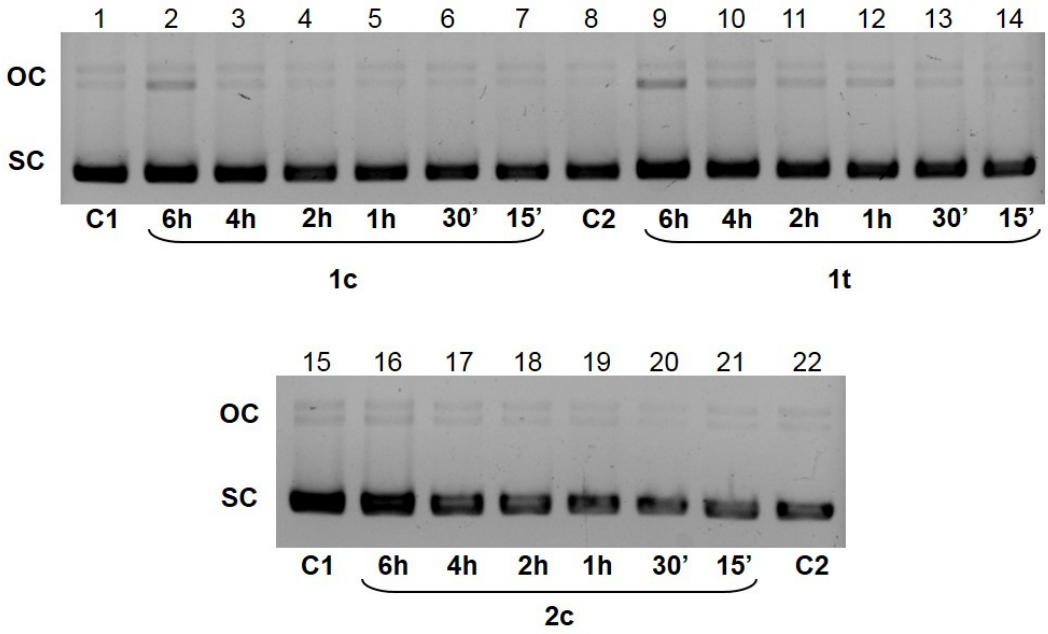

Figure S1. Electropherograms of dsDNA plasmid pUC19 after exposure to a 50 μM solution of ruthenium complexes **1c** (lanes 2–7) and **1t** (lanes 9–14), as well as osmium complex **2c** (lanes 16–21) for different exposure times (15 min to 6 h) in comparison to untreated controls C1 and C2 (lanes 1, 8, 15, 22).

3. Conclusions and Outlook

Previous studies have suggested possible advantages in using other transition-metal ions than platinum as the basis for anticancer drugs that give the chance of using additional coordination sites, alterations in ligand affinity and substitution kinetics. Ruthenium-based compounds have attracted the interest of researchers because of the opportunity to use this metal for creation of novel drugs suitable for treating tumors with a rather selective cytotoxicity against tumor cells. The aim of the current study was to investigate biological properties of novel transition metal complexes influencing their anticancer drug profiles. Many publications confirmed that metal-based compounds other than those of platinum work in a different way; however, there is relatively little information on mechanisms of action and involved pathways. There is a chance to extend the range of applied chemotherapeutic agents by combining various metal ions and ligands with subsequent investigation of their properties and activities, focusing on the most promising combinations.

We studied novel Ru- and Os-based nitrosyl complexes with azole heterocycles, the striking difference in the activity of which was attributed to higher lability of the Ru−NO bond in comparison to the Os−NO bond and to the ability of mitochondria to activate NO release leading to cell death. In the course of ruthenium anticancer drug development, Ru(II)–cymene complexes with various substituted 3-hydroxyflavones were found to exhibit not only high antiproliferative activity in human cancer cell lines but were also found to inhibit human topo2α activity, which correlated with their cytotoxic potency. The compound library of organometallic complexes featuring flavonoid ligands has been extended by three Ru(II)-, Os(II)- and Rh(III)-arene complexes, in which a flavonol ligand containing a piperonyl group was designed to imitate the general structure of 3',4'-dihydroxyflavonols and to elucidate the important features for topoisomerase inhibition. The obtained results suggest that these complexes are potent inhibitors of cancer cell growth at a low micromolar concentration range and act as catalytic inhibitors of topo2α. A series of novel 1,3-dioxoindan-2-carboxamide-based complexes, designed to combine the attributes of half-sandwich complexes and the topo2α inhibiting properties of the ligand scaffold, were able to inhibit catalytic activity of the topo2α enzyme in the concentration range of their IC50 values, in contrast to the free ligand. Thus, the coordination of the bioactive ligand scaffold to the organometallic fragments has only a minor impact on the cytotoxicity, whereas there is a distinct impact on topo2α inhibition properties of the complexes and potency of inducing apoptosis of specifically the rhodium-based analog. Novel Ru(II)-, Os(II)-, Rh(III)- and Ir(III)-based thiomaltol complexes showed a significantly higher topo2α inhibitory capacity compared to the free ligand and act as topo2α catalytic inhibitors. Moreover, structure-activity relationships of these complexes in mammary carcinoma cell lines with different levels of topo2α expression as well as the analysis of their antiproliferative activity in a newly generated enzyme

down-regulated cell line variant confirm that the sensitivity of the cells to the different drugs depends on the level of enzyme expression. In addition, a theoretical analysis of the intramolecular contacts between these metal complexes helped to indicate the pocket which is most likely binding site of the protein domain what was not previously done for this class of compounds. The combination of these findings suggests that topo2α is a possible target for these complexes, but probably the mechanism of inhibition is not simple and additional studies and more complex analysis is required to more clearly understand the mode of action. Nevertheless, these compounds may serve as potential pharmacophores for further rational design of topo2 catalytic inhibitors.

Molecular target identification is of central importance to drug discovery. Each of the approaches to research of target identification and mechanism of action has its own strengths and limitations, and of course different technical performance characteristics. Laboratories that have experience in chemistry or biochemistry can aim for direct biochemical approaches, whereas groups with a high degree of computational experience can first use methods that research databases for clues. Of course, there is no "right answer" about which method is best and we are suggesting that the combination of approaches will be most fruitful. Since there is ongoing and rapidly growing interest in the design of metal-based anticancer agents capable to overcome the drawbacks of clinically applied chemotherapeutics, the proposed research will improve our knowledge of transition metal-based complexes and would benefit the field of metallopharmaceuticals.

4. References

1. Sarkar S, Horn G, Moulton K, Oza A, Byler S, Kokolus S, Longacre M (2013) Int J Mol Sci 14(10), 21087–113
2. Vogelstein B, Kinzler KW (2004) Nat Med 10(8), 789–99
3. National Cancer Institute, accessed 22/2/16, http://cancer.gov/
4. Hanahan D and Weinberg RA (2000) Cell, Vol 100, 57–70
5. Hanahan D and Weinberg RA (2011) Cell, Vol 144, 646–674
6. McFarland CD, Korolev KS, Kryukov GV, Sunyaev SR, Mirny LA (2013) Proc Natl Acad Sci USA 110(8), 2910–5
7. Podlaha O, Riester M, De S, Michor F (2012) Trends in Genetics 28(4), 155–163
8. Akavia UD, Litvin O, Kim J, Sanchez-Garcia F, Kotliar D, Causton HC, Pochanard P, Mozes E, Garraway LA, Pe'er D (2010) Cell 143(6), 1005–17
9. Eifert C, Powers SR (2012) Nature Reviews Cancer 12, 572–578
10. Yates LR, Campbell PJ (2012) Nat Rev Genet 13(11), 795–806
11. Torre LA, Bray F, Siegel RL, Ferlay J, Lortet-Tieulent J, Jemal A (2015) Global Cancer Statistics, 2012. CA Cancer J Clin 65, 87–108
12. Peto J (2001) Nature, 411(6835), 390–5
13. Ezzati M, Henley SJ, Lopez AD, Thun MJ (2015) Int J Cancer, 116(6), 963–71
14. Grewal P, Viswanathen VA (2012) Clin Liver Dis, 16(4), 839–50
15. Lim U, Subar AF, Mouw T, Hartge P, Morton LM, Stolzenberg-Solomon R, Campbell D, Hollenbeck AR, Schatzkin A (2006) Cancer Epidemiol Biomarkers Prev 15(9), 1654–9
16. Cross AJ, Sinha R (2004) Environ Mol Mutagen 44(1), 44–55
17. Bouayed J, Bohn T (2010) Oxid Med Cell Longev 3(4), 228–237
18. Seeram NP, Henning SM, Niu Y, Lee R, Scheuller HS, Heber D (2006) J Agric Food Chem 54(5), 1599–1603
19. Mukhtar H, Ahmad N (2000) Am J Clin Nutr 71(6), 1698s–1702s
20. Challier B, Perarnau JM, Viel JF (1998) Eur J Epidemiol 14(8), 737–47
21. Cancer Atlas, accessed 15/2/16, http://canceratlas.cancer.org/
22. Ferlay J, Soerjomataram I, Dikshit R, Eser S, Mathers C, Rebelo M, Parkin DM, Forman D, Bray F (2015) Int J Cancer 136(5), E359–E386
23. Cancer Stat Facts: Cancer of Any Site. National Cancer institute, assessed 25/06/2018, https://seer.cancer.gov/
24. Urruticoechea A, Alemany R, Balart J, Villanueva A, Viñals F, Capellá G (2010) Curr Pharm Des 16(1), 3–10

25. Baba AI, Câtoi C. (2007) Comparative Oncology. Bucharest: The Publishing House of the Romanian Academy, Chapter 19, Principles of anticancer therapy
26. Chabner BA, Roberts TG (2005) Nature Reviews Cancer 5, 65–72
27. Corrie PG (2008) Medicine 36(1), 24–28
28. Moudi M, Go R, Yong Seok Yien C, Nazre M (2013) Int J Prev Med.; 4(11): 1231–1235
29. Clarke MJ (2003) Coordination Chemistry Reviews 236, 209–233
30. Muhammad N, Guo Z (2014) Current Opinion in Chemical Biology 19, 144–153
31. Wang D, Lippard SJ (2005) Nature Reviews Drug Discovery 4, 307–320
32. Apps MG, Choi EH, Wheate NJ (2015) Endocr Relat Cancer 22(4), R219–33
33. Osheroff N (1998) Biochimica et biophysica acta (1400), 1–2
34. Null PA, Hudson J, Gorbsky JG (2002) Cell Growth Differ 13(7), 325–33
35. Pommier Y, Leo E, Zhang H, Marchand C (2010) Chem Biol 17(5), 421–33
36. Pommier Y (2013) ACS Chem Biol 8(1), 82–95
37. Khadka DB, Cho WJ (2013) Expert Opin Ther Pat 23(8), 1033–56
38. Larsen AK, Escargueil AE, Skladanowski A (2003) Pharmacol Ther 99(2), 167–81
39. Li H, Xie N, Gleave ME, Dong X (2015) Oncotarget 6(24), 20474–84
40. Murphy MB, Mercer SL, Deweese JE. (2017) Advances in Molecular Toxicology 11, 203-240
41. Wendorff TJ, Schmidt BH, Heslop P, Austin CA, Berger JM (2012) J Mol Biol. 424(3–4): 109–124
42. Palermo G, Stenta M, Cavalli A, Dal Peraro M, De Vivo M (2013) J Chem Theory Comput.; 9(2):857–62
43. Ali Y, Abd Hamid S (2015) Tumor Biol
44. Allen TM (2002) Nature Reviews Cancer 2, 750–763
45. Pardoll DM (2012) Nat Rev Cancer 12(4), 252–64
46. Medici S, Peana M, Nurchi VM, Lachowicz JI, Crisponi G, Zoroddu MA (2015) Coord Chem Rev 284, 329–350
47. Lainé AL, Passirani C (2012) Curr Opin Pharmacol 12(4), 420–6
48. Romero-Canelón I, Sadler PJ (2013) Inorg Chem 52(21), 12276–91
49. Jungwirth U, Kowol CR, Keppler BK, Hartinger CG, Berger W, Heffeter P (2011) Antioxid Redox Signal 15(4), 1085–1127
50. Thompson DS, Weiss GJ, Jones SF, Burris HA, Ramanathan RK, Infante JR, Bendell JC, Ogden A, Von Hoff DD (2012) Journal of Clinical Oncology 30:15, 3033–3033
51. Bergamo A, Gaiddon C, Schellens JH, Beijnen JH, Sava G (2012) J Inorg Biochem 106(1), 90–9
52. Hanif M, Babak MV, Hartinger CG (2014) Drug Discov Today 19(10), 1640–8

53. Meier-Menches SM, Gerner C, Berger W, Hartinger CG, Keppler BK (2017) Chem Soc Rev; 47(3), 909–928
54. Jakupec MA, Kandioller W, Schoenhacker-Alte B, Trondl R, Berger W, Keppler BK (2017) Trends and Perspectives of Ruthenium Anticancer Compounds (Non-PDT). Chapter 14, doi: 10.1002/9783527695225.ch14.
55. Dwyer FP, Sargeson AM (1953) J. Am. Chem. Soc., 75 (4), 984–985
56. Geldmacher Y, Oleszak M, Sheldrick WS (2012) Inorganica Chimica Acta 393, 84–102
57. Leunga C-H, Zhonga H-J, Chanb S-H D, Ma D-L (2013) Coord Chem Rev 257, 1764–1776
58. Ndagi U, Mhlongo N, Soliman ME (2017) Drug Des Devel Ther, 11, 599–616
59. Zou T, Ching A, Lum T, Lok C-N, Zhang J-J, Che C-M (2015) Chem Soc Rev, 44, 8786–8801
60. Palma G, D'Aiuto M, Rea D, et al. (2014) Biochem Pharmacol, 13(13), 1603–1615